

GCO PUBLICATION No. 1/84

PREDICTION OF SOIL SUCTION FOR SLOPES IN HONG KONG

M.G. Anderson

**Geotechnical Engineering Office
Civil Engineering Department
HONG KONG**

GCO PUBLICATION No. 1/84

PREDICTION OF SOIL SUCTION FOR SLOPES IN HONG KONG

M.G. Anderson

**Geotechnical Engineering Office
Civil Engineering Department
HONG KONG**

© Hong Kong Government

First published, September 1983

Reprinted, December 1984

Reprinted, October 1985

Reprinted, August 1996

Prepared by:

Geotechnical Engineering Office,
Civil Engineering Department,
Civil Engineering Building,
101 Princess Margaret Road,
Homantin, Kowloon,
Hong Kong.

This publication is available from:

Government Publications Centre,
Ground Floor, Low Block,
Queensway Government Offices,
66 Queensway,
Hong Kong.

Overseas orders should be placed with:

Publications (Sales) Office,
Information Services Department,
28th Floor, Siu On Centre,
188 Lockhart Road, Wan Chai,
Hong Kong.

Price in Hong Kong: HK\$132

Price overseas: US\$24 (including surface postage)

An additional bank charge of **HK\$50** or **US\$6.50** is required per cheque made in currencies other than Hong Kong dollars.

Cheques, bank drafts or money orders
must be made payable to **HONG KONG GOVERNMENT**

FOREWORD

This Report was prepared by Dr M.G. Anderson of the Department of Geography, University of Bristol, England as his final report on the project carried out under PWD Agreement CE 3/81. The project was begun in July 1982 and completed in September 1983.

A number of Geotechnical Control Office staff made significant contributions to the work reported here. In particular, Mr J.M. Shen made valuable contributions to many areas of the project. Mr W.C. Kwan carried out the chunam mix study, and Mr C.K. Chan undertook the chunam permeability study, facilities and support being provided by the Public Works Central Laboratory.

Dr P.E. Kneale assisted in selected bibliographic searches. Report typing and preparation of the majority of the figures were undertaken by the Geotechnical Control Office. Selected figures and plates 2.1 & 2.2 were prepared by the Department of Geography, University of Bristol.

Assistance in the establishment of the field site at Clearwater Bay Road was provided by the Highways Office.

A handwritten signature in black ink, appearing to read 'E.W. Brand', with a stylized, cursive script.

E.W. Brand
Principal Government Geotechnical Engineer

CONTENTS

	<u>Page No.</u>
Foreword	1
Glossary	6
List of Tables	7
List of Figures	9
List of Plates	16
1. INTRODUCTION	17
1.1 Background to the project requirements	17
1.2 Objectives and scope	18
2. SOIL SUCTION INSTRUMENTATION REVIEW	20
2.1 Introduction	20
2.2 Manual tensiometer systems for recording soil water potentials	21
2.2.1 "Jetfill" tensiometers	21
2.2.2 "Quick Draw" tensiometers	21
2.3 Automatic tensiometer systems for recording soil water potentials	21
2.3.1 Scanivalve based unit for soil water potential monitoring	21
2.3.2 Institute of Hydrology, U.K., pressure transducer tensiometer system	23
2.4 Response times of tensiometer systems	24
2.5 Thermal conductivity sensors	24
2.6 Discussion	25
3. MODELLING SOIL WATER CONDITIONS	26
3.1 Background to modelling approaches	26
3.1.1 Soil moisture deficit approaches	26
3.1.2 Soil water finite difference models	28
3.2 Outline of the models used in this study	30
3.2.1 Basic model structure	30
3.2.2 Procedures for the estimation of unsaturated permeability	31

	<u>Page No.</u>
3.2.3 Evaporation estimation	33
3.2.4 Modelling perched water tables	34
3.2.5 One and two dimensional models	36
3.2.6 Summary of input variables to the soil water model	37
4. DATA ACQUISITION	39
4.1 Data requirements	39
4.2 Chunam soil water characteristics	39
4.2.1 Chunam suction-moisture curves	39
4.2.2 Permeability determinations of chunam	40
4.2.3 Relationship of chunam mix to permeability	42
4.3 Soil suction comparisons on a chunam and grass slope	46
4.3.1 Site details and instrumentation	46
4.3.2 Soil suction response to storms	47
4.3.3 The prediction of soil suction response	47
4.3.4 Direction of soil water movement and implications for modelling	49
4.4 The effect of backslope topography on soil suctions	50
4.4.1 Site description and instrumentation	51
4.4.2 Backslope soil water conditions	52
4.5 Vegetation - runoff relationships	54
4.5.1 Background to data requirements	54
4.5.2 Available runoff/vegetation data	54
4.5.3 Runoff plot requirement	55
5. GENERAL APPLICATIONS OF SOIL CHARACTERISTIC CURVES AND RELATED DATA	57
5.1 Initial application of suction-moisture curves	57
5.1.1 Determination of 'a' and 'b' coefficients	57
5.1.2 Utilisation of suction moisture curves to estimate water table rise	58
5.1.3 Modification of the existing criteria for the issue of a landslip warning	60
5.1.4 Summary of principal applications of suction-moisture curves	62

	<u>Page No.</u>
5.2 Predicting the effects of cracks in chunam	63
5.2.1 Establishment of a model to predict flow through chunam cracks	63
5.2.2 Application of the model of effective chunam permeability to field conditions	66
5.2.3 Summary of modelling crack effects in chunam	67
6. APPLICATIONS OF MODELLING CAPABILITY	68
6.1 One dimensional vertical infiltration model	68
6.1.1 Validation of vertical infiltration model	68
6.1.2 Summary of infiltration model verification	70
6.1.3 Predictions of soil water conditions in decomposed volcanics	70
6.1.4 Predictions of chunam 'effectiveness' using the vertical infiltration model	72
6.1.5 Modelling surface cover effects - vegetation	73
6.2 Validation of two dimensional soil water model	76
6.2.1 Application of two dimensional soil water model to Tai Po, St. Christopher Bend site	76
6.3 Discussion of modelling utility for design purposes	78
6.3.1 Choices of available models to make predictions of soil suctions	78
6.3.2 Summary of circumstances in which soil water conditions can be accurately estimated for design purposes	79
7. CONCLUSIONS AND RECOMMENDATIONS	80
7.1 Design conclusions	80
7.1.1 Cover	80
7.1.2 Materials	81
7.1.3 Prediction of soil water conditions	82
7.1.4 Instrumentation for soil suction	83
7.2 RECOMMENDATIONS FOR FURTHER WORK	83
8. REFERENCES	85
TABLES	93
FIGURES	121
PLATES	230
APPENDIX A	239

Glossary

a	'intercept' in the log-log regression of suction moisture curve (see equation 3.22)
b	gradient in the log-log regression of suction-moisture curve (see equation 3.22)
q	flux $m^{-2}s^{-1}$
B	crack width of chunam per metre m
B ₁	effective crack width of chunam per metre m
B _∞	effective crack width of chunam per metre at depth m
H	head m
I	hydraulic gradient
I _T	throughfall rain intensity ms^{-1}
K	permeability ms^{-1}
K _e	effective permeability ms^{-1} (see equation 5.14)
K _i	permeability of intact chunam ms^{-1}
K _s	saturated permeability ms^{-1}
K(θ)	permeability at moisture content θ ms^{-1}
θ	volumetric water content m^3m^{-3}
θ _s	volumetric water content at saturation m^3m^{-3}
ψ	soil suction kPa
ψ _e	soil suction at air entry ('bubbling pressure') kPa

List of Tables

<u>Table</u> <u>No.</u>		<u>Page No.</u>
1.1	Summary of selected reports relating to soil suction research in Hong Kong	93
1.2	Principal tensiometer sites in Hong Kong up to 1982	94
1.3	Soil suction study - research design	95
2.1	Selected examples of reports detailing tensiometer and thermal conductivity systems	96
2.2	Response times of tensiometer - transducer systems	97
3.1	Selected soil water finite difference models	98
3.2	Summary of model equations	99
3.3	Input variables to soil water model	100
4.1	Permeability of chunam from field samples	101
4.2	Trial mixes for laboratory reconstituted chunam samples of Tai Po decomposed volcanics and King's Park decomposed granite	102
4.3	Trial mixes for laboratory reconstituted chunam samples of Clear Water Bay Road decomposed granite	103
4.4	Variation of area shrinkage with age for chunam of Tai Po decomposed volcanics	104
4.5	Variation of area shrinkage with age for chunam of King's Park decomposed granite	105
4.6	Variation of area shrinkage with age for chunam of Clear Water Bay Road decomposed granite .	106
4.7	Permeability of trial mix chunam samples	107
4.8	Instrumentation details for Tai Po St. Christopher Bend site	108
4.9	Selected studies relating to vegetation and runoff production	109
4.10	Characteristics of grass species commonly used in Hong Kong	110

		<u>Page No.</u>
5.1	Illustrative relationships of crack geometry	111
5.2	Predicted permeability of cracks from equation 5.11	112
5.3	Slope locations for chunam crack survey	113
5.4	Summary of chunam crack survey	114
5.5	Summary of crack seepage and effective chunam permeability	115
6.1	Sites selected for 1 dimensional model verification	116
6.2	Statistical estimates of extreme rainfalls	117
6.3	Summary of infiltration and runoff for the simulations undertaken in Figure 6.9	118
6.4	Summary of principal data accuracy required for finite difference models	119
6.5	Acceptable circumstances for establishing soil suction conditions for design purposes.	120

List of Figures

<u>Figure</u>		<u>Page No.</u>
<u>No.</u>		
1.1	Selected measurements of lowest recorded suctions in colluvium	121
1.2	Selected measurements of lowest recorded suctions in decomposed granite	122
1.3	Selected measurements of lowest recorded suctions in decomposed volcanics	123
1.4	Selected measurements of lowest recorded suctions in slopes protected by chunam	124
1.5	Illustration of the procedure for the soil suction prediction model outlined by McFarlane (1981)	125
1.6	Water content and suction changes in the saturated and unsaturated zones	126
1.7	Principal field sites used in the research programme	127
2.1	Installation procedures for "Jetfill" tensiometers in uniform soils. Method (A) for depths to 1.5 m, method (B) for depths greater than 1.5 m	128
2.2	8 mm ceramic cup tensiometer (2100 series - Soil-Moisture Equipment Corporation) with flexible tube.	129
2.3	"Quick Draw" tensiometer (Soil-Moisture Equipment Corporation)	130
2.4	Response times of "Quick Draw" tensiometer (after Sweeney 1982)	131
2.5	Tensiometer design for use with automatic scanivalve system (after Anderson and Burt, 1977)	132
2.6	Institute of Hydrology pressure transducer tensiometer system	133
2.7	Measuring circuit for temperature - compensated matric potential sensor (after Phene, Hoffman and Austin, 1973)	134

<u>Figure</u>		<u>Page No.</u>
<u>No.</u>		
2.8	Mean voltage readout of the MCS 600 sensor with suction (from MCS 600 System User's Manual)	135
2.9	Response time of the MCS 600 sensor in laboratory testing using a glacial till (after Lee, 1983)	136
3.1	Illustration of the SMD concept (after Leach and Herbert, 1982)	137
3.2	Diagrammatic representation of (a) 1 dimensional and (b) 2 dimensional soil water models.	138
3.3	Diagrammatic representation of 3 dimensional 'SHE' model structure	139
3.4	Governing equations used in soil water model (note evaporation and base conditions may be varied)	140
3.5	Basic one dimensional soil water model structure	141
3.6	Illustrations of two types of instability in soil water modelling	142
3.7	Estimation of unsaturated permeability using the M-Q method, compared with that of Marshall and experimental methods	143
3.8	Sine based evaporation concept	144
3.9	Concept for evaporation model (after Ballick et al, 1981)	145
3.10	Four methods for considering pore pressures induced by perched water table	146
3.11	Solutions to equation 3.28	147
3.12	Selected solutions to equation 3.29	148
3.13	Illustration of one and two dimensional models used in this study	149
3.14	Suggested strategy for the incorporation of field variability into the modelling framework	150
3.15	Flow diagram for top computational point of soil water model	151
3.16	Flow diagram illustrating overall model approach (also see figure 3.15)	152

Figure

<u>No.</u>		<u>Page No.</u>
4.1	Suction moisture curves for volcanic chunam	153
4.2	Suction moisture curves for granitic chunam	154
4.3	Suction moisture curve for granitic chunam	155
4.4	Ponding and burette methods used to determine the permeability of chunam .	156
4.5 a	Particle size distributions for soils used in chunam mixes	157
4.5 b	Controls on the shrinkage and permeability of chunam	158
4.6	Site plan of the chunam slope, Clear Water Bay Road (see figure 1.7)	159
4.7	Site plan of the grass slope, Clear Water Bay Road (see figure 1.7)	160
4.8	Tensiometer locations at the Clear Water Bay Road Site (see figure 4.6 and 4.7)	161
4.9	Resistance envelopes for the grass and chunam slopes at Clear Water Bay Road	162
4.10	Soil suctions on chunam slope relating to the storm of 6 May 1983	163
4.11	Soil suctions on grass slope relating to the storm of 6 May 1983	164
4.12	Soil suctions on chunam slope relating to the storm of 26-28 May 1983	165
4.13	Soil suctions on grass slope relating to the storm of 26-28 May 1983	166
4.14	Soil suctions on chunam slope relating to the storm of 17 June 1983	167
4.15	Soil suctions on grass slope relating to the storm of 17 June 1983	168
4.16	Summary of principal soil water conditions on the chunam and grass slope	169
4.17	Significance of differences between lowest storm suctions at 3 m depth on chunam and grass slopes using discriminant analysis	170

Figure

No.

Page No.

4.18	Significance of differences between lowest storm suctions at 4 m depth on chunam and grass slopes using discriminant analysis	171
4.19	Plot of equations 4.6 and 4.7	172
4.20	Plot of equations 4.8 and 4.9	173
4.21	Summary of prediction procedure for estimating both lowest storm suction and subsequent suction recovery	174
4.22	Plot of equations 4.10 and 4.11	175
4.23	Comparison of observed and predicted suctions during recovery on chunam slope (3 m depth)	176
4.24	Comparison of observed and predicted suctions during recovery on grass slope (3 m depth)	177
4.25	Hydraulic gradients at top slope location A (see figure 4.6) on chunam slope for selected storms	178
4.26	Directions of near surface soil water movement at the Clear Water Bay Road Site (see figure 4.6 and 4.7)	179
4.27	Suction-moisture curves for the CDG on the chunam slope at Clear Water Bay Road (see figure 4.6)	180
4.28	Suction-mositure curves for the CDG on the grass slope at Clear Water Bay Road (see figure 4.7)	181
4.29	Tai Po, St. Christopher Bend, Study site (see figure 1.7)	182
4.30	Typical piezometer responses. P1 and P3 are at the same elevation (109.3 mPD)	183
4.31	Instrumentation plan, showing tensiometer, piezometer and horizontal drain locations	184
4.32	Storm of July 11-14 1980 with the associated soil water conditions on July 12 and July 16 1980 at 1.5 m depth	185
4.33	Storm of August 5-9 1980 with the associated soil water condition on August 5 and August 8 1980 at 1.5 m depth	186

Figure

No.

Page No.

4.34	Orthogonals to total potential lines for July 12 1980 illustrating soil water convergence at 1.5 m depth	187
4.35	Discharge from three horizontal drains in July 1980 - note the relatively higher discharge from drain A located at the focus of the backslope topography	188
4.36	Predicted response of soil suction to slope plan curvature (positive concave) by (a) permeability group and (b) storm size. (after Anderson, 1982)	189
4.37	Relationship of failed and 'stable' cut slopes to unconfined strength, slope plan curvature and slope angle for three permeability groups. (after Anderson, 1983)	190
4.38	Variation of runoff with rainfall. (after Hsu et al, 1983)	191
4.39	Summary of runoff production on chunam and grass slopes (after Hsu et al, 1983)	192
5.1	Selected soils plotted on 'a' and 'b' coefficients (see equation 3.22)	193
5.2	Plot of equation 5.2 used to predict the effect of a protective cover	194
5.3	Definition diagrams for equations 5.3-5.6	195
5.4	Water table response in selected soils as predicted by equation 5.6. Soil depth 10 m	196
5.5	Water table response in selected soils as predicted by equation 5.6. Soil depth 20 m	197
5.6	Current procedure (1983) for the issue of a landslide warning	198
5.7	Illustration of a suggested method for improving the current (1983) landslide warning procedure	199
5.8	Plots of the two hypothetical storms in figure 5.7 on the current (1983) landslide warning relationships	200

Figure

No.

Page No.

5.9	Examples of past storm suction recovery	201
5.10	Definition diagram for crack model - see equations 5.7-5.9	202
5.11	Seepage predicted by the crack model under the conditions specified	203
5.12	Effective permeability of chunam predicted by the crack model	204
5.13	Alternative approaches to the estimation of K_e in terms of regular and irregular crack spacing.	205
5.14	Predicted effective chunam protection	206
5.15	Illustration of rainfall intensities in relation to permeability values.	207
6.1	Suction moisture curves used in soil water simulations at locations 1-3	208
6.2	Simulations of soil water conditions at Realty Ridge	209
6.3	Simulation of soil water conditions at Chater Ridge using 1 dimensional soil water model (section 3.0)	210
6.4	Suctions reported by Sweeney (1982) for a site in Mid-Levels	211
6.5	Simulation of soil water conditions based upon the site reported by Sweeney (1982)	212
6.6	Simulation of soil suctions at Clear Water Bay site, chunam slope, location C (see figures 4.6 and 4.14)	213
6.7	Simulation of soil suctions and Clear Water Bay site, grass slope, location I (see figure 4.7 and 4.15)	214
6.8	Simulation of soil water conditions at Tai Po, St. Christopher Bend site (see figure 4.31)	215
6.9	Simulation of soil water conditions resulting from even intensity rainstorms as shown	216
6.10	Sensitivity of resulting soil suctions to changes in rainfall distribution within a 24 hour storm (see figure 6.9)	217

Figure

No.

Page No.

6.11	Sensitivity of resulting minimum suctions to permeability changes with regard to the 24 hour storm shown in figure 6.9	218
6.12	Simulation of soil water conditions with chunam cover. Lowest suctions shown	219
6.13	Simulation of soil water conditions with chunam cover. Lowest suctions shown	220
6.14	Predicted effectiveness of chunam using crack model coupled to soil water model	221
6.15	Two simplified conditions of the production of runoff (b and c)	222
6.16	Input parameters used in soil water model to illustrate vegetation - runoff relationships (see figures 6.17 and 6.18)	223
6.17	Infiltration, as a percentage of storm rainfall, shown for selected values of K_1	224
6.18	Infiltration, as a percentage of storm rainfall, shown for selected values of K_1	225
6.19	Summary of implications of initial vegetation runoff generation models shown in figure 6.15	226
6.20	Hypothetical relationships which may emerge from runoff plots and soil water simulations	227
6.21	Two dimensional simulation of soil water conditions at Tai Po, St. Christopher Bend site (see figure 4.31)	228
6.22	Summary of selected permeability determinations made in Hong Kong.	229

List of Plates

<u>Plate</u>		<u>Page No.</u>
<u>No.</u>		
2.1	Prototype tensiometer - scanivalve system (after Anderson and Burt, 1977)	230
2.2	Redesigned tensiometer - scanivalve system employing microprocessor control unit (after Anderson and Kneale, 1980 a)	231
4.1	Chunam slope instrumented as shown in figure 4.6.	232
4.2	Grass slope instrumented as shown in figure 4.7.	232
4.3	Jetfill tensiometers installed at location C on chunam slope (see figure 4.6).	233
4.4	Raingauge location on chunam slope (see figure 4.6).	233
4.5	Tai Po, St. Christopher Bend site	234
5.1	Crack survey - slope 89 - see table 5.3	235
5.2	Crack survey - slope 98A - see table 5.3	235
5.3	Crack survey - slope 99 - see table 5.3	236
5.4	Crack survey - slope 102 - see table 5.3	236
5.5	Crack survey - slope 106 - see table 5.3	237
5.6	Crack survey - slope 112 - see table 5.3	237
5.7	Crack survey - slope 113 - see table 5.3	238
5.8	Crack survey - slope 114 - see table 5.3	238

1. INTRODUCTION

1.1 BACKGROUND TO THE PROJECT REQUIREMENTS

Research into elements of soil suction has been undertaken in Hong Kong since 1978. Commencing with a research programme into measurement methods (PWD report number 8, 1979), the work expanded to research into laboratory methods and to a field programme of suction instrumentation. In the former case the accuracy of water retention curve estimation was a major element, whilst the field programme sought to establish suction levels in different materials and under different types of cover (chunam and grass). Table 1.1 summarises the main reports relating to this research, together with selected findings. Table 1.2 summarises the principal tensiometer sites established by the G.C.O. up to 1982. It is evident therefore, that there is a substantial amount of available information in the following general fields :

- (i) laboratory experience for suction-moisture determination and associated accuracies of different methods.
- (ii) variability of suction-moisture curves in both natural and remoulded materials.
- (iii) field experience in soil suction monitoring, together with reliability, accuracy and installation procedures of different systems (see for example G.C.O. 1981).

Figures 1.1-1.4 illustrate summary findings from certain of the tensiometer installations reported in table 1.2.

For both colluvium and decomposed granite (DG) there is significant field evidence to suggest that suction is lost even during relatively dry years. A possible exception is the site reported by Sweeney (1982), although more continuous data is perhaps required here before this site can be assessed fully.

By contrast figures 1.3 and 1.4 suggest that there is the possibility of maintained suctions within the decomposed volcanics at depth (figure 1.3) and under chunam.

Compared with field monitoring based inference, the predictive capability for soil suction is somewhat more limited. McFarlane in PWD (1981) established a statistical scheme for suction prediction.

This is summarised in figure 1.5. This scheme involves the relocation of soil suction response to storm rainfall, on an arbitrarily established rainfall axis, as shown in the figure. This repositioning of rainfall response is shown in figure 1.5(c). The resulting curve defines the suction change with rainfall. Therefore initial suction and total rainfall can be used to determine the minimum suction resulting from a rainfall event. Whilst selected families of exponentially based curves can be established this way, such a method does not allow for positive pressures to be established. From the physical processes of soil water redistribution in the unsaturated zone, and the continuity between the unsaturated and saturated soil water phases (figure 1.6) the method outlined in figure 1.5 cannot be viewed as particularly satisfactory.

This limited predictive capability must be seen against the background of both available data and current requirements to predict suction. It is possible to isolate significant areas in the pre-existing soil suction programme which now become necessary, and indeed possible, to address more firmly :

- (a) No existing information on chunam permeability or soil water retention characteristics.
- (b) No comprehensive field study of suction/pore pressure responses under different covers. (Selected single point observations on slopes are available as outlined in table 1.2).
- (c) No application of soil water finite difference models to predict soil suction/pore water pressure. (Leach and Herbert (1982) outline a finite difference model that relates to ground water response on the Mid-Levels).
- (d) No information on runoff characteristics of different vegetation types which is a necessary pre-requisite for enhancing predictive capabilities of soil suction by methods such as those outlined in (c).

It is these elements above that allow the establishment of a comprehensive research programme, aimed to meet objectives arising out of current needs.

1.2 OBJECTIVES AND SCOPE

Given the available work undertaken in Hong Kong with regard to soil suction research reported in 1.1, the following objectives were established for the current project :

- (a) To determine the effect of different surface coverings upon the soil suction regime of the underlying slopes.
- (b) To evaluate the relative importance of slope material and topography in controlling suction.
- (c) To examine and develop a prediction model for soil suction appropriate to objectives (a) and (b).
- (d) To review current soil suction instrumentation capabilities and assess the need for further development in the context of requirements for Hong Kong.

These research objectives demanded that a decision be made at the onset of the programme, as to the optimum way of progressing within the available time and resources of the project.

A substantial field programme of monitoring could have been proposed, with site selection being based upon essentially a priori criteria and judgements, in regard of that site selection which would be most likely to enunciate the principal controls on soil suction as required to meet the above objectives.

A second element of uncertainty is introduced by such a strategy, and that relates to the question of recurrence interval between rainstorm events and

design. An entirely empirical proposal obviously has no control on the range of precipitation data to be experienced, and hence on the eventual scope of the outcome in terms of general applicability of the findings.

An experimental design was thus selected which sought to maximise the potential inference in regard to the objectives, but which simultaneously demanded field resources that could be met within the available resources. In this regard it was felt that a simulation model requiring only parameterisation and no calibration from historical suction data was an appropriate methodology by which to meet the long term (say 1 in 10 or 1 in 100 year) design demands. The implication of such a scheme is the requirement for a limited amount of input data e.g. suction-moisture curves, some of which were already available for Hong Kong materials (tables 1.1 and 1.2), but others of which (such as chunam properties) would need to be determined. This strategy, it is contended, would serve the dual role of completing certain important base line material property research in Hong Kong, whilst simultaneously facilitating more far-reaching design conclusions to be established, than would be feasible if a purely empirical monitoring exercise were to be undertaken.

Table 1.3 shows the structure of the research design that was established for this project on the basis of the above review. The empirical work included thus sought to be both free standing (in allowing selected empirically based conclusions to be drawn) and to be a constituent element in the predictive capability.

2. SOIL SUCTION INSTRUMENTATION REVIEW

2.1 INTRODUCTION

Soil suction instrumentation can be divided into two types according to the methodology of the monitoring system: tensiometric methods which are suitable for recording suctions up to approximately 80-90 kPa, and thermal conductivity sensors which are capable of providing estimates of soil suction up to 1 500 kPa. Both systems may be of a manual reading type or automatic.

These groups of systems will be reviewed from the standpoint of their appropriateness to Hong Kong conditions and requirements, and to determine whether as a result of that review, there is need in Hong Kong to develop further instrumentation for soil suction monitoring.

Table 2.1 presents a selected list of installations and reviews that have recently been undertaken in this field. The methodology of the two systems has been much researched.

A tensiometer measures soil suction by obtaining equilibrium across a high air entry porous medium between the soil suction and a confined reservoir of water within the tensiometer system. As soluble salts are free to pass through the porous medium, the osmotic component of suction is eliminated and the tensiometer measures only the matric component of suction. A useful treatment of the components of suction is given by Krahn and Fredlund (1972). At a temperature of 20°C at sea level water boils or cavitates at a pressure of about 97 centibars, i.e. at approximately 1 atmosphere (or bar) of pressure below atmospheric pressure. This places an upper limit on the tensiometer range for measuring matric suction as the water in the tensiometer system cavitates as 1 bar of suction is approached. For sites at significant elevations above sea level, the range of the tensiometer is further reduced. It is of interest to note that fine grained soils can contain water at matric suctions of much greater than 1 bar without cavitation of the water. Apparently this is because water in the very fine pores of the soil takes on a molecular structure that can sustain very high tensions or suctions (Croney and Coleman, 1952). A further problem is that even though the tensiometer is filled with de-aired water, air in solution in the soil water diffuses through the high air entry medium during the equalisation process. This air starts to come out of solution at about 85 centibars suction at sea level and can reduce the accuracy of soil suction measurements. This figure is reduced by approximately 3.5 centibars for every 300 m increase in elevation.

Significant research on the heat dissipated sensor was undertaken in 1939 by Shaw and Baver. They concluded that heat conductivity of a soil gives a reliable index of the moisture content of the soil, and that changes in the salt concentration of the pore fluid did not materially affect the heat conductivity of the soil. Subsequent research sought to overcome certain of the problems encountered using the thermistor and electrothermal methods of combining the heating element and temperature indicator. Analytical and design research undertaken by Phene, Hoffman and Rawlins (1971) resulted in the development of a sensor manufactured by Moisture Control System Corporation, known as the MCS 6000 sensor. A similar instrument was built by Watertech of Australia and is reported in Department of Main Roads, N.S.W. Australia, Laboratory Report IR11, 1977. Both MCS Corporation and Watertech are no longer trading and such equipment is no longer commercially available.

2.2 MANUAL TENSIO METER SYSTEMS FOR RECORDING SOIL WATER POTENTIALS

2.2.1 'Jetfill' tensiometers

Jetfill tensiometers have been available from Soil Moisture Corporation for several years, and have proved to be robust and accurate for the measurement of soil suction in Hong Kong and elsewhere. G.C.O. (1980) details the mode of operation and specification of these units, and McFarlane (1981) has discussed installation procedures (Figure 2.1).

There is no other commercial unit available, as far as the author is aware, that is equivalent, nor are there any improvements that can be made for the purpose for which the jetfill tensiometers are designed. A smaller unit (2100 series - Figure 2.2) is available with a ceramic cup approximately 8 mm diameter (see Ingersoll 1981).

2.2.2 'Quick Draw' tensiometers

The 'Quick Draw' tensiometer (Figure 2.3) is an adaptation of the jetfill tensiometer, designed to give very rapid response times, and is intended for portable use. The principal restriction is the available probe depth - a maximum of approximately 0.5 m. Notwithstanding this limitation, response times are very rapid. Figure 2.4 illustrates results given by Sweeney (1982) in an application in Hong Kong. Similar results have been obtained by the author in both the Caribbean and U.K.

As can be seen from Figure 2.3, the high air entry ceramic tip is connected to a vacuum dial gauge by means of a very small bore capillary tube, which runs inside the tensiometer rod. As Sweeney (1982) observes, the internal water volume of the unit is very small, so that the detrimental effect of the large thermal expansion and contraction of water is reduced to an insignificant level. This allows soil suction measurements to be made quickly and accurately, even when the temperature of the tensiometer is greatly different from that of the soil.

2.3 AUTOMATIC TENSIO METER SYSTEMS FOR RECORDING SOIL WATER POTENTIALS

2.3.1 Scanivalve based unit for soil water potential monitoring

Transducer-tensiometer systems for the measurement of soil water potentials in both natural and artificial slopes have been reported in the literature (Table 2.1). Burt (1978) describes such a system in detail with a single transducer serving 22 tensiometers through a Scanivalve fluid switch. Plate 2.1 illustrates a prototype system used for a 3-year field research programme. A number of successful field applications of such instrumentation have now been reported (G.C.O., 1980, and Anderson and Burt, 1977, for example) and there is therefore no need here to outline the system in full. However, in all reported applications of such systems the transducer outputs to a chart recorder. To obtain the necessary accuracy of soil water potentials for all 22 tensiometers, a chart speed of $1-2 \text{ mm min}^{-1}$ is required. Where the interest is to examine detailed potential variation over storms with durations of several hours, and to monitor the subsequent drainage process, this can be extremely consumptive of power if the chart recorder is rated at 0.3 Amp hr. under continuous operation (the JJ Educational Measurement

CR 552B recorder, for example, has a current consumption in this range). High current consumption from 12 volt cells at remote field sites, combined with a demand for continuous data and perhaps infrequent field site visits, renders such a chart recorder based system to be of extremely limited utility.

With such demands as these in terms of data and site visits, it was seen as highly desirable to have developed and tested a unit which could effectively replace the chart recorder element in the transducer-tensiometer system. Plate 2. illustrates the unit that was constructed and subjected to U.K. field trials. Two enclosures are visible, together with a 12 volt rechargeable cell. The Scanivalve enclosure on the right comprises the bulkhead fittings taking the hydraulic lines from the tensiometers elsewhere on the hillslope to the Scanivalve switch mounted centrally in that enclosure. The 'reading line' from the Scanivalve, kept as short as possible to maintain high accuracy, is shown connected to the transducer. The essential elements of this enclosure are identical to the Scanivalve system described by Burt (1978). The output from the transducer passes to the electronic enclosure housing the microprocessor unit and thermal printer.

It is this enclosure that replaces the former chart recorder, and represents the principal innovative element in the system. Here solid state electronics with microprocessor and associated memory banks have been incorporated. All components are mounted on printed circuit board and use CMOS integrated circuit technology. The system has been designed to economise on power consumption and enable a wide variety of functions to be performed. Numerical Decode Switches are used to preset (i) the number of tensiometers required to be read (maximum 22), (ii) the time (minutes) each tensiometer is connected by the Scanivalve to the transducer (the dwell time), (iii) the interval time (hours) between each complete cycle of readings, and (iv) the real time. When the real time is entered into the unit the quartz clock is activated thus providing an accurate time base for all subsequent automatic operations. The current consumption of the electronic unit represents a major advance over conventional chart recorder based systems. In continuous operation a total power consumption of approximately 50 milliamps can be expected, and when shut down, the drain on the battery is approximately 20 milliamps.

Two references can be included within the cycle of readings. The first is open to atmosphere, and the second can be connected to a pressure reference equivalent to the full-scale range of the transducer. In this way, the calibration of the transducer is automatically checked in each sequence of readings. Each time the transducer is connected to the zero reference, a reading is obtained and stored in the microprocessor. This stored reading is then subtracted from all subsequent readings. In this manner, an auto-zeroing facility has been incorporated. The print-out indicates on a single line the day number, real time, station number and water pressure or suction in the range -9.99 m to +9.99 m. For pressures or suctions outside this range, the units digit and two decimal places remain the only ones recorded. For practical purposes this is hardly restrictive since for a given elevation potential position the soil water potential would have to be capable of changes in excess of approximately one atmosphere between readings for any confusion to be possible. The thermal dot matrix printer thus has a maximum capacity of 18 characters per line, and print out is on heat sensitive paper 57 mm wide with the automatic winding of printed paper incorporated. For each station dwell time, three readings are printed at equally spaced intervals during that time. In this way, it is possible to detect drift which may be indicative of air in a tensiometer line. Thus this diagnostic capability

renders the printer system almost as good as a conventional chart recorder in this regard; in all other respects the microprocessor unit is clearly superior. The printer unit can, of course, be replaced by a tape output device and, with the appropriate modem, the output can be transmitted on a telephone line.

Whilst the sealed 12 volt rechargeable lead-acid accumulator should power the system on continuous operation for a period of approximately four weeks, in the event of the battery discharging to the point at which erroneous readings are likely, 'Battery Low' is displayed on the printer and the complete system is immediately shut down.

The principal specifications of the system are as follows:

Transducer : Range -100 to +200 kPa (enabling the system to monitor positive and negative pore water pressures)

Stiffness $3 \times 10^{-9} \text{ m}^5 \text{ kN}^{-1}$

Tubing : Stiffness $0.5 \times 10^{-9} \text{ m}^5 \text{ kN}^{-1}$
(see G.C.O. 1980)

Scanivalve : Drive = WSS - 24

Wafer = W06022/1P - 24T

Response times : dependent upon transducer and tubing stiffness but Table 2.2 summarises a selection of such systems showing response times to be generally of the order of 60 seconds.

The transducer design which the author assembled at Bristol, U.K., and which was adopted for the Mid-Levels study (G.C.O. 1980) is shown in Figure 2.5. The tensiometers consist of a 22 mm external diameter, one bar air entry porous ceramic cup glued to a cylindrical perspex body of a similar diameter. The manufacturers quoted transmission rate of water through the cup wall is $5.3 \text{ ml hr}^{-1} \text{ cm}^{-2}$ per 100 kPa of pressure difference across the cup wall. A rubber bung through which a longer reading line and a shorter de-airing return line pass, forms a seal at the upper end. The two lines are made from twin polythene covered nylon tubing 2.7 mm I.D. and 4.7 mm O.D. The de-airing line can either be terminated at the soil surface above the tensiometer, or returned to a centrally located de-airing board housed with the scanivalve and electronic enclosure.

2.3.2 Institute of Hydrology U.K. pressure transducer tensiometer system

Announced in November 1982 by the Institute of Hydrology, is a pressure transducer tensiometer (PTT) system, manufactured under licence by Geotechnical Instruments.

This unit differs from the system reported in 2.3.1 above, only in that each ceramic cup has its own transducer. Whilst this dispenses with the need

for a Scanivalve fluid switch system, the configuration is significantly more expensive, since it requires one transducer per ceramic cup.

Three variants have been developed: basic non-purgeable, purgeable and borehole. The resolution of soil suction measurement claimed by the manufacturers is 0.1 kPa.

The non-purgeable PTT is simply a standard 50 mm x 25 mm porous pot, cemented to a collar which mates via an O-ring seal to a pressure transducer. The porous pot is filled with de-aerated water before installation and must be removed from the soil periodically for refilling.

The purgeable PTT employs the same type of porous pot and transducer but is also fitted with purging tubes and valves. Figure 2.6 illustrates the purgeable unit.

The borehole PTT uses the non-purgeable units with the porous cup shrouded and potted with plaster of paris into an open-sided mounting.

2.4 RESPONSE TIMES OF TENSIO-METER SYSTEMS

Response time information is critical to the employment of transducer tensiometer systems. Notwithstanding this obvious requirement to maximise the full potential of such systems in terms of tensiometer reading frequency using automatic systems, there is only a restricted number of studies that have examined field response times. Table 2.2 summarises certain of the information available. In general, response times are of the order of 60 seconds, and in consequence a 3 minute connection time to each tensiometer on a fully automatic system may be considered appropriate. Anderson and Kneale (1980) showed that recovery to 99% of the equilibrium value could be achieved for step changes of 10 kPa within 120 seconds, with tensiometers installed in Oxford Clay. The use of tubing as specified in G.C.O. (1980) for the tensiometer connections to the Scanivalve enclosure, a very short (30 cm or less) 'reading' line from the Scanivalve to the transducer, and pre-installation pressure testing of all the components and fittings, are the principal design guides which will ensure response times are of the order of 1-2 minutes.

2.5 THERMAL CONDUCTIVITY SENSORS

The rate of heat dissipation in a porous material of low heat conductivity is sensitive to water content, therefore the water content of a porous material can be measured by supplying a heat source at a point centred within this material, and by measuring the temperature rise at that point. Figure 2.7 shows the basic circuit design for the MCS equipment - the sensor is used as a heating element and a temperature measuring device. Thus the sensor consists of a diode which is surrounded by a heating coil and embedded in a porous medium. In a complete study of the MCS 6000 sensor Lee (1983) reports the following principal findings. Firstly, the sensitivity in the range 0-100 kPa is ± 6 kPa. Above 200 kPa the results from the sensor must be very much open to question - see Figure 2.8. However a principal constraint on its use is the time required for the sensor to give a stable reading. On the desorption cycle, that time increases with a

decrease in the water content. Whilst for the absorption cycles, the response time exhibits a greater degree of non-linearity. Figure 2.9 shows that in either case response times are of the order of 160 hours, illustrating the severe constraints on such systems (see Table 2.2) for transient soil water conditions of interest in Hong Kong materials.

The available reports on the Watertech system, being similar to the MCS 6000, are rather imprecise. The Department of Main Roads, N.S.W. Australia (1977) report the principal problems to relate to equipment malfunction - they make no report of response times or accuracy.

2.6 DISCUSSION

For the purpose of measuring soil suctions in the range 0-80 kPa in Hong Kong, it is clear that the field evidence of both installation procedures and response times as regards manual tensiometer systems, has shown the Jetfill tensiometer to be appropriate for most requirements. The use of automatic tensiometer systems in Hong Kong should take the form of the system described in 2.3.1 with the tensiometers shown in Figure 2.5. The output device should be either an electrosensitive printer or cartridge data logger. Thermal printers have shown too great a level of long term unreliability to be considered suitable.

The thermal conductivity sensors have too great a response time to be considered for most applications in Hong Kong. However, if suctions in the range 80-200 kPa were required to be determined, such a system, despite the restrictions noted in 2.5 above, is the only available system.

Considering the commercially available tensiometric systems reviewed above, together with the tensiometer design shown in Figure 2.5, there is no justification for any instrumentation development specific to Hong Kong soil suction monitoring needs. The response times and installation procedures for the systems reported in 2.2 and 2.3 are known and established, and meet current practice needs.

3. MODELLING SOIL WATER CONDITIONS

3.1 BACKGROUND TO MODELLING APPROACHES

3.1.1 Soil Moisture Deficit Approaches

Soil moisture deficit is a widely used concept in the context of hydrological modelling. The concept has received much attention specifically in the context of aquifer recharge modelling, as well as in terms of agricultural applications. In both these regards recharge of soil water for a specific time interval may be stated as:

$$R_f = E_a + R_o + \Delta S \quad (3.1)$$

where R_f = rainfall
 E_a = actual evapotranspiration
 R_o = runoff
 ΔS = change in soil moisture deficit

or as

$$\Delta S = R_f - R_o - E_a$$

Of course, there is some difficulty in the actual calculation of recharge using equation. There is difficulty in knowing exactly how to measure and evaluate actual evapotranspiration. In addition, the recharge process is dependent on flow in the unsaturated zone which is subject to hysteresis. This aspect will be treated in more detail in the following section ; it is sufficient at this stage to note certain approximations inherent in the SMD approach. Leach and Herbert (1982) note Rushton et al's (1979) application of equation 3.1 in which they suggest that some recharge should occur even when the SMD is zero. They go on to define the necessary conditions appropriate to the SMD approach.

During a particular time interval, actual change in storage is

$$\Delta S = F (R_f - R_o - E_p)$$

the function F being the slope of the drying curve of the vegetated soil and E_p is the potential evapotranspiration.

It is assumed that the actual evapotranspiration takes place at the potential rate (i.e. $F = 1$) up to the root constant (RC) above which the actual evapotranspiration falls to 1/10 the potential rate (i.e. $F = 1/10$).

The root constant is a measure of the amount of water readily available within the root zone of the soil and is effectively equal to depth of root zone multiplied by effective porosity of the soil (expressed in millimeters of water).

In practice actual evapotranspiration will continue at the reduced rate until a maximum deficit (D) is reached and beyond which no soil moisture is available.

The following three conditions must be considered:

- (i) $0 \leq S < R_C$ then $E_a = E_p$
- (ii) If $R_C < S < D$ then
$$\begin{aligned} a_s/s &= F(R_f - R_o - E_p) \\ E_a &= (1 - F)(R_f - R_o) + F.E_p \end{aligned}$$
- (iii) If $S = D$ $E_a = 0$

Notwithstanding the above discussion, a perhaps even more restrictive element in the SMD approach however is the fact that for a given time increment all changes within the balance formulation are effected instantly. This aspect poses perhaps the most severe constraint on the SMD concept when one wishes to use it in terms of equivalence to soil suction in cases with a high resolution space-time requirement, since it operates essentially as a linear reservoir (Figure 3.1). Notwithstanding these general comments, SMD approaches have been attempted in a general spatial context. Malone and Shelton (1982) for example, illustrate the relationship between SMD and frequency of failure for landslides in Hong Kong 1978-1980. Whilst this study does illustrate the general accordance between slide occurrence and SMD it must be stated that some 11% of the slides they illustrate occurred with an SMD greater than 10 mm. This testifies to results we would expect from the foregoing discussion, namely that whilst the majority of slides may occur with saturated or near saturated conditions, there are important exceptions. Leach and Herbert (1982) and Leach (1982) utilise the SMD concept more specifically in modelling terms, in their study of a groundwater recharge model as applied to the Mid-Levels. Here, for computational purposes the slope section is modelled by two lines of nodes, a near surface sequence and one at depth with recharge being estimated by SMD (equation 3.1) at the near surface nodes.

This example is introduced into the discussion since it illustrates an important requirement usually attaching to the employment of SMD in hydrology modelling, namely that of model calibration. In the case of the Leach (1982) model, this calibration process resulted in adjustments being made to the storage coefficients in the colluvium and the CDG and minor adjustments had to be made in the shape of the $\bar{\alpha}$ index curve. In effect such adjustments represent the accommodation of inaccuracies in the modelling approach, and although SMD cannot be adjusted (since, in effect, S is a forcing function defined by measured input data - equation 3.1, Figure 3.1) by the model set up, there are inevitably errors in the recharge component which are implicitly adjusted by accommodation. Such a scheme requirement renders the SMD approach appropriate for general post-dictive conditions relating to slide mechanics (e.g. Crozier and Eyles, 1980), and for inclusion in predictive models for which an adequate length of calibrating data is available (e.g. Leach, 1982). We have observed that SMD cannot be accurately calculated by the use of equation 3.1, although it must be recorded that maps of SMD are prepared, for example, on a weekly basis for the U.K. by the Meteorological Office.

A more explicit approach to modelling was required in the current research programme, since a wide range of conditions were required to be simulated for which no pre-existing soil suction or pore pressure information was available. Accordingly, a physical modelling approach was taken. This approach contrasts sharply with the soil moisture deficit approach of course.

3.1.2 Soil water finite difference models

For three dimensional flow in a homogenous isotropic media Darcy's Law is represented by:

$$\vec{V} = -k(\theta) (\nabla \phi) \quad (3.2)$$

where \vec{V} = the discharge velocity
 ϕ = total potential
 θ = moisture content
 $K(\theta)$ = hydraulic conductivity

The equation of continuity can then be written:

$$\frac{\partial(\rho\theta)}{\partial t} = -\nabla \cdot \rho \vec{V} = -\left[\frac{\partial(\rho V_x)}{\partial x} + \frac{\partial(\rho V_y)}{\partial y} + \frac{\partial(\rho V_z)}{\partial z} \right] \quad (3.3)$$

where ρ is the density of water. If density change can be neglected

$$\frac{\partial\theta}{\partial t} = -\nabla \cdot \vec{V} \quad (3.4)$$

combining Darcy's Law and the equation of continuity gives

$$\frac{\partial\theta}{\partial t} = \nabla \cdot [K(\theta) \nabla \phi] \quad (3.5)$$

If we now assume that the absorption potential, chemical potential, osmotic-pressure potential and thermal potential may be neglected, then the total potential can be written

$$\phi = \psi + Z \quad (3.6)$$

where ψ = moisture potential
 Z = gravitational potential

Equation (3.5) now becomes:

$$\frac{\partial\theta}{\partial t} = \nabla \cdot [K(\theta) \nabla (\psi + Z)] = \nabla \cdot [K(\theta) \nabla \psi] + \frac{\partial K(\theta)}{\partial Z} \quad (3.7)$$

For homogeneous soil:

$$D(\theta) = K(\theta) (d\psi/d\theta) \quad (3.8)$$

where D = soil moisture diffusivity

thus equation (3.7) can be written:

$$\frac{\partial\theta}{\partial t} = \nabla \cdot [D(\theta) \nabla \theta] + \frac{dk}{d\theta} \frac{\partial\theta}{\partial z} \quad (3.9)$$

Equation (3.9) is sometimes known as the non-linear Fokker - Planck equation. For vertical flow only this reduces to:

$$\frac{\partial\theta}{\partial t} = \frac{\partial}{\partial z} \left[D(\theta) \frac{\partial\theta}{\partial z} \right] + \frac{dk}{d\theta} \frac{\partial\theta}{\partial z} \quad (3.10)$$

If we now substitute equation (3.8) into equation (3.10) we have:

$$\frac{\partial \theta}{\partial t} = \frac{\partial}{\partial z} \left[K(\theta) \frac{\partial \theta}{\partial z} \right] + \frac{\partial K}{\partial z} (\theta) \quad (3.11)$$

which is equivalent to the Richards equation:

$$C(\psi) \frac{\partial \psi}{\partial t} = \frac{\partial}{\partial z} \left[K(\psi) \frac{\partial \psi}{\partial z} \right] + \frac{\partial K(\psi)}{\partial z} \quad (3.12)$$

where $C(\psi) = d\theta/d\psi$ = volumetric water capacity.

If we follow the logic of Bruce and Whisler (1973) equation (3.12) can be rewritten to include soil depth dependent changes in physical properties:

$$C(\psi, z) \frac{\partial \psi}{\partial t} = \frac{\partial}{\partial z} \left(K(\psi, z) \frac{\partial \psi}{\partial t} \right) + \frac{\partial K(\psi, z)}{\partial z} \quad (3.13)$$

This relatively well established and lengthy analysis is of course based upon an empirical relationship - Darcy's Law (equation 3.2). Although this was established for saturated soils, this application extends it to unsaturated soils with the requirement for single value relationships between k , θ and ψ . This validity of Darcy's Law is generally held to be good for Reynolds numbers less than 1.0, and whilst slight departures from Darcy's Law have been observed for nearly impermeable clays, such details are generally not important and in soil water modelling Darcy's Law is assumed to apply.

There are two principal areas which have been investigated in the last 15 years or so and which are especially critical to the empirical utilization of the equations detailed above in simulations. These relate firstly to the determination of the k - θ and ψ - θ relationships, and secondly to the variability of those and related parameters in the field.

Whilst numerous experimental determinations of hysteresis in soil hydraulic properties have been made, they are far less common than determinations of the drying curves of θ - ψ due to experimental difficulties. Experiments that have been undertaken, largely in materials with high hydraulic conductivity, have shown hysteresis in θ - ψ and k - ψ (e.g. Topp and Miller 1966; Topp 1969; Poulovassilis 1970; Talsma 1970 and Tzimas 1979). Little information is however available as to the degree of hysteresis in the θ - ψ relation, and no information as to the hysteretic or non-hysteretic nature of the k - θ relation for undisturbed field soils (Tzimas 1979). The summary of most findings in this field suggests that hysteresis associated with k tends to be small enough to ignore in most applications. Secondly it is theoretically evident that hysteresis in these relationships should be more pronounced in sands than clays (low hydraulic conductivity materials) - see Hillel and Vanbavel 1976. Experimental evidence does not always support the significance of hysteresis however. Gillham et al. 1979 used a finite difference solution of the Richards equation (3.12) to compare hysteretic and non-hysteretic behavioural responses in a laboratory column of sand. They found a non-hysteretic simulation of a slow drainage-rewet experiment predicted the pressure head distribution as accurately as did the hysteretic simulation. As Gillham et al. suggest, further experimentation is needed to assess the generality of this result. Watson et al. (1975) found hysteresis to be significant in a field soil, but in considering soil variability, they speculated that a mean ψ - θ relationship might be satisfactory to account for water movement.

A number of soil water simulation models have been developed, and the selected characteristics of certain such models are summarised in Table 3.1. Finite difference models of this form do not lend themselves to as great a degree of generalisation as finite element models. Accordingly, the models listed in Table 3.1 relate to a specific set of site conditions. Figures 3.2, 3.3 illustrate this point further, with Figure 3.2a showing the basic elements in the Jensen (1981) model. This model, developed for plant growth studies, emphasises the detailed processes of transpiration and interception loss at the soil surface, but does not include perched water table or multi-layer soil elements of varying permeability. By contrast, the two dimensional model of Hillel (1977) consolidates the surface and root zone evapotranspiration processes into a single function; again perched water table conditions are excluded. In three dimensions similar decisions have to be made relating to the degree of process consolidation that is acceptable. Figure 3.3 shows the basic structure for the S.H.E. (1981) Institute of Hydrology model. This model is not yet operational.

3.2 OUTLINE OF THE MODELS USED IN THIS STUDY

3.2.1 Basic Model Structure

The basic model structure employed in this analysis is shown in Figures 3.4 and 3.5. The profile used was of finite depth and divided into NL compartments of different thickness. The water movement between compartments obeyed Darcy's Law in finite difference form (equation 3.12). The soil surface incorporated a detention capacity, the maximum for which must be specified. When no precipitation occurs, evaporation takes place according to a sine function algorithm which is described in more detail below. Runoff takes place when the surface detention capacity is filled and rainfall intensity exceeds the infiltration rate. The average hydraulic conductivity for flow through the boundary between adjoining cells I and J is weighted according to its thickness:

$$K_{IJ} = (K_J \cdot T_J + K_I \cdot T_I) / (T_J + T_I) \quad (3.14)$$

where T is the cell thickness.

The flux through the bottom boundary of the NL cells could either be taken to be equal to the hydraulic conductivity of the bottom cell, or to zero. The flux between each cell then followed Darcy's Law in discrete form:

$$Q_I = (\phi_J - \phi_I) \cdot K_{IJ} / (T_J + T_I) \quad (3.15)$$

where ϕ is the total potential for the respective cell. Unsaturated flow was assumed to take place in the vertical plane, whilst saturated flow was allowed to occur in both horizontal and vertical planes.

In the field, the description of infiltration is highly complicated since the initial and boundary conditions are usually not constant while the soil characteristics may vary with time and space. Haverkamp et al. (1973) have illustrated the variety of finite difference solutions employing different forms of the non-linear Fokker-Planck equation (3.9) and different ways of discretization. They were able to show that the six numerical models

examined yielded comparable results, which were not significantly different from the measured water contents. The scheme followed here is essentially that of the CSMP method (Hillel 1977); an explicit scheme. Whilst Haverkamp et al. showed the CSMP method to require a larger execution time than the implicit models they examined, it has a definite advantage in the relative ease of programming. The execution time may be reduced by increasing the layer thickness and adjusting the time step as a function of the soil water diffusivity. If D_{\max} is the maximum value of the soil water diffusivity in the soil profile at time t , the CSMP method with a rectangular integration method is stable when:

$$\Delta t < (r \cdot (\Delta z)^2 / D_{\max}) \quad (3.16)$$

where Δz is the layer thickness

r a coefficient (Staple (1966) used $r = 0.15-0.30$ for a loam, whilst Haverkamp et al. 1973 set $r = 0.50$ for a sand).

In this study the values for r were used as indicated, together with $r = 0.10$ for a clay (a highly conservative value - see Pall et al. 1981). Thus the instability criterion was used to determine Δt given Δz . If desired of course the criterion can be reversed such that Δz is determined given Δt .

There is a second source of instability which is process based and which must be noted.

Hillel (1980) has reviewed the occurrence of instability during the flow of water in unsaturated soil through crusts. However, Raats (1973) observed that profile layering is not a prerequisite for wetting front instability. Raats hypothesis, based on the Green and Ampt infiltration model provides the following criterion for the onset of instability:

$$\Omega > (L - \psi_c) / K_L \quad (3.17)$$

where Ω = the hydraulic resistance of the crust
(thickness divided by hydraulic conductivity)
 L = depth to the wetting front
 ψ_c = pressure head at the wetting front
 K_L = hydraulic conductivity of the subcrust.

Thus instability of the wetting front is favored by high crust resistance, a small value of $-\psi_c$ (high antecedent wetness of the subcrust soil) and a large value of K_L . Figure 3.6 provides an example of the instability criteria for both the numerical solution (equation 3.16) and the wetting front (equation 3.17). Obviously the former is much the more important in this analysis.

3.2.2 Procedures for the estimation of unsaturated permeability

The soil moisture-hydraulic conductivity and soil moisture-matric suction relationships have to be defined to allow modelling of the water flux through both saturated and unsaturated conditions.

Either empirical curves can be used for this purpose, or a suction-moisture curve can be assumed and the hydraulic conductivity soil moisture relationship derived. This latter procedure ensures physical consistency and is now well established. It was considered sensible to avoid any experimental errors in this area, and thus the K- ψ curve was derived from the following relationship (Campbell 1974, Millington and Quirk 1959 and Jackson 1972 provide details of the theory, whilst Hillel 1977 exemplifies its use in a simulation study directed to ecological problems):

$$K_i = K_s (\theta_i/\theta_s)^P \frac{\sum_{j=1}^M ((2j+1-2i)\psi_j^{-2})}{\sum_{j=1}^M ((2j-1)\psi_j^{-2})} \quad (3.18)$$

where K_i corresponds to θ_i , θ_s , and K_s refer to the respective parameter values at saturation and the summations are made over the j - θ increments for which the calculation is made. Equation 3.18 is the so called Millington-Quirk (MQ) method.

Thus from selected $\theta - \psi$ curves, physically consistent K- θ curves can be obtained.

Jackson (1972) showed that equation 3.18 could be used to provide acceptable estimates of K (see Figure 3.7), and he suggested the use of $P = 1$ which has been shown to describe the $\theta - \psi$ -K relationships well for a range of soils (see too Whisler 1976). Hysteresis in $\psi - \theta$ was not incorporated into the current model.

An alternative estimation procedure for unsaturated permeability is the Campbell (1974) method. Campbell showed that the scaling of K_s to K can be successfully effected by the following simple relationships:

$$K = K_s (\theta/\theta_s)^{2b+2} \quad (3.19)$$

where b is the coefficient in the relationship

$$\psi = \psi_e (\theta/\theta_s)^{-b} \quad (3.20)$$

This latter equation simply indicates that on a log-log plot, the suction moisture curve becomes linear, defined by two parameters, a and b .

Since: $\log \frac{\psi}{\psi_e} = \log A + B \log \frac{\theta}{\theta_s}$

and thus $\log \frac{\psi}{\psi_e} = \log A + B (\log \theta - \log \theta_s)$ (3.21)

where $(\log \theta_s)$ is a constant of course, then the gradient, b , is independent of the units employed, and thus for convenience of calculation equation 3.21 can be rewritten as

$$\log \psi = -a - b \log \theta \quad (3.22)$$

The principal restriction of this method is that a suction value of 0 kPa cannot be reached, and so it is appropriate to consider saturation to occur at 1 kPa. Other than this element of uncertainty at low suctions, the method is substantially easier to compute than the M-Q method.

In the analysis undertaken here, the M-Q method is used in the finite difference model because of its consistent performance over the complete suction range to saturation, whilst the Campbell method is employed in analysis, where representation of the $\theta - \psi$ curve by two parameters is deemed advantageous.

A further potential complication in the soil water retention curves is that related to surface crusting effects. Whisler et al. 1979 discuss two principal methods of representing this process. One approach is to impose a boundary condition of a decreasing flux as a function of time. A second, and more physically realistic approach is to let the soil water retention characteristics change with time. Whisler et al. propose use of the following adjustments:

$$\begin{array}{ll} K(\psi, z) = K_i & 0 < t \leq t_{c1} \\ K(\psi, z) = K_i - B_1 (t - t_{c1}) K_i & t_{c1} < t \leq t_{c2} \\ K(\psi, z) = B_2 K_i & t_{c2} < t \leq t_r \end{array}$$

t_r = time rainfall stops

t_{c1} = time crust starts to form

t_{c2} = time crust fully formed

K_i = the unadjusted value of conductivity

B_1 and B_2 are constants determining the rate of conductivity decrease.

This scheme therefore provides for a linear change in soil properties (θ_s can be similarly treated) with a then constant value for these properties. No comment is made as to the functions which may describe the reversal of this effect to facilitate this procedure in a multiple, rather than single event model. However, this procedure was included as a subroutine in the overall model, to provide an option for crust formation. It is however evident, as reported by Whisler et al., that more data needs to be obtained to more realistically model crusting phenomena and to assign appropriate linear functions.

What is clear though, is that there is a basis here for utilizing such concepts to simply reflect vegetation induced runoff by interception. This is further commented on in Chapter 6.

3.2.3 Evaporation estimation

Two approaches to modelling evaporation could be undertaken in the model. Firstly a simple isothermal evaporation routine was used. This function allowed evaporativity, E_0 (the maximum and limiting rate of evaporation possible from the soil as long as the surface is kept sufficiently wet) to vary as a sine function during the day:

$$E_0 = E_{\max} \sin (2\pi t/86400) \quad (3.23)$$

where t = time in seconds from sunrise

E_{\max} = the maximum midday evaporativity when the soil moisture content in the top cell exceeds the air dry value θ_d , evaporation takes place at rate E_0 (i.e. flux (1) = $-E_0$, see Figure 3.5). After the top cell dries to its minimum matric potential the evaporation rate becomes equal to the rate of upward transmission of moisture by the profile or to E_0 whichever is the smaller.

The obvious attraction of this procedure is its simplicity, with only the requirement of specifying E_{\max} . The night time evaporation rate was set equal to 1/100 of the maximum daytime value. Figure 3.8 details a summary of this procedure.

A more complete model of evaporation however is provided by assumptions of non-isothermal conditions. The energy balance approach requires knowledge of the factors contributing to the thermal balance at the evaporation surface. (Figure 3.9).

Following Wiesner (1970) we can set up a surface energy balance:

$$Sa - I = G + H + L + E \quad (3.24)$$

where the radiation terms are:

Sa = incoming radiation into a surface of albedo g ,
 and I is the thermal IR radiation
 G = heat flux from ground
 H = heat flux from air
 L = latent heat
 E = evaporation

(In the notation of Weisner 1970 $Sa - I$ is equivalent to $R_c (1-r) - R_b$ where r is the albedo and R_b the thermal IR)

The net radiation, R_n (the left hand side of equation 3.24) is the summation of the solar energy input (modified by the albedo) (Sa) and the thermal IR input (I). The thermal model detailed in Balick et al. (1981) can be used to calculate R_n , H and L such that E can be estimated.

3.2.4 Modelling perched water tables

In terms of the application requirements here with regard to Hong Kong conditions, it is a necessary prerequisite that perched water tables should be included in the modelling framework, and that pore pressures be evaluated at selected points throughout the perched zone. The mechanisms that can induce positive pore pressures are either a reduction in permeability, or theoretically, entrapment of air during infiltration. This latter process is ignored in all soil water physics approaches to the estimation of soil water conditions, and extensive work in the 1970's by Morel-Seytoux and others has not led to any requirement to incorporate such a process in current applications.

Figure 3.10 illustrates four possible approaches to the generation of positive pore pressures in the context of perched water tables.

Firstly, the condition that as soon as part of the column is saturated ($\psi < \psi_e$), hydrostatic conditions are developed. This is an extreme situation and one which would represent a worst condition, reflecting for example a transient condition of perching above boulders in colluvium. Secondly, a similar situation, but one in which hydrostatic conditions are only generated if $\gamma_1 > \gamma_2$. Both of these two conditions are considered within a homogeneous soil, and may prove so transitory that they would be inappropriate to base further inference on.

The third and fourth conditions (Figure 3.10) reflect the occurrence of perching at a K_1/K_2 interface occasioned by a permeability reduction.

In the third condition we can set the criteria that $\gamma_1 = \gamma_2$ and that $K_2 < K_1$.

The maximum pore pressure (P_{max}) at the interface can then be expressed as:

$$\frac{P_{max}}{h - x} = 1 - (K_2/K_1)^{0.5} \quad (3.25)$$

from the following analysis.

At time t a water column has descended a distance x into a medium with permeability K_2 .

Let p be the pore water pressure at the K_1/K_2 interface. Then the hydraulic gradients are:

$$i_1 = \frac{h - x - p_0}{h - x} = 1 - \frac{p}{h - x} \quad (3.26)$$

$$i_2 = \frac{p + x}{x} = 1 + \frac{p}{x}$$

For continuity, flux = $K_1 i_1 = K_2 i_2 = \frac{dx}{dt} n$

when n = effective porosity.

Let $\alpha = K_2/K_1$, and $B = x/h$ then from the continuity of flux and after simplification we have

$$\frac{p}{h} = \frac{(1 - \alpha) B (1 - B)}{\alpha (1 - \beta) + \beta} \quad (3.27)$$

and $\frac{p}{h} \max$ occurs at $\beta = (\alpha^{0.5}) / (1 + \alpha^{0.5})$

and $\frac{p}{h} \max = (1 - \alpha) / (1 + \alpha^{0.5})^2$

$$\text{thus } \frac{P_{max}}{h - x} = (1 - \alpha^{0.5}) \quad (3.28)$$

Condition 3 on Figure 3.10 therefore considers the solution to equation 3.28 in which the maximum pressure at the interface during the passage of the column of water is generated. Solutions to equation 3.28 in terms of both (P_{max}/h) and $(P_{max}/(h-x))$ are shown in Figure 3.11.

Of course this again represents a 'worst' solution, since p is a function of time. This dynamic condition is reflected in equation 3.27 which can be rewritten:

$$\frac{P_t}{h_t} = \frac{(1 - \alpha) \beta_t (1 - \beta_t)}{\alpha (1 - \beta_t) + \beta_t} \quad (3.29)$$

and a solution given in terms of time t . Figure 3.12 illustrates the solution under the conditions of K_1 , h and n specified. Here $t = 10^4 T$ secs i.e. $T = 1$ represents 2.78 hours, $T = 10 = 27.8$ hours. Thus as α reduces i.e. K_2 becomes much less than K_1 , the relatively high pore pressures at the K_2/K_1 interface are sustained for increasingly longer periods.

This dynamic condition (equation 3.29) reflected in Figure 3.12, was considered the most realistic one to be incorporated into the finite difference model, and accordingly this equation was adopted to provide solutions to p for all times t . Pore pressure conditions above and below the interface to the saturated/unsaturated boundary were thus calculated by multiplying P_t/h_t by the previously determined distances from the end points of saturation to the interface, thus pressures decline pro rata from the interface to zero at the top and base of the saturated column.

3.2.5 One Dimensional and Two Dimensional Models

The scheme as so far described allows for infiltration and vertical flow in heterogeneous soils with pore pressure estimations made according to equation 3.29 for all locations within perched water tables (see table 3.2).

To generalise this model to two dimensions requires further approximations. In coupling several one dimensional models (Figure 3.5) together to form a two dimensional model (Figure 3.2b) it is convenient to employ the Dupuit-Forchheimer assumptions. These assumptions state that in a system of gravity flow toward a shallow sink (i.e. the toe of the slope) all the groundwater flow is horizontal, and that the velocity at each point is proportional to the slope of the water table but independent of depth. Hillel (1977) observes that these assumptions are not correct in the strict sense but they provide feasible solutions in a very simple form. Thus if the effective gradient is taken to be equal to the slope of the water table (dh/dx) above each point, and allowing only horizontal flow we have:

$$Q = K_s h \frac{dh}{dx} \quad (3.30)$$

where h is the height of the water table above an impervious floor. Using this procedure, groundwater flow can be induced on a horizontal flow basis, cell to cell. Figure 3.13 illustrates the two models used in this study. There are several constraints on the two dimensional model however which should be noted here. Firstly, it does not accommodate horizontal flow from perched water table zones - all water movement down to the groundwater is

assumed to be vertical. Secondly, there is a problem with the geometry of the computational points on steep slopes, since to effect simulations at significant backslope distances, a very large number of points are required involving unduely large computational times. Thirdly, in application, there is the prerequisite for knowing the complete distribution of K and $\theta - \psi$ curve throughout the entire slope section. Finally the unsaturated soil water/groundwater interface can cause instability problems in finite difference calculations and so the model is not easy to establish in a generally applicable form.

In terms of the current investigation, the two models were used as follows:

- 1 dimensional : for the examination of cover effects on near surface soil water conditions
for the examination of soil water conditions at depth (up to 20 m) providing there is evidence of dominant vertical flow in the profile, providing the data input (see 3.2.6) could be obtained from readily available site information
- 2 dimensional : for representation of soil water conditions when the K and $\theta - \psi$ distributions throughout the entire slope were known
when groundwater conditions were controlled strictly by the boundary or infiltration condition as modelled (i.e. there was no other form of recharge to the modelled section)
when the slope geometry permitted the estimation procedure to be sufficiently conservative in the total number of computational points.

It must be stressed, that there is no generally applicable soil water forecasting model that can be applied to all situations of interest in Hong Kong. The fact that the groundwater condition is but one boundary condition and this itself cannot be adequately forecasted in Hong Kong at specified locations, serves to emphasise the problems faced by attempts to provide answers to questions relating to the transient states of soil suction on a basis sufficiently general to be compatible with requirements.

Notwithstanding this factor which is inherent in the problems under investigation as outlined in Section 1.2, the following chapters provide examples of model applications, pursuant of these aims which it is argued are appropriate given the constraints given in this section.

3.2.6 Summary of input variables to the soil water model

Table 3.2 summarises the data input requirements for the 1-D model. The additional input for the 2-D model is the height of each computational column above an assumed impervious plane (Figure 3.2b) and the horizontal distances between computational points.

The question of field variability is an important one in assessing the results from simulation procedures of this type. The optimal procedure here is to establish the distributions of field variability for the input parameters (Table 3.3). These distributions would then be input as part of the simulation procedure, with in each run of the program, values of each parameter being stochastically selected from the appropriate distribution. In this manner, the robustness of the simulated outcomes will fully reflect field induced uncertainty and permit more realistic assessments to be made regarding the likelihood of a specified condition occurring, such as saturation throughout a profile for example.

The ICL machine does not have suitable stochastic sampling distributions available (as they are on many IBM and Honeywell systems using 'Genstat' and similar software) and thus such a scheme (as outlined in Figure 3.14) could not be modelled in the subsequent applications. It is most important in terms of inference, that this point is recalled when those results are assessed.

Figure 3.15 shows a flow chart of the principal components relating to computation of the upper most soil water conditions in the model ie. soil surface conditions. Note that in the current application no stochastic variability was undertaken for the reasons mentioned. Figure 3.16 shows the nature of the operations in the model undertaken for each time increment. There is no provision for **surface** runoff generation other than by infiltration excess ie. the effect of vegetation canopy runoff, as well as transpiration processes are excluded. In such an approach it is suggested that the simplest possible way of modelling vegetated surfaces is to apply an "effective" rainfall concept. This would take the form of reducing rainfall available for infiltration by a given amount appropriate to specified vegetation types. If this were unsuitable, then as figure 3.15 shows, it is necessary to examine the modelling strategy in more detail by refining the **evapotranspiration** processes for example, along the lines perhaps suggested by Jensen (1981).

The concept of vegetation surface inclusion is treated in more detail in the following sections. It is sufficient at this stage to note that the requirement for input variables may be expected to depart from those implied by table 3.2 as further information relating to vegetation runoff characteristics in Hong Kong, are obtained in the current project.

4. DATA ACQUISITION

4.1 DATA REQUIREMENTS

Commensurate with the objectives and the available resources, three areas of empirical work were identified as being potentially the most productive and the most central.

- (a) To maximise the modelling work in this project, as well as subsequent analyses, chunam suction-moisture curve and associated saturated permeability determinations should be made.
- (b) To explore the effect of cover two requirements were seen:
 - (i) the establishment of a chunam and adjacent grass slope which would be monitored for soil suction,
 - (ii) the establishment of plot studies utilizing different vegetation cover, so that the bulk runoff could be ascertained with the ultimate aim of accommodating vegetation in the finite difference model.
- (c) To analyse the effect of backslope topography on soil water conditions experienced in a cut face. This aspect involves the analysis of data acquired by the author and D.P. McNicholl in a previous project.

The basis of this selection of empirical work was made, as was outlined in 1.2, with a view to obtaining sufficient field data to permit significant conclusions to be drawn, whilst simultaneously providing data for model parameterisation and verification. As discussed in 1.0 this is seen as all important in a design context, since different recurrence interval storms can be input to such finite difference models as were outlined in 3.0, only when such data is available.

With the exception of the very limited data available for b(i) above (McFarlane, 1980), all the areas of data acquisition were new in the Hong Kong context.

4.2 CHUNAM SOIL WATER CHARACTERISTICS

4.2.1 Chunam suction-moisture curves

The modelling approach detailed in 3.0 allows chunam cover to be included, providing that it can be assigned a suction-moisture curve and a saturated permeability.

Since no suction-moisture curves for chunam had been undertaken previously, it was necessary to acquire such data within the current project. Samples of granitic and volcanic chunam were taken in the field from the following locations:

Granitic chunam : King's Park {old chunam}
King's Park {new chunam}
Clear Water Bay Road {upper}
Clear Water Bay Road {lower}
Lung Cheung Road

Volcanic chunam : Lam Po Road {two samples}
Tai Po, St. Christopher Bend {new chunam}
Tai Po, St. Christopher Bend {old chunam}

Figures 4.1 - 4.3 show the derived suction moisture curves. The single most noteworthy feature of these curves is of course the steepness of both the drainage and wetting curves. This represents a point of convenience in modelling since, in effect, the only discriminating element is the volumetric moisture content at saturation, when the sensitivity of finite difference modelling output is accounted for. This aspect is discussed further in 6.0.

4.2.2 Permeability determinations of chunam

Whilst very limited empirical data testifies to the higher maintained suctions under properly maintained chunam (Figure 1.4), McFarlane (1980)), the permeability of chunam has not been evaluated. This is an important pre-requisite for modelling (see Table 3.3) as well as for comparisons with rainfall intensity, as has been discussed. Two studies were therefore undertaken with regard to chunam permeability. Firstly samples were taken from field sites, and the results of those analyses are presented in this section. Secondly, the effect of the mix proportions on the permeability of newly formed chunam is examined in 4.2.3.

Sampling for chunam permeability was undertaken on the samples used for the determination of the suction moisture curves as given in 4.2.1.

As specimens of 100 mm diameter were required, field samples had to be larger. Their sizes were more or less 300 mm x 300 mm. Cracks were deliberately avoided.

Various methods were used for final trimming. Due to the brittle nature of chunam, coring was not successful. Most of the samples were prepared by sawing.

Two tests were undertaken to determine chunam permeability. Firstly, a ponding test was undertaken. In this test, water was allowed to pond over the test specimen and found its way out only through the specimen. The variation of remaining water head with time was monitored. In effect, it was a falling head permeability test.

The apparatus set up (Figure 4.4) was extremely simple, thus saving a lot of errors arising out of unnecessary complications. A transparent plastic cylinder of 100 mm internal diameter was mounted over the specimen which was trimmed to a diameter of 100 mm. The contact was kept watertight by a sealant which provided some structural strength during handling. Two kinds of sealants had been used, namely paraffin wax and silicon sealant. The former had to be applied in layers and because of this, watertightness was not always possible. On the other hand, the latter sealant which was manufactured by Z-bond could be applied easily. Its only disadvantage was that it required a day's time for curing before the actual test could be carried out.

The specimen with the cylinder was then soaked in water for saturation. Afterwards, the cylinder was filled with water which was then allowed to seep through the soil to an outside trough which held water up to the top of the specimen, thereby avoiding withholding of water by suction. Outflow head could be maintained by overflowing or manual removal of excess water if the flow rate was slow.

The water head used was limited by the length of the cylinder which was 0.2 m long. Under a head of that order of magnitude, the chunam specimen usually required a week to finish the test. For such a long period, evaporation might account for a large quantity of water loss. A cap with a small air vent was provided to minimize evaporation.

The second permeability test employed was a falling head test.

The apparatus for this test was a triaxial cell and a burette. Water was allowed to run from the burette through the base of the triaxial cell into the test specimen. Flow was confined to the specimen by plastic membrane together with the use of O-rings (Figure 4.4).

It had been considered to use lateral pressure to confine the flow into the specimen only. However, the triaxial cells available in the laboratory employed all-around cell pressure for lateral pressure simulation, hence if flow was to be induced, the water head required would be very large. Meanwhile, an alternative arrangement using O-rings faced another difficulty. Because of the irregularities of the sides of the chunam specimens, O-rings could not fit perfectly around them. As a solution, a smooth-sided paraffin wax ring was cast around the specimen to shield off the irregularities.

The calculation basis of this procedure is as follows:

Let a = cross-sectional area of burette
 A = cross-sectional area of sample
 h = water head at time t
 h_0 = water head at time zero
 H = height of sample
 K = coefficient of permeability

In time t ,

$$Q = a \frac{dh}{dt}$$

By Darcy's Law,

$$\frac{Q}{A} = Ki$$

where i = hydraulic gradient

$$i = \frac{h}{H}$$

$$a \frac{dh}{dt} = KA \frac{h}{H}$$

$$\frac{dh}{h} = \frac{KA}{aH} dt$$

$$\ln h = \frac{KA}{aH} t + \ln h_0 \quad (4.1)$$

Therefore, a semi-log plotting of water head against time will give a straight line with a slope equal to $\frac{KA}{aH}$, from which the coefficient of permeability can be evaluated.

Generally, the method using burette gave a higher value for the coefficient of permeability. This can be attributed to two facts. One reason is that in this method, the water head was higher ranging from 0.8 m the highest to 0.2 m the smallest, whereas in the alternative method-ponding, the water head ranged from 0.2 m to zero. The permeability of chunam may not be constant over these two ranges of water head. Secondly, there seemed to be a substantial amount of side leakage between specimen and wax ring in the burette method. This can be reflected in the results : the burette method gives a permeability three hundred times that given by the ponding method.

The ponding method is a close simulation of possible site conditions. The actual ponding depth will seldom exceed 0.2 m especially on slope surfaces.

Table 4.1 details the full results of the chunam permeability tests.

Except for one specimen, the permeability values were quite constant and repeatability of results was high. The only exception is the sample from Lower Clearwater Bay Road. Over a period of ten days, the permeability varied from 5×10^{-7} m/s to 7×10^{-8} m/s and finally settled down to the latter value. This is probably due to silting up of pores by fines.

For chunam made from decomposed granite, the coefficient of permeability was recorded to be in the range of 10^{-7} to 10^{-8} m/s. An average of 1.2×10^{-7} m/s.

For chunam made from decomposed volcanics, the coefficient of permeability ranged from 10^{-8} to 10^{-9} m/s, with an average of 1.4×10^{-8} m/s. The lower value reflects a higher proportion of fines in decomposed volcanics.

4.2.3 The relationship of chunam mix to permeability

A total of 30 trial mixes were made in this study. 12 mixes were laboratory reconstituted chunam from King's Park Decomposed Granite and another 12 mixes from Tai Po Decomposed Volcanics, King's Park Decomposed Granite and Tai Po Decomposed Volcanics were preferred because significant amounts of suction related engineering data were already available from previous investigations. The 12 mixes for each soil type were made according to the mix proportions given in Table 4.2. Water content was varied accordingly in each case to produce the necessary workability. The remaining 6 mixes were made with Clear Water Bay Road Decomposed Granite to obtain site - specific data for the present study. The mix proportions for the 6 mixes are given in Table 4.3. Again, water content was varied accordingly in each mix to produce the necessary workability. Ordinary Portland cement was used for the trial mixes, the brand being Golden Eagle. The water used for the trial mixes was tap water. Kwan (1983) provides detailed information on the particle size distributions of the soils used.

Cylindrical moulds of nominal internal diameter 73 mm and nominal thickness 42 mm were used in the preparation of samples.

Moulds for the chunam samples were removed one day after mixing. The samples were left indoors, and air cured. No special curing was made.

The formation of cracks in chunam is directly related to its shrinkage property. The area shrinkage is relevant in respect of crack formation in view of the fact that chunam plaster on slopes is very thin when compared to its area extent. The Geotechnical Manual for Slopes (G.C.O. 1979) states: 'chunam should be applied to the surface in two layers each not less than 20 mm thick'.

It is noted that other factors as well may contribute to crack formations. Field observations show that chunam made of coarse sand generally has cracks wider than those of fine soils. High water - cement ratio will also lead to severe cracking in the chunam.

During curing of the samples, measurements of the diameter of the samples were made daily for seven days. Three diameters, spaced evenly, were marked on the samples. The diameters were measured by a screw gauge. The percentage shrinkage is calculated from the following formula:

$$\text{percentage shrinkage} = \left(1 - \frac{\text{average measured area}}{\text{average original area}}\right) \times 100\% \quad (4.2)$$

Since the cement and lime content of the trial mixes vary and there may be cases in which cement and lime contents are nil, the water to soil ratio was adopted for comparison and analysis instead of the usual approach of water to cement ratio. The amount of water in each trial was adjusted so that all the trial mixes were consistent with their workabilities. Since there is not a quantitative measurement of workability for chunam, the required workability is a matter of personal judgement. Due to the silty nature of the Tai Po Decomposed Volcanics, the mixes were very cohesive. Compaction of the mixes by method of tamping was not practicable. King's Park Decomposed Granite is sandy and much less cohesive. Clear Water Bay Road Decomposed Granite is gravelly sand and chunam made from it has properties approaching that of concrete. The determination of the required workabilities depends largely on experience.

Measurement of the area shrinkage of the chunam samples began one day after the preparation of the mixes when the moulds were removed. All the samples were left indoors and air cured. The temperature and humidity changes were very small and their effects on the curing of the samples were minimal. Tables 4.4 - 4.6 show the variation in area shrinkage with age for the chunam for all the trials undertaken. Comparisons within these tables reveal that chunam mixes of Tai Po Decomposed Volcanics are generally more susceptible to shrinkage than that of King's Park Decomposed Granite with chunam mixes of Clear Water Bay Road Decomposed Granite the least susceptible. A comparison of the particle size distribution curve for the three soil types indicates a gradual transition from high silt content (Tai Po Volcanics) to high sand content with the presence of gravel (Clear Water Bay Road granites). A significant portion of the shrinkages occurs in the first 7 days of curing, although Ho (1978) reported in a recent study that more than 70% of the shrinkage was obtained at the end of 60 days. The comparatively large proportion of shrinkage obtained in the first 7 days for the trial mixes here may be attributed to small size of the samples and the curing condition. Less humid conditions and smaller samples both lead to drying of the sample at a faster rate. Cracks were generally not observed in the samples except for a few cases which have low cement and lime content.

It is desirable to isolate and identify the principal controls on shrinkage. The data in Tables 4.4 - 4.6 in association with the cement,

and lime content and water to soil ratio (as given by the trial numbers - Tables 4.2 - 4.3) were subjected to multiple regression analysis.

Let Y = % area shrinkage at age of 7 days
 X_1 = cement to soil ratio
 X_2 = hydrated lime to soil ratio
 X_3 = water to soil ratio

The form of the regression model is :

$$\hat{Y} = A + B_1X_1 + B_2X_2 + B_3X_3 \quad (4.3)$$

The following are the results for chunam mixes of the two soil types:

(a) Chunam of Tai Po Decomposed Volcanics

$$\hat{Y} = 5.3 - 71.8X_1 - 24.6X_2 + 20.2X_3 \quad (4.4)$$

adjusted R^2 = 0.81

standard error = 2.0% area shrinkage

standardized regression coefficients:

$$\beta_1 = -0.67$$

$$\beta_2 = -0.54$$

$$\beta_3 = 0.55$$

Negative values of the partial regression coefficients for cement and lime contents (X_1 and X_2 respectively) imply that the increase in cement or lime content will reduce the area shrinkage. Other things being equal, the standardized partial regression coefficient β 's indicates that one standard deviation unit change of the cement to soil ratio (β_1) would introduce the greatest change in shrinkage and one unit change in lime to soil ratio (β_2) the least.

(b) Chunam of King's Park Decomposed Granite

$$\hat{Y} = -0.49 - 31.2X_1 - 10.8X_2 + 16.1X_3 \quad (4.5)$$

adjusted R^2 = 0.57

standard error = 0.83% area shrinkage

standardized regression coefficients:

$$\beta_1 = -1.06$$

$$\beta_2 = -0.86$$

$$\beta_3 = 0.87$$

In this case, only 57% of the variance in shrinkage is explained by cement, lime and water content jointly as indicated by the adjusted R^2 . Again, negative values of β_1 and β_2 indicate that increases in cement or lime content will reduce shrinkage. Also, one standard deviation unit change of the cement to soil ratio introduces the greatest change in shrinkage and the effect of lime content on shrinkage is the least.

It is however important to recall that the water to soil ratio and the cement, lime content are not strictly independent. Regression equations show that increases in lime and cement content reduce shrinkage. At the same time, increase in lime and cement content leads to an increase in water content which acts to nullify the effect.

The second stage of the laboratory experiment sought to determine the control that mix proportions have on permeability.

The falling head method (4.2.2) was used to measure the permeability of the chunam samples. No leakage from any part of the apparatus or the sides of the sample was observed. Hence complete water-tightness could be assumed.

Generally, the permeability values were quite constant and repeatability of results was high. There were two samples the permeability of which dropped nearly an order of magnitude over a period of one week. This is probably due to silting up of pores by fines. A case which had been encountered before (Chan (1982)). There were also two cases in which the permeability increases. The increase may be attributed to the higher degree of saturation of the sample during the running of the permeability test. Saturation of the samples was undertaken by percolation and no check of the degree of saturation was made. Checking of saturation would require the application of back pressure and the use of triaxial test apparatus. Since at least six tests would run at any one time, it was not practicable to saturate the samples by back pressure.

Table 4.7 details the permeability results obtained. Comparison of these results with those of field samples (Table 4.1) shows the laboratory reconstituted samples have values lower than the site samples. The difference may be up to an order of magnitude for some soil types. Laboratory reconstituted mixes were under more stringent quality control than the site mixes and this factor, as well as aging may account for the observed differences.

Mix No. 1 of each soil type is simply the permeability of compacted remoulded soil. Bearing in mind that laboratory result may be 2 orders of magnitude lower than comparable field tests, close agreement of results was obtained. With the addition of cement or lime, it would drastically reduce the value of permeability.

Controls on the chunam trial permeability values (Table 4.7) were sought. No statistically significant relationships were found between permeability and % area shrinkage, cement and lime content, or water content. It is more probable that the conservative variation in permeability that was observed, is due to such factors as the compaction of chunam mix during preparation.

Figure 4.5 summarises the controls on chunam performance in the context of mix variation which can be stated as follows:

- (a) The standard specification 1:3:20 mix, i.e. mix No. 7, compared with other mixes has low shrinkage and medium to low permeability.
- (b) The permeability of intact chunam is unrelated to the mix properties.
- (c) The principal effect of mix variation is thus related to chunam shrinkage.

- (d) Particle size distribution of the soil part of chunam mixes is the most important determining factor of the properties of the mixes (see Tables 4.4 - 4.6). Chunam mix of fine soil is associated with large drying shrinkage and lower permeability.
- (e) Both cement and lime stabilize the soil. Increase in cement or lime content alone reduces the shrinkage. Increase in water content results in larger shrinkage. Statistical correlation indicates that the effect of change in cement content is most prominent while lime content is the least.
- (f) Since variation of cement and lime content necessitates a corresponding change in water content, there exist an optimum cement content. The existence of such an optimum content for lime is not so obvious regarding the influence on shrinkage. For fine material, high cement content is desirable (lime content proportions are irrelevant). For coarser material, cement and lime content assume equal importance. The actual proportions are unimportant providing the cement content is 1:20 or greater.

4.3 SOIL SUCTION COMPARISONS ON A CHUNAM AND GRASS SLOPE

4.3.1 Site details and instrumentation

Two slopes some 300 m apart on Clear Water Bay Road (see Figure 1.7) were selected for instrumentation. It is important to recall, that previous work in Hong Kong (McFarlane, 1980) had made only point comparisons between grass and chunam slope responses. A more comprehensive instrumentation plan was therefore sought in this investigation - one which would allow comprehensive conclusions to be drawn regarding the slope behaviour as a whole, and secondly a plan that would provide for sufficient resolution of data that could be used to verify the application of the soil water model (3.0).

Plans of the two slopes are given in Figures 4.6 and 4.7 together with the depth and location of Jetfill tensiometer positions. Figure 4.8 gives the tensiometer locations in profile, the deeper locations being seen to accord with the depth of interest in stability terms, as can be seen from the resistance envelopes for both sites (Figure 4.9).

Plates 4.1 and 4.2 show the two sites, and illustrate the similar backslope spur topography, being CDG. Plate 4.3 shows the detail of one tensiometer installation (group C on the top berm of the chunam slope - Figure 4.6), whilst Plate 4.4 shows the location of the raingauge, currently being installed, on the lower berm of the chunam slope. The rainfall data used in the analysis in this report is from G.C.O. raingauge KO4, which is some 0.8 km from the site.

Daily readings from all the tensiometers commenced on April 24, 1983, and analysis of the data through to 1 July 1983 is undertaken in this report.

The quality of the chunam cover is extremely good (Plate 4.4).

4.3.2 Soil Suction response to storms

During the April - July 1983 period there were some eleven storms ranging in terms of total precipitation from 5 mm to 285 mm (the storm of June 17, 1983).

The broad pattern of storm response is shown with regard to three storms of markedly different storm precipitation. Figures 4.10 and 4.11 show the unchanging pattern of soil suctions to 9.5 mm of rainfall on 6 May 1983. Figures 4.12 and 4.13 show the response to 254.5 mm between 0000 hours on 26 May and 1300 hours on 28 May 1983. A significantly more intensive storm on June 17 1983 (recurrence interval in excess of 2 years) is shown in Figures 4.14 and 4.15 together with the associated responses.

From these data several general features are apparent:

- (a) generally, soil suction contours are approximately parallel to the slope face in both the chunam and grass slopes to the maximum instrumented depth of 4 m,
- (b) there is evidence to show that significant recharge occurs from the upslope unprotected area on the chunam slope during prolonged low intensity rainfall (see Figure 4.12).
- (c) the chunam slope, excepting the circumstance outlined in (b), maintains higher suctions than the grass slope. This aspect can be analysed further. Figure 4.16 illustrates the mean suction difference, at 3 m and 4 m depth, between the grass and chunam sites, based on the lowest suctions resulting from the storms in the study period. Suction differences exceed 5 kPa in locations other than the top slope and base slope locations. Whilst these mean differences are significant, they do not by themselves imply a consistent difference between the two slopes for all storms. To ascertain whether such a sustained difference exists, then it is appropriate to employ discriminant analysis. Figure 4.17 and 4.18 show the results of the analysis in which the only site that does not exhibit a significant difference between grass and chunam is at the lowest slope location at 4 m depth.

4.3.3 The prediction of soil suction response

Within the restricted amount of data available it was considered appropriate to attempt a multiple regression estimation of the suction recovery in the post storm period at a variety of depths.

The first analysis undertook a prediction of the resulting suctions ('RESU') for different days ('TIME') after the cessation of rainfall, with the start suction conditions ('STSU') being the lowest suctions during the storm.

Input into the first analysis were all observations at 1 m depth of lowest storm suctions, and the recovery suctions for all days after the storms for which no rainfall was recorded. Separate regressions were undertaken for the chunam and grass slopes at 1 m depth, and then the analysis repeated for 3 m depth. The results were as follows:

1 m depth:

$$\text{Chunam} \quad \text{RESU} = -0.2323 + 0.0401.\text{TIME} + 1.0519.\text{STSU} \quad (4.6)$$

$$r = 0.941$$

$$\text{standard error} = 2.17 \text{ kPa}$$

$$\text{Grass} \quad \text{RESU} = 0.7012 + 0.0539.\text{TIME} + 0.9704.\text{STSU} \quad (4.7)$$

$$r = 0.947$$

$$\text{standard error} = 1.87 \text{ kPa}$$

3 m depth:

$$\text{Chunam} \quad \text{RESU} = 0.9242 + 0.0085.\text{TIME} + 0.9919.\text{STSU} \quad (4.8)$$

$$r = 0.987$$

$$\text{standard error} = 1.14 \text{ kPa}$$

$$\text{Grass} \quad \text{RESU} = 1.6644 + 0.0160.\text{TIME} + 0.9409.\text{STSU} \quad (4.9)$$

$$r = 0.954$$

$$\text{standard error} = 1.73 \text{ kPa}$$

Variable definitions:

RESU : resulting suction (kPa), TIME days after the rainfall has ceased

TIME : days after rainfall ceased

STSU : lowest storm induced suction (kPa) at the location on the slope that it is desired to predict the recovery suction (RESU), TIME days after rainfall has ceased

These relationships are graphed in Figures 4.19 - 4.20. They illustrate several points:

- (a) the linear increase in suction with time (upto 5 days) after cessation of rainfall. At 1 m depth on grass, the rate of suction increase exceeds that of the chunam slope to satisfy the evapotranspiration demand. At 3 m depth, the rates of suction increase are similar on both slopes - in this case of course such increases are gravity drainage (suction-moisture) controlled.
- (b) given the very high correlation coefficients and low standard errors, it is appropriate to consider these equations as useful predictors of the resulting suctions at all positions on the slopes. The entry points to the use of these equations are solely therefore the lowest suction resulting from the storm at the point of interest on the slope (STSU) and the number of days after the storm for which the recovery suction is required.

As more data becomes available, then such equations should be recomputed - recall the limited 3 month data availability at the time of writing.

Of course, establishment of similar relationships, using total storm rainfall ('RAIN') and pre-storm suction ('PRSU') is possible. Figure 4.21 shows the possibility of such a relationship configuration in which these two variables could be used to predict lowest storm suction, which then becomes the entry point to equations 4.6 - 4.9. Figure 4.22 shows the prediction of lowest storm suctions, from total rainfall and pre-storm suctions, at 3 m depth. The relationships were as follows:

3 m depth:

$$\text{Chunam} \quad \text{LOSU} = -0.6384 - 0.0106.\text{RAIN} + 0.9563.\text{PRSU} \quad (4.10)$$

$$r = 0.984$$

$$\text{standard error} = 1.30 \text{ kPa}$$

$$\text{Grass} \quad \text{LOSU} = 0.8346 - 0.0187.\text{RAIN} + 0.9033.\text{PRSU} \quad (4.11)$$

$$r = 0.960$$

$$\text{standard error} = 1.76 \text{ kPa}$$

Variable definitions:

LOSU : lowest resulting suction (kPa) from a storm of 'RAIN' mm

RAIN : total storm rainfall mm

PRSU : Pre-storm soil suction (kPa) at location on the slope that it is desired to predict the lowest storm induced suction (LOSU), which can then be the entry point (STSU) to equations 4.6 - 4.9.

It is therefore of interest, given the significance of the above relationships, to effect the complete prediction scheme, as outlined in Figure 4.21 for 3 m depth for all the available storms in the study period.

Thus if equations 4.8 and 4.10 are coupled for the chunam slope at 3 m depth, the resulting suctions, TIME days after a storm, can be predicted from total storm rainfall (RAIN) and pre-storm suction (PRSU) at the point of interest. Figure 4.23 illustrates the predicted and observed resulting suctions for all days of recovery (up to 5) for all 11 storms in the study period. Figure 4.24 graphs the corresponding comparisons for the grass slope. The maximum error in both cases is approximately 5 kPa, with a consistently much better performance for the majority of observations.

As increased data becomes available, with longer recovery periods occurring, then more representative equations corresponding to (4.6) - (4.11) can be established. It is nevertheless encouraging from a predictive standpoint, that what data has been obtained, indicates a commonality of drainage response over the entire slope lengths. This being so, a case is argued in 5.3 that one application of the recovery relationships lies in modification of the current (1983) landslide warning index for Hong Kong.

4.3.4 Direction of soil water movement and implications for modelling

For the vertical tensiometer profiles an analysis in terms of total potential was undertaken to ascertain the existence, or otherwise, of a

vertical flux over the period of available data. As would be anticipated, in all cases a vertical flux was shown to dominate conditions within each profile. What is of interest, however is, the dominance of this flux during and after the storm of 26-27 May 1983 at the chunam top slope location, where the data in Figure 4.12 has shown significant recharge to be occurring from the unprotected backslope area. Figure 4.25 illustrates the nature of the fluxes for profile A (see Figure 4.6), the topslope location on the chunam slope for a selection of three storms.

But of course of greater significance are the soil water flow directions in the entire slope. This can be crudely estimated by drawing orthogonals to the total potential lines, which themselves have to be estimated by interpolation (see Figure 4.26a) because of the enforced instrumentation location points in relation to the slope geometry (Figure 4.8). Figures 4.26b and 4.26c show the range of flow directions up to 4 m depth estimated in this manner. The flow directions are thus dominantly vertical on the basis of total flux calculations (as opposed to vertical flux components - Figure 4.25). The implications here are that, like selected instances in the Mid-Levels, it is appropriate to consider a one dimensional simulation procedure for an examination of general response in these relatively shallow depths with, of course variations in start moisture conditions as appropriate. A requirement, whether 1-D or 2-D modelling is undertaken, is the acquisition of suction moisture curves. Compatible with the chunam suction-moisture curves for this site (Figure 4.2), suction-moisture curves for the CDG at the two slopes were obtained from each berm location. These curves are given in Figures 4.27 and 4.28, in preparation for the modelling undertaken at this site which is reported in 6.0.

4.4 THE EFFECT OF BACKSLOPE TOPOGRAPHY ON SOIL SUCTIONS

The site at Clear Water Bay Road, the preliminary results for which have been presented in 4.3, illustrates conditions of soil suction response under essentially one dimensional control. However, in topographically more complex conditions, and especially where there are significant hillslope hollows immediately backslope, then the dominant controls on soil suction response in the near surface zone need no longer be one dimensional. Moreover, the groundwater response in such conditions need not be infiltration controlled, but may be influenced by complex three dimensional interactions. This has clear implications for modelling strategies (6.0). Also, in terms of possible maintenance of zones of near surface saturation, several studies have shown that hollows or dishes in backslope topography can initiate soil water convergence (Anderson & Kneale 1982). The result is a concentration of higher pore pressures (or lower suctions) than in cut slopes where the back slope topography is regular. Where the convergence process occurs in humid temperate climates it has been demonstrated that localised zones of saturation can be maintained for several days and weeks in the absence of rainfall.

Soil water movement is governed by total potential ϕ which is the sum of the soil water potential, ψ , and the elevation potential Z . The usual expression is $\phi = \psi + Z$ and all variables are quoted in length terms (m). ψ can be positive for positive pore pressures and negative for negative pore pressures (soil suction). Z is measured from an arbitrary datum and will dominate the total potential, and hence soil water behaviour, in steep topography. Under these circumstances we may expect soil flow paths (ortho-

gonals to equipotential lines) to be reasonably approximated by orthogonals to topographic contours as has been noted in 4.3.4. Conversely, in shallow topography, seasonal or storm induced variations in the soil water potential, Ψ , may exceed Z , and hence the pattern of soil water movement on such slopes may not be effectively controlled by topography alone, but be more related to local antecedent soil water conditions. Such contrasting soil water flow path patterns (static in steep topography, and temporarily variable in shallow topography) have been exemplified by Anderson and Kneale (1982) in natural slopes in the UK.

Extending this knowledge to the conditions prevalent in Hong Kong, we might expect the following principles to apply

- (a) in the typically steep topography, the soil water flow paths should be relatively static,
- (b) where hillslope hollows exist, these will give rise to pronounced zones of soil water convergence,
- (c) where soil water convergence does occur it will result in locally higher soil water content, higher pore pressures, or indeed in the more permeable materials such as colluvium, the establishment of piping in such zones. (Jones, 1981)

4.4.1 Site description and instrumentation

A site at St. Christopher Bend near Tai Po Road (Figure 1.7) had been instrumentated and monitored by Anderson and McNicholl (1983) and the site was found to be suitable for a comprehensive study of the important relationship between topography and soil water conditions. Figure 4.29 shows the general location of the site which is a road cutting 45 m high at the crest and trending roughly south east - north west. Two contrasting backslope topographies are evident. To the west of the cut slope crest on the south side of the cutting is a pronounced hillslope hollow, whilst to the east of the same cut face, is a rectilinear slope. Two piezometers, at the same ground level elevation (109 m), can reasonably be associated with those respective topographies. The piezometer P1 is at the rectilinear backslope/cut face boundary, whilst piezometer P3 corresponds to the hillslope hollow configuration. Binnie & Partners' (1979) stability report for the slope indicates the upper four berms to be in zone B (highly weathered) material, while the two lower berms are in zone D rock. The ends of the slope are formed in volcanic rocks but the central part is intrusive (probably granodiorite). In addition a shear zone extends diagonally across the face from just south of piezometer P4 in an easterly direction (Figure 4.29). As is often the case in Hong Kong, there is a layer of colluvium in the hillslope hollow and other areas of the backslope. Plate 4.5 shows a general view of the site. Of particular interest is the response of the two piezometers P1 and P3. Figure 4.30 shows a typical type of response, with the general ground water level being some 6 m lower adjacent to the rectilinear slope (piezometer P1) than at P3. This difference, whilst narrowing during storm events, is still appreciable considering the ground elevation of the piezometers is identical (109.3 m).

From an initial appraisal of the site, a possible mechanism that may explain such locally different ground water elevations is that of soil water convergence in the hollow area backslope of P3. It is noteworthy that seepage was observed in the cut face at a location corresponding to the hillslope

hollow outfall. This field observation combined with the evidence of studies already referred to, was a useful guide to the placement of tensiometers in the hillslope hollow area. Jetfill tensiometers were employed and the exact locations of these installations are shown in Figure 4.31. In addition, horizontal drains were already installed on the lower three berms as shown. With the exception of location T8, all tensiometer locations had tensiometers at 1.5 m depth; table 4.8 provides the tensiometer depths and piezometer information for all the sites shown on Figure 4.31.

Tensiometer, piezometer and horizontal drain records were taken during two principal periods 1 June 1980 - 10 October 1980 and between 1 June 1981 - 1 October 1981. In particular the tensiometer data was intended to identify the presence of soil water convergence processes near surface, should they exist.

4.4.2 Backslope soil water conditions

For the storms occurring within the study period, convergence was found to exist within the instrumented hollow area (Figure 4.29). Two storms were selected for further investigation and soil water conditions were mapped at 1.5 m depth. Figures 4.32 and 4.33 illustrate the marked nature of the topographically induced soil water convergence. Figure 4.32 shows contraction of the zone of positive pressures to take place after the storm, whilst Figure 4.33 illustrates the maintenance of a saturated zone after five days without precipitation (July 30 - August 4 1980). The subsequent storm commencing August 5 results in a significant expansion of that area where pore water pressures exceed 0 kPa. In both these examples it is to be noted that the soil water potential lines are, in many instances, orthogonal to the topographic contours - a clear indication of the significant soil water convergence. If there was no soil water convergence occurring, then soil water potentials at a given depth (in this case 1.5 m) should be the same at all points over the slope. This point is further illustrated by plotting orthogonals to total potential lines. Figure 4.34 illustrates such a plot for the 12 July data, showing convergence to be focusing close to piezometer P3 at a point nearly coincident to horizontal drains A and B. From this figure it can be seen that out of the fourteen horizontal drains on berm 3, only four exhibited any flow during the study period, and these were located in the region of the cut face corresponding to the zone of convergence already noted. Flow from these drains (Figure 4.35) shows an approximate four day delay, and is appreciably higher at drain A than elsewhere.

The maintenance of a zone of saturation in the centre of the hillslope hollow is a factor worthy of further comment. It can be seen from Figure 4.33, that such a zone at 1.5 m depth is still relatively extensive even though there had been no rainfall in the previous five day period, as we have observed. This can be taken as an indication that during much of the wet season, topographic convergence provides for a probably permanent zone of saturation which varies in extent according to antecedent rainfall, and which must serve to preferentially charge the groundwater in this restricted locality. The efficiency of this mechanism is of course dependent upon the detailed variation of permeability with depth throughout the catchment area that could potentially contribute to convergence. All that can be said here is that convergence is seen here to manifest itself in a saturated zone. The detailed variation of permeability with depth is unknown, but it is likely that the upper layers are more permeable and that diminution of permeability with depth occurs at similar depths below ground surface. This is particularly

the case where there is a layer of colluvium over the residual soils as in the hillslope hollow. These factors together would result in perching of water near surface and facilitating increasingly marked topographic convergence of soil water.

In a situation in which a topographic hollow occurs at the immediate backslope vicinity of a cut face, then it would appear that

- (a) There is the possibility of soil water convergence in the backslope hollow causing, and maintaining, a zone of saturation within the soil at shallow depths.
- (b) Further, this zone of saturation may be sufficient to surcharge the underlying local groundwater conditions at that point.
- (c) The results in terms of the groundwater conditions are :
 - (i) the maintenance of higher groundwater in the vicinity of the zone of near surface soil water convergence, but a relatively small, infiltration induced, response to storm rainfall
 - (ii) the maintenance of lower groundwater conditions at similar ground elevations away from the zone of saturation (e.g. P1 on Figure 4.29) - see Figure 4.30. However, in these locations storm responses are very pronounced (e.g. 2 m in response to 0.268 m of rainfall).
- (d) The much more pronounced groundwater response to rainfall away from the topographic hollow (i.e. piezometer P1) is likely therefore to be induced by groundwater interaction parallel to the cut face - stimulated by the infiltration induced rise at P3, setting steeper lateral hydraulic gradients. Such rises, as measured at P1 are, as we have commented and as the simulation has suggested, far too large to be induced by vertical infiltration alone.

In demonstrating the occurrence, at a single site, of soil water convergence, its likely relationship to groundwater levels and horizontal drain discharge differences in relatively short distances, there remains the question of generalising the results of such soil water mechanisms to other sites. It is evident, that in a general sense, due regard must be taken of topographic features backslope from cut faces, but it is a matter beyond this project to establish 'convergence criteria' for the parameter modification of standard stability analyses in such circumstances. Anderson and Kneale (1982) have shown that analytically derived indices from saturated flow equations under specific assumptions, may prove useful in this regard. For example, Beven and Kirkby (1979) derived the index $a/\tan \beta$ (where a = area drained per unit contour length, and β = local slope angle); this index is high in hillslope hollows, and lower elsewhere and has been shown to be successful in predicting zones of soil water convergence.

Elsewhere, generalisation of soil water convergence process has been achieved in regard of cut slopes in residual volcanic materials in the Caribbean. Anderson (1982, 1983) has shown that with regard to soil suctions at shallow depths (less than 5 m) the effect of topography (i.e. soil water convergence) as measured by slope plan curvature, diminishes with decreasing permeability (Figure 4.36a and 4.36b). Moreover, such a topographically

induced soil water condition lends itself as a significant discriminator in the context of deriving failure bounds in relation to shallow slips (Figure 4.37).

4.5 VEGETATION - RUNOFF RELATIONSHIPS

4.5.1 Background to data requirement

The effect of cover differences (chunam and grass - Plates 4.1 and 4.2) has been explored in the context of two sites using available data to date. Whilst this has allowed certain tentative conclusions to be drawn, there remains the question of making comparisons with other vegetation types. There are three ways in which this could be achieved:

- (a) a substantial empirical programme of monitoring could be mounted,
- (b) a smaller instrumentation scheme could be established to provide base-line data and to provide the necessary information to parameterise the top computational point in the soil water model (3.0) such that vegetation can be accommodated in the simulation,
- (c) the existence of pre-existing data be established and utilized.

In terms of the general research philosophy as outlined in 1.2, a substantial field investigation programme with the available resources could not be justified.

As has been shown, modelling intact chunam is relatively straightforward. In the context of cover effects on soil water conditions, with the saturated permeabilities and suction-moisture curves having been determined (4.2.1), then the chunam can be modelled directly as part of the soil profile, albeit with markedly different characteristics. With the processes of interception, detention and root zone permeability changes in regard to vegetated surfaces, then the existing model cannot accommodate both the increased number of processes in the upper layer together with their variation in respect of particular forms of vegetation combinations.

To aid the model refinement at the coarsest level, runoff data for different vegetation covers is required. Such data could then be used to derive an 'effective rainfall' which would be regarded as that available for infiltration to the soil surface. This is of course the minimum of information that is required to effect top boundary changes to the modelling structure, and the mechanics of that modification are outlined in 6.1.2. The immediate requirement here is some knowledge of runoff production from differing vegetation covers.

4.5.2 Available runoff/vegetation data

An extensive literature search was undertaken to ascertain the availability of runoff data for different vegetation types. In summary, nearly all available material that could be found, was inappropriate to Hong Kong conditions on the basis that the slopes studies were too shallow and the rainfall regime was too dissimilar to the high intensity tropical rainfall experienced here. Table 4.9 summarises selected material from that literature search. This situation forced the analysis to centre on work

undertaken in Hong Kong alone. In this regard two pieces of work are relevant to this study. Firstly the work reported by Hsu (1983) in which a chunam and a grass slope were monitored for runoff. The slopes at the Chinese University of Hong Kong were some 50 - 60 m², with the chunam slope being at 45° and the grass slope at 40.5°. Figure 4.33 shows results from two storms of different intensity. Reanalysis of their results was undertaken and presented in the form of Figure 4.39. Of particular interest from these results is the fact that the grass slope generates significant runoff (20-35%) for storms of moderate intensity.

Certain caution needs to be exercised in the interpretation of the numerical results from this study however. The small plot size will be recalled, and with it the very small runoff volumes that are recorded, even in the most intense storms. To effect a measurable stage rise (maximum 30 cm), the recording V-notch weir was designed with a 2.12° angle. There is no evidence in the report to detail calibration of the weir with the British Standard weir flow formulation quoted in the report. If indeed no calibration was made it is most likely that the absolute discharge values are in error, although the comparative response of chunam and grass may still be valid.

The second area of direct relevance to the work here is that relating to grass and tree species planting practice in Hong Kong. This is fully documented in G.C.O. (1983). Table 4.10 illustrates the principal grasses used, and emphasises that most of the work in Hong Kong to date has concentrated on planting and establishment rates in association with erosion control. Appended to Table 4.10 is a qualitative assessment of possible runoff production from different grasses (Forbes, personal communication). It must be stressed that there is as yet, no field evidence in Hong Kong for runoff discrimination by grass, or other vegetation types, and that the possible runoff production inclusion in Table 4.10 is a personal assessment that there may well be expected to be significant differences in runoff by grasses currently employed in Hong Kong.

4.5.3 Runoff plot requirement

From the foregoing discussion, it is evident that both to acquire runoff data from different vegetation covers employed in Hong Kong, and to enable modifications to be made to the top boundary condition of the soil water model, it was necessary to establish plot studies within the current project. Only in this manner it is argued can the effect of cover be adequately assessed, bearing in mind the near absence of relevant data as we have observed. At the time of writing, runoff plots were being established, or in the planning stage:

- (a) Chunam : Clear Water Bay Road (Plate 4.1)
- (b) Grass : Clear Water Bay Road (Plate 4.2)
- (c) Grass : Tsuen Wan (Figure 1.7)
- (d) Shrubs and grass : Tsuen Wan (Figure 1.7)
- (e) Mature shrubs and trees : Tsuen Wan (Figure 1.7)
- (f) - (h) Newly seeded plots : Chuk Yuen (Figure 1.7)
- (i) Grass fill slope : Kohima Barracks (Figure 1.7)

The approximate plot size for all sites is 400 m^2 and necessary drainage modification, as required, are currently underway. Runoff will be recorded by Clarke water level recorders (maximum stage 225 mm) using 7 day clockwork mechanisms.

Whilst Nassif and Wilson (1975) have shown that the effect of slope angle on infiltration rates in grass slopes is negligible on slopes in excess of 25° , it was considered desirable to establish three trial plots (f - h) on the same slope location. This allows hydroseeding and turfing to be undertaken on two plots, with a change to the standard hydroseeding mix to be undertaken on the third plot.

Thus, having established the need for undertaking the empirical work with regard to vegetation - runoff data in Hong Kong, it is anticipated that results from the above mentioned plots will be available in 1984.

5. GENERAL APPLICATIONS OF SOIL CHARACTERISTIC CURVES AND RELATED DATA

5.1 INITIAL APPLICATION OF SUCTION-MOISTURE CURVES

In 3.2 it was shown that suction-moisture curves can be approximated in many instances by a straight-line relationship on a log-log plot, with regression coefficients a and b . This fact has great potential in the utilisation of these curves and the following sections detail the estimation of the coefficients a and b for selected Hong Kong soils together with applications of these coefficients to the estimation of cover effects and in terms of landslide warning improvements for Hong Kong. It is firstly necessary to estimate the a and b parameters.

5.1.1 Determination of a and b coefficients

The data in McFarlane (1981) were analysed in detail and indeed a linear relationship is obtained on a log-log plot. The values of " a " and " b " were obtained for each sample tested. Figure 5.1 shows the values of " a " plotted against " b " for the samples tested and for the 5 results presented in Campbell (1974). Rawls et al (1981) present statistical data on moisture contents at 33 and 1500 kPa suction for various soil types. The values of " a " and " b " as determined from these data are also shown in Figure 5.1. It is seen that different soil types are grouped in different parts of the plot. This provides a classification of soil based on suction-moisture characteristics similar to Casagrande's plasticity chart based on soil consistency. A lower limit of all the points is conveniently represented by the line $a = \frac{b}{3} - 1$. It is seen that soils of similar grading lie on a straight line, but that position on the line varies tremendously depending on soil structure. For the Tai Po Volcanic, the " b " value ranges from 31 to 36 for the natural material and from 15 to 30 for the remoulded material. The variation in " b " value can be attributed to the difference in remoulding moisture content. For the King's Park Granite, while the " b " value of the natural material is around 6, it ranges from 11 to 18 for the remoulded material. This time no simple explanation for the variation of b is found.

For practical purposes, the proposed moisture-suction relationship can be considered valid up to 1 kPa suction, where field saturation can be deemed to occur. This is a convenient end point since $\log 1 = 0$ and 1 kPa also represents the limit of precision of measurement of field suction. The average degree of saturation at 1 kPa suction as calculated from the proposed moisture-suction relationship (taking into account volume change) is 92% for the granite and 96% for the volcanic.

One of the great advantages of being able to express the moisture suction curve in the form $\log \psi = -a - b \log \theta$ is that unsaturated permeabilities can be estimated easily from it. Several methods have been proposed for obtaining unsaturated permeabilities from numerical integration of the soil suction-moisture curve based on idealized model of an assembly of fine capillary tubes of various diameters. These methods are found to be quite accurate when the permeabilities are normalized (matched) by a measured value at one water content, generally at saturation. Campbell (1974) showed that when the suction moisture relationship can be expressed in the form $\log \psi =$

- a - b log θ , the unsaturated permeability can be expressed in the form:

$$K = K_s \left(\frac{\theta}{\theta_s} \right)^{2b+3} \quad \text{in terms of } \theta, \text{ or} \quad (5.1)$$

$$K = K_s \left(\frac{\psi_s}{\psi} \right)^2 + \frac{3}{b} \quad \text{in terms of } \psi. \quad (5.2)$$

Taking field saturation to be represented by a suction of 1 kPa as before, the above equation is plotted in Figure 5.2 for different values of b. This figure can be used to estimate the effect of a protective cover (such as chunam) in reducing infiltration and maintaining suction. When the rate of infiltration is limited to an amount less than the saturated permeability of the soil, the suction in the soil will be kept at the value where the unsaturated permeability is equal to the rate of infiltration. From the graph it can be seen that for b = 6 to 30 obtained for Hong Kong soils, protective covers 10, 100 and 1000 times less permeable than the soil would maintain suctions of 2 to 3, 6 to 9 and 16 to 27 kPa respectively.

In this analysis it is assumed that the empirical equation derivations relating moisture content and soil suction (used to estimate b) exhibit correlation coefficients in excess of 0.95, since utilization of equation (5.2) in the manner described and illustrated in Figure 5.2 depends on using a regression equation as X on Y, although computed for Y on X.

5.1.2 Utilization of suction moisture curves to estimate water table rise

The suction-moisture curve gives of course a measure of volumetric moisture content at specified suctions. In the context of water table rise through vertical infiltration, it is therefore implicit, that, given known soil water conditions in the profile to the water table, the amount of infiltration required to raise the water table x metres, establishing a new soil water profile, can be estimated. To ease the method of computation and analysis, it is more convenient to consider a solution as estimated by drainage. Initial trials at estimation of a solution by wetting were not completely successful. To complete a solution by drainage, the following assumptions are made:

- (a) Infiltration takes place vertically, there being no other form of recharge
- (b) The soil is homogeneous
- (c) The water table is horizontal
- (d) Both initial and final soil water conditions in the profile are hydrostatic
- (e) The suction moisture content of soil can be described by a linear log-log plot (equation with coefficients a and b)

There is therefore no hysteresis, and saturation occurs at 1 kPa. (ψ is suction in kPa and θ the volumetric water content).

From an initial condition with the water table at the surface, assume that drainage from below lowers the water table by an amount H, then the amount of drainage is given by:

$$I = \int_0^H (\theta_s - \theta_x) dx \quad (5.3)$$

where θ_x is the volumetric moisture content of the soil at a distance x metres from the water table. (see Figure 5.3a)

$$\begin{aligned} \text{Since } \log \psi &= - (a + b \log \theta) && (a \text{ and } b \text{ treated as positive}) \\ &= - (\log 10^{-a/b} + \log \theta^b) \\ &= - \log 10^{a/b} \theta^b \end{aligned}$$

$$\text{then } \psi = (10^{a/b} \theta^b)^{-1}$$

$$\text{or } \theta = \frac{1}{10^{a/b}} \cdot \frac{1}{\psi^{1/b}} \quad (5.4)$$

For hydrostatic equilibrium, $\psi = \gamma_w x + 1$

$$\theta_s - \theta_x = 10^{-a/b} - 10^{-a/b} \psi^{-1/b} = 10^{-a/b} (1 - (\gamma_w x + 1)^{-1/b})$$

$$\int_0^H (\theta_s - \theta_x) dx = 10^{-a/b} \int_0^H (1 - (\gamma_w x + 1)^{-1/b}) dx$$

$$\begin{aligned} &= 10^{-a/b} \left[x - \frac{1}{\gamma_w} \frac{(\gamma_w x + 1)^{1 - 1/b}}{1 - \frac{1}{b}} \right]_0^H \\ &= 10^{-a/b} \left[H - \frac{(\gamma_w H + 1)^{1 - \frac{1}{b}}}{\gamma_w (1 - \frac{1}{b})} + \frac{1}{\gamma_w (1 - \frac{1}{b})} \right] \end{aligned} \quad (5.5)$$

Equation 5.5 gives the depth of water (m) drained, in lowering the water table from the surface to depth H . Of course, the amount of water drained in this manner is equivalent to that water (infiltration) required to raise the water table from H to the surface. This can then be generalised to provide the infiltration, I (M), necessary to raise the water table from depth H_2 to H_1 :

$$\begin{aligned} I = 10^{-\frac{a}{b}} &\left[\left(H_2 - \frac{(10H_2)^{1 - \frac{1}{b}}}{10(1 - \frac{1}{b})} + \frac{1}{10(1 - \frac{1}{b})} \right) - \right. \\ &\left. \left(H_1 - \frac{(10H_1)^{1 - \frac{1}{b}}}{10(1 - \frac{1}{b})} + \frac{1}{10(1 - \frac{1}{b})} \right) \right] \end{aligned} \quad (5.6)$$

Thus, in H_2 metres of soil (initial depth to water table) I m of infiltration are required to raise the water table $(H_2 - H_1)$ metres (Figure 5.3b).

In equation (5.6) with respect to equation (5.5), $\gamma_w H + 1$ is approximated by $10H$.

Using equation (5.6), parameterised for specific soils by coefficients a and b from Figure 5.1, then for a soil depth (H_2) of 10 m, Figure 5.4 shows the response of selected soils to given amounts of infiltration. Figure 5.5 shows the corresponding results for a 20 m depth of soil. These figures show the relatively greater responses for the volcanic soils compared to granitic soils for similar infiltration amounts.

5.1.3 Modification of the existing criteria for the issue of a landslide warning

The current (1983) practice for issue of a landslide warning incorporates a relationship between recorded rainfall on days 1-15 and day 16 rainfall, as shown in Figure 5.6. Such an index measure is likely to overestimate risk, since no account is taken of drainage in the 1-15 day rainfall. The presence of a large storm can, therefore, have a significant distorting effect. It is proposed that some improvement to the current procedure can be made from the work reported here.

The proposed modification to the index employs, for the depth of interest selected in the context of landslide risk, observed or predicted suction recovery, combined with the drainage model given in equation 5.6. The modified index is illustrated with respect to the June 17 1983 storm of 285 mm.

Figure 5.7 shows the recorded rainfall, together with two hypothetical storms which will be used to illustrate the difference between the two methods of warning estimation.

Consider the soil suction at 0.9 m depth, location J at Clear Water Bay Road site (Figure 4.7). Figure 5.7 shows the measured suction in response to the June 17 storm. If conditions are then taken to be hydrostatic, the water table depths can be estimated during the period as shown in Figure 5.7. It is then, for the given material as characterised by coefficients a and b , a matter of substitution in equation 5.6 for two water table depths, to determine the amount of drainage taking place between two selected times. This drainage can then be interpreted as an amount by which the rainfall in the 1-15 day index should be reduced by at any time.

This estimation was undertaken for the Clear Water Bay site as shown. H_1 was set at 2 m on 23 June, and H_2 set at 2.6 m on 26 June to estimate the response to hypothetical storm 1. For hypothetical storm 2, H_2 was set at 2.8 m on 30 June. Accordingly, drainage losses were calculated by equation 5.6 and subtracted from the 1-15 day rainfall. Figure 5.7 illustrates the 1-15 day rainfall estimations by the modified index and the current summation index, for the two hypothetical storms. Figure 5.8 plots the positions of these storms in relation to the warning line. It is clear that for the intense storm 2, the current index would have prescribed the issue of a warning, whilst the modified index (in accommodating drainage) would not have done so, in fact by a significant margin.

Whilst the method outlined may provide a more realistic framework for detailing the antecedent conditions, it should be noted that the following elements are required to apply the procedure :

- (a) the selection of the parameters 'a' and 'b' (see figure 5.1) which have been adopted to describe the suction-moisture curve. The question of both the spatial variability within materials and the between material differences in suction moisture curves becomes a key element. Clearly a conservative ('safe') approach of straightward simplicity is to select, for universal application of the method, the steepest suction-moisture curve determined for material in Hong Kong. This upper bound will represent conditions of least drainage, and be associated with the highest values of the gradient b.
- (b) the selection of a depth of interest. This is a requirement so that the hydrostatically implied water table depth can be assessed (see figure 5.7).
- (c) the determination of suction recovery to provide for estimation of the falling water table. There are three possibilities :
 - (i) measurements of past storm suctions as dictated by the likely occurrence of storms, following a particularly large event (e.g. June 17 1983). In this case, then sites must be selected which are considered in some way representative.
 - (ii) Recovery of suction can be predicted as has been shown by equations 4.6 - 4.9.
 - (iii) Perhaps most usefully however, are rates of similar suction recovery in past storm conditions as shown in figure 5.9. Further soil suction data could be analysed confirm these rates at given depths.

It should be noted that both from the data used to obtain figure 5.9 (see figures 4.19 and 4.20) and from the Clear Water Bay Road application of the proposed model (figure 5.7) a linear rate of drainage, in the context of mm rainfall equivalent, is observed. This may well therefore serve to support the application of a simpler linear reduction technique to antecedent rainfall in the 1-15 day index, without the need to resort to the more detailed method outlined here. This possibility is currently being examined by J. Premchitt.

5.1.4 Summary of principal applications of suction-moisture curves

- (a) Suction-moisture relationships in residual and remoulded Hong Kong soils are linear in a log-log plot over a wide range of suctions and therefore can be described by two parameters a and b where $-a$, $-b$ are the intercept and gradient of the straight line in the plot.
- (b) Different soil types and soil structures are reflected in the values of a and b . A graphical plot of a against b provides a classification based on suction-moisture characteristics (Figure 5.1) similar to Casagrande's plasticity chart based on soil consistency.
- (c) Remoulded soils of similar grading exhibit a wide range of suction-moisture characteristics depending on the remoulding conditions. For Tai Po Volcanic this can be attributed almost entirely to the remoulding moisture content. For King's Park Granite the interaction between remoulding moisture content and density are too complex to allow simple analysis.
- (d) Ratio of unsaturated to saturated permeability can be estimated by Campbell's method (Figure 5.2) and from it the effect of surface protection cover in maintaining suction can be assessed. Protective covers 10, 100 and 1000 times less permeable than the soil would maintain suctions of 2 to 3, 6 to 9 and 16 to 27 kPa respectively in one-dimensional infiltration.
- (e) For the ideal case of one dimensional infiltration under initially hydrostatic conditions, the responsive rise of water table to infiltration can be estimated from the suction moisture characteristics (Figures 5.4 and 5.5). A water table in natural Tai Po Volcanic would respond much more violently than one in natural King's Park Granite, for the same amount of infiltration. This can be attributed to the higher initial degree of saturation in the volcanic. Remoulded soils would exhibit a wide range of response depending on the structure of soil produced by remoulding.

- (f) The current landslip warning index can be modified by accounting for drainage in post storm conditions. The modified index utilises the suction-moisture curve, and the drainage model outlined in equation 5.6.

5.2 PREDICTING THE EFFECTS OF CRACKS IN CHUNAM

In section 4.2 initial data relating to chunam characteristics in terms of permeability and suction-moisture curves were obtained. In that section, the analysis dealt with chunam as being intact. The laboratory investigation on the effect of the chunam mix on the resulting characteristics of the chunam, showed conclusively that shrinkage was the major result of mix variations.

In the field, the consequence of such shrinkage is of course cracking, and it is therefore necessary to consider evaluating cracked chunam in the context of determining the effectiveness of chunam cover in reducing infiltration.

Cracked chunam effectiveness can be evaluated in two ways, either a model for flow through cracked chunam could be established and a selective field study undertaken to parameterise such a model, or a substantial field programme of monitoring could be undertaken. The resources of the project together with the range of solutions desired, made it desirable that the former approach was taken.

5.2.1 Establishment of a model to predict flow through chunam cracks

A seepage model, outlined by Harr (1962) was adopted and used for this purpose. Here a crack of width B and vertical extent (chunam thickness) H is assumed. The flux passing through the crack can then be determined by:

$$B = \frac{8q}{K\pi^2} \sum_{n=1}^{\infty} \frac{e^{-(2n-1)\alpha}}{(2n-1)^2} \quad (5.7)$$

$$\text{where } \alpha = \frac{\pi KH}{q}$$

and where K = soil permeability ms^{-1}
 B = crack width m
 q = flux m^2s^{-1}
 H = chunam thickness (head) m

Since α is a function of q , q can be found only by iteration.

Of major interest in terms of effective chunam protection is the effective crack width (B_1 - see figure 5.10) and the effective width at depth when the seepage becomes parallel (B_∞). The former spread immediately under the chunam can be given as:

$$B_1 = \frac{4q}{K\pi^2} \sum_{n=1}^{\infty} \frac{1 + e^{-2(2n-1)\alpha}}{(2n-1)^2} \quad (5.8)$$

whilst the spread at depth becomes:

$$B_{\infty} = q/K \quad (5.9)$$

Table 5.1 illustrates solutions to equations 5.7-5.9 with $H = 0.05$ m, $K = 1 \times 10^{-6} \text{ ms}^{-1}$ and selected values of crack width B . It is to be noted from these results that the ratio of $B:B_{\infty}$ is approximately 1:10.

However, before such a model can be considered suitable for application it is necessary to determine the crack permeability with respect to the soil permeability below, since in the above solution it is assumed that there is no head loss within the crack. The following parallel plate flow model (Massey, 1970) can be used:

$$Q = \frac{bB^3}{12\mu} \left(\frac{dp^*}{dx} \right) \quad (5.10)$$

where b = length of crack
 B = crack width
 p^* = piezometric head
 $\frac{dp^*}{dx}$ = piezometric head gradient along direction of flow
 ρ = density of fluid
 g = gravitational acceleration
 i = hydraulic gradient
 μ = viscosity
 (see Figure 5.10)

By Darcy's Law equation 5.10 reduces to

$$K = \frac{bB^3}{12\mu} \rho g \quad (5.11)$$

for unit area calculation.

If the crack spacing is regular and of distance S , then the total length of transverse and longitudinal cracking per unit area is

$$b = \frac{2}{S}$$

and thus

$$K = \frac{B^3}{S} \left(\frac{\rho g}{6\mu} \right) \quad (5.12)$$

Taking $\mu = 1.0 \times 10^{-3} \text{ kg m}^{-1} \text{ s}^{-1}$ at 20°C then (5.12) can be evaluated for different crack widths (B) and crack spacing (S), thereby providing estimates of crack permeability. Selected estimations are provided in Table 5.2. Calculations show the unrestricted permeability of cracks in chunam is likely to approximate 10^{-3} ms^{-1} , which is far greater than the underlying soils. Thus, it can be assumed that the flow in cracks is governed by the soil permeability, and by equations 5.7-5.9.

On this basis then, values of flux for different crack widths, and soil permeabilities, assuming a crack depth of 50 mm have been calculated (utilizing equations 5.7-5.9). Figure 5.11 shows the change in flux for changing crack widths. These results show that the influence of crack width is small, since the effective crack width B_{∞} is controlled principally by the head (H).

The solutions presented in figure 5.11 confirm the minimal head loss that occurs in the crack prior to entry. Taking a 1 mm crack at 1 m spacing with a soil permeability of $K = 1 \times 10^{-5} \text{ ms}^{-1}$, then from Figure 5.11 $q = 4.38 \times 10^{-6} \text{ m}^2 \text{ s}^{-1}$ and from Table 5.2 $K = 1.64 \times 10^{-3} \text{ ms}^{-1}$. Since head $H = q/K$ by Darcy's Law then the actual head loss = $1.3 \times 10^{-4} \text{ m}$, or 0.27% of the total head of 0.05 m.

With these conditions it therefore becomes possible to estimate the equivalent permeability of chunam. The total flux through the chunam (Q_T) is given by:

$$Q_T = Q_i + Q_c \quad (5.13)$$

where Q_c = flux through the crack
and Q_i = flux through the intact chunam

For a unit area the effective chunam permeability (K_e) is

$$K_e = K_i + q_o \left(\frac{2}{S} \right) \quad (5.14)$$

where K_i is the permeability of intact chunam, with crack spacing S as defined in equation 5.12. Figure 5.12 illustrates the effective permeability of chunam (K_e), based on solutions to equations 5.7-5.9 and 5.14 with a crack width of 12 mm. This illustrates the dependency of the effective chunam permeability on the permeability of the underlying soil.

Thus, the effective permeability of chunam can be estimated by use of the crack model (equations 5.7-5.9), knowledge of the intact permeability of chunam (K_i - see Section 4.2) and the crack spacing (see equation 5.14).

Having established the methodology for this estimation procedure, a limited crack survey was undertaken to present an evaluation of chunam performance based on the model procedure outlined. It is to be noted that a laboratory investigation in which the principal aim was to validate the model predictions (equations 5.7-5.9) had been initiated but was incomplete at the time of writing.

5.2.2 Application of the model of effective chunam permeability to field conditions

A field survey of chunam cracks was undertaken in order to parameterise the crack model (equations 5.7-5.9) and thereby to facilitate an estimation of effective chunam permeability. Eight sites were selected for this analysis. These are detailed in table 5.3. The quality of the chunam was classified in the 'CHASE' report on the basis of visual inspection only.

The field survey, carried out for these eight sites followed the procedures below:

- (a) an area with a crack density representative of the chunam surface was selected
- (b) a 1 m^2 area was marked on the surface
- (c) the widths of the cracks and their corresponding cumulative length within the area were measured
- (d) for large extents of chunam, two areas were selected for measurement in order to improve the representative aspect of the survey. These were designated areas A and B.

Table 5.4 summarises the data obtained, and plates 5.1-5.8 illustrate the actual sites.

The crack length and width data obtained was then used to estimate the flow through the cracks, according to the relationships shown in Figure 5.11. Ignoring hairline cracks, this summation of total seepage was evaluated for each site and is shown in table 5.5. The seepage, together with the intact chunam permeability, taken to be $1 \times 10^{-8} \text{ ms}^{-1}$ (see Table 4.1) allows the effective chunam permeability, K_e , to be calculated by equation 5.14, where regular crack spacing is now replaced by total length estimation (Table 5.4) as shown in Figure 5.13.

Figure 5.14 summarises the effective permeability predictions made on the basis of the field survey and the crack model as reported in Table 5.5. These results suggest that for soils of high permeability ($1 \times 10^{-4} \text{ ms}^{-1}$) the condition of the chunam needs to be good for the chunam to be considered effective. In Figure 5.14, good protection is considered to be an effective chunam permeability of less than $1.0 \times 10^{-6} \text{ ms}^{-1}$ the duration of rainfall is the only important factor (see Figure 5.15).

In the interpretation of Figure 5.14 and Table 5.5 several factors must be noted:

- (a) the effective permeability, in association with crack condition (poor - average) is a predicted association by equation 5.7-5.9.
- (b) the model used for the prediction assumes no void space below the chunam. Field conditions frequently suggest the presence of such a void (hence a likely increase in effective crack width B_{∞} - Figure 5.10). We might therefore expect the protection level of chunam to be lower by this factor than Figure 5.14 would suggest.
- (c) the crack model assumes the crack to be formed by two parallel plates. Departures from this condition in the field may lower head losses within the crack and this factor may increase the protection shown in Figure 5.14.

5.2.3 Summary of modelling crack effects in chunam

- (a) A model has been outlined which predicts flow through cracks under specified conditions (equations 5.7-5.9).
- (b) This model can be used to estimate the effective permeability of chunam with cracks (Figures 5.12 and 5.13, equation 5.14).
- (c) From a field crack survey, chunam effective permeability was predicted for poor to average chunam condition cover, as defined by the CHASE report (Figure 5.14).
- (d) From the standpoint of rainfall intensity, an effective chunam permeability of $1 \times 10^{-6} \text{ms}^{-1}$ or less needs to be achieved (Figure 5.15). This is the distinction made in the summary graph (Figure 5.14).
- (e) Selected factors have been outlined which may serve to reduce or increase the effective permeability of chunam for a specific crack distribution. These are factors such as vertical crack irregularity and void space at the chunam-soil interface that are not modelled.
- (f) The effective permeability of $1 \times 10^{-6} \text{ms}^{-1}$ renders the slope independent of rainfall intensity (Figure 5.15), and in consequence, only dependent on rainfall duration.
- (g) Whether $1 \times 10^{-6} \text{ms}^{-1}$ is a sufficiently low effective permeability to render the underlying soil free from saturation under specific rainfall duration recurrence intervals, can only be answered by reference to simulation studies undertaken by the soil water model outlined in Section 3.0.

6. APPLICATIONS OF MODELLING CAPABILITY

6.1 ONE DIMENSIONAL VERTICAL INFILTRATION MODEL

The basis of this model has been outlined in section 3.0, together with the general circumstances in which it can be used. Before any application can be made using the model with respect to evaluating the performance of chunam, or indeed any other purpose, it is necessary to undertake a series of validation tests : The programme of validation tests is outlined in the following section, after which the effectiveness of different slope covers are simulated.

6.1.1 Validation of vertical infiltration model

Table 6.1 details the five locations which were selected for the validation programme. A range of geology, storms, cover, and simulation depths were selected.

For the Mid-Levels sites (locations 1-3), permeability values were taken from the Mid-Levels report figures 3.1-3.3. Suction - moisture curves were used as shown in table 6.1. Curves additional to these already referenced were required, and figure 6.1 shows these for CDV and colluvium. The former curve was established in the laboratory, whilst that for colluvium was a matched curve from the PSD data given in the Mid-Levels report (tables B1-B3) (after Arya and Paris, 1981). All simulations assumed a surface detention capacity of 0.02 m, with the exception of the chunam site at Clearwater Bay in which surface detention was set to zero. The simulation iteration time used was 30 seconds.

Location (1)

Figure 6.2 shows the results for the simulation of the August 30 storm at Realty Ridge. The simulation was started on 29 August 1980 at 000 hours and run through at the 30 second calculation time interval, to 5 September 1980. The predictions for 5 September are shown (at 0900 hours), together with the minimum suctions simulated during the seven day period. It must be noted here that such minimum suctions as shown, do not necessarily occur simultaneously throughout the profile. The predictions for 5 September are generally in error by less than 5 kPa.

Location (2)

In colluvium, field evidence suggests suctions tend to zero throughout profiles to depths of up to 20 m (figure 1.1) figure 6.3 shows the results of simulating the storm of May 9-11, 1981 at Chater Ridge. Start conditions used were those measured, as shown, and the simulated end of storm suctions (72 hours) accord very closely with the measured values - everywhere better than 5 kPa.

Location (3)

Sweeney (1982) reports a Mid-Levels site in CDG with recorded suctions to 38 m depth (see figure 6.4). There are no storm response data for this site, but the general thesis of Sweeney's report

is the suggestion of maintained suctions. As this is the deepest recorded suction data for Hong Kong it was considered appropriate to undertake a simulation, the only element of 'validation' being the presumed absence of saturation throughout the profile. Figure 6.5 shows the result of simulating the May 1981 rainstorm (figure 6.3) on the 'start' conditions shown for 13 September 1980 in figure 6.4 (being reasonable wet season values). From the results of the simulation it can be seen that suction is maintained, although near zero values are recorded within the colluvium. In figure 6.5 it is the worst suctions for each depth during the storm and five day post storm period that are plotted.

Location (4)

On the chunam slope of Clear Water Bay Road (plate 4.1), location C was selected (figure 4.6) for the simulation. It has already been shown that flow is dominantly vertical throughout the chunam slope to the instrumented depth of 4 m (figure 4.26). Using the chunam permeability determined for this site in addition to the suction moisture curve, a simulation was undertaken of the response to the 17 June 1983 rainstorm event (see figure 4.14). Figure 6.6 shows the measured and predicted suctions in the six day period 16-21 June 1983. The simulation time increment used was 20 seconds, although in the graphed comparison only predicted values at times coincident with the observed values are plotted. Correspondence between measured and predicted values is seen to be good with again errors less than 5 kPa with the exception of 0.9 m depth, where errors are seen to be approximately 6 kPa after June 18 (post storm).

Location (5)

At the grass slope at the Clear Water Bay site, location I was selected for the simulation of the same 17 June 1983 storm. Figure 4.7 details the exact location which corresponds to location C on the chunam slope. Figure 6.7 shows the measured and predicted values. In this instance because of nature of the surface cover, the data from the Chinese University runoff study was used to provide an estimate of runoff due to the vegetation. For the storm of 17 June this would be estimated from figure 4.39 to be approximately 40%. Thus 60% of the rainfall shown in figure 4.15 was applied to the model. This aspect of incorporating vegetation type in the model as the top boundary condition is treated fully in section 6.1.3. The predictive performance at this location is relatively poor. The principal reason for this is seen to be incomplete knowledge of the vegetation canopy induced runoff, together with root zone permeability.

Location (6)

At Tai Po, St. Christopher Bend this formed part of a two dimensional simulation which is reported in section 6.2 below. However, the one dimensional model was used at location T3 at this study site (see figure 4.31) to simulate conditions relating to the storm of 10-14 July 1981. The suction moisture curve used was that for colluvium (figure 6.1b) and CDV at 2 m (figure 6.1a). Start conditions were these shown in figure 6.8 for 10 July and the permeabilities used were the measured permeabilities for colluvium

and CDV (G.C.O. (1982) figures 3.1 and 3.2). Figure 6.8 shows that hydrostatic pore pressures were recorded in the near surface zone to 2 m depth (representing local perching of water). The model, as set up could accommodate perched water induced by permeability decrease. Due to the absence of further field data a constant permeability of $2 \times 10^{-8} \text{ ms}^{-1}$ was applied from 0.3 m to 6 m. Indications are therefore of a decrease in permeability within this zone. This example again emphasises the near overriding importance of knowledge of the permeability in order to predict soil water response to desired levels of accuracy; emphasizing the observations to be made in the following section.

6.1.2 Summary of infiltration model verification

- (a) For locations 1-4 (table 6.1) there is generally good agreement between measured and predicted soil suction values. The relatively constant permeability with depth within given geologies at certain locations has been noted, and this must account for the good performance of the one-dimensional model as shown.
- (b) In locations 1-3 no runoff modification to the rainfall was made i.e. it was assumed that all rainfall was available for infiltration. The interest here is the good performance of the model at the two Mid-Levels sites where there is mature vegetation, suggesting the absence of canopy runoff. Available storm loss data for the Mid-Levels (G.C.O. 1980 table 2.5 and figure 2.7) are generally supportive of this, although the quality of the data is acknowledged to be poor.
- (c) Chunam protection has been shown to be capable of being modelled satisfactorily (location 4). However, due to the thin upper layer in the model representing chunam, instability was found to occur in several trial runs due to too large a time increment for simulation and a correspondingly too small a computational point distance (see figure 3.5).
- (d) For grass slopes, the evidence confirms the known requirement to have accurate knowledge of canopy induced runoff and root zone permeability, before adequate simulations can be satisfactorily undertaken. This aspect is treated in Section 6.1.3.
- (e) The specific conditions which are suitable for the vertical infiltration model and the data input accuracy needs are outlined in section 6.3.

6.1.3 Predictions of soil water conditions in decomposed volcanics

In section 1.1 it was shown that what limited field evidence there was in terms of soil suction for Hong Kong, suggested that in most materials. Other than perhaps, the CDV, suctions were reduced to zero in wet season conditions. It is therefore of interest to examine the predictions of the vertical infiltration model in this regard.

The model was set up with the following input data :

Suction - moisture curve : CDV figure 6.1

Saturated permeability	: G.C.O. (1982) figure 3.3
Start conditions in profile	: G.C.O. (1981) figure C2.18 (as figure 6.2)
Surface detention	: 0.02 m

The storm rainfall to be used represents a problem of resolution in utilising finite difference models. Table 6.2 shows the rainfall for various recurrence intervals in Hong Kong. There is of course no information on the distribution of rainfall within the specified duration. However, the finite difference model as structured for the research project had the capability to input hourly rainfall. Thus, an even intensity of rainfall has to be assumed to give the worst conditions for suction maintenance in any specified duration. This was the initial strategy adopted. Figure 6.9 shows the results of applying 1 in 100 year rainstorms of specified duration (2 hour to 15 day) as given in table 6.2, on the profile conditions as specified above (lowest suctions are plotted).

The depth of the elimination of soil suction is of course dependent upon storm duration, with the 48 hour and 7 day storms inducing perching at the 5-10 m depth range. The 15 day storm now yields a depth of saturation less than the 7 day since the rain intensity falls to a value just below the saturated permeability of the soil. Table 6.3 summarises the runoff and infiltration results.

It is to be recalled that the storms used in figure 6.9 are of even intensity. The effect of redistribution of the specified rainfall within the storm duration is worthy of examination. Figure 6.10 illustrates changes that were made to the 1 in 100 year 24 hour storm to illustrate this factor. Storm reallocations (1-3) produce little change in the lowest suctions recorded at each depth. Storm (4) however produces a measurable increase in the minimum recorded suction, since for 20 of the 24 hours the rainfall is at a rate less than the saturated permeability of the lowest soil layer (K_3 - figure 6.9).

Undertaking a similar sensitivity analysis, but this time with respect to the saturated permeability of each of the three soil layers yields much more significant changes in predicted suctions. Figure 6.11 shows the result of both increasing and decreasing the permeabilities used in figure 6.9 by half an order of magnitude. This magnitude of change is within the measurement error of such determinations in the field, as shown by figures 3.1-3.3 in G.C.O. (1982).

For a decrease in permeability by half an order of magnitude then significant suctions are maintained to depths below 7 m; whilst an increase in permeability of the same amount renders the profile saturated to approximately 20 m depth.

The salient aspects of this analysis are therefore :

- (a) With vertical infiltration only, suctions in CDV can be destroyed by 1 in 100 year storms to depths of 18 m, if the permeability is taken as $1 \times 10^{-6} \text{ ms}^{-1}$.
- (b) Permeabilities less than this value will ensure the maintenance of suctions at progressively shallower depths.

- (c) The evidence clearly shows a requirement to provide permeability data to an accuracy better than half an order of magnitude (see figure 6.11). Failure in this regard will negate any conclusions such as (a) and (b) above.
- (d) The analysis on which the above conclusions are based represents a condition in which lateral throughflow is absent. Such conditions in implying a downslope increase in throughflow discharge would of course lead to less favourable conditions for suction maintenance than those illustrated by figure 6.9.
- (e) The rainfall intensities used in the analysis represent the least favourable from the standpoint of soil suction maintenance, since they are computed as equal rain intensity for the entire storm duration. Trial variations of within-storm intensities reveal suction responses significantly less than changes associated with permeability variations (figure 6.10).

6.1.4 Predictions of chunam 'effectiveness' using the vertical infiltration model

The analysis of chunam permeability and suction-moisture curves in section 4.1, together with the crack model summarised in figure 5.14 facilitates a more detailed assessment of chunam performance by making use of the vertical infiltration model.

Here, layer 1 of the model was set to comprise the chunam surface, having 3 computational points or cells (see figure 3.5) with two subsequent soil layers to 9 m depth. Of course there are innumerable combinations of permeability, rainfall and start conditions that can be used in such a modelling scheme. In addition, it must be noted that the analysis of chunam performance summarised in figure 5.14 assumes a constant permeability of soil with depth. On the grounds just outlined therefore it might be expected that revisions to the chunam effective performance (figure 5.14) could be revised by results from modelling (section 3.0) these conditions of soil heterogeneity and start conditions not so far considered.

A standard suction-moisture curve for chunam was adopted; that of figure 4.2 c, and the suction-moisture curve adopted for the soil was that corresponding to CDG figure 4.27 b. Start conditions in the profile were those of figure 6.4 i.e. a mean start suction of approximately 20 kPa. Two rainfall events are shown here. Firstly, the 9-11 May 1981 event (figure 6.3) of 228 mm was used, and secondly the 1 in 10 year 3 day event distributed according to that event was generated from figure 2.4 in G.C.O. (1982).

Figures 6.12 and 6.13 show the results of simulations using the conditions outlined, and portraying the lowest recorded suction at each depth in a 200 hour simulation period (storm length 72 hours).

Figure 6.12 shows the improvement rendered by a decrease in chunam effective permeability of one order of magnitude to 10^{-7} ms^{-1} . Under the 1 in 10 year event the perched water table, present when $K_e = 10^{-6} \text{ ms}^{-1}$, is absent when $K_e = 10^{-7} \text{ ms}^{-1}$. This result is consistent with the summary plot of figure 5.14 and table 5.5. In that table the conditions in figure 6.12

plot as poor protection ($K_e = 10^{-6} \text{ ms}^{-1}$) and good protection ($K_e = 10^{-7} \text{ ms}^{-1}$) respectively. Although in figure 5.14 this latter condition is classified as good protection (since K_e is two orders of magnitude less than the underlying soil), it is observed from figure 6.12 b that it is just insufficient to prevent saturation occurring.

An increase of K_e to 10^{-8} ms^{-1} under the same storm conditions ('very good' protection as classified by table 5.5 and figure 5.14) renders the soil profile safe from saturation under the 1 in 10 year event used.

As has already been observed, the rainfall conditions represent the worst possible from the standpoint of the destruction of soil suction, since an even rain intensity was used in the model for each of the three day rainfall totals. It is well known that there is considerable intensity variation which would serve to better maintain soil suctions than figure 6.12 and 6.13 would suggest.

From these simulations, as well as others undertaken, it is appropriate to consider $K_e = 10^{-7} \text{ ms}^{-1}$ as a level of protection that under normal field start conditions and typical 1 in 10 year events should maintain at least low suctions. The large permutations of conditions that are possible in relation to this problem cannot all be simulated, but the indications from this analysis are that of $K_e = 10^{-7} \text{ ms}^{-1}$ is an acceptable and realistic boundary value for practical purposes.

It is appropriate in the light of this analysis to refine the associations shown in figure 5.14, to clearly elucidate good protection (i.e. $K_e < 10^{-6} \text{ ms}^{-1}$), and protection likely to ensure the maintenance of some degree of suction (i.e. $K_e < 10^{-7} \text{ ms}^{-1}$). Figure 6.14 shows the appropriate refinement. The associations here were established by the following procedure which obviously has the potential to be more thoroughly researched :

- (a) Determine soil permeability (or estimate from available sources).
- (b) Determine permeability of intact chunam (an estimate from this study should be adequate - see table 4.1).
- (c) Undertake field crack survey (as outlined in section 5.2).
- (d) Use the crack model to determine the flow through the total recorded cracks (as outlined in section 5.2.2)
- (e) Make a preliminary assessment of chunam effectiveness (as shown in table 5.5 and figure 5.14).
- (f) If desired, input the effective permeability determined in (d) (equation 5.14) into the soil water finite difference model in association with the soil permeability (a) to examine the protection under storm types of particular interest.

6.1.5 Modelling surface cover effects - vegetation

The verification procedure of the vertical infiltration model illustrated the need to evaluate the top model boundary conditions in some detail when it is desired to incorporate vegetation (figure 6.7).

In order to provide a modelling capability that can accommodate vegetation cover for Hong Kong then it was considered that three steps were necessary :

- (a) establishment of runoff plots to provide data on vegetation - runoff relationships.
This need has been discussed in section 4.5;
- (b) to examine whether a simple "effective rainfall" concept, having acquired the data in (a), can be used in the current model with sufficient accuracy and discrimination for different vegetation types;
- (c) to evaluate whether, depending on the results of (b), it is necessary to model the processes of transpiration and surface hydraulic behaviour of the vegetation in a more detailed deterministic manner.

As has been outlined in section 4.5, the runoff plots as tabulated in section 4.5 are being established. Prior to the data acquisition in the 1984 wet season however, it is possible to prescribe simple procedures that can be utilised when the runoff data become available.

A basic model of vegetation control on runoff production and infiltration can be envisaged; figure 6.15. In this model two conditions are shown. Firstly, that the vegetation canopy is such that the rain intensity allowed to reach the ground surface is less than the permeability (K_1) of the root zone. Under such conditions no soil surface runoff is possible of course, and any recorded runoff from such a configuration must be initiated at the canopy level, and entirely due to the vegetation therefore.

The second condition shown in figure 6.15, is that in which the vegetation allows a rain intensity through the canopy at a rate which exceeds K_1 . Under these circumstances, soil surface runoff will be generated. Since the throughfall rain intensity exceeds K_1 , the presence of the vegetation, in terms of runoff production at least, is irrelevant.

These basic postulates have a series of related assumptions which must be examined before any uses can be proposed for this initial scheme :

- (a) the runoff induced by the canopy is time invariant
- (b) the hydraulic resistance to flow on the canopy surface is time invariant
- (c) the root zone permeability can be measured in the field, given the steep slope geometry.
- (d) surface detention can be determined in the field for parameterising the soil water model, as discussed below.
- (e) on steep slopes, it is assumed that surface detention allows vertical infiltration, and that the slope is thereby recharged irrespective of slope angle.

If these assumptions and conditions can be accepted then illustrative simulations, using the vertical infiltration model can be used to demonstrate interpretation of data ensuing from the runoff plots.

A profile was set in the vertical infiltration model with start moisture conditions, permeability and suction-moisture curve as shown in figure 6.16. In effect, this represents a profile of CDG in the high permeability range (G.C.O. 1982 figure 3.2). With these conditions, and a surface detention capacity of zero, figure 6.17 shows, for a 1 in 100 2 hour rain storm, the simulated percentage runoff as K_1 varies and the canopy induced runoff changes. Thus in the model, for an assumed 20% canopy runoff (being an assumed characteristic of a particular vegetation type) then 80% of the rainfall (0.8×219 mm - see table 6.2) is made available to the soil surface in the model for infiltration, surface detention storage and possible soil surface runoff. Since 0.8×219 mm in 2 hours corresponds to an intensity of $2.4 \times 10^{-5} \text{ ms}^{-1}$, then at a K_1 value of this, there can be no soil surface runoff.

An equality line (figure 6.17) is thus established. Above this line the vegetation is the dominant barrier, since all the rain that penetrates the canopy can enter the soil (model (b) in figure 6.15). Below this equality line the soil permeability is the dominant barrier. For a given K_1 within this zone, runoff production is a constant, although of course the canopy/soil surface proportions may vary.

With increased surface detention, the runoff responses change. Figure 6.18 illustrates the situation with a soil surface detention capacity of 2 cm - all other conditions are as for figure 6.17. The presence of vegetation is now more important, since the throughfall from the canopy can be stored (water which in the former case - figure 6.18 - would have runoff on the soil surface). This process is shown by the dropping of the breakpoint in the runoff lines.

The procedure for interpretation of the effectiveness of vegetation can be illustrated by reference to figure 6.18 :

- (a) storm size 219 mm in 2 hours
- (b) estimated soil surface detention of 2 cm
- (c) use figure 6.18, derived by simulation for these conditions
- (d) estimate K_1 - say $K_1 = 2.1 \times 10^{-5} \text{ ms}^{-1}$
- (e) obtain total measured runoff - say 35% of storm
- (f) locate K_1 on Y axis of figure 6.18
- (g) move along that K_1 line to the point at which 35% runoff is encountered
- (h) since this point lies above the equality line, then the vegetation is effective (model b, figure 6.15)
- (i) with 0% canopy runoff (i.e. no vegetation) then for $K_1 = 2.1 \times 10^{-5} \text{ ms}^{-1}$ then 10% runoff would result.
- (j) therefore $35\% - 10\% = 25\%$ more runoff occurs than would occur, without the presence of vegetation
- (k) with zero surface detention, and no vegetation for $K_1 = 2.1 \times 10^{-5} \text{ ms}^{-1}$ (figure 6.17) then the runoff generated would be 30%.

This example can be made additionally clear by stating that for 35% runoff to be observed, only 10% runoff is generated by the soil surface

conditions, with the K_1 value of $2.1 \times 10^{-5} \text{ ms}^{-1}$. Hence for 35% runoff, the soil must be unsaturated, and thus all the runoff observed is attributable to vegetation. Figure 6.19 summarises the salient elements of the relationships.

As runoff data becomes available, then it may be possible to assign vegetation type/species to the respective zones above or below the line which demarcates the importance, or unimportance, of vegetation in runoff generation - see figure 6.20.

The simulation model is required for this analysis, since, as can be seen from figure 6.18 the impact of soil surface detention capacity can be significant in terms of moving the vegetation discrimination line away from the permeability/throughfall intensity equality line.

The simulations undertaken here, and presented in figures 6.17 and 6.18 relate to one storm only. As runoff data from the plots that are being established becomes available, then this data can be analysed in the manner outlined in this section for a variety of storm conditions, in order that an average performance of a particular vegetation type can be assessed.

This is, as outlined at the beginning of this section, the first simple form of analysis that should be attempted. Implicit are the assumptions as discussed, which may necessitate more detailed modelling of the top boundary to achieve adequate resolution for vegetation - runoff relationships.

6.2 VALIDATION OF TWO DIMENSIONAL SOIL WATER MODEL

The form of the two dimensional soil water model has been outlined in section 3.2, and is shown diagrammatically in figure 3.5. It is apparent that, as has already been stated in section 3.2 there are specific demands that such a model places on the user that considerably exceed that of the one dimensional model. The principal additional input requirements are :

- (a) knowledge of permeability throughout the slope
- (b) estimation that the groundwater boundary conditions in the field are as modelled
- (c) a slope geometry that permits the model to be adequately set up in terms of a realistic number of computational points.

Clearly, these requirements under Hong Kong conditions and with available data sources are not easy to meet. However, the model was tested at Tai Po, St. Christopher Bend, where certain basic data was available and it was considered further in sights into the modelling restrictions could be gained.

6.2.1 Application of two dimensional soil water model to Tai Po, St. Christopher Bend site

The storm of 10-14 July 1980 was used for the simulation, a storm which has already been observed to induce a 0.4 m rise in piezometric level at the study site piezometer P3. The site plan is given in figure 4.31

and the storm and piezometer response in figure 4.30. Initial moisture conditions were obtained from tensiometer locations T3, T8 and T14; and it was along this transect that the simulation was undertaken. Soil water conditions below the maximum tensiometer depth were extrapolated linearly to the groundwater as given by piezometer P3. The permeability and suction-moisture curve used for this site have already been given in section 6.1. Figure 6.21 shows the results of modelling the soil water response to the storm of 11-14 July. Of principal interest is the discipation of the surface zone of saturation with time, and the charging of the groundwater through vertical unsaturated flow. This mechanism, from the start conditions on July 11 is sufficient to account for a 0.4 m rise in groundwater at P3 by July 13, 1980. This accords with the observed condition (figure 4.30).

It is possible to make limited but useful comparisons of the performance of the soil water simulation model as compared with alternative approaches currently available. Since the model described here, predicts groundwater response, comparisons can be made with predictions from the wetting band theory of Lumb (1975), as exemplified in the GCO Manual (1979). This latter approach pre-supposes direct rainfall addition to the groundwater, albeit at a rate which is a function of material permeability, as given by :-

$$h = \frac{Kt}{n(S_f - S_o)} \quad (6.1)$$

where K = permeability (ms^{-1})
 t = rainfall duration (s)
 n = porosity
 S_f = final degree of saturation
 S_o = initial degree of saturation
 h = rise in ground water level (m)

An alternative approach to the wetting band theory has been developed, and reported in section 5.1.2. In a uniform soil with negative hydrostatic conditions extending from the ground surface to a water table, then with a given suction - moisture curve for the soil, the amount of infiltration required to produce a given groundwater rise can be evaluated. This procedure provides only for initial and final conditions that are hydrostatic (negative hydrostatic above and positive hydrostatic below the water table).

If we compare the predictions of groundwater response by these methods for the July 11-14 storm, then the following results are obtained :

Measured response at P3	0.37 m
Predicted responses :	
(1) Wetting band theory	8.64 m
(2) Suction - moisture curve method	5.00 m (Section 5.12)
(3) Soil water simulation model	0.40 m

The transient nature of soil water conditions above the water table, are not well accommodated by either the wetting band theory or the suction - moisture curve method. This explains the better performance of the soil water simulation model.

Nevertheless, although the two dimensional model has performed well on the transect selected, other transects in the same locality were much less successful on the principal basis that the lower boundary condition of the model (i.e. the groundwater) was inappropriately configured for the field conditions. The site, as has already been outlined (section 4.4) is one in which convergence of soil water has been shown to occur in backslope conditions, and aside from that zone of convergence, groundwater conditions are most likely dominated by three dimensional processes.

There are a set of conditions that can be detailed in which soil water finite difference models may be useful in the context of estimating both the effectiveness of cover and the prediction of soil water conditions in different materials. These aspects are discussed in the following section.

6.3 DISCUSSION OF MODELLING UTILITY FOR DESIGN PURPOSES

6.3.1 Choices of available models to make predictions of soil suctions

Essentially there are three types of 'models' available :

- (a) empirical relationships of the form given in equations 4.6-4.11 where observed data are related by multiple regression methods.
This technique in terms of strict statistical inference, does not allow estimation of soil suctions for recurrence interval storms that are required for design, unless such models incorporate that data from historical records. In addition, a potential weakness in the context of general utility is that such an approach need have no physical basis.
- (b) finite difference approaches of the form used in this report and discussed in section 3.0. Having a strong physical basis, it has been shown that such models have high resolution capability in terms of predicting soil water conditions in the unsaturated zone. There is however, from the standpoint of general utility an increased demand in such models for clear assessments of the input data accuracy, since of course no calibration in the model is involved. Table 6.4 summarises the principal types of accuracy required in the context of applications made in this report.
From this table, as well as from the results of figure 6.11, it is clear that knowledge of permeability to a very high field accuracy is required to substantiate for example, the maintenance or otherwise, of soil suction by the use of finite difference models at a particular site. This point is re-emphasised by cross reference to figure 6.22 which summarises selected permeability determinations for Hong Kong. However, one of the clear advantages such models have is their parsimonious

data input requirement (table 3.3) when compared with the resolution of output. In addition, all the required input data variables relate to routine site investigation information or to laboratory derived elements (e.g. suction - moisture curve) of which there are an increased amount available (see section 4.0).

- (c) finite element approaches, which have certain advantages over finite difference models. The primary advantages are those of generality and treatment of the boundary conditions (see Papagiannakis, 1982 and table 6.4). Whilst the general model equations and accuracy needs parallel those of the finite difference models, programming solutions for finite difference models are easier. Within the available time for the project, and bearing in mind the specific requirements of the research, time was not available to develop a general finite element model. It is contended here that the finite difference approach was appropriate given these balance of advantages.

6.3.2 Summary of circumstances in which soil water conditions can be accurately estimated for design purposes

The general distillation of approaches and data needs given in 6.3.1 and table 6.4 can be used to prescribe sets of field circumstances in which the methods outlined in this report can be expected to provide acceptable estimates of soil water conditions. These field conditions are summarised in table 6.5. Empirical evidence is only acceptable under very restricted conditions. This then is seen to automatically involve the use of forward explicit finite difference schemes if actual soil suction is the principal focus of the predictive capability.

Such model structures have been shown to be analytically capable of providing the forecasting requirement. However, a large number of field conditions may affect the boundary conditions of such formulations in ways that cannot be easily modelled. The upper (surface cover) and lower (groundwater) boundaries have both seen to be major limitations in this regard. Elements of this report have sought to exemplify these conditions - these are cross referenced in table 6.5. The upper boundary condition is generally easier to satisfy than the groundwater boundary under Hong Kong conditions in the context of finite difference model requirements. Again, it must be recalled that currently no accurate groundwater prediction model is available for sites within Hong Kong, and yet this represents just the lower boundary condition for soil suction forecasting requirements. This point emphasises both the sensitive nature of the soil suction forecasting models, and the current inevitability of their spatially restricted utility to Hong Kong.

However, the research programme here has sought to emphasise that such models provide the principal predictive capability for soil suction, and that general statements can be successfully made especially in regard of the maintenance of suctions in different materials (section 6.1.3) and of the effects of surface cover (section 6.1.4) within the general limitations of table 6.5

7. CONCLUSIONS AND RECOMMENDATIONS

7.1 DESIGN CONCLUSIONS

7.1.1 Cover

There are three, progressively less restrictive criteria by which to judge the effectiveness of chunam :

- (a) Maintenance of soil suction beneath the cover :

Both field and modelling evidence (figure 6.14) suggest the necessity of having the effective permeability (K_e) of the chunam less than 10^{-7} ms^{-1} to achieve maintenance of suctions for 1 in 10 year rainfall events. Effective permeability is defined by equation 5.14.

- (b) Providing significant protection in terms of percentage surface runoff generated (suctions not now necessarily maintained).

An effective permeability of 10^{-6} ms^{-1} in relation to rainfall provides significant protection (see figure 5.15). This condition is in fact achieved by a wide range of chunam quality and underlying soil permeabilities (see figure 5.14).

- (c) Prevention of infiltration under conditions of high soil permeability (10^{-4} ms^{-1}) and chunam in 'bad' condition.

Even under these extreme conditions chunam affords some protection against the volume of water allowed to infiltrate into the slope. Table 5.5 shows typically that in those circumstances $K_e = 1 \times 10^{-5} \text{ ms}^{-1}$, which still prevents of the order of 40% of rainfall infiltrating in storms typified by that shown in figure 5.15.

The question as to whether any types of vegetation cover can provide equivalent protection in those categories can only be ascertained after results from the runoff plots (currently being established) are known. The methodology for making those assessments, once the runoff data has been obtained, has been established (section 6.1.5).

Other more detailed conclusions relating to chunam cover from field and laboratory work undertaken are principally :

- (a) The intact permeability of chunam has been shown to be insensitive to the exact mix proportions. Within the mix trials undertaken and reported in section 4.0, K_s was consistently lower than $9 \times 10^{-9} \text{ ms}^{-1}$. Intact field samples show a permeability in the range $2 \times 10^{-7} \text{ ms}^{-1}$ to $2 \times 10^{-9} \text{ ms}^{-1}$ (section 4.0). This discrepancy is assumed to be the product of age.
- (b) Significant recharge of a chunamed slope has been shown to occur from the upslope unprotected area. The downslope

extent of this influence is limited however, being confined to part of the upper most slope sector only. Unless detailed permeability estimates are available for the entire upper slope and backslope sector, two dimensional simulations cannot be used to estimate the degree of protection required backslope to meet specified requirements relating to pore water conditions in the slope.

- (c) Below this upper zone influenced by recharge, vertical infiltration has been shown to dominate the remainder of the chunamed slope studied during the wet season. The implications here are that one dimensional infiltration simulation models are appropriate for design and cover maintenance prediction needs (see section 6.1.2).
- (d) The mean difference in suction at mid-slope locations between a comparable chunam and grassed slope has been shown to be in excess of 10 kPa at depths up to 4 m (see figure 4.16).

7.1.2 Materials

- (a) In colluvium and CDG there is ample field evidence, (section 1.1) which is supported by selected simulation results, (section 6.0) to show that even in relatively dry years (e.g. 1980 - Mid-Levels Study) soil suctions in the upper 20 m of such materials are reduced to zero.
- (b) Simulations have shown that even where empirical evidence implies the maintenance of suctions in such materials (e.g. Sweeney 1982 - CDG), then for a 1 in 10 year rainfall event such suctions may be lost.
- (c) In CDV there is selected field evidence to show that suctions may be maintained at depths below about 15 m (see section 1.1). This ascertainment is supported by simulations only under fairly restrictive conditions.
- (d) The principal restriction is the need, as demonstrated by the simulations undertaken in section 6.1, to have knowledge of the saturated permeability with depth, to better than half an order of magnitude.
- (e) Specific sites in CDV may be capable of sustaining suctions at depths of 15-20 m against 1 in 100 year storms. Before such a claim could be made however, the results here indicate a firm requirement to have reliable estimates of Ks to the accuracy specified (section 6.3) at all depths of interest. From the permeability variation known to exist on a point to point basis, it is perhaps unlikely that this requirement can be met in many circumstances.

For the reason given in (e) it is considered impossible to generalise soil suction behaviour simply in terms of material type alone.

7.1.3 Prediction of soil water conditions

Two prediction procedures for soil suction have been outlined. An empirical statistical model has been established for the prediction of soil suctions under both grass and chunam in CDG (Clear Water Bay Road Site - section 4.3.3). Predictions of post-storm suction recovery are shown to be good (figures 4.23 and 4.24).

To enable longer term recurrence interval conditions to be evaluated a numerical simulation procedure was adopted. The principal findings from this analysis are :

- (a) It is unlikely that two dimensional finite difference models of soil water movement (of the type outlined in section 3.0) can be used for making reliable predictions under Hong Kong conditions. Principally this is because of the limited information available related to saturated permeability.
- (b) Where vertical profile data in terms of permeability is available, then one dimensional infiltration models for heterogeneous soils have been shown to perform well in the selected applications that have been made in this study, for CDG, CDV, colluvium and chunam (section 6.0).
- (c) Before such one dimensional models can be used for design purposes, the scheme outlined here needs to be refined in three principal areas to achieve acceptable generality of application :
 - (i) Stochastic variability of the input data needs to be incorporated so that the outcomes fully reflect the known field conditions (see section 3.2).
 - (ii) Alternative schemes to the M-Q method for estimation of unsaturated permeability should be evaluated. Available evidence however, which is reviewed in section 3.2.2, suggests this to be the most minor of the modifications which should be examined.
 - (iii) When runoff data from the study plots becomes available then it will be necessary to re-define the upper boundary conditions of the model outlined in section 3.0 so that associations can be made with specific vegetation types.
- (d) Particular attention must be paid to the model boundary conditions to ensure they realistically reflect the field conditions and processes pertaining to surface cover and groundwater. It has been shown that backslope topography can initiate processes (three dimensional soil water convergence and groundwater movement) that may not be capable of being modelled in either one or two dimensions. Such boundary condition requirements (outlined in section 6.3) restrict the suitability of such one and two dimensional models to specific field cases, principally : rectilinear slopes, where groundwater is either directly controlled by infiltration or is well below the toe of the slope, and where permeability, together with the other required input data are known (see table 6.5).

- (e) A simple model, based upon soil water drainage under hydrostatic start and finish conditions has been proposed as a possible procedure to improve the current landslip warning method. It has been shown (section 5.1.3) that such a method can quite significantly change the circumstances for the issue of a landslip warning, since soil drainage is a constituent element in the proposed model.

7.1.4 Instrumentation for soil suction

Currently available soil suction monitoring equipment has been reviewed. The conclusion from this review is that the current practice adopted in Hong Kong, both as regards installation procedures and equipment specification is satisfactory. In the light of commercially available equipment there appears no justification for further equipment development at the current time.

7.2 RECOMMENDATIONS FOR FURTHER WORK

It is recommended that consideration be given to the following work being undertaken immediately :

- (a) Incorporation of vegetation specification into 1-D soil water model :

The runoff data from the projected runoff plots to be used :

- (i) to evaluate the performance of the different vegetation types in preventing infiltration in accordance with the simulation procedure outlined in section 6.1.5.
- (ii) specify vegetation type in terms of effective rainfall, thereby characterising the vegetation in the simplest possible terms for inclusion in the existing model.
- (iii) if such a simple scheme provides insufficient resolution, as could be expected, then vegetation runoff production must be modelled dynamically (albeit in simple terms).

- (b) Modification of landslip warning procedure

The proposed method for refining the current procedure outlined in section 5.1.3 should be tested against available field data, and assessed as a means of justifying a simple linear reduction in rainfall, as has been discussed.

- (c) Verification of chunam crack model (section 5.0)

The model used for the estimation of the effective permeability of chunam (section 5.2.1) requires laboratory verification. Simulation results in section 6.0 are undertaken with values that are deemed

to be effective chunam permeability, but there remains the need to verify experimentally that the crack impact, in terms of chunam permeability, is as the model used here predicts (figure 5.12). At the time of writing, this project had been initiated, but no results were available on either the suitability of the experimental procedure or the chunam flux results.

The following items represent longer term research proposals, which may be undertaken when the results from the runoff plots are known :

(a) Refinement of 1-D soil water model for 'design' purposes :

As detailed in section 7.1.3, there is a need to fully generalise the current research program to accommodate variability in field parameters (e.g. establish an 'n' soil layer model, with stochastic variable sampling), and to ensure the program is entirely 'user friendly'.

(b) Role of vegetation in slope stability :

On the assumption that runoff-vegetation relationships can be established and employed in the soil water model as suggested in section 6.1.5, then such a scheme should be combined with the corresponding root strength patterns so that the total impact of vegetation on slope stability can be assessed.

(c) Degree of backslope protection recommended for chunam slopes :

The qualitative association of recharge from upslope unprotected areas with the downslope zone of influence under the chunamed surface (section 4.3) requires further investigation. Either an empirical study needs to be undertaken or a numerical simulation procedure could be established, providing sufficient field data on material permeability and soil retention characteristics was forthcoming. In these circumstances confidence could then be placed upon results from a two dimensional simulations.

8. REFERENCES

- Anderson, M.G. 1982. Predicting pore-water pressures in road cut slopes in the West Indies. Applied Geography, 2, 55-68.
- Anderson, M.G. 1983. Road-cut slope topography and stability relationships in St. Lucia, West Indies. Applied Geography, 3, 105-114.
- Anderson, M.G. and Burt, T.P. 1977. Automatic monitoring of soil moisture conditions in a hillslope spur and hollow. J. Hydrology 33, pp. 27-36.
- Anderson, M.G. and Kneale, P.E. 1980a. Soil moisture investigation - Wootton Bassett. Department of Transport, EID, Report 2 on EID 6/3/04, 14pp.
- Anderson, M.G. and Kneale, P.E. 1980b. Topography and hillslope soil water relationships in a catchment of low relief. J. Hydrology, 47, 115-128.
- Anderson, M.G. and Kneale, P.E. 1980c. Pore water changes in a road embankment. Highway Engineer, 25, 193-195.
- Anderson, M.G. and Kneale, P.E. 1982. The influence of low angled topography on hillslope soil water convergence and stream discharge. J. Hydrology, 57, 65-80.
- Anderson, M.G., McNicholl D.P. and Shen, J.M. 1983. On the effect of topography in controlling soil water conditions, with specific regard to cut slope piezometric levels. Hong Kong Engineer (submitted paper)
- Arya, L.M. and Paris, J.F. 1981. A physioempirical model to predict the soil moisture characteristic from particle-size distribution and bulk density data. Soil Sci. Soc. Am. J., 45, 1023-1030.
- Ashcroft, B. 1983. Vegetation establishment on hostile sites Hong Kong Engineer, 11, 33-35.
- Balick, L.K., Link, L.E., and Scoggins, R.K. 1981. Thermal modeling of terrain surface elements. U.S. Army Engineer Waterways Experiment Station Technical Report EL-81-2.
- Barnett, A.P. Carrecker, J.R. and Abruna, F. 1972. Soil and nutrient losses in runoff with selected cropping treatments in tropical soils. Agron J., 64, 391-395.
- Beven, K. and Kirkby, M.J. 1979. A physically based variable contributing area model of basin hydrology Hyd. Sci Bull, 24, 43-69.
- Binnie and Partners (Hong Kong) 1979. Report on stability of cut slopes at M.S. 43/13½ Tai Po Road Improvement - Stage 1. Unpublished report G.C.O. Data Bank.
- Boels, D., Van Gils, J.B.H.M., Veerman, G.J. and Wit, K.E. 1978. Theory and system of automatic determination of soil moisture characteristics and unsaturated hydraulic conductivities. Soil Sci. 126, pp. 191-199.

- Bondurant, J.A. 1971. Quality of surface irrigation runoff water. Trans. Am. Soc. Agric. Eng., 14, 1001-1003.
- Branson, F.A. 1975. Natural and modified plant communities as related to runoff and sediment type, in Hasler, D (ed). Coupling of Land and Water Systems Ecological Studies 10, 157-172.
- Branson, F.A. and Owen, J.R. 1970. Plant cover, runoff and sediment yield relationships on Mancos Shale in Western Colorado. Water Resources Research, 6, 783-790.
- Bruce, R.R. and Whishler, F.D. 1973. Infiltration of water into layered field soils. Ecological Studies, 4, Physical aspects of soil water and salts in ecosystems, 77-89.
- Burt, T.P. 1978. An automatic fluid scanning switch tensiometer-system. British Geomorphological Research Group, Technical Bulletin 21.
- Campbell, G.S. 1974. A simple method for determining unsaturated hydraulic conductivity from moisture retention data. Soil Science, 117, 311-314.
- Carson, M.A. and Kirkby, M.J. 1972. Hillslope form and Process. Cambridge University Press, 475pp.
- Chan, C.K. 1982. Permeability of chunam surfacing Geotechnical Control Office. Unpublished report on FWD CE 3/81, 20pp.
- Chipp, P.N., Clare, D.G., Henkel, D.J. and Pope, R.G. 1982. Field measurement of suction in colluvium covered slopes in Hong Kong in Proc. 7th S.E. Asian Geotechnical Conf., McFeat-Smith, I. and Lumb, P. (eds) H.K.I.E., 49-62.
- Colbeck, S.C. 1976. On the use of tensiometers in snow hydrology, J. of Glaciology, 17, pp. 135-140.
- Croney, D., Coleman, J.D. and Bridge, P.M. 1952. The suction of moisture held in soil and other porous materials. Road Research Technical Paper No. 24, London, H.M.S.O.
- Crozier, M.J. and Eyles, R.J. 1980. Assessing the probability of rapid mass movement. Third Australia - New Zealand Conf. Geomechanics, Wellington, 2-47.
- Department of Main Roads, N.S.W. Australia, 1977. Investigation of soil moisture conditions and seasonal moisture variations in Illawarra Division. Materials and Research Laboratory report 1R.11.
- Emmett, W.W. 1970. The Hydraulics of overland flow on hillslopes U.S. Geol. Survey Prof. Paper 662-A.
- Ezaki, T. 1981. Studies on the turfing work for the protection of cutting slope 3, on the mechanism of surface erosion and the protection effects by vegetation. Bull. Ehime University Forest., Japan, 18, 125-142.

- Ezaki, T, Fushimi, T and Fujihisa, M 1979 Studies on the use of Japanese weeds for the protection work of bare slopes 6. The runoff characteristics of rainfall on the cutting slope of the forest road. Bull Ehime University Forest, Japan, 16, 149-156.
- Feddes, R.A., Bresler, E., and Neuman, S.P. 1974. Field test of a modified numerical model for water uptake by root systems. Water Resources Research, 10, 1199-1206.
- Feddes, R.A. Kowalik, P., Newman, S.P. and Bresler, E. 1976. Finite element and finite difference simulation of field water uptake by plants. Hydrological Sciences Bulletin, 21.
- Federer, C.A. 1973. Forest transpiration greatly increases streamflow recession. Water Resources Research, 9, 1599-1604.
- Fitzsimmons, D.W. and Young, N.C. 1972. Tensiometer-pressure transducer system for studying unsteady flow through soils. Trans. Am. Soc. Agric. Eng. 15, pp. 272-275.
- Forbes, J.E. 1983. Protecting trees in development areas Hong Kong Engineer, 11, 37-39.
- Freeze, R.A. 1969. The mechanism of natural groundwater recharge and discharge. 1. One-dimensional, vertical, unsteady, unsaturated flow above a recharging or discharging groundwater flow system. Water Resources Research, 5, 153-171.
- Freeze, R. A. 1980. A stochastic conceptual analysis of rainfall-runoff processes on a hillslope. Water Resources Research, 16, 391-408.
- Frere, M.H. 1976. Nutrient aspects of pollution from Cropland. ARS-USDA report ARS-H-2.
- G.C.O. 1979. Geotechnical Manual for Slopes. Public Works Department, Hong Kong 227pp.
- G.C.O. 1980. Mid-Levels study, Part 2A, Vol. 9, Part 10 field instrumentation.
- G.C.O. 1981. Mid-Levels study; Hydrology subject report volume 2 Appendices. Geotechnical Control Office, Hong Kong.
- G.C.O. 1982. Cutslopes in Hong Kong Assessment of Stability by empiricism Public Works Department, Hong Kong.
- G.C.O. 1982. Mid-Levels study. Public Works Department, Hong Kong 264pp.
- G.C.O. 1983. Geotechnical Manual for Slopes (2nd edition), Public Works Department, Hong Kong.
- Gilham, R.W, Kulte, A., and Heerman, D.F. 1979. Measurement and numerical simulation of hysteretic flow in a heterogeneous porous media. Proc. Soil Sci. Soc. Am., 43, 1061-1067.

- Gilmour, J.T. and Marx, D.B. 1981. Soluble salt concentrations in runoff water from soils previously cropped to rice Proc. Soil Sci Soc Am, 45, 1198-1201.
- Gummaa, G.S. 1978. Spatial variability of insitu available water. Unpublished Ph. D. Univ. of Arizona, Tucson, Arizona.
- Harr, H.E. 1962. Groundwater flow and seepage, McGraw Hill, New York, 315pp.
- Harr, R.D. 1977. Water flux in soil and subsoil on a steep forested slope. J. of Hyd. 33, pp. 37-58.
- Haverkamp, R., Vauclin, M., Touma, J., Wierenga, P.J., and Vachaud, E. 1977. A comparison of numerical simulation models for one-dimensional infiltration. Proc. Soil Sci. Soc. Am., 41, 285-294.
- Hillel, D. 1977. Computer Simulation of Soil Water Dynamics, IDRC, Ottawa.
- Hillel, D. 1980. Fundamentals of Soil Physics. Academic Press, New York.
- Hillel, D. and Van Bavel, C.H.M. 1976. Simulation of profile water storage as related to soil hydraulic properties. Proc. Soil Sci. Soc. Am., 40, 807-815.
- Ho, K.H. 1978. The properties and application of chunam surfacing Department of Civil Engineering. Hong Kong University, unpublished dissertation.
- Hsu, S.I., Lam, K.C. and Chan, K.S. 1983. A study of soil moisture and runoff variation in hillslopes. Department of Geography Chinese University of Hong Kong, Occasional Paper 45, 57pp.
- Hudson, N.W. and Jackson, D.C. 1959. Erosion Research Report of Progress 1958-9, Federation of Rhodesia and Nyasaland : Ministry of Agriculture.
- Ingersoll, J.E. 1980. Soil tensiometers for use at temperatures below freezing. (Unpublished report).
- Ingersoll, J.E. 1981. Laboratory and field use of soil tensiometers above and below 0°C. CRREL Special Report 81-7.
- Jackson, R.D. 1972. On the calculation of hydraulic conductivity. Soil Science Society of America, 36, 380-382.
- Jackson, T.J. 1980. Profile soil moisture from surface measurements. Journal of Irrigation and drainage division, Proc. Am. Society Civil Engineers, IR2, 81-92.
- Jensen, K.H. 1981. Application of soil water flow theory in field simulation. Nordic Hydrology, 12, 167-184.
- Jones, J.A.A. 1981. The nature of soil piping. A review of research British Geomorphological Research Group, Monograph 3, GeoBooks Norwich 301 pp.

- Klute, A. and Peters, D.B. 1962. A recording tensiometer with a short response time. Proc. Soil Sci. Soc. Am. 26, pp. 87-88.
- Kowsar, A. 1982. Water harvesting for afforestation III Dependence of tree growth on amount and distribution of precipitation. Soil Sci. Soc. Am. J. 46, 802-807.
- Kowsar, A., Mehdizadeh, P. Vaziri, E and Boersma, L 1978. Water harvesting for afforestation. II Survival and growth of trees. Soil Sci. Soc. Am. J., 42, 650-657.
- Krahn, J. and Fredlund, D.G. 1972. On total, matric and osmotic suction. Soil Science, 114, 339-348.
- Kwan, W.C. 1983. Chunam Study. Geotechnical Control Office, unpublished report on PWD CE 3/81 30pp.
- Leach, B. 1982. The development of a groundwater recharge model for Hong Kong. Hydrol. Sci. Bul.
- Leach, B. and Herbert. R. 1982. The genesis of a model for the study of a steep hillside in Hong Kong Q. J. Eng. Geol. 15, 243-259.
- Lee, R.K.C. 1983. Measurement of soil suction using the MCS 6000 sensor. University of Saskatchewan, unpublished M.S. thesis, 162pp.
- Lull, H.W. 1964. Ecological and siviculture aspects in Chow, V.T. (ed) Handbook of Applied Hydrology McGraw Hill.
- Lumb, P. 1975. Slope failures in Hong Kong. Q.J. Eng. Geol., 8, 31-65.
- McFarlane, J. 1980. Soil suction measurements in Hong Kong Soil - Instrumentation and preliminary results. Public Works Department Hong Kong. Unpublished report.
- McFarlane, J. 1981. Suction-moisture relationships in residual and remoulded Hong Kong soils. P.W.D. Materials Division, Report 24.
- McKim, H.L., Berg, R.L., McGraw, R.W., Atkins, R.T. and Ingersoll, J. 1976. Development of a remote-reading tensiometer/transducer system for use in subfreezing temperatures. Conference on Soil Water Problems in Cold Regions, Edmonton, pp. 31-45.
- McKim, H.L., Walsh, J.E. and Arion, D.N. 1980. Review of techniques for measuring soil moisture in situ. CRREL Special Report 80-31.
- Malone, A.W. and Shelton, J.C. 1982. Landslides in Hong Kong 1978-1980. Am. Soc. Civ. Eng. Conf., Hawaii, 425-441.
- Massey, B.S. 1970. Mechanics of fluids.
- Mendizadeh, P., Kowsar, A., Vazin, E. and Boersma, L. 1978. Water harvesting for afforestation. I Efficiency and Lifespan of asphalt cover. Soil Sci Soc Am J., 42, 644-649.
- Millington, R.J. and Quirk, J.P. 1959. Permeability of porous media. Nature, 183, 387-388.

- Nassif, S.H. and Wilson, E.M. 1975. The influence of slope and rainfall intensity on runoff and infiltration. Hydrological Sciences Bulletin, 20.
- Nielsen, D.R., Biggar, J.W. and Erh, K.T., 1973. Spatial variability of field measured soil water properties. Hilgardia, 42, 215-259
- P.W.D. 1979. Final report for the use of psychrometers for measurement of soil suction in Hong Kong. Materials Division, Public Works Department, Report 8.
- Pall, R., Jarrett, A.R., and Morrow, C.T. 1981. Transient soil moisture movement through layered soils using a finite element approach. Am. Soc. Agric. Eng., Trans., 24, 678-683.
- Papagiannakis, T. 1982. A steady state model for flow in saturated - unsaturated soils. Department of Civil Engineering, University of Saskatchewan, unpublished M.S. thesis.
- Phene, C.J., Hoffman, G.J. and Austin, R.S. 1973. Controlling automated irrigation with soil matric potential sensor Trans. Am. Soc. Agric. Eng., 16, 773-776.
- Phene, C.J., Hoffman, G.J. and Rawlins, S.L. 1971. Measuring soil matric potential insitu by sensing heat dissipation with a porous body. I Theory and sensor construction. Soil Sci. Soc. Am. Proc., 35, 27-32.
- Poulovassilis, A. 1970. The hysteresis of pore water in granular porous bodies. Soil Science, 109, 5-12.
- Raats, P.A.C. 1973. Unstable wetting fronts in uniform and nonuniform soils. Proc. Soil Sci. Soc. Am., 37, 681-685.
- Rawls, W.J., Brakensiek, D.L. and Saxton, K.E. 1981. Soil water characteristics, Am. Soc. Agric. Eng. Paper 81-2510.
- Renard, K.G. 1977. Erosion research and mathematical modelling in Toy, T.J. (ed) Erosion : Research Techniques Erodibility and Sediment Delivery Geobooks, Norwich.
- Rice, R. 1969. A fast response field tensiometer system; Trans. Am. Soc. Agric. Eng. 12, pp. 48-50.
- Rushton, K.R. and Ward, C. 1979. The estimation of groundwater recharge. J. Hydrol., 41, 345-361.
- S.H.E. 1981. Systeme Hydrologique Europeen, a short description. Unpublished manuscript.
- Sanchez, P.A. 1976. Properties and management of soils in the Tropics. John Wiley, Chichester, 618pp.
- Schmugge, T.J., Jackson, T.J. and McKim, H.L. 1980. Survey of methods for soil moisture determination. Water Res. Res., 16, pp 961-979.

- Sellers, P.J. and Lockwood, J.G. 1981. Numerical simulation of the effects of changing vegetation type on surface hydro climatology. Climatic Change, 3, 121-136.
- Shen, J.M. 1983. Suction moisture relationships in residual and remoulded Hong Kong Soils and their applications. Geotechnical Control Office, unpublished report, 16pp.
- Staple, W.J. 1966. Infiltration and redistribution of water in vertical columns of loam. Proc. Soil Sci. Soc. Am., 33, 645-651.
- Suarezde Castro, F. and Rodriguez A. 1955. Perdidas por erosion de elementos nutritivos bajo diferentes cubiertas vegetales y con varias practicas de conservacion de suelos. Federacion Nacional de Cafeteros de Colombia Bol Tec. 14
- Sweeney, D.J. 1982. Some in situ soil suction measurements in Hong Kong's residual soil in Proc. S.E. Asian Geotechnical Conference, HKIE, 91-105.
- Talsma, T. 1970. Hysteresis in two sands and the independent domain model. Water Resources Research, 6, 964-970.
- Topp, G.C. 1969. Soil water hysteresis measured in a sandy loam and compared with the hysteretic domain model Proc. Soil Sci. Soc. Am. 33, 645-651.
- Topp, G.C. and Miller, E.E, 1966. Hysteretic moisture characteristics and hydraulic conductivities for glass-bead media. Proc. Soil Sci. Soc. Am., 30, 156-162.
- Towner, G.D. 1980. Theory of time response of tensiometers. Journal Soil Science, 31, pp. 607-621.
- Tzimas, E. 1979. The measurement of soil-water hysteretic relationships on a soil-monolith. Journal of Soil Science, 30, 529-534.
- United States Department of Agriculture, 1968. Moisture-tension data for selected soils on experimental watersheds. Agricultural Research Service Reports ARS-41-144.
- Viessman, W., Knapp, J.W., Lewis, G.L. and Harbaugh, T.E. 1977. Introduction to Hydrology. Harper and Row. 691pp.
- Ward, R.C. 1976. Principles of Hydrology. McGraw Hill.
- Watson, K.K. 1965. Some operating characteristics of a rapid response tensiometer system; Water Res. Res., 1, pp 577-586.
- Watson, K.K. and Jackson, R.J. 1967. Temperature effects on a tensiometer-pressure transducer system. Proc. Soil Sci. Soc. Am. 31, pp 156-160.
- Watson, K.K., Reginato, R.J., and Jackson, R.D. 1975. Soil water hysteresis in a field soil. Proc. Soil Sci. Soc. Am., 39, 242-246.

- Whisler, F.D. 1976. Calculating the unsaturated hydraulic conductivity and diffusivity. Soil Science Society of America, 40, 150-151.
- Whisler, F.D., Curtis, A.A., Niknam, A., and Ronkens, M.J.M. 1979. Modelling infiltration as affected by surface crusting in Surface and Subsurface Hydrology. Morel-Seytoux, H.J., Salas, J.D., Sanders, T.G., and Smith, R.E. (eds) Water Resource Publications, Fort Collins, 400-413.
- Wiesner, C.J. 1970. Hydrometeorology Chapman and Hall, London.
- Williams, T.H. Lee 1976. An automatic scanning and recording tensiometer system. J. of Hyd., 39, pp 175-183.
- Young, N.C. 1968. Using a tensiometer-pressure transducer apparatus to study one and two-dimensional imbibition. M.Sc. thesis, Univ. Idaho, Moscow, Idaho.

Table 1.1 - Summary of selected reports relating to soil suction research in Hong Kong

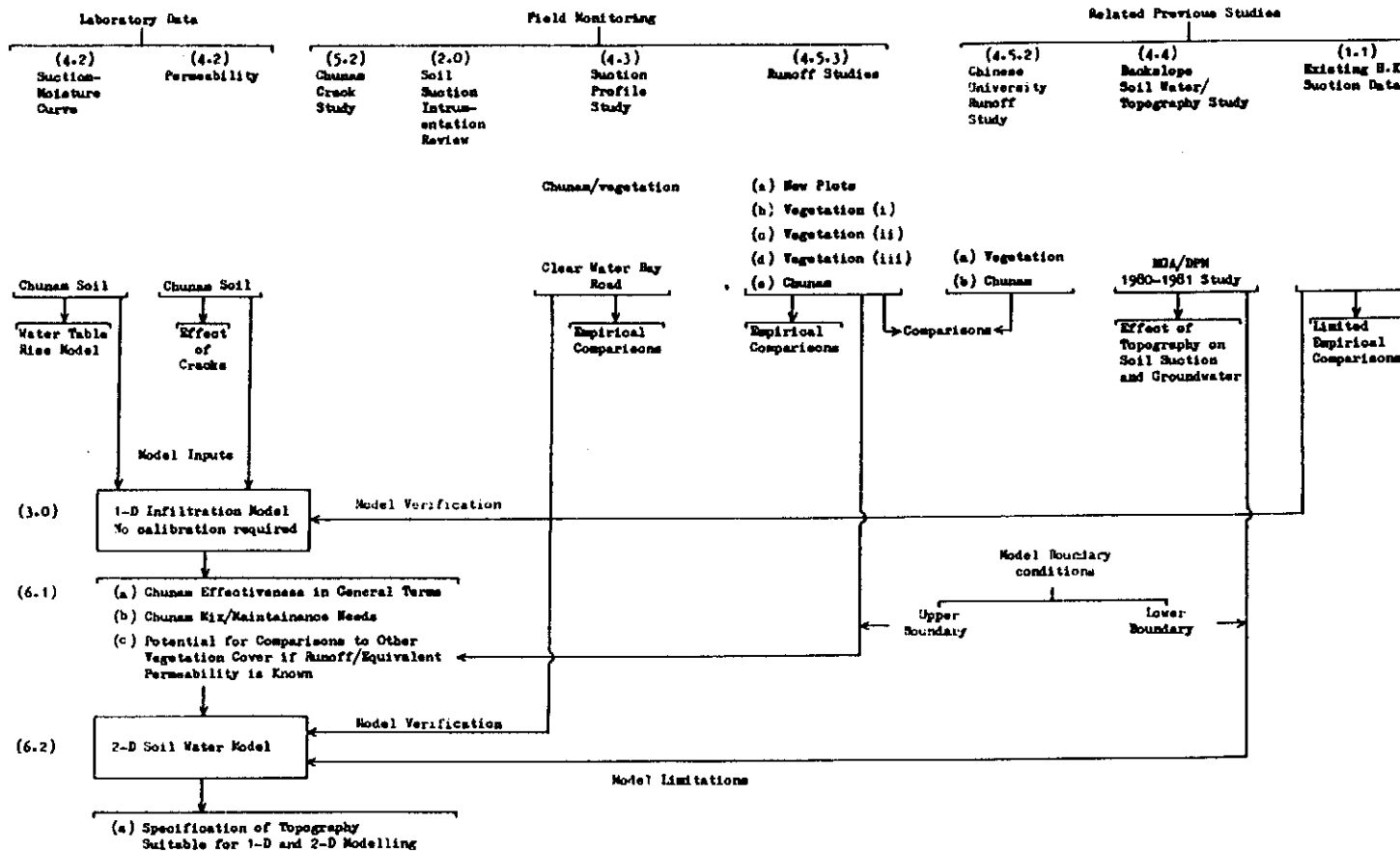
Date	Report	Remarks
1978	Soil Suction Research - Binnie and Partners' Proposal Meeting reports	Psychrometers affirmed to be insufficiently reliable in 0-2 bar range.
1979	Materials Division Report No. 8 - Final report on the Use of Psychrometers for Measurement of Soil Suction in Hong Kong	Testing programme emphasising measurement capability in 0-1 bar range, showing that thermocouple psychrometers cannot give reliable measurements in this range.
1979	Soil Suction Research - Interim report	First use of tensiometers in Hong Kong. Installations at H.K.U., Mid-Levels and Chai Wan emphasising need to study remoulded samples for suction.
1980	Methods for the Determination of Soil Suction-moisture Relationships - P.W.D. Interim report	Pressure plate, ceramic plate and volumetric pressure plate extractor methods outlined.
1980	Soil Suction Measurements in Hong Kong Soil - Instrumentation and Preliminary Results, P.W.D. Interim report	Five sites with single tensiometer installations.
1981	An Evaluation of the Accuracy of Soil Suction-moisture Relationships Using Volumetric Pressure Plate Extractors P.W.D. Materials Division Report No. 20	Possible error in degree of saturation of 10%.
1981	Suction-moisture Relationships in Residual and Remoulded Hong Kong Soils P.W.D. Materials Division Report No. 24	Variability of suction-moisture relationship in undisturbed samples.
1981	Soil Suction and Its Relation to Rainfall P.W.D. Materials Division Report No. 25	Prediction model established for soil suction - rainfall.
1981	Mid-Levels Study Hydrology Subject Report Volumes 1 and 2	Tensiometer equipment installation and testing, together with detailed over-storm results from automatic tensiometer systems
1982	Mid-Levels Study G.C.O.	Extensive tensiometer suction data reported for Mid-Levels.

Note : (1) Sites used and referred to in this report are shown in figure 1.7.

Table 1.2 - Principal tensiometer sites in Hong Kong up to 1982

Site	Geology	Date	No. of tensiometers	Remarks
Mid-Levels	DG DV	1980	> 200	Mid-Levels Study (G.C.O. 1982) Installation in caissons up to 10 m deep.
King's Park	DG	1980	19	Vegetated cut slope, chunamed cut slope chunamed fill slope.
Lung Cheung Road	DG	1980	15	Chunamed and vegetated cut slope
Kennedy Town	DV?	1980	8	No-fine concrete covered cut slope and vegetated natural slope.
Po Shan Road	DV	1980	3	Grassed slope.
Hong Kong Sanitarium	DG	1980	12	Grassed fill slope, vegetated natural.
		1981	18	Slope and spray concrete protected fill slope.
So Uk Estate	-	1981	11	Chunamed fill slope.
Pak Tin Estate	-	1981	9	Chunamed fill slope.
Tai Po, St. Christopher Bend	DV	1980 1982	53	Chunamed cut slope and vegetated backslope hollow.

Table 1.3 Soil suction study research design



Note : Numbers in brackets refer to sections in this report.

Table 2.1 - Selected examples of reports detailing
tensiometer and thermal conductivity systems

TENSIOMETER SYSTEMS	THERMAL CONDUCTIVITY SENSORS
<p><u>Field installations ($>0^{\circ}\text{C}$)</u></p> <p>Anderson and Burt (1977) (2.3.1) Anderson and Kneale (1980) (2.3.1) Rice (1969) Williams (1978) (2.3.1) Watson (1967) Harr (1977) Sweeney (1982) (2.2.2) Chipp <u>et al.</u> (1982) (2.2.1, 2.3.1) G.C.O. (1980) (2.2.1, 2.3.1)</p> <p><u>Field installation ($\leq 0^{\circ}\text{C}$)</u></p> <p>Colbeck (1976) Ingersoll (1980), (1981) McKim <u>et al.</u> (1976)</p> <p><u>Reviews of tensiometric techniques</u></p> <p>Ingersoll (1981) McKim <u>et al.</u> (1980) Schmugge <u>et al.</u> (1980)</p> <p><u>Response times (empirical and theoretical)</u></p> <p>See Table 2.2</p>	<p><u>Field installations</u></p> <p>Lee (1983) (2.5.1) Department of Main Roads, (1977) N.S.W., Australia Phene, Hoffman and Austin (1973)</p> <p><u>Review of thermal conductivity methods</u></p> <p>Lee (1983)</p>

Note: (1) Numbers in brackets following the year of publication refer to the relevant section in this report, detailing the equipment used in the investigation.

Table 2.2 - Response Times of Transducer-Tensiometer Systems

Authors	Date	Cup Material	Cup Air Entry Value	Transducer Sensitivity	Empirical/Theoretical	Soil Material	Response Time	Level of Accuracy
Klute, A. and Peters, D.B.	1962	fritted glass	-	$3 \times 10^3 \text{ mb.cm}^{-3}$	E	-	1 sec	-
Watson, K.K.	1965	ceramic	86cm water 1300cm water	$1 \times 10^2 \text{ psi.cm}^{-3}$ $1 \times 10^2 \text{ psi.cm}^{-3}$	E E	sand sand	0.1 sec 29.6 sec	-
Watson, K.K. & Jackson, R.J.	1967	ceramic	1300cm water	$5 \times 10^{-5} \text{ cm}^3 \text{ mbar}^{-1}$	T	-	9.1 sec	-
Young, N.C. (36)	1968							
Fitzsimmons, D.W. & Young, N.C.	1972	porvic (polyvinyl chloride)	-	$3 \times 10^4 \text{ mb.cm}^{-3}$	E	depending on material & saturation	1 sec to 60 sec	-
Williams, T.H.L.	1978	ceramic	1000cm water	$1 \times 10^{-4} \text{ cm}^3 \text{ mbar}^{-1}$	T	-	1 sec	-
Boels, D. et al	1978	ceramic	-		T	heavy clay-wet -medium -dry sandy clay-wet loam-medium -dry	60 sec 98 sec 60 sec 125 sec 450 sec	1% 1% 1% 1% 1%
Towner, G.D.	1980				T			
Anderson, M.G. & Kneale, P.E.	1980	ceramic	1000cm water		E	clay	100 sec	-

Table 3.1 - Selected soil water finite difference models

	Model Dimension		Hysteresis in $\theta-\psi$		Lower Boundary Condition Dynamic		Stochastic Parameter Variability of Input		Dynamic Evaporation Included		Pressure Calculations throughout Perched Water Table	
	1D	2D	Yes	No	Yes	No	Yes	No	Yes	No	Yes	No
Freeze (1969)	/		/		/			/		/		/
Feddes (1974)	/			/	/			/	/			/
Hillel & Van Bavel (1976)	/			/	/			/	/			/
Hillel (1977)		/	/	/	/			/	/			/
Jackson (1980)	/			/	/			/	/			/
Freeze (1980)		/	/		/		/			/		/
Pall et al (1981)	/			/	/			/	/			/
Jensen (1981)	/			/	/			/	/			/
This study	/	/		/	/			/	/		/	

Note : (1) A review paper by Haverkamp et al (1977) compares numerical solutions to the Fokker-Planck equation.

Table 3.2 - Summary of model equations

Condition	Equation	Application
Saturated Flow	Darcy's Law (3.15)	Basis of soil water movement extended to unsaturated flow
	Darcy's Law with Dupuit-Forchheimer approximations (3.30)	Groundwater movement in 2-D model
	Pore water pressures in perched water table (3.29)	Estimation of transient pore pressures throughout perched water table
Unsaturated Flow	Millington-Quirk (3.18)	Estimation of unsaturated permeability for specified soil moisture content
Boundary Conditions	Evaporation (3.23)	Sine based forcing function for evaporation at top computation point
	Model base	Set drainage to 0 (impermeable base) or to any selected condition up to permeability of base computation point
	Surface detention	Set to a specified value to represent surface ponding effects

Note : (1) The effect of vegetation canopy-induced runoff is not yet modelled; the results of the studies described in section 4.3 are awaited. Saturation excess runoff is generated.

Table 3.3 - Input variables to soil water model

Input variables	Units
Moisture content at saturation (layers 1 - 3)	$m^3 m^{-3}$
Maximum evapotranspiration	m
Surface detention capacity of soil	m
Saturated permeability (layers 1 - 3)	ms^{-1}
Suction - moisture curve (layers 1 - 3)	$m^3 m^{-3}$ and m
Hourly or daily precipitation	m
Time precipitation starts	hour
Initial moisture contents at all points	$m^3 m^{-3}$
Number of computational points in each soil layer	-
Distance between each computational point	m
Simulation time step increment	s
Simulation run time	hour

Note : (1) The base boundary condition must be set (see figure 3.4)

(2) There is no requirement to input unsaturated permeability - suction relationships, as the M-Q method (equation 3.18) is used in the program.

Table 4.1 - Permeability of chunam from field samples

Sample Location		Permeability (ms ⁻¹)	
		Using Burette	Using Ponding
Decomposed Granite	King's Park	1.5×10^{-7}	
	Upper Clearwater Bay Road	1.4×10^{-7}	5.2×10^{-8}
	Lower Clearwater Bay Road		6.9×10^{-8}
	Lung Cheung Road		2.3×10^{-7}
Decomposed Volcanics	Po Lam Road (P1)	6.0×10^{-6}	1.6×10^{-8}
	Po Lam Road (P2)	7.5×10^{-6}	2.2×10^{-8}
	Tai Po (MB) - New	8.9×10^{-7}	2.6×10^{-9}

Table 4.2 - Trial Mixes for laboratory reconstituted chunam samples of
Tai Po Decomposed Volcanics & King's Park Decomposed Granite

		Parts by weight of <u>Hydrated Lime</u> per 20 parts of soil			
		0	1	3	5
Parts by weight of Cement per 20 parts of soil	0	Test Base-line (1)	(2)	(3)	(4)
	1	(5)	(6)	(7) Standard PWD Specification	(8)
	2	(9)	(10)	(11)	(12)

Note : Numbers (2) refer to test number.

Table 4.3 - Trial mixes for laboratory reconstituted chunam samples of Clear Water Bay Road Decomposed Granite

		Parts by weight of <u>Hydrated Lime</u> per 20 parts of soil			
		0	1	3	5
Parts by weight of <u>Cement</u> per 20 parts of soil	0	Test # ₁ Base- line			4
	1			7 Standard PWD Specification	
	2	9		11	12

Table 4.4 - Variation of area shrinkage with age for
chunam of Tai Po Decomposed Volcanics

Trial Mix No.	% shrinkage at ages (in days)						
	1	2	3	4	5	6	7
1	-	11.0	15.0	17.3	-	-	17.9
2	-	10.1	11.9	12.5	-	-	13.1
3	-	8.1	-	10.5	-	11.1	11.7
4	3.3	8.1	-	10.5	-	11.0	11.0
5	2.3	-	4.6	5.2	5.8	5.9	6.1
6	-	4.0	4.6	4.5	4.8	-	4.9
7	2.2	4.8	5.4	-	6.0	6.1	6.1
8	3.2	5.9	6.3	-	6.7	6.8	6.8
9	1.2	2.9	3.2	-	4.2	4.4	4.5
10	1.4	1.9	-	2.3	2.4	2.5	2.6
11	2.0	3.5	-	4.4	4.4	4.4	4.4
12	2.2	3.7	-	4.2	4.4	-	4.6

Note : (1) Trial Mix No. 7 is PWD Specification

Table 4.5 - Variation of area shrinkage with age for
chunam of King's Park Decomposed Granite

Trial Mix No. (see Table 4.2)	% shrinkage at ages (in days)						
	1	2	3	4	5	6	7
1	3.4	3.8	-	4.2	-	4.6	4.6
2	1.2	1.5	-	1.9	-	2.2	2.4
3	1.2	1.9	-	2.6	-	2.3	2.4
4	2.0	-	3.2	3.4	-	3.5	3.6
5	0.2	-	0.4	0.9	-	0.9	1.3
6	1.1	-	1.4	1.6	-	1.6	1.8
7	0.2	0.2	0.3	-	0.7	-	0.7
8	0.3	0.4	0.4	-	0.7	-	0.7
9	0.2	-	0.2	-	0.5	0.6	0.6
10	-	0.7	-	0.9	1.1	-	1.0
11	0.5	-	0.5	-	0.6	0.8	0.9
12	-	1.0	-	1.2	1.4	-	1.4

Note : (1) Trial Mix No. 7 is PWD Specification

Table 4.6 - Variation of area shrinkage with age for
chunam of Clear Water Bay Road Decomposed
Granite

Trial Mix No.	% shrinkage at ages (in days)						
	1	2	3	4	5	6	7
1	2.2	-	1.8	1.8	-	1.8	1.8
4	1.7	-	2.0	2.0	2.1	2.0	1.9
7	0.1	0.3	-	-	-	0.3	0.3
9	-0.1	0.0	-	-	0.0	0.1	0.1
11	0.7	0.9	-	-	0.8	0.8	0.8
12	1.1	-	0.7	0.6	-	0.7	0.7

Note : (1) Trial Mix No. 7 is FWD Specification

Table 4.7 - Permeability of trial mix chunam samples

		Parts by weight of hydrated lime per 20 parts of soil			
		0	1	3	5
Parts by weight of cement per 20 parts of soil	0	7.05×10^{-8}	4.3×10^{-8}	1.2×10^{-9}	6.6×10^{-9}
		6.3×10^{-8}	3.1×10^{-9}	5.7×10^{-9}	5.8×10^{-9}
	1	8.5×10^{-9}	8.6×10^{-9}	2.1×10^{-9}	5.5×10^{-9}
		1.28×10^{-8}	1.71×10^{-8}	9×10^{-9}	1.7×10^{-9}
	3	2.4×10^{-9}	4.2×10^{-9}	1.8×10^{-9}	2.2×10^{-9}
		7.8×10^{-9}	2.6×10^{-9}	2.0×10^{-9}	2.2×10^{-9}

King's Park
Decomposed
Granite



Tai Po
Decomposed
Volcanics

Table 4.8 Instrumentation details for Tai Po, St. Christopher Bend Site

Tensiometer locations					
Depths (vertical) m					
Location Number	0.3	0.75	1.0	1.5	2.0
T1	X	X		X	
T2	X	X		X	
T3	X		X	X	X
T4	X	X		X	
T5	X	X		X	
T6	X	X		X	
T7				X	
T8	X	X	X	X	
T9	X	X		X	
T10	X		X	X	X
T11	X	X		X	
T12	X			X	
T13				X	
T14				X	X
T15				X	X
T16				X	
T17	X		X	X	X
T18				X	
T19			X	X	X
T20			X	X	X
T21			X	X	X
Piezometer Locations					
Location Number	Ground Level		Tip depth below G.L. (m)		
P1	109.3		20.7		
P2 A/B	124.1/124.1		36.6/19.5		
P3	109.3		16.7		
P4 A/B	102.6/102.6		14.0/6.7		

Table 4.9 - Selected studies relating to vegetation and runoff production

General Texts

Carson and Kirkby (1972)
 Sanchez (1976)
 Viessman et al (1977)
 Lull (1964)
 Ward (1976)

Vegetation type and runoff

Barnett et al (1972)
 Suarez de Castro, Rodriguez (1972)
 Branson & Owen (1970)
 Branson (1975)
 Mehdizadeh et al (1978)
 Kowsar et al (1978)
 Kowsar (1982)
 Ezaki (1981)
 Ezaki et al (1979)
 Federer (1973)
 Hudson & Jackson (1959)

Runoff, water quality and vegetation

Gilmour & Marx (1981)
 Frere (1976)
 Bou durant (1971)

Modelling vegetation/runoff relationships

Sellers and Lockwood (1981)
 Emmett (1972)
 Hillel (1977)
 Renard (1977)
 Feddes et al (1976)

Hong Kong Studies of vegetation and vegetation/runoff

Hsu et al (1983)
 Ashcroft (1983)
 Forbes (1983)

Table 4.10 - Characteristics of grass species commonly used in Hong Kong

Grass*	Botanical Name	Height (m)	Characteristics	Possible Runoff Production
Bahia	<i>Paspalum notatum</i>	0.3-0.5	Root system is extensive and strong, effective for erosion control, compatible with shrub and tree planting, well adapted to wide range of sites, good shade, drought and wear tolerance; early growth rate may be slow.	High
Bermuda	<i>Cynodon dactylon</i>	0.3	Root system is extensive, effective for erosion control, well adapted to a wide range of sites; browns in winter.	Low
Buffel	<i>Cenchrus ciliaris</i>	0.7-1.5	Root system is extensive and strong, fire and drought tolerant, will grow on infertile sites.	-
Carpet	<i>Axonopus compressus</i>	0.1-0.2	Root system shallow but effective for erosion control, usually planted by sprigging/turfing; prefers moist conditions, browns in the winter.	-
Cantipede	<i>Eremochloa ophiuroides</i>	0.20	Will grow on infertile sites, easily established, effective for erosion control.	-
Rhodes	<i>Chloris gayana</i>	0.5-1.0	Tufted**, aggressive, fire tolerant.	High
Perennial Rye	<i>Lolium perenne</i>	0.1-0.9	Quick germination and good early growth, winter sowing recommended; does not survive very hot weather.	-
Weeping Love	<i>Eragrostis curvula</i>	0.5-0.9	Tufted**, aggressive; chokes out other grasses, browns in winter.	High
<p>Legend :</p> <p>* All species listed are perennial (long-lasting)</p> <p>** Tufted denotes a cluster of shoots arising from a common root system, and may not be as effective for erosion control as nontufted grasses.</p>				

Table 5.1 - Illustrative relationships of crack geometry

Crack width (B) m per metre	Under surface effective crack width (B_1) m per metre	flux (q) m^2s^{-1}	Effective crack width at depth (B_∞) m per metre
0.0005	0.019	3.75×10^{-8}	0.038
0.001	0.022	4.40×10^{-8}	0.044
0.002	0.026	5.14×10^{-8}	0.051
0.003	0.029	5.73×10^{-8}	0.057
0.004	0.031	6.20×10^{-8}	0.062
0.005	0.033	6.60×10^{-8}	0.066

Notes : (1) Solutions based on $K = 1 \times 10^{-6} ms^{-1}$, $H = 0.05$
see equations 5.7-5.9.

(2) See Figure 5.10 for definition diagram.

Table 5.2 - Predicted permeability of cracks from equation 5.11

Crack Spacing m	Crack width (B) m					
	5.00E-4	1.00E-3	2.00E-3	3.00E-3	4.00E-3	5.00E-3
0.250	8.18E-4	6.54E-3	5.23E-2	1.77E-1	4.19E-1	8.18E-1
0.500	4.09E-4	3.27E-3	2.62E-2	8.83E-2	2.09E-1	4.09E-1
1.000	2.04E-4	1.64E-3	1.31E-2	4.41E-2	1.05E-1	2.04E-1
2.000	1.02E-4	8.18E-4	6.54E-3	2.21E-2	5.23E-2	1.02E-1
5.000	4.09E-5	3.27E-4	2.62E-3	8.83E-3	2.09E-2	4.09E-2

Note : Permeability values in ms^{-1}

Table 5.3 - Slope locations for chunam crack survey

'CHASE' report slope number	Location	Coordinates	Chunam Condition
89	Ngau Chi Wan Platform Road	22075N 40225E	Bad
98	Ngau Chi Wan Road	21775N 40300E	Average
99	Old Clearwater Bay Road	21650N 40700E	Average
102	Fei Ngo Shan Road	21725N 41275E	Average
106	Jats Incline Road	23500N 40700E	Poor
112	Jats Incline Road	22925N 40225E	Bad
113	Jats Incline Road	22900N 40250E	Bad
114	Jats Incline Road	22925N 40275E	Poor

Table 5.4 - Summary of chunam crack survey

'CHASE' Slope No.	89	112	113	106	114		98		99	102
Chunam Condition	Bad	Bad	Bad	Poor	Poor		Average		Average	Average
					A	B	A	B		
Crack Widths mm										
Hair Crack	3350		1530	8840	720	1170	1080	1780	1890	1750
0.5 mm	2790			350			320	330	670	630
1.0	650	3620	1890		640	1270	510			
1.5	410					380				
2.0			2210		490	3050				
3.0					750	510				
4.0		50	250			1330				
5.0										
6.0			85							

Note : Numbers in table are the total length of cracks of given crack width in a 1 m² area.

Table 5.5 - Summary of crack seepage and effective chunam permeability

'CHASE' Slope No.			89	112	113	106	114		98		99	102
Chunam Condition			Bad	Bad	Bad	Poor	Poor		Average		Average	Average
							A	B	A	B		
Chunam Permeability	Soil Permeability											
1.0E-8	1.E-6	q	1.53E-7	1.43E-7	2.10E-7	1.33E-8	9.45E-8	3.40E-7	4.00E-8	1.40E-8	2.50E-8	2.30E-8
		K_e	1.63E-7	1.53E-7	2.20E-7	2.33E-8	1.45E-7	3.50E-7	5.00E-8	2.40E-8	3.50E-8	3.30E-8
	1.E-5	q	1.53E-6	1.43E-6	2.10E-6	1.33E-7	9.45E-7	3.40E-6	4.00E-7	1.40E-7	2.50E-7	2.30E-7
		K_e	1.54E-6	1.44E-6	2.11E-6	1.43E-7	9.55E-7	3.41E-6	4.10E-7	1.50E-7	2.60E-7	2.40E-7
	1.E-4	q	1.53E-5	1.43E-5	2.10E-5	1.33E-6	9.45E-6	3.40E-5	4.00E-6	1.40E-6	2.50E-6	2.30E-6
		K_e	1.53E-5	1.43E-5	2.10E-5	1.33E-6	9.45E-6	3.40E-5	4.00E-6	1.40E-6	2.50E-6	2.30E-6

- Notes : (1) q is seepage through cracks based on crack model (equations 5.7-5.9) ($m^3 s^{-1}$)
(2) K_e is effective chunam permeability based on equation 5.13 (ms^{-1})
(3) All permeability values are ms^{-1} .

Table 6.1 - Sites selected for 1 dimensional model verification

Location	Geology	Permeability ms ⁻¹	Suction moisture curve	Profile Depth m	Storm date	Slope cover
1. Realty Ridge	<u>COLLUVIUM</u> CDV	2.0×10^{-5} 1×10^{-6}	figure 6.16 figure 6.1 a	11	30 August 1980	Mature vegetation
2. Chater Ridge	COLLUVIUM	2×10^{-5}	figure 6.1 b	9	10 May 1981	Mature vegetation
3. Site 2, Shaft A ⁽¹⁾ (Sweeney, 1982)	<u>COLLUVIUM</u> CDG	2×10^{-5} 1×10^{-6}	figure 6.1 b figure 4.27b	35 ⁽²⁾	10 May 1981	Bare ground
4. Clearwater Bay Road	<u>CHUNAM</u> CDG	5.2×10^{-8} 3.0×10^{-6}	figure 4.27b figure 4.27b	4	17 June 1983	Chunam protected
5. Clearwater Bay Road	CDG	3.0×10^{-6}	figure 4.27b	4	17 June 1983	Thin-medium grass cover
6. Tai Po St. Christopher Bend	<u>COLLUVIUM</u> CDV	1×10^{-5} 2×10^{-6}	figure 6.1 b figure 6.1 a	3	10-14 July 1980	Dense grass - slope 8°

Notes : (1) No detailed validation is possible because of non-regular recording of suction data.

(2) Deepest records of suction for Hong Kong.

TABLE 6.2 - STATISTICAL ESTIMATES OF EXTREME RAINFALLS

Duration	Rainfalls for various return periods (1, 2)				
	2	5	10	100	1000
Hours: 1	68.2	88.5	102	144	185
2	94.3	128	150	219	286
4	119	169	203	307	409
8	146	213	257	395	530
24	214	309	371	567	759
Days: 2	253	366	440	675	904
4	311	441	527	796	1061
7	358	495	585	868	1148
15	483	642	747	1078	1402
31	668	847	965	1336	1700
Months: 3	1200	1480	1660	2240	-
6	1800	2250	2550	3480	-

- Notes:
1. Rainfalls in mm, return periods in years.
 2. Based on Royal Observatory records, 1884-1939 and 1947-77.

Table 6.3 - Summary of infiltration and runoff for the simulations undertaken in Figure 6.9

Duration	1 in 100 year storm					
	2 hour	8 hour	24 hour	48 hour	7 day	15 day
Rainfall (mm) (Table 6.2)	219	395	567	796	868	1 078
Infiltration (mm) given start condition (Fig. C 2.18 G.C.O.1981)	34	97	250	400	868	1 078
Runoff (% of storm)	84.4	75.4	55.9	49.7	0	0
Run time to derive suction minima (see Figure 6.9)	240	240	240	240	480	480

Table 6.4 - Summary of principal data accuracy required for finite difference models

	Qualitative Accuracy needed	Absolute accuracy guide	Source in this report	Remarks
<u>Input variable</u>				
K	very high	better than half an order of magnitude	figure 6.11	can be difficult to achieve (see Nielsen et al (1973), G.C.O. (1982))
$\theta - \psi$	moderate	within usual field variability range		tests undertaken by author at Bristol
surface detention	high for specific applications e.g. vegetation runoff studies	2 cm	figure 6.17 and 6.18	scarcity of published sources
rainfall	within-storm intensity not too sensitive	-	figure 6.10	
<u>Boundary Conditions</u>				
Upper	(1) Vegetation	high	empirical guide- lines to be determined (see Section 6.15)	figures 6.7, 6.17 and figure 5.12
	(2) Chunam	high in terms of crack density		
Lower : Groundwater	Appropriate field conditions to be complied with by model	see table 6.5	figure 6.21	will <u>severely</u> limit 2-D model applica- tions in Hong Kong especially coupled with permeability needs.

Table 6.5 - Acceptable Circumstances for Establishing Soil Suction Conditions for Design Purposes

	ACCEPT- ABLE	UNACCEPT- ABLE	NOTES
A. EMPIRICAL EVIDENCE			
Rainfall			
(i) 1 in 10 year event of acceptable even intensity	X		
(ii) All other storms		X	But gives guide to processes and soil water start conditions to be used in modelling
B. MODELLING EVIDENCE			
Topography			
(i) straight slope condition	X		See Section 6.1.1
(ii) spur cut	X		
(iii) hollow cut		X	
(iv) backslope variable topography		X	See Section 4.4 May be acceptable if it can be demonstrated that convergence of soil water can be accommodated by, say, wet initial conditions in a 2-D model
Cover			
(i) chunam	X		Acceptable if crack survey, or effective permeability of chunam, can be provided - see Section 5.2.
(ii) vegetation		X	Acceptable only if the upper boundary condition can be expressed in terms of effective rainfall or effective permeability as a minimum - see Section 6.1.5.
Geology			
(i) hard rock		X	Joint controlled conditions predominate.
(ii) decomposed	X		Acceptable if permeability variations can be accommodated by the model structure - see Section 6.1.3
(iii) soil	X		
Groundwater			
(i) direct infiltration control	X		
(ii) more complex groundwater controls		X	perhaps induced by geologic or topographic controls

- Notes :
- (1) Unacceptability of a single characteristic is a sufficient criteria for rejection of a complete site acceptance of soil suction in design.
 - (2) Acceptable conditions for the modelling approach presupposes (a) appropriate laboratory and field input data (see Table 6.4) and (b) field conditions, especially in terms of permeability variation, that can be accommodated by the model.
 - (3) An acceptable modelling outcome can only be regarded as such, providing it can be shown that, with stochastic sampling from field parameter distributions, the outcomes yield suctions at the location of interest (see Figure 3.14).

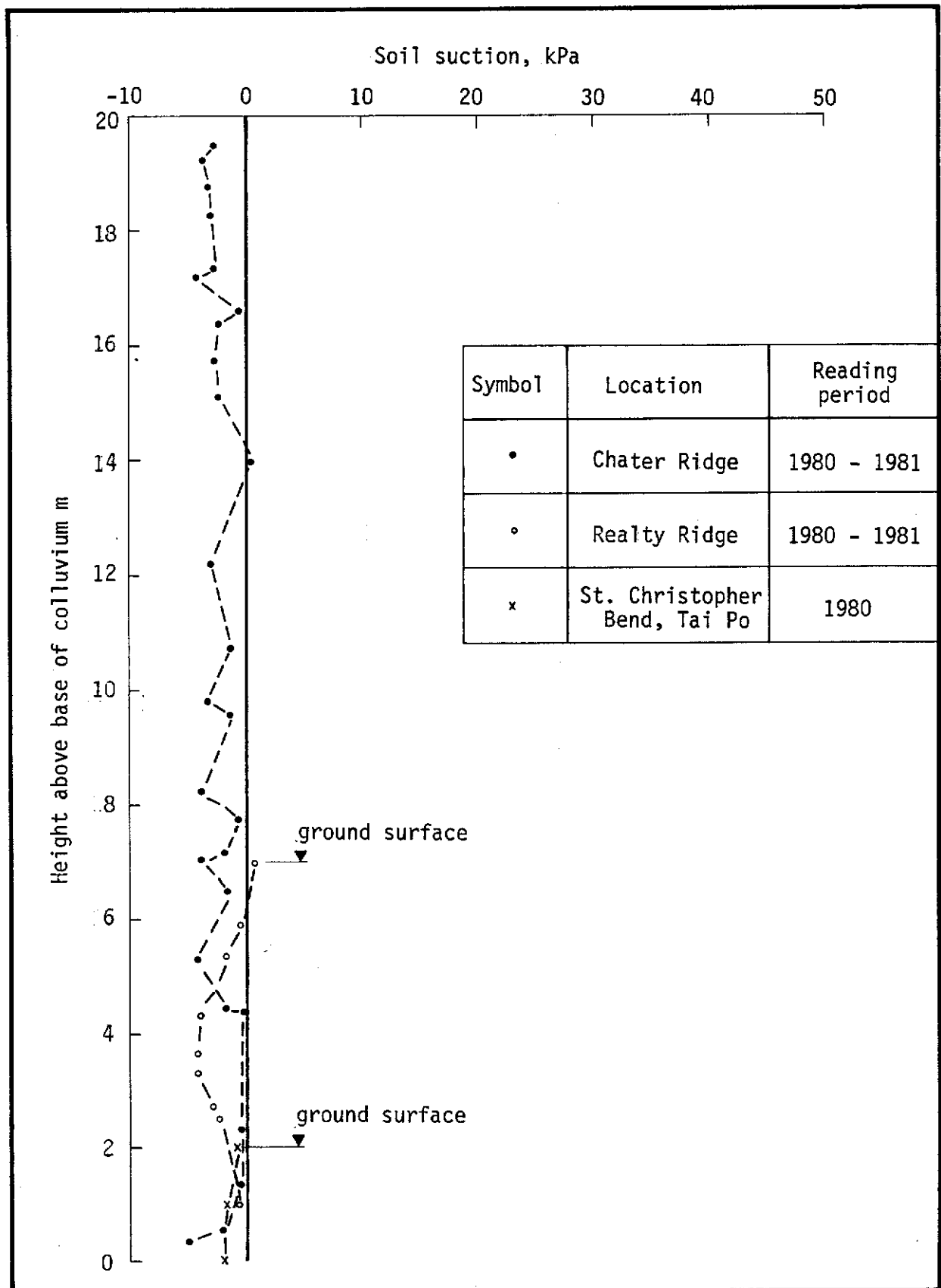


Figure 1.1 - Selected measurements of lowest recorded suctions in colluvium

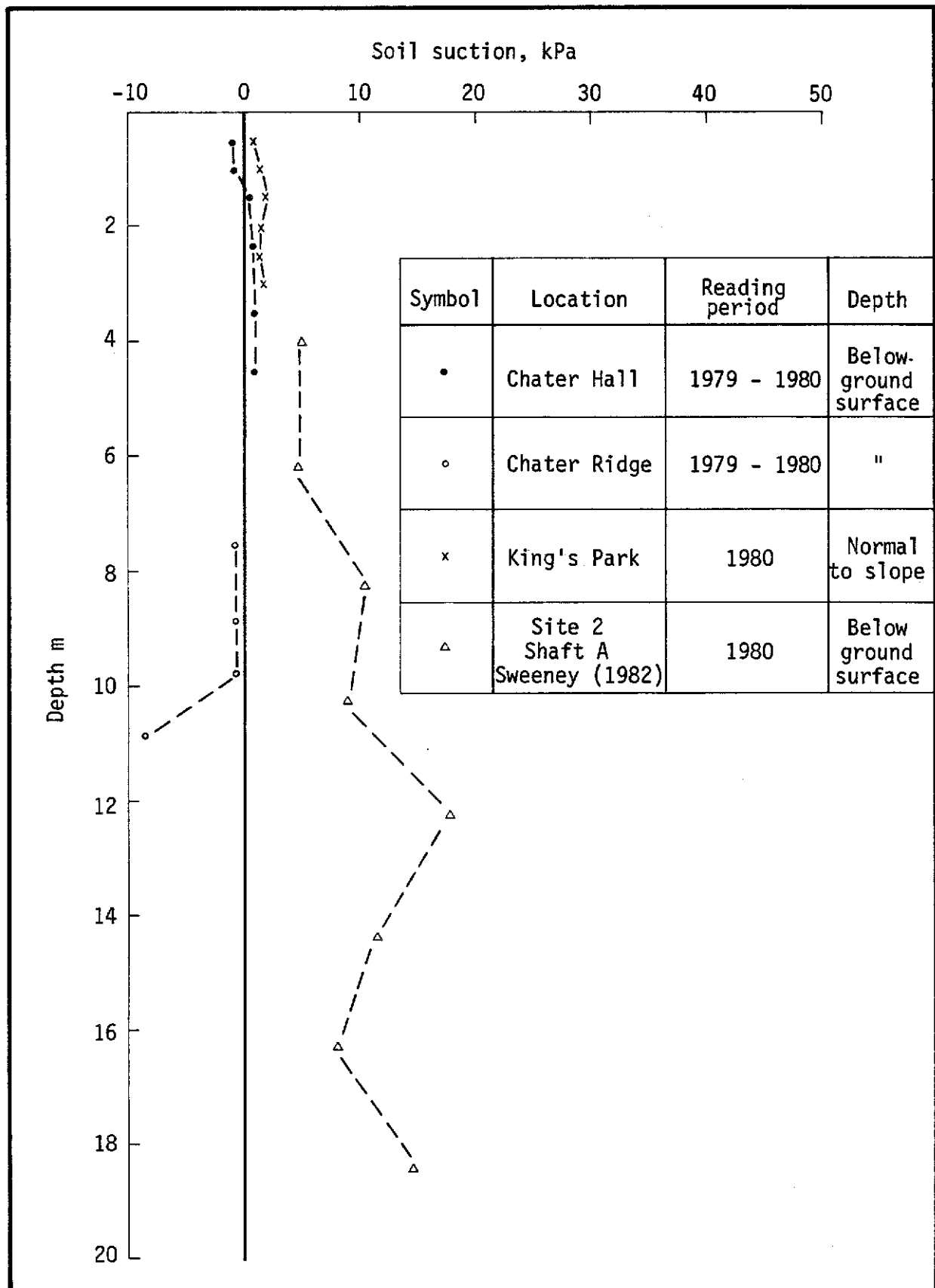


Figure 1.2 - Selected measurements of lowest recorded suctions in decomposed granite

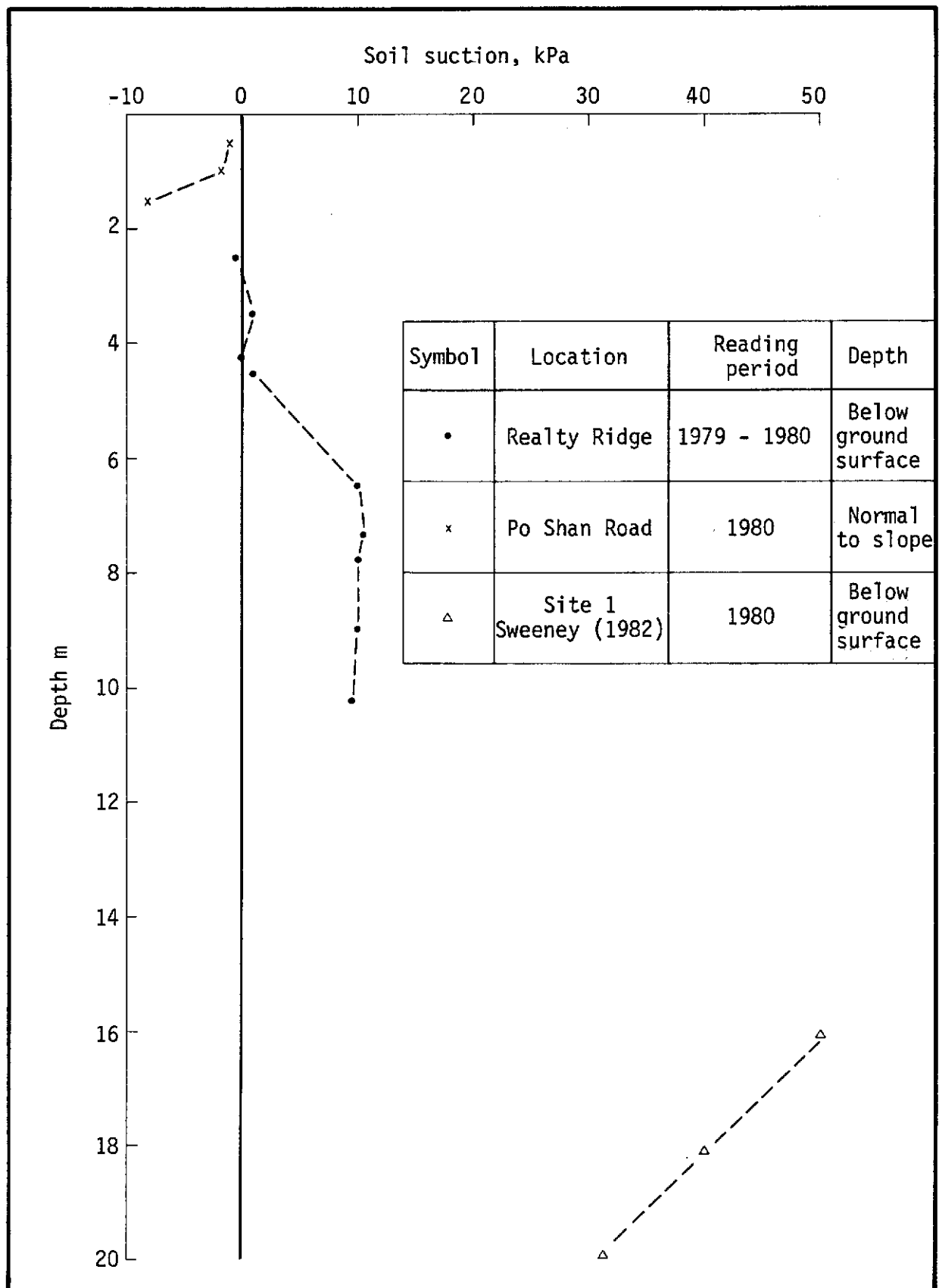


Figure 1.3 - Selected measurements of lowest recorded suctions in decomposed volcanics

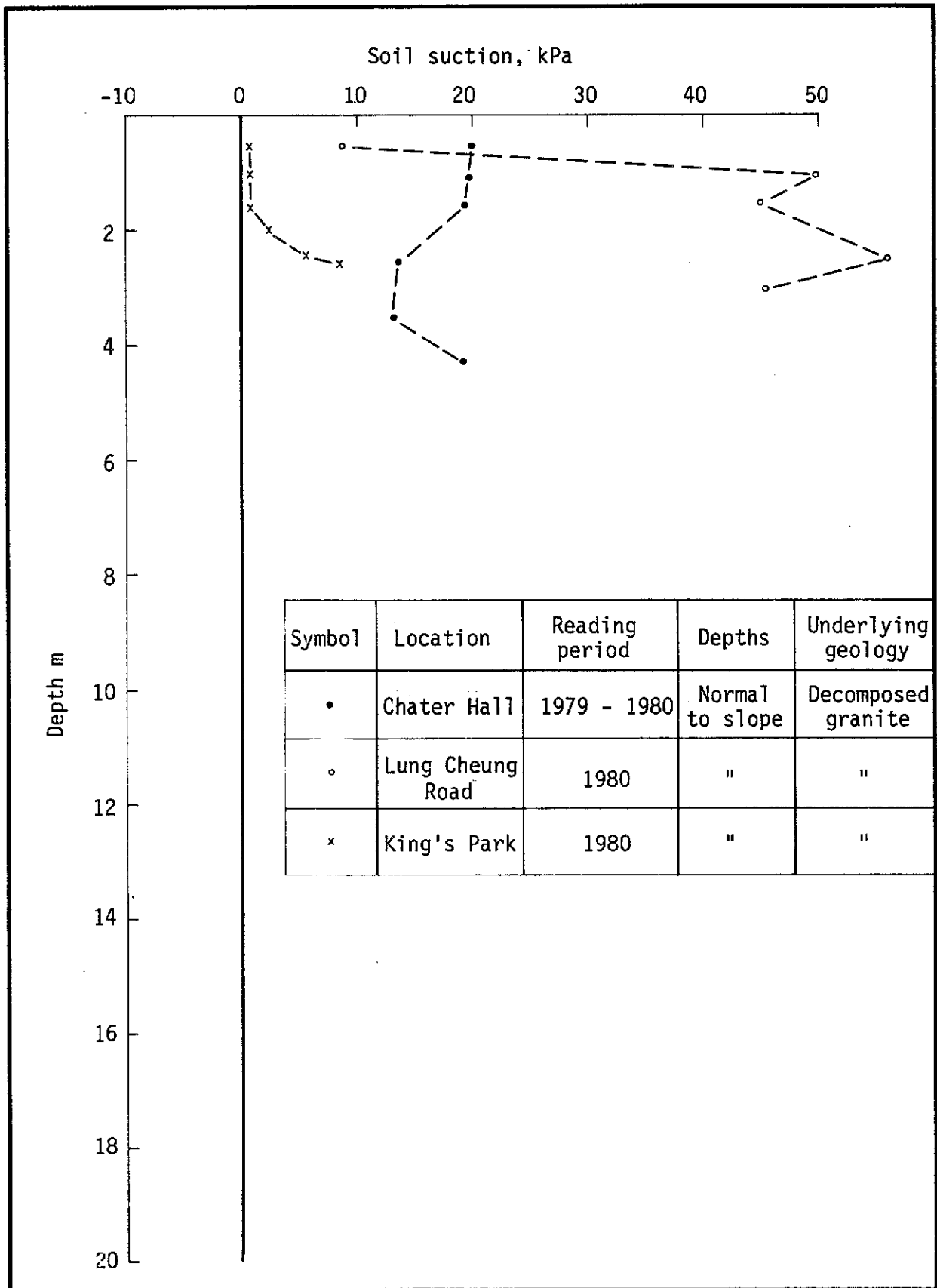


Figure 1.4 - Selected measurements of lowest recorded suctions in slopes protected by chunam

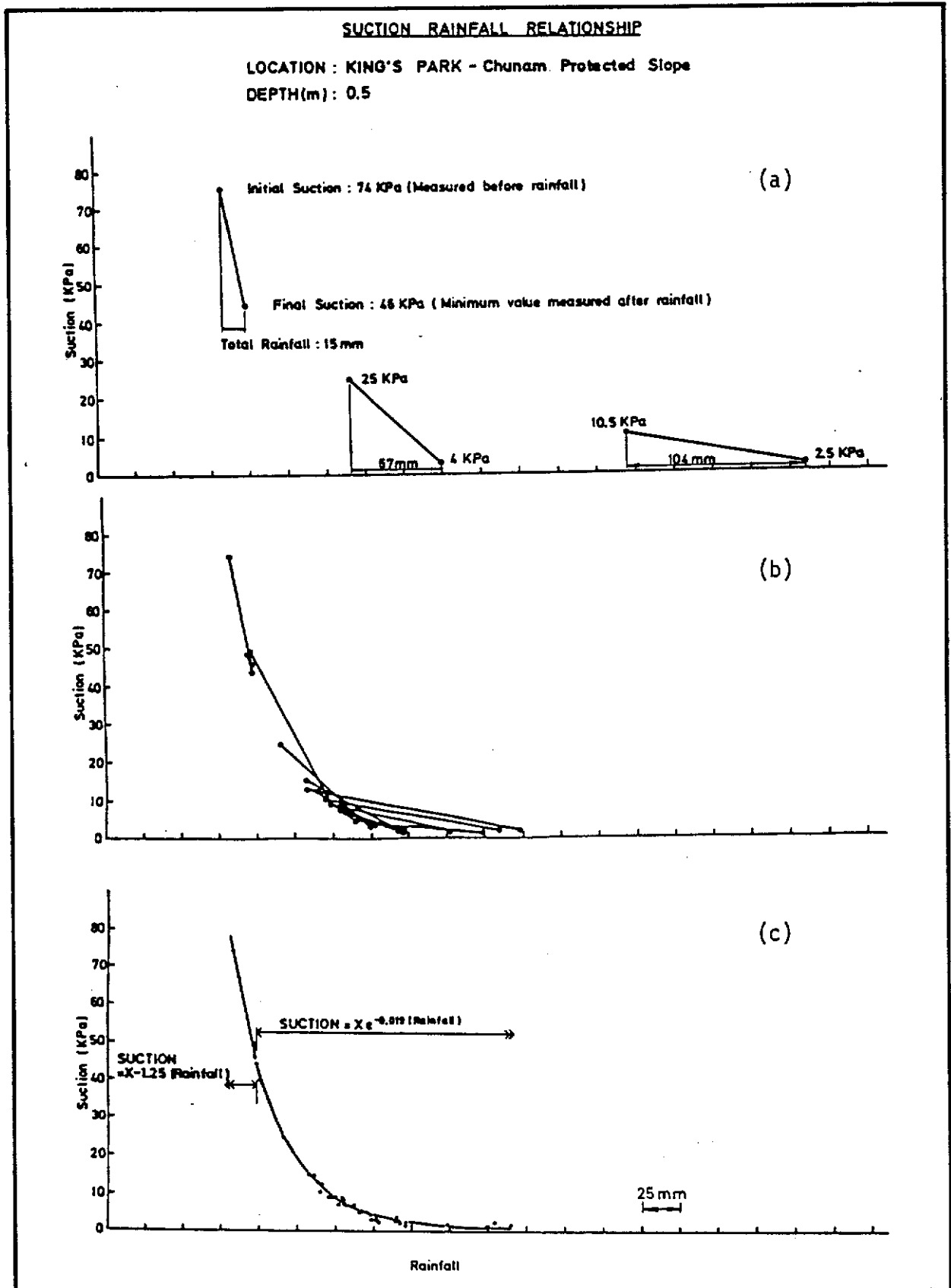


Figure 1.5 - Illustration of the procedure for the soil suction prediction model outlined by McFarlane (1981)

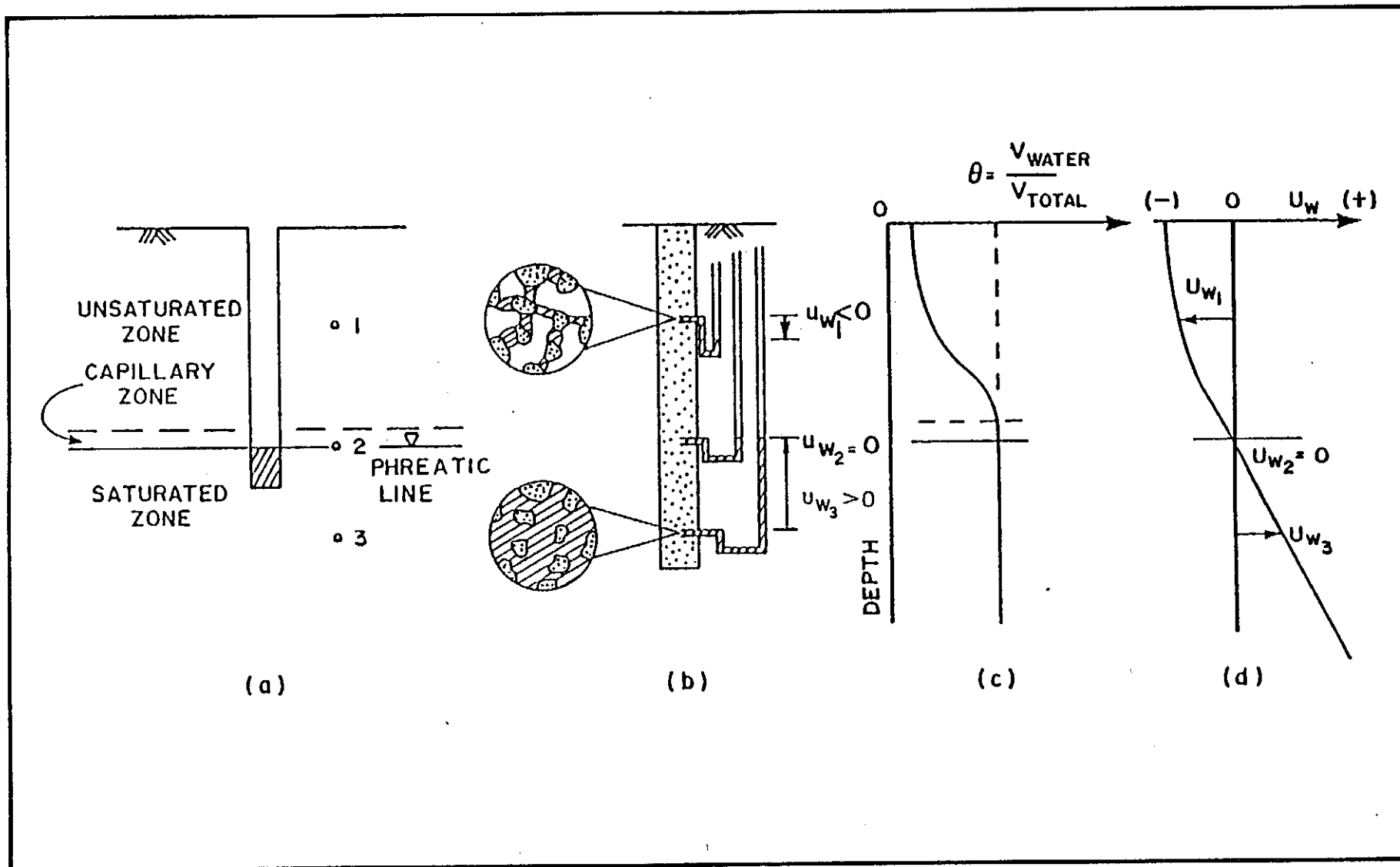


Figure 1.6 - Water content and suction changes in the saturated and unsaturated zones
(after Papagiannakis, 1982)

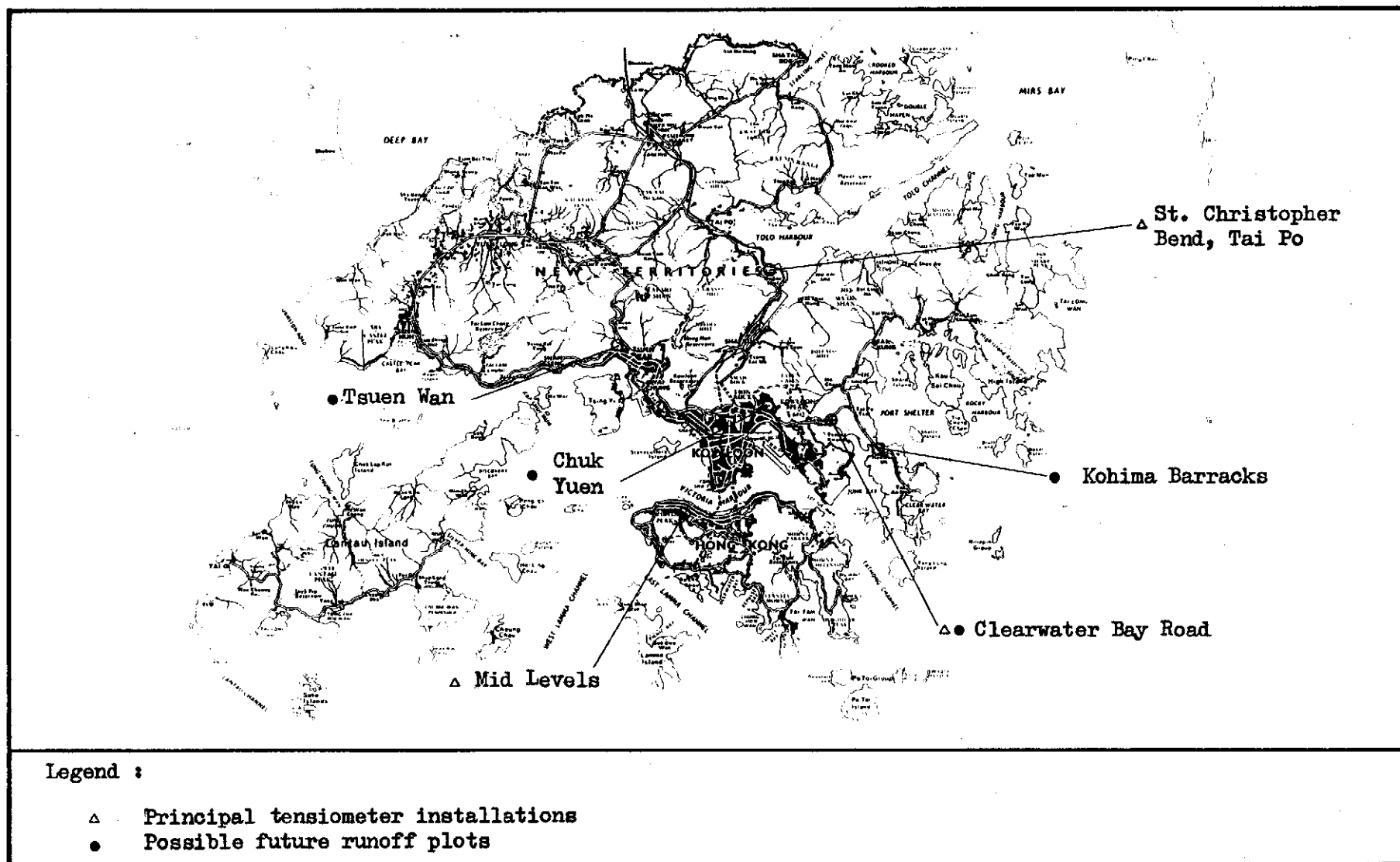


Figure 1.7 - Principal field sites used in the research programme

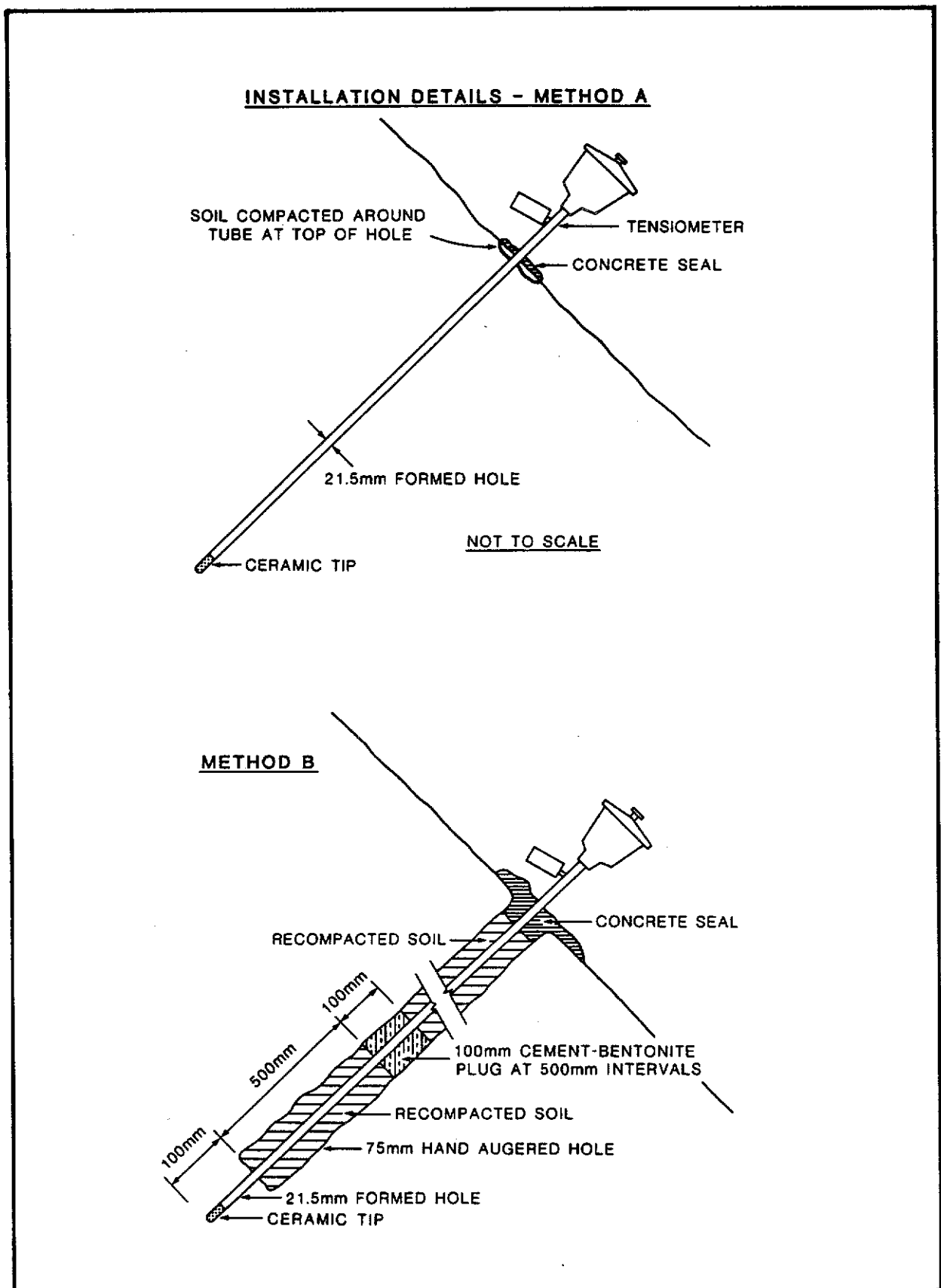


Figure 2.1 - Installation procedures for "Jetfill" tensiometers in uniform soils. Method (A) for depths to 1.5 m (B) for depths greater than 1.5 m

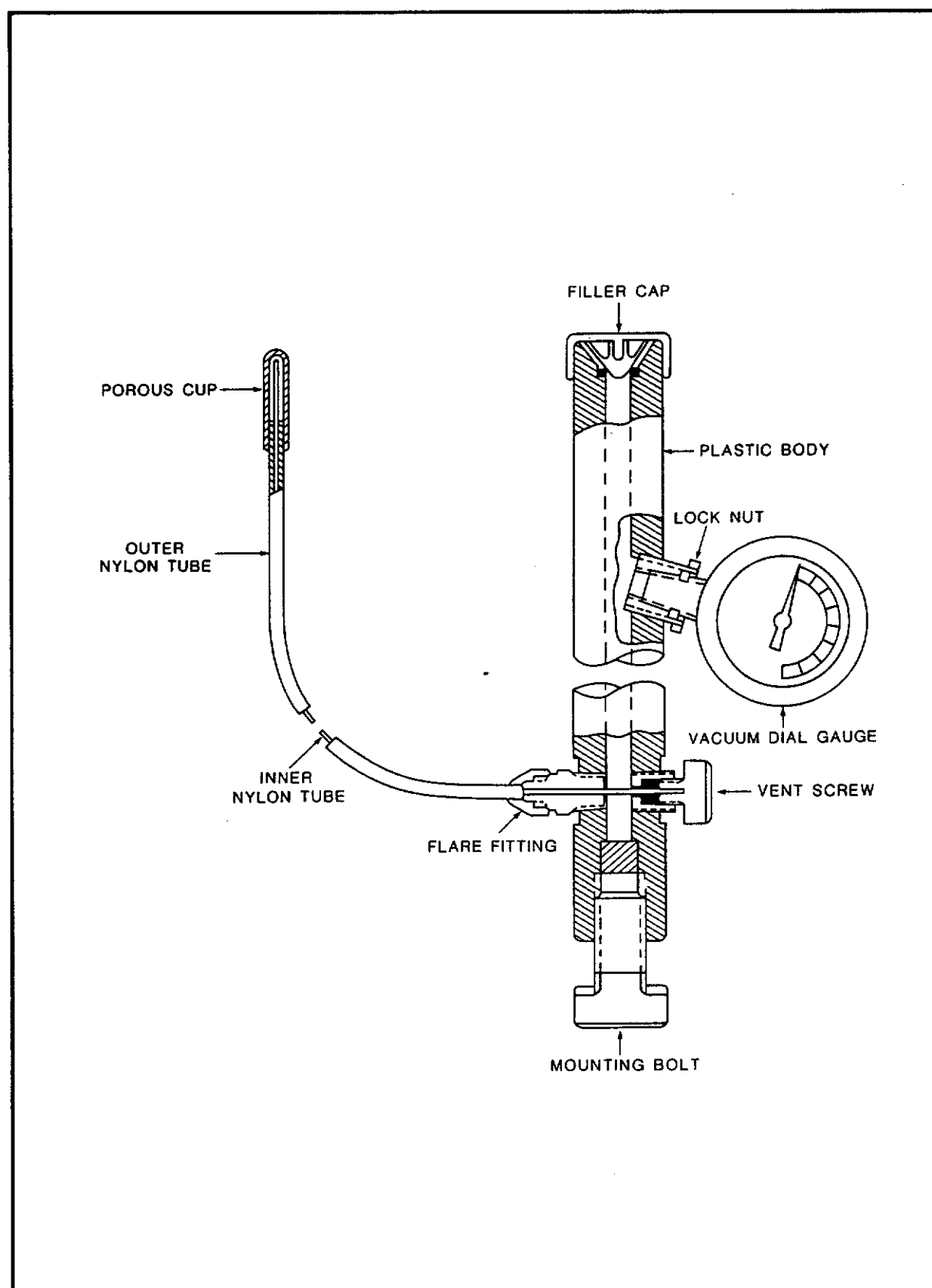


Figure 2.2 - 8 mm ceramic cup tensiometer (2100 series - Soil-Moisture Equipment Corporation) with flexible tube

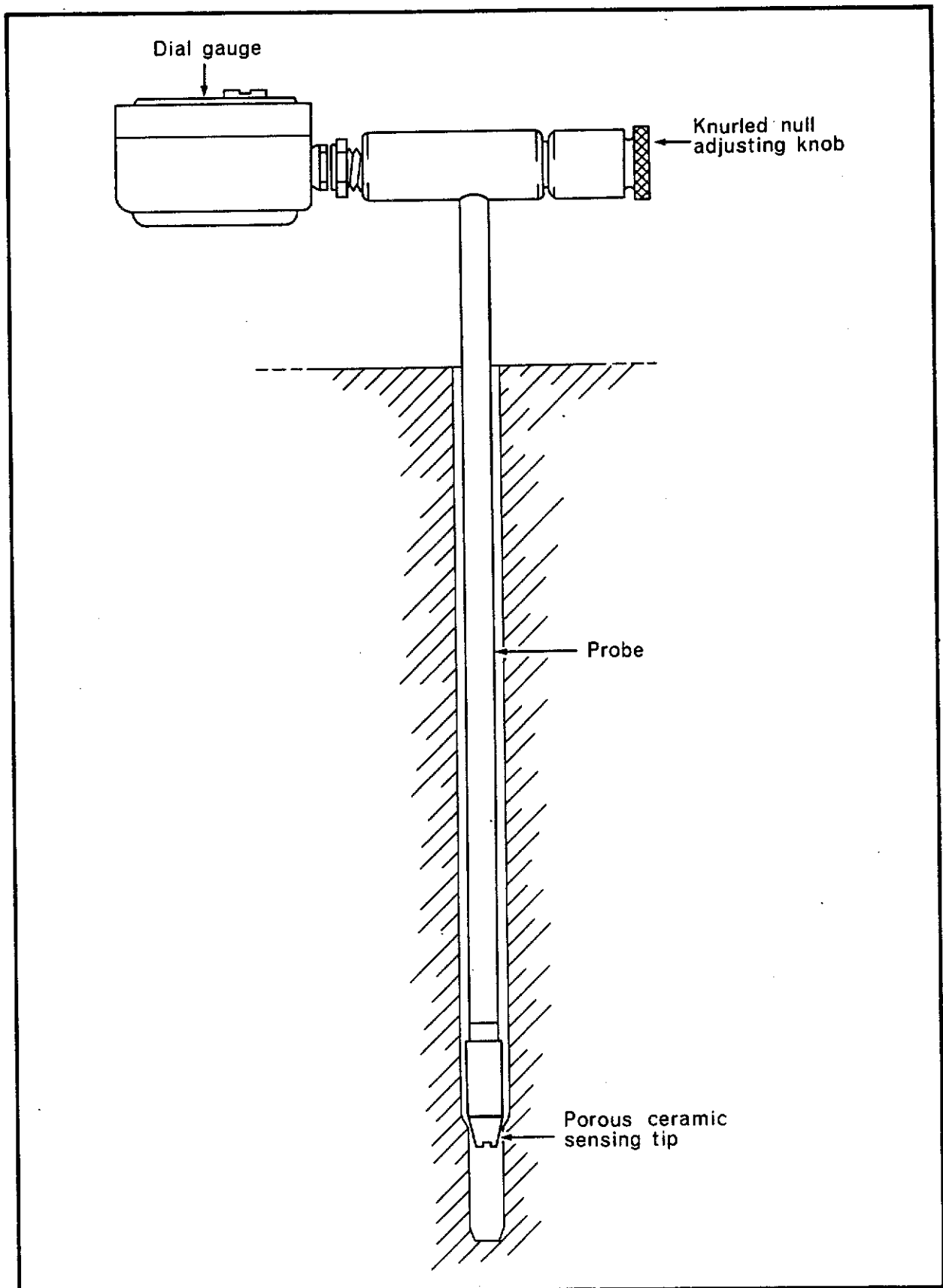


Figure 2.3 - "Quick Draw" tensiometer (Soil-Moisture Equipment Corporation)

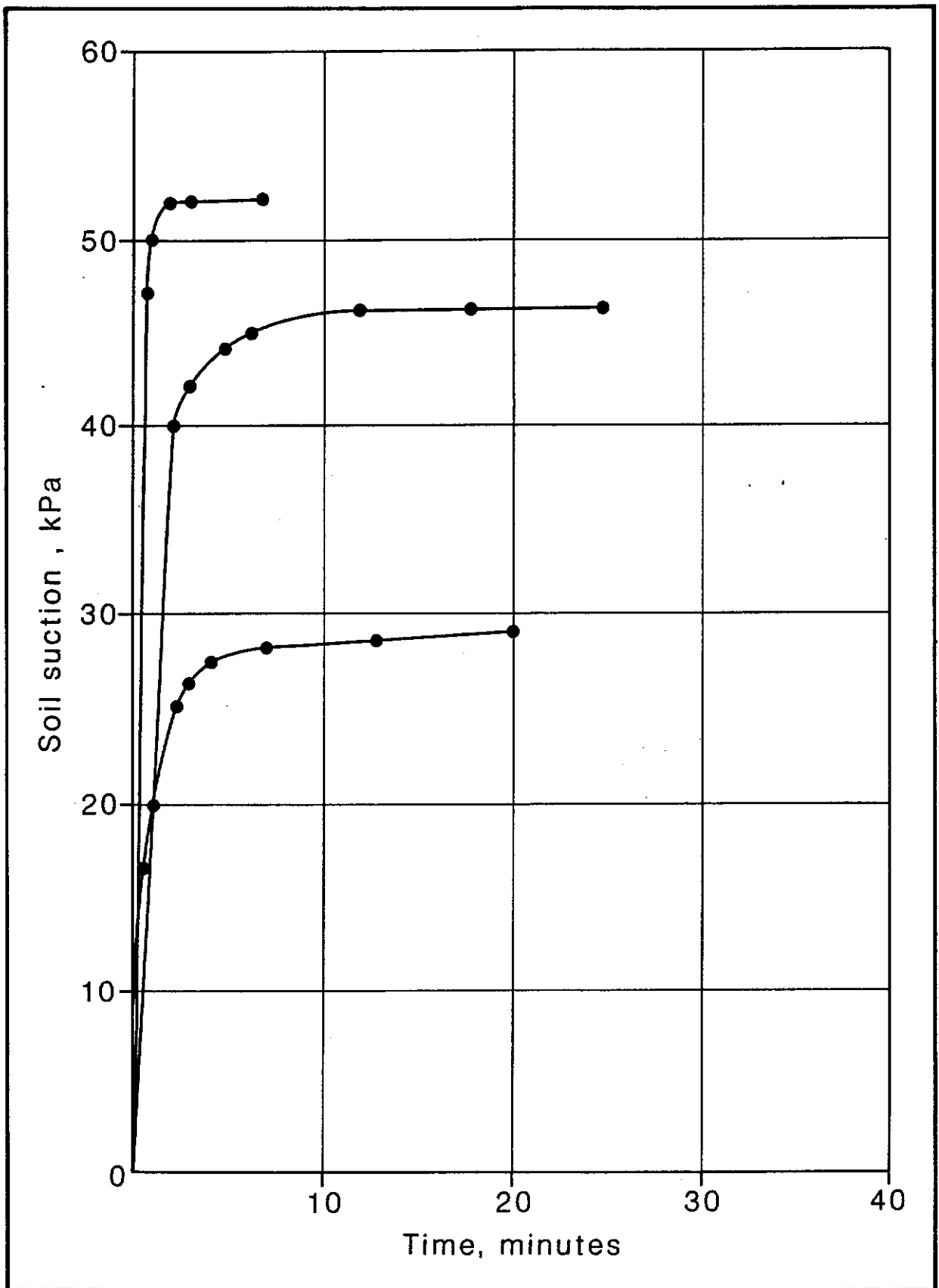


Figure 2.4 - Response times of "Quick Draw" tensiometer (after Sweeney 1982)

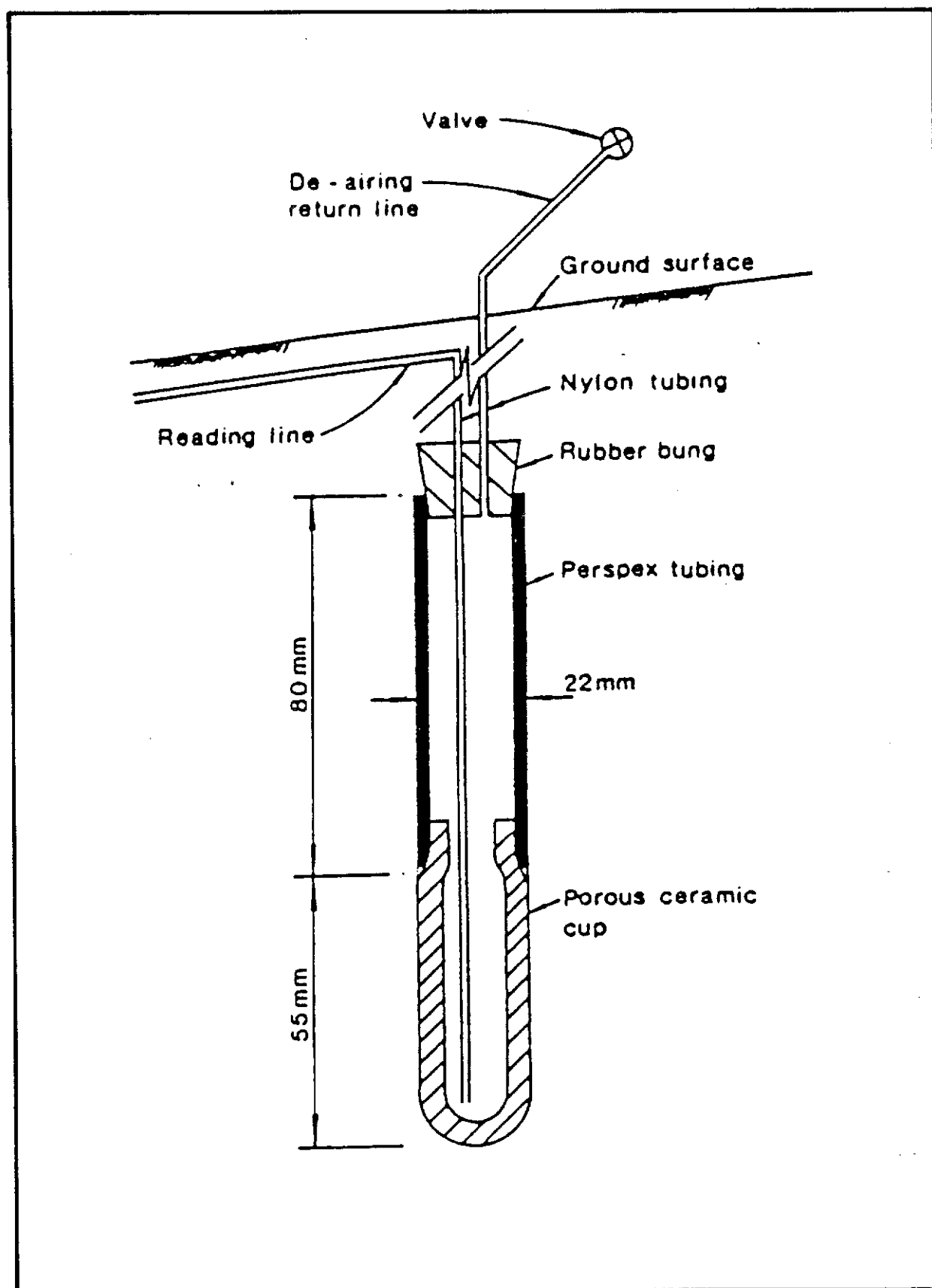


Figure 2.5 - Tensiometer design for use with automatic scanivalve system (after Anderson and Burt, 1977)

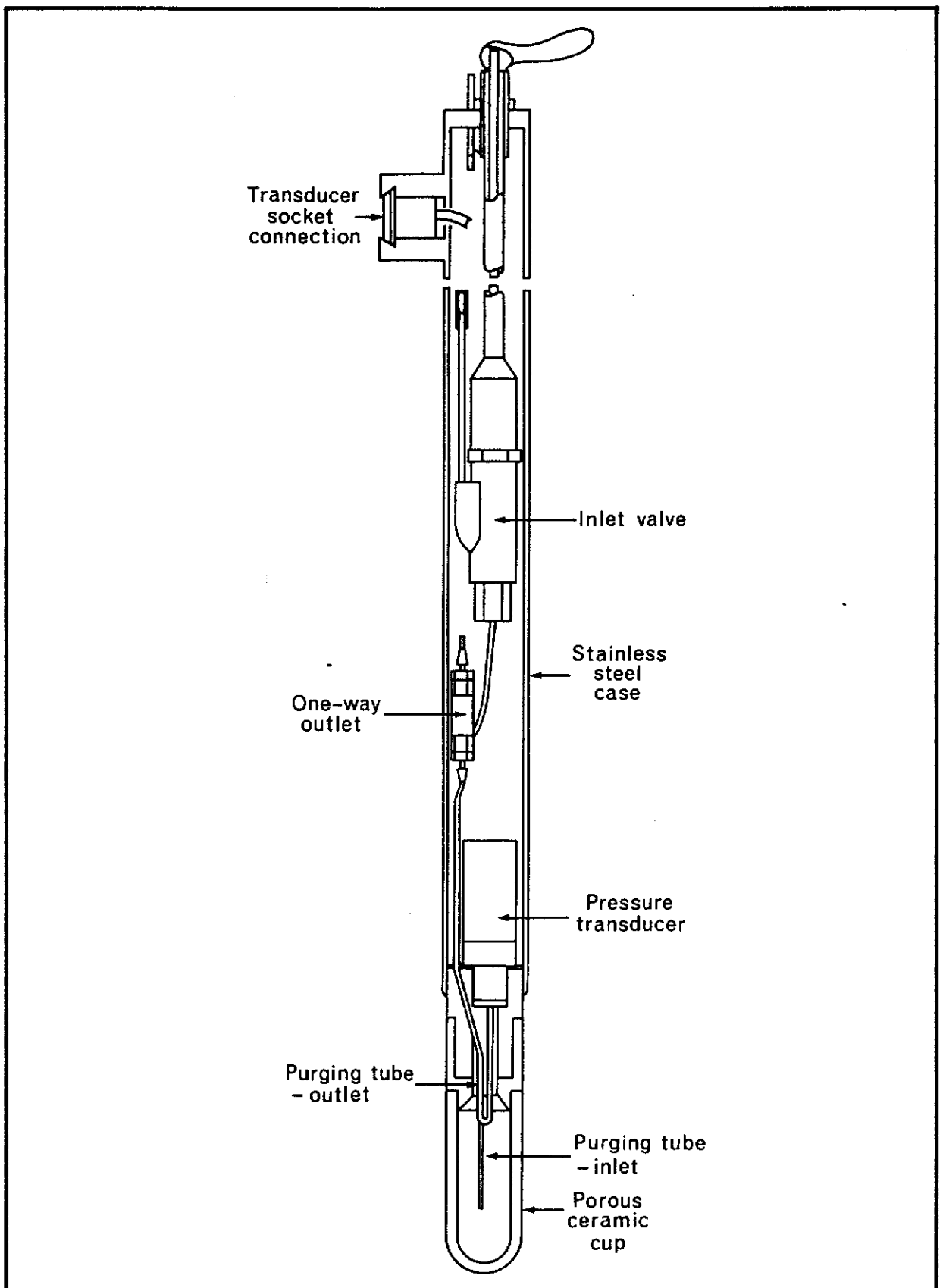


Figure 2.6 - Institute of Hydrology pressure transducer tensiometer system

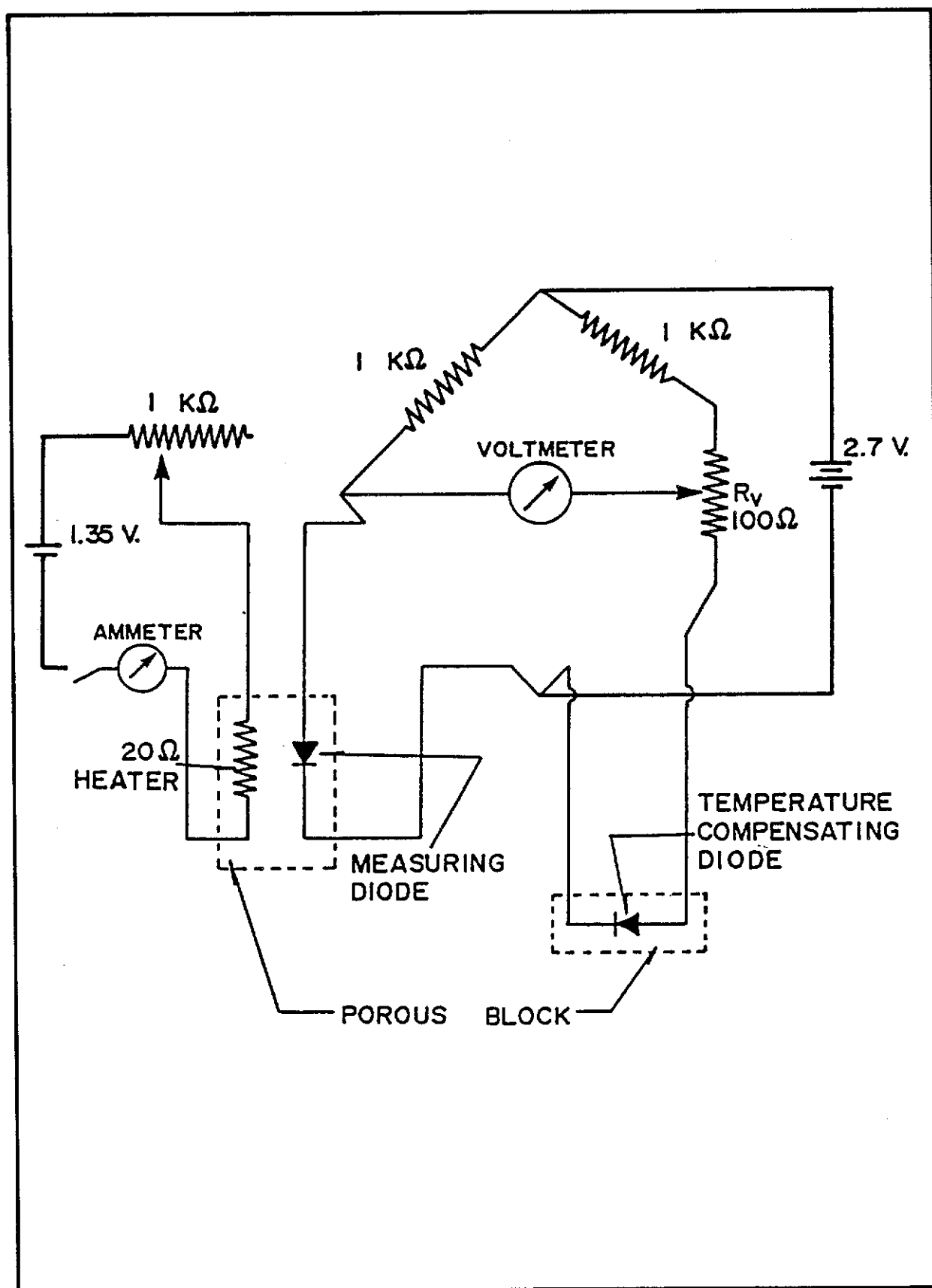


Figure 2.7 - Measuring circuit for temperature - compensated matrix potential sensor (after Phene, Hoffman and Austin, 1973)

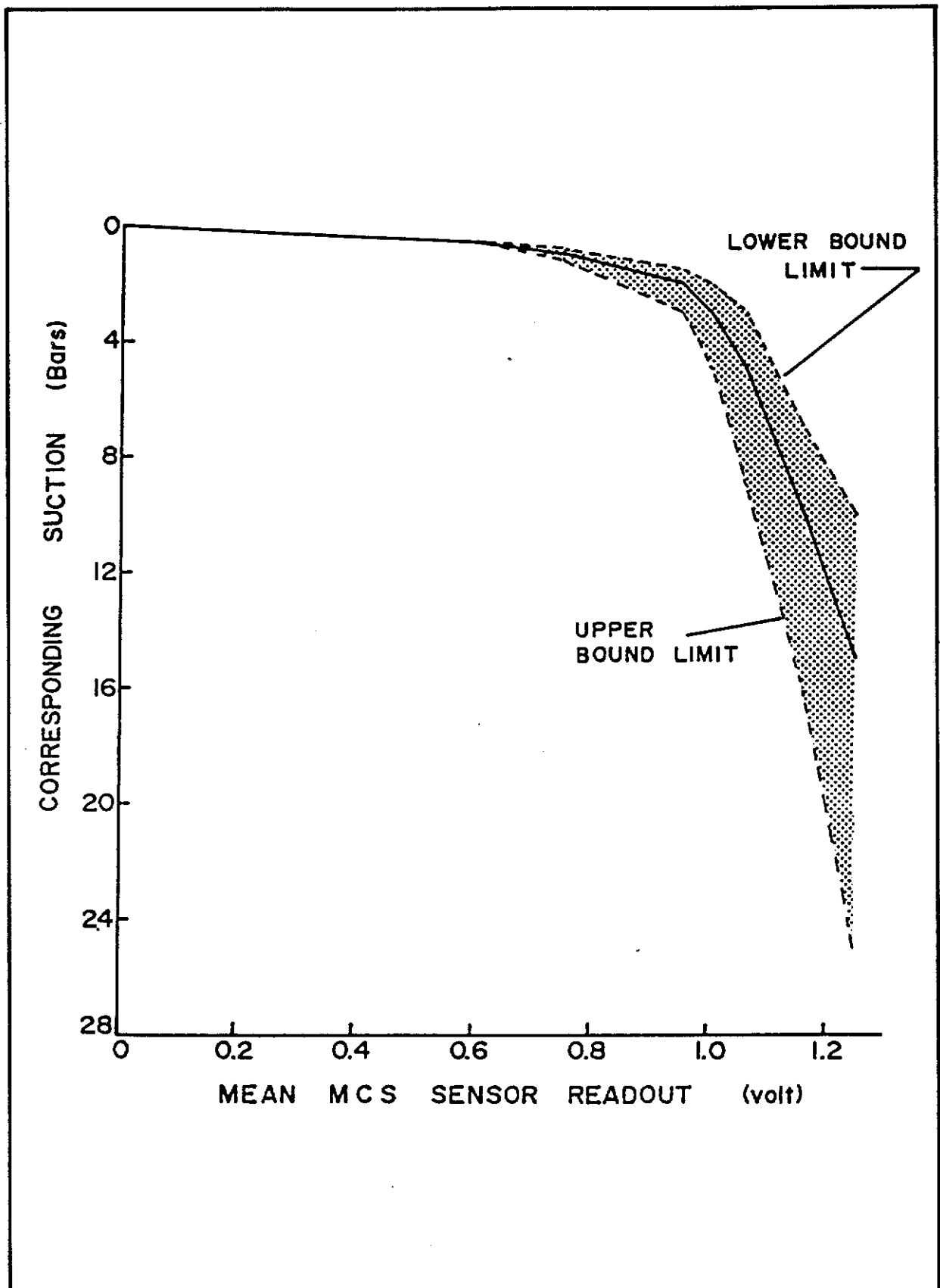


Figure 2.8 - Mean voltage readout of the MCS 600 sensor with suction
(from MCS 600 System User's Manual)

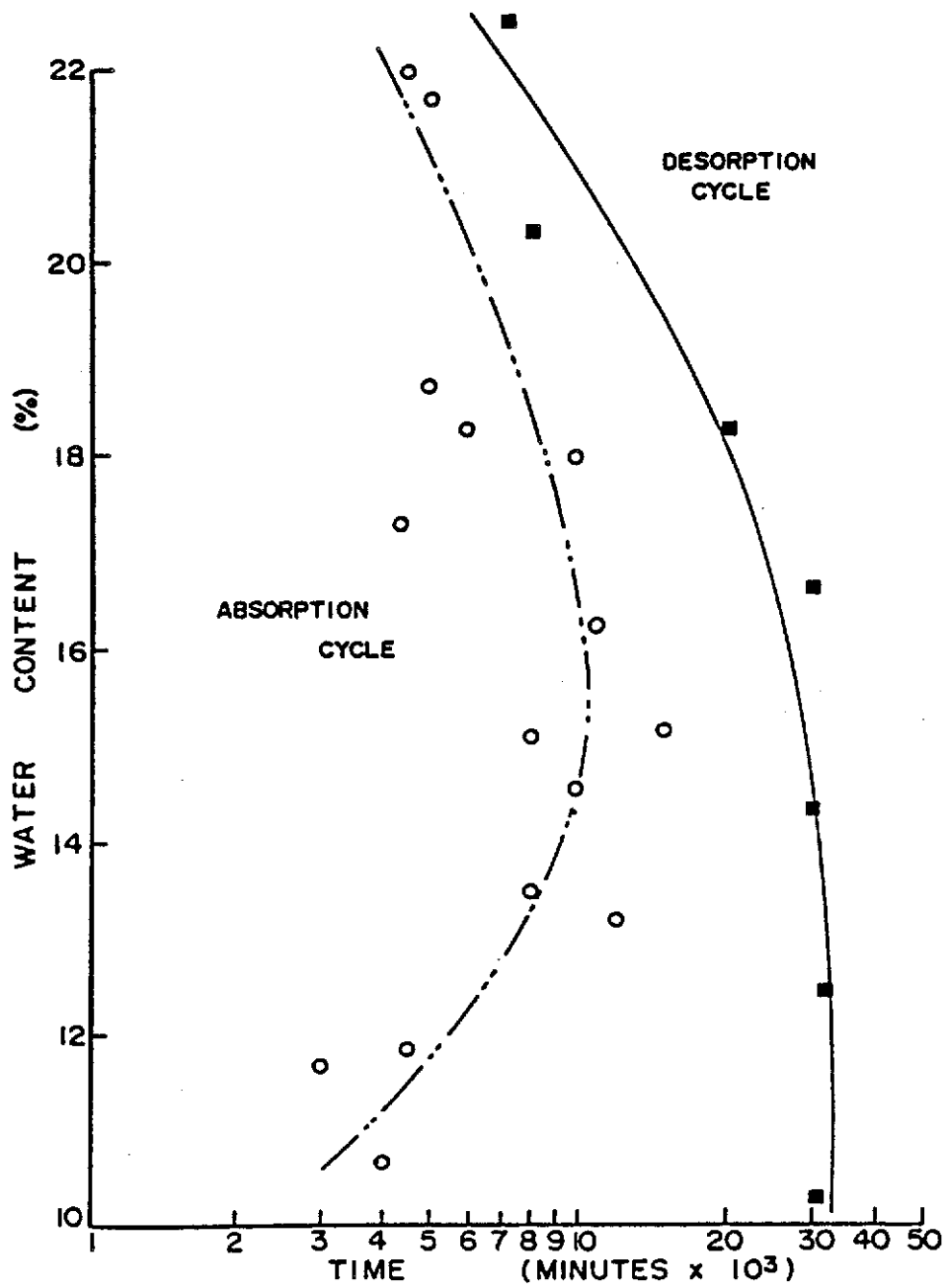


Figure 2.9 - Response time of the MCS 600 sensor in laboratory testing using a glacial till (after Lee, 1983)

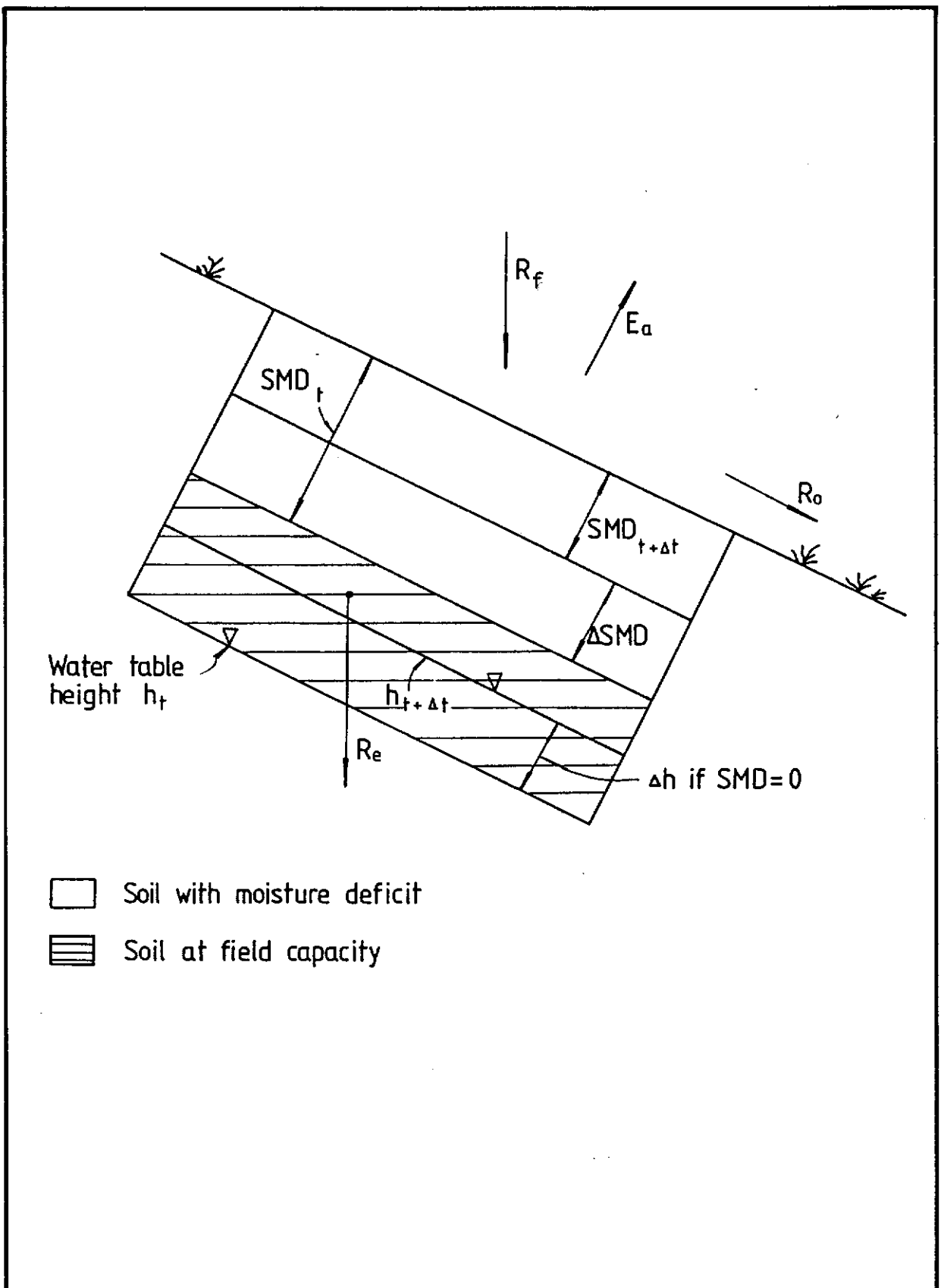


Figure 3.1 - Illustration of the SMD concept (after Leach and Herbert, 1982)

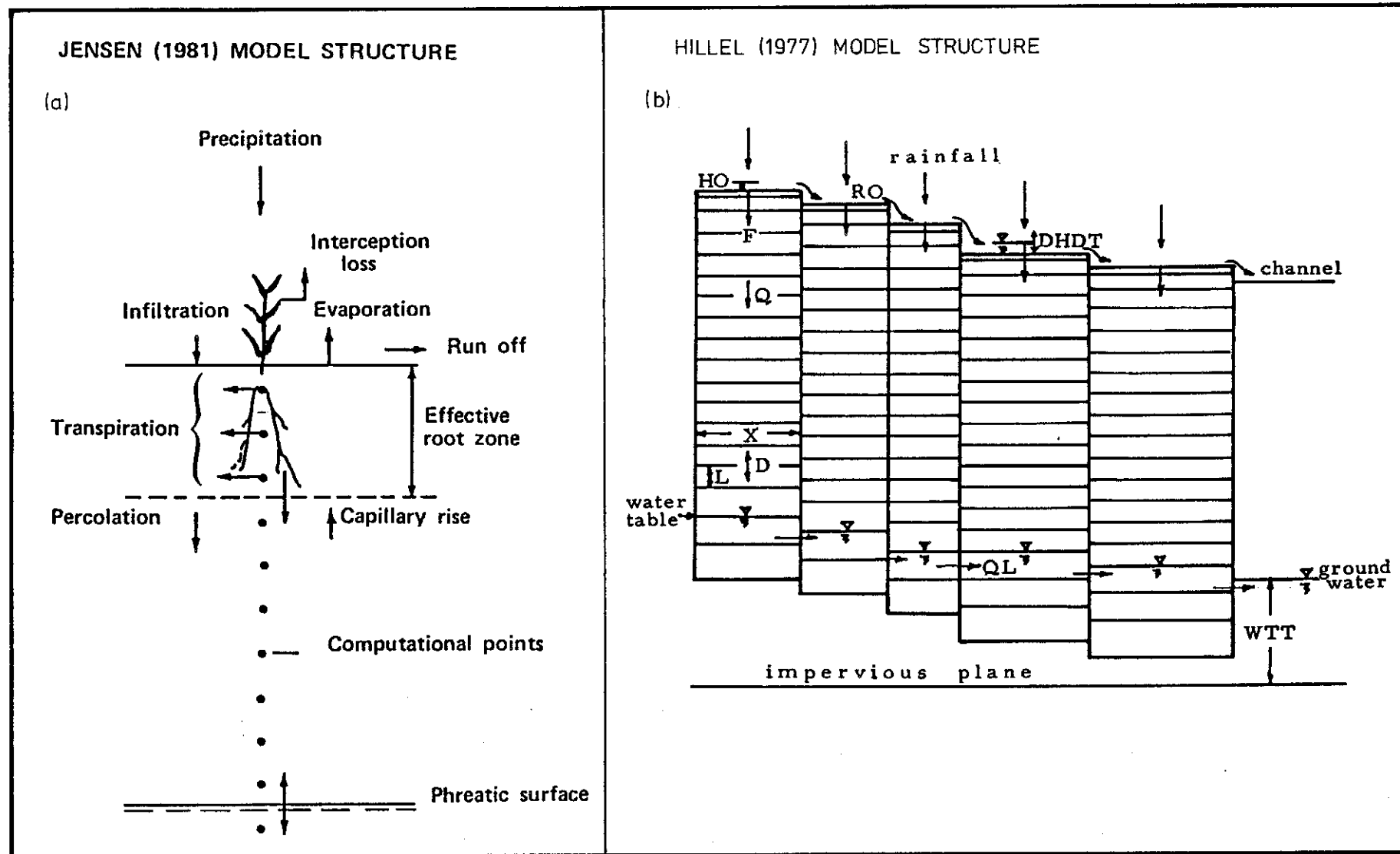


Figure 3.2 - Diagrammatic representation of (a) 1 dimensional and (b) 2 dimensional soil water models

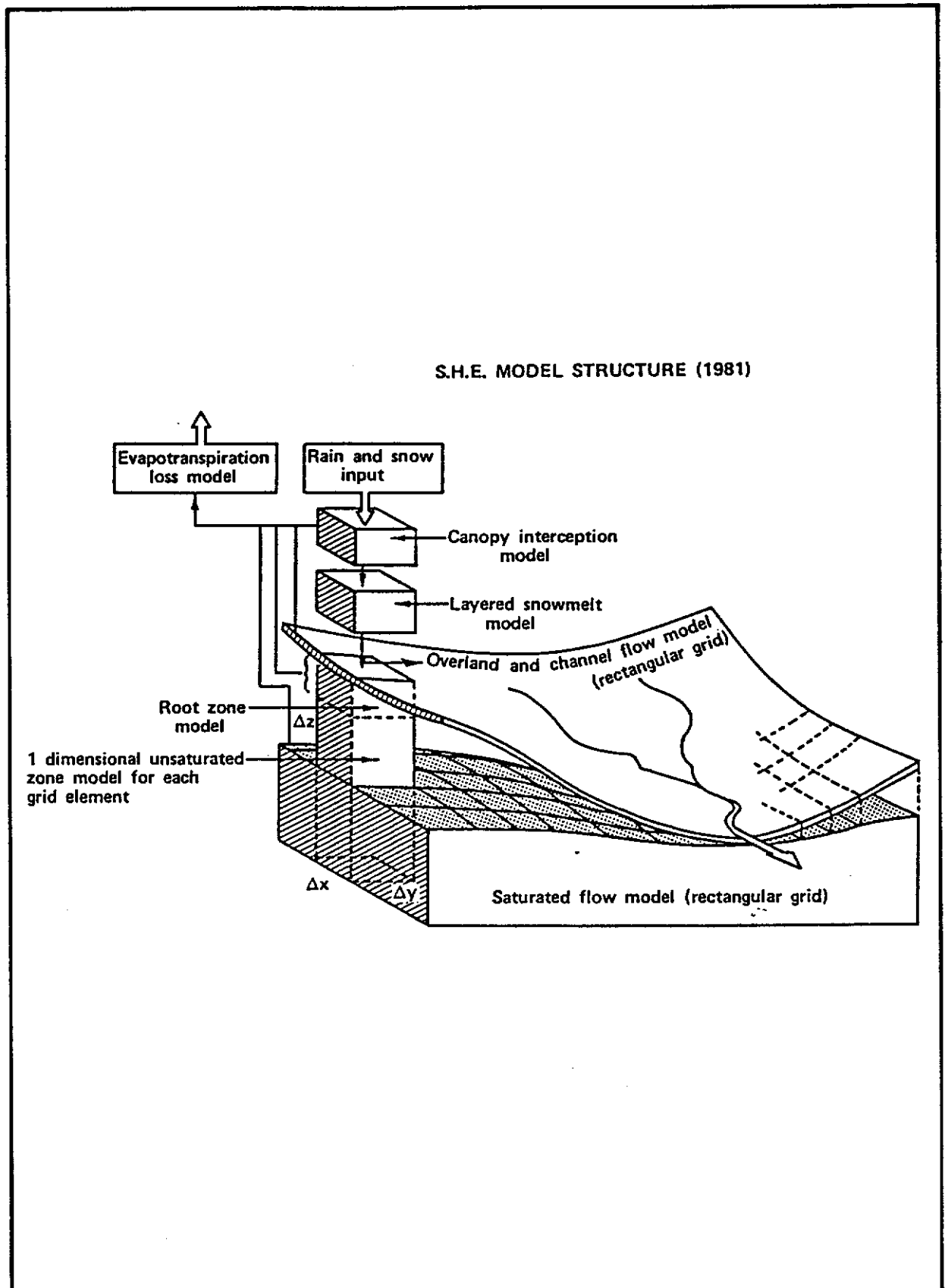


Figure 3.3 - Diagrammatic representation of 3 dimensional 'SHE' model structure

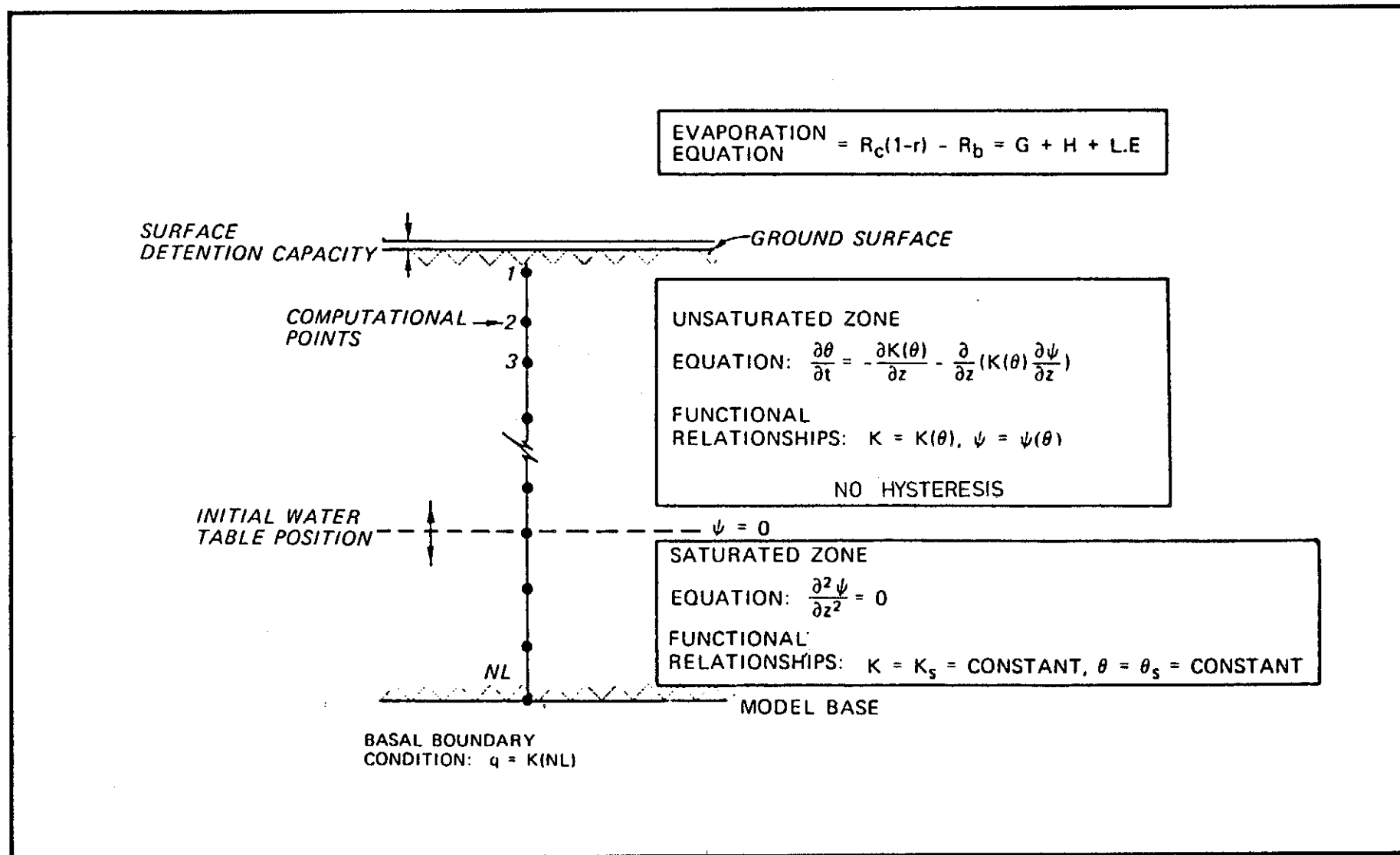


Figure 3.4 - Governing equations used in soil water model (note evaporation and base conditions may be varied)

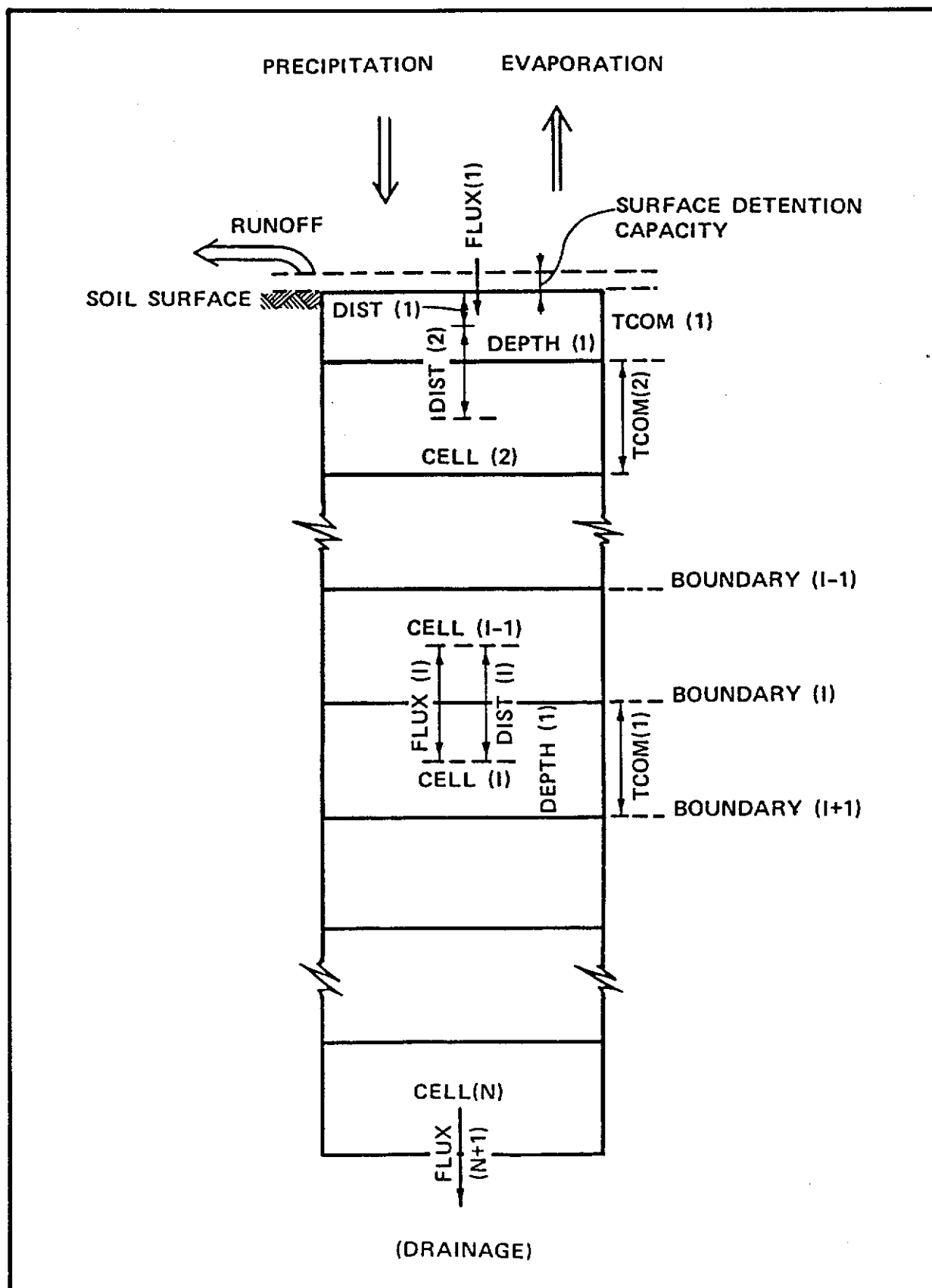
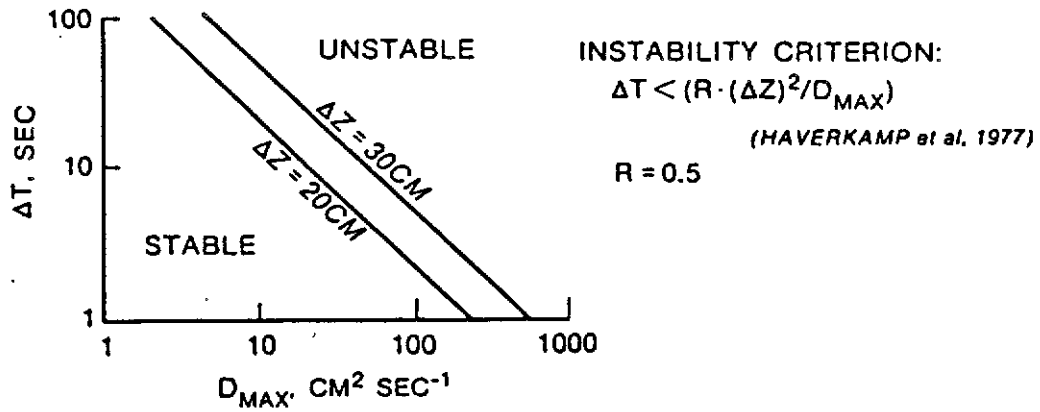
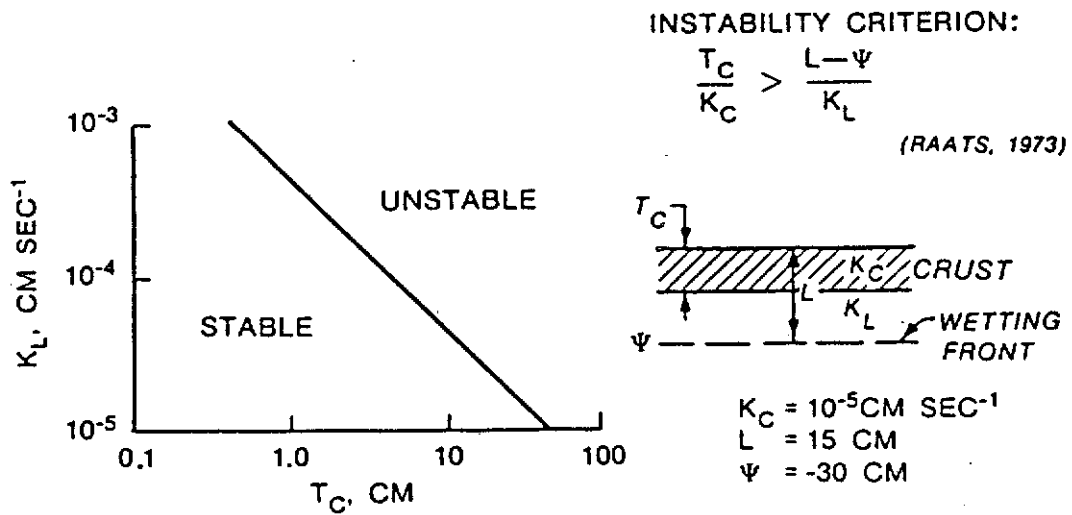


Figure 3.5 - Basic one dimensional soil water model structure



a. NUMERICAL SOLUTION STABILITY



b. WETTING FRONT STABILITY

Figure 3.6 - Illustrations of two types of instability in soil water modelling

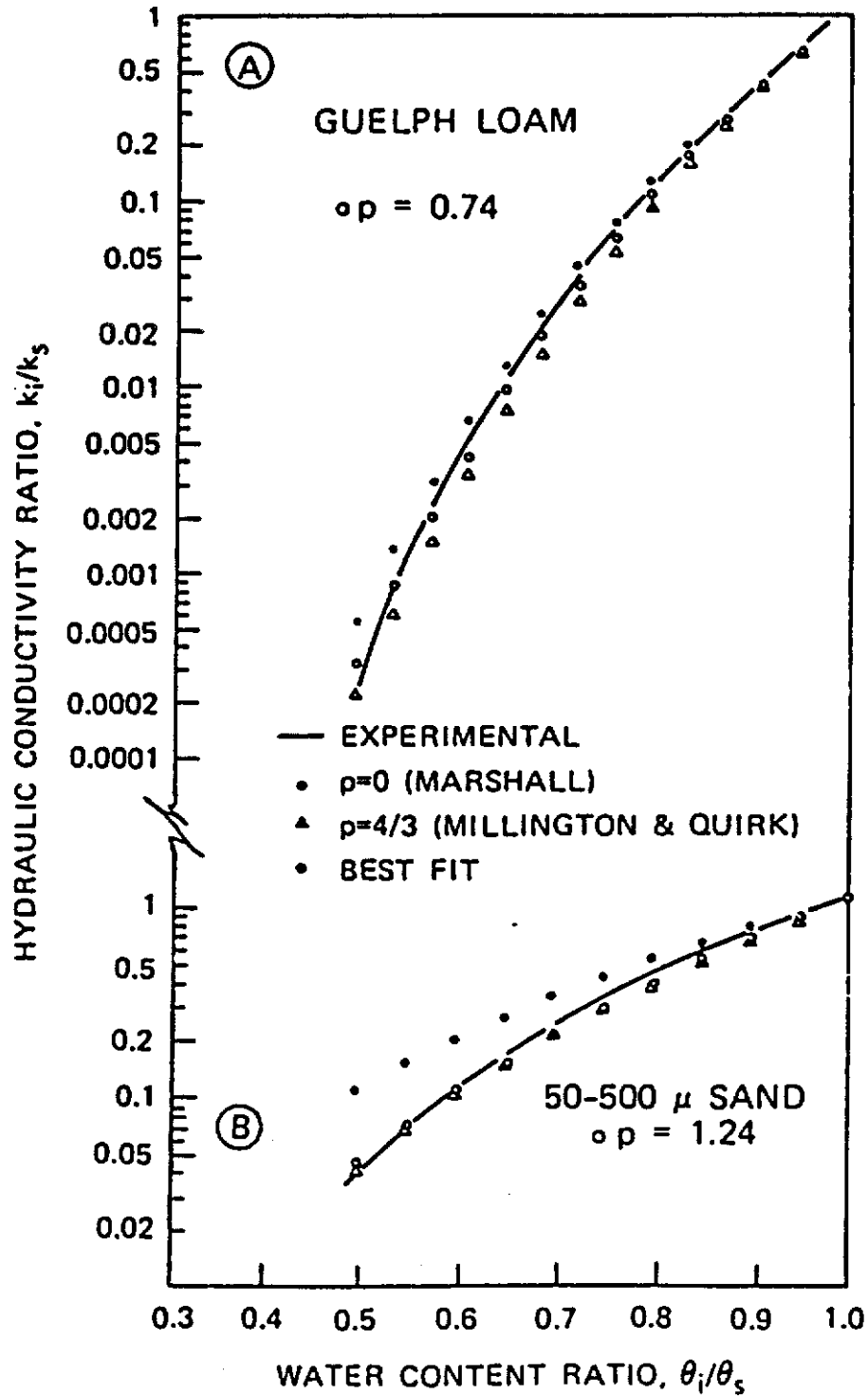


Figure 3.7 - Estimation of unsaturated permeability using the M-Q method, compared with that of Marshall and experimental methods

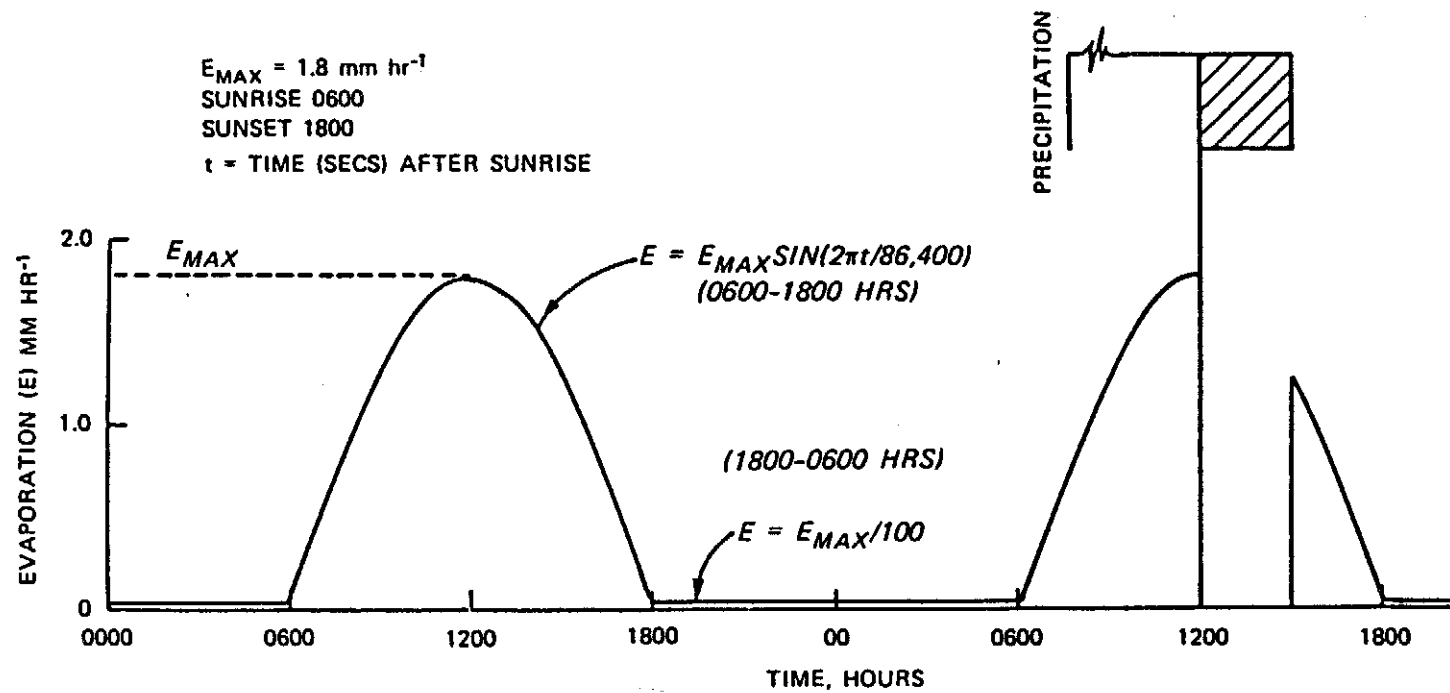


Figure 3.8 - Sine based evaporation concept

CONCEPT FOR EVAPORATION MODEL

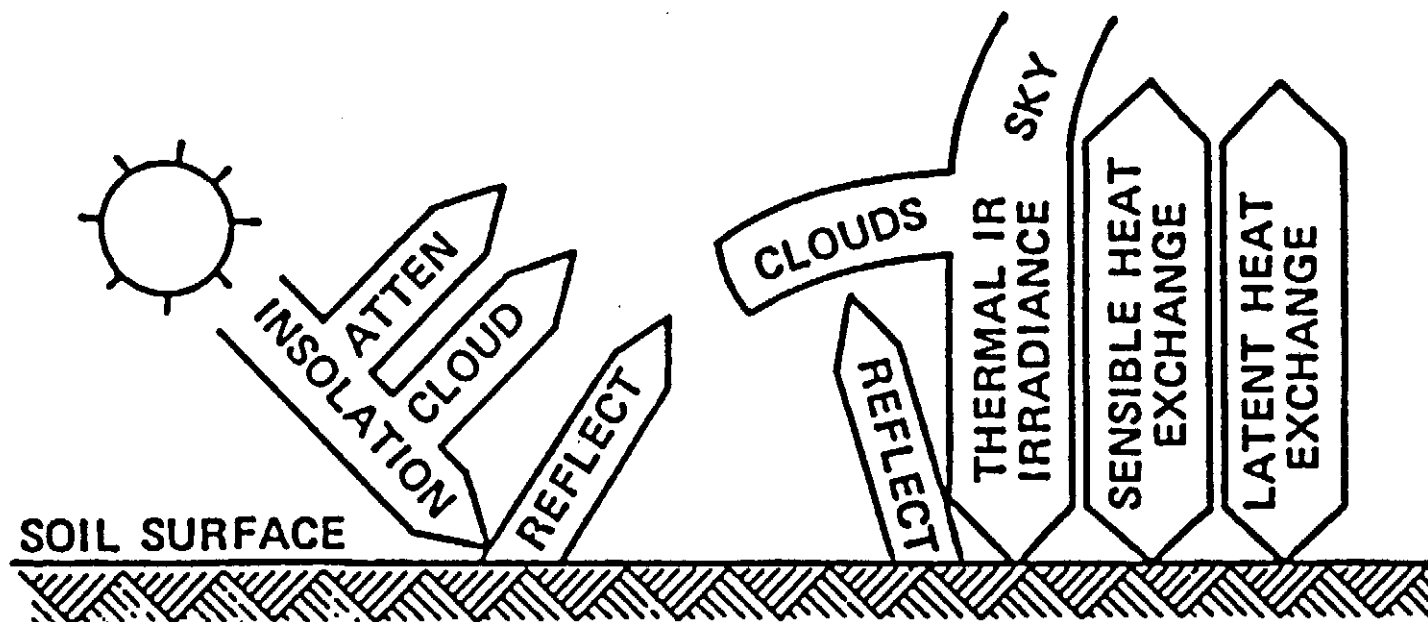


Figure 3.9 - Concept for evaporation model (after Ballick et al, 1981)

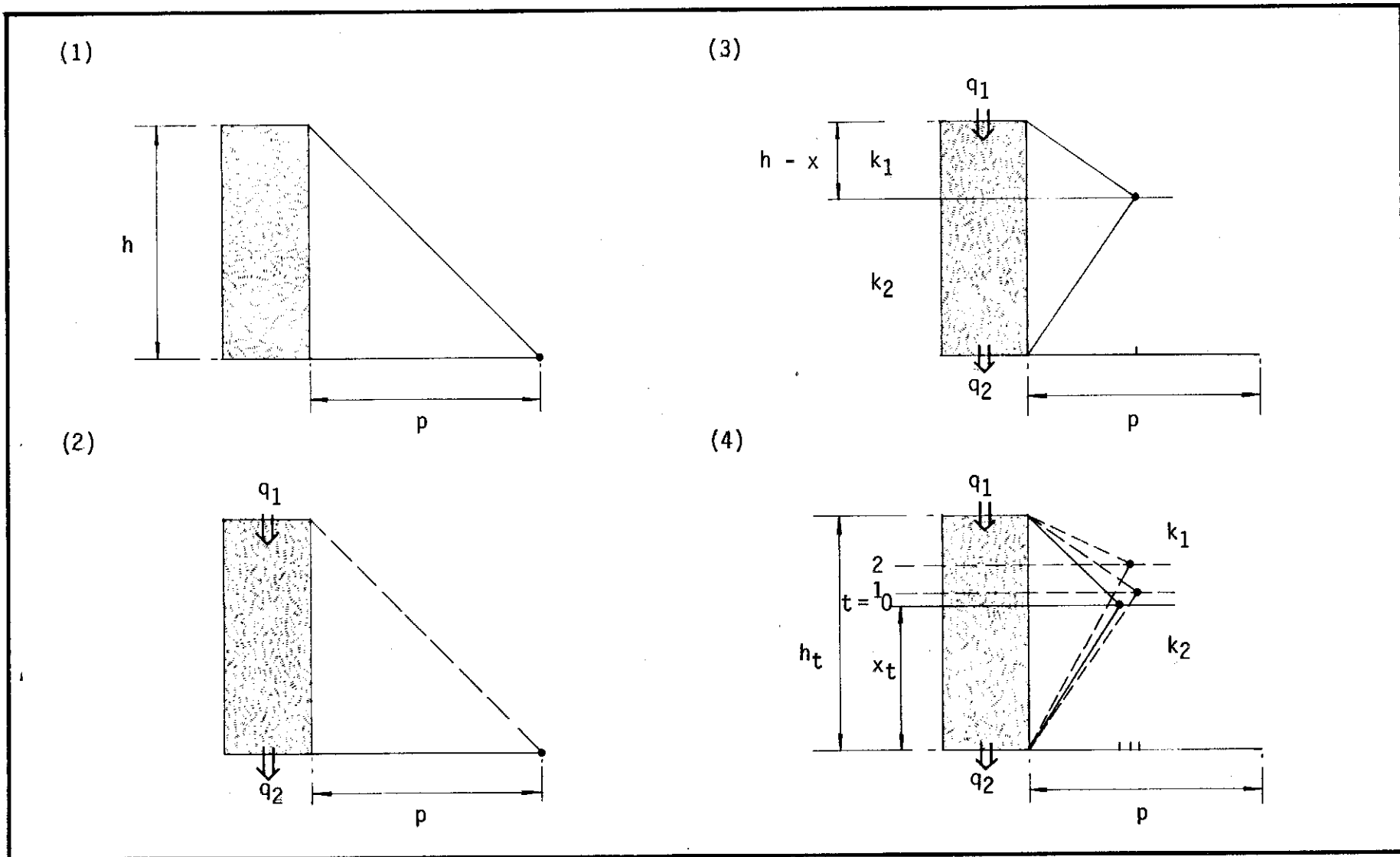


Figure 3.10 - Four methods for considering pore pressures induced by perched water table

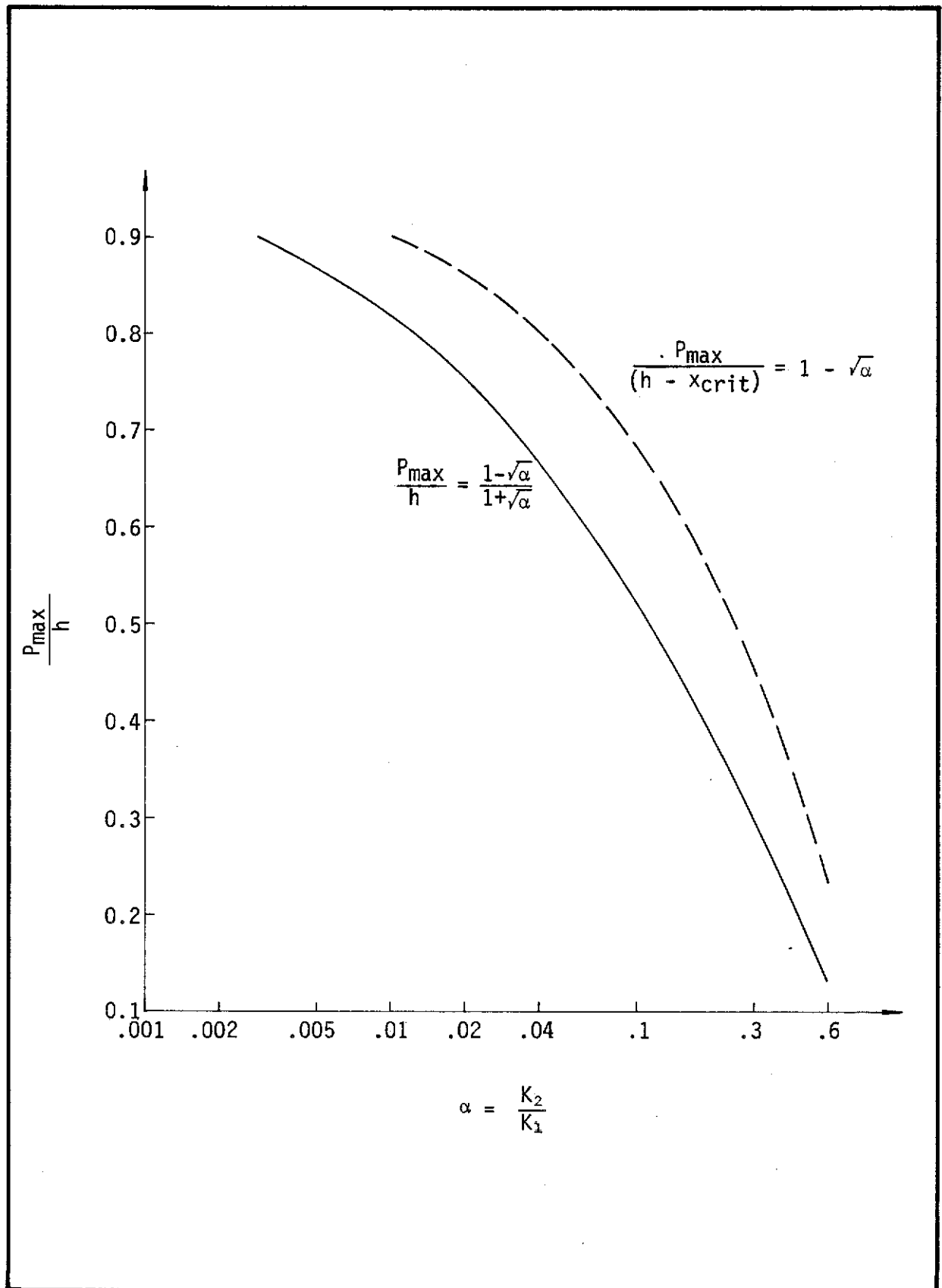


Figure 3.11 - Solutions to equation 3.28

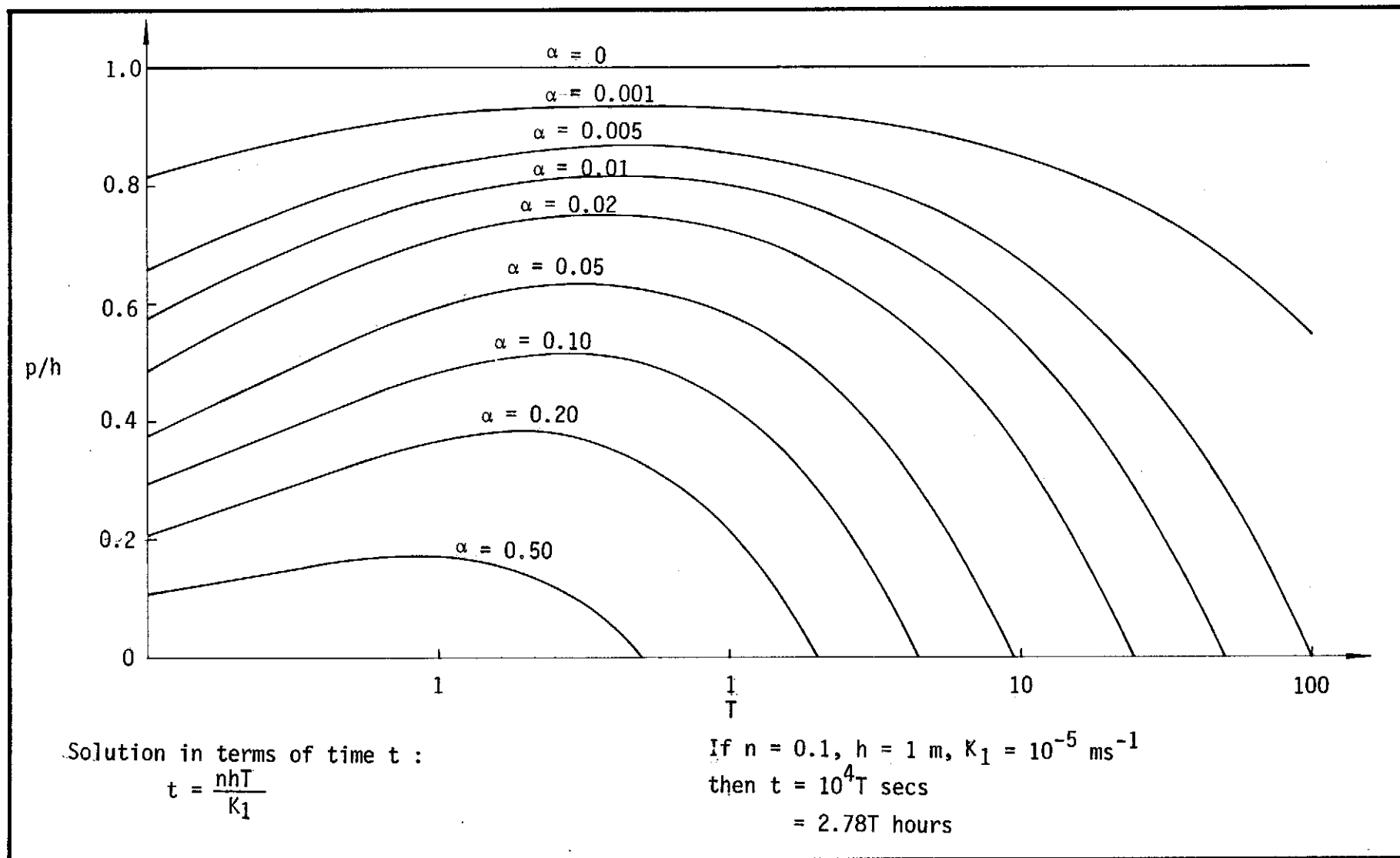


Figure 3.12 - Selected solutions to equation 3.29

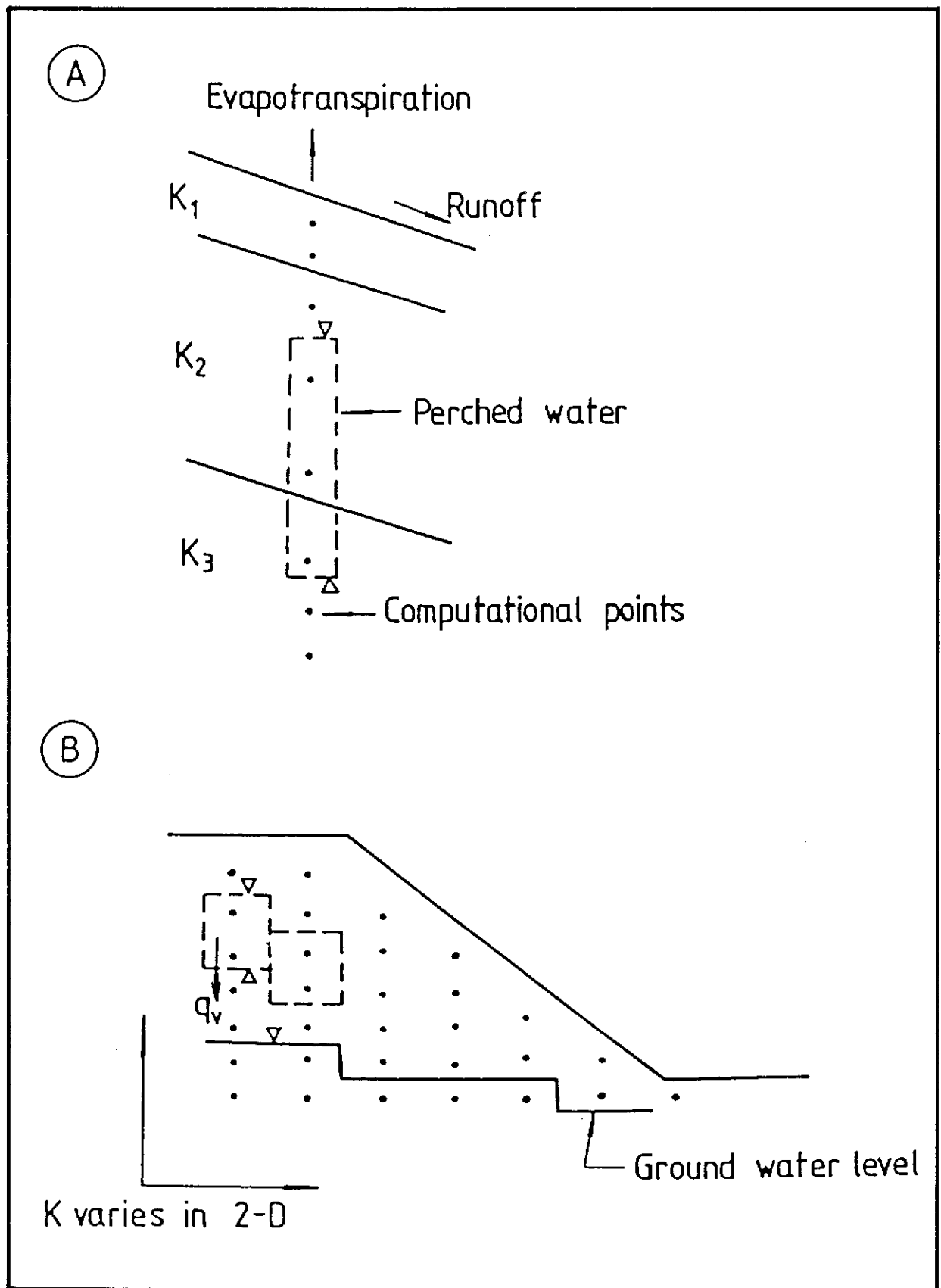


Figure 3.13 - Illustration of one and two dimensional models used in this study

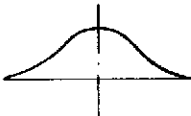
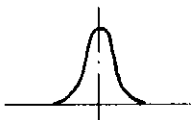
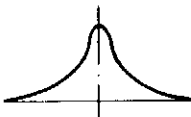
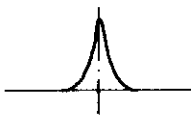
Variable	Field variability	Sample sources	Stochastic generation of input data - n runs			Summary of run results
Permeability		Nielsen et al (1973)	1 ↓	2 ↓ n	Probability of occurrence of given soil water condition
Surface detention capacity		-	↓	↓		
Initial moisture/suction		McKim et al (1980)	↓	↓		
Moisture content for suction-moisture curve		Gummaa (1978)	↓	↓		
· · · n'						
Legend : ↓ random selection of variable value for a particular run, in accordance with field variability distribution						

Figure 3.14 - Suggested strategy for the incorporation of field variability into the modelling framework

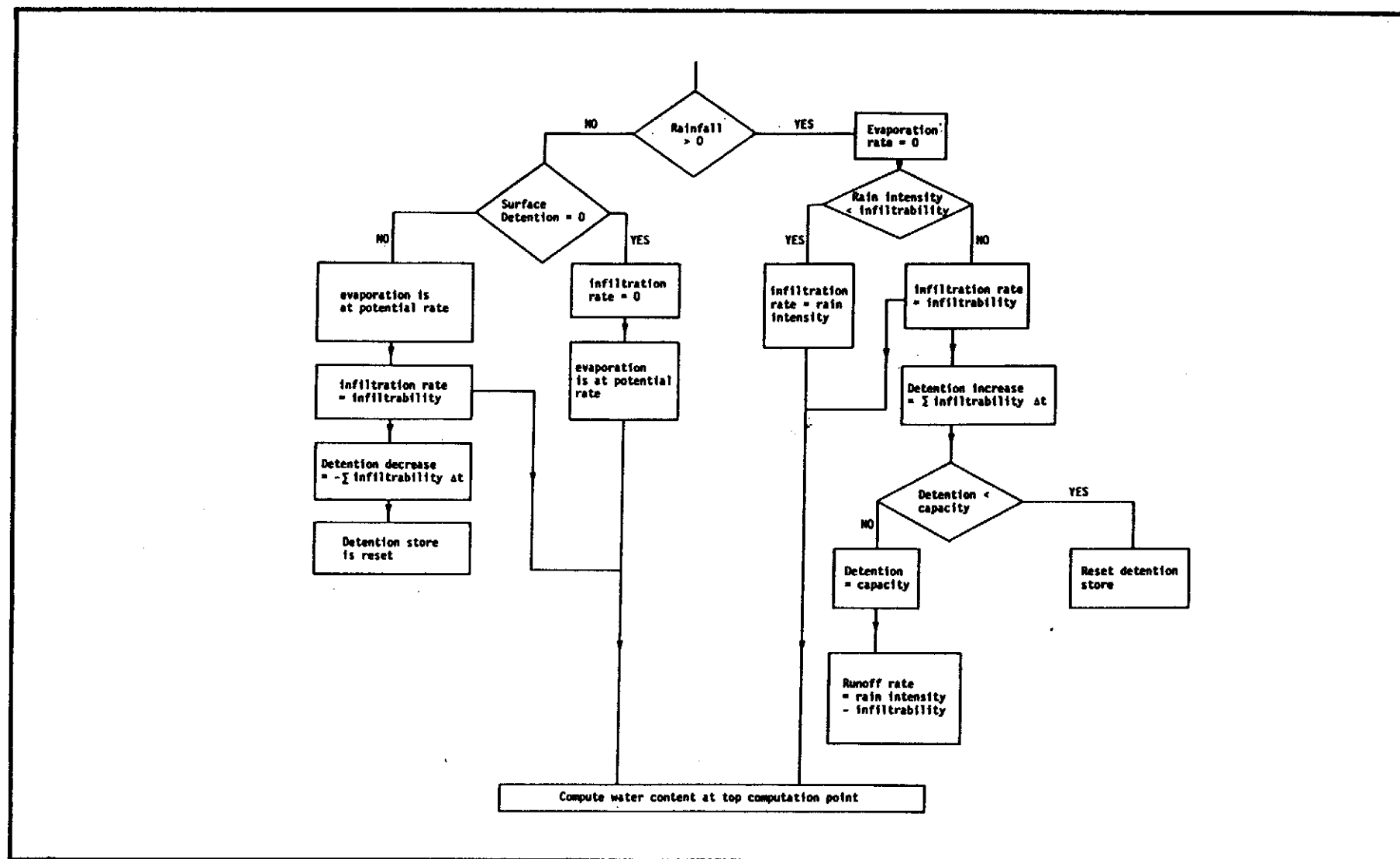


Figure 3.15 - Flow diagram for top computational point of soil water model

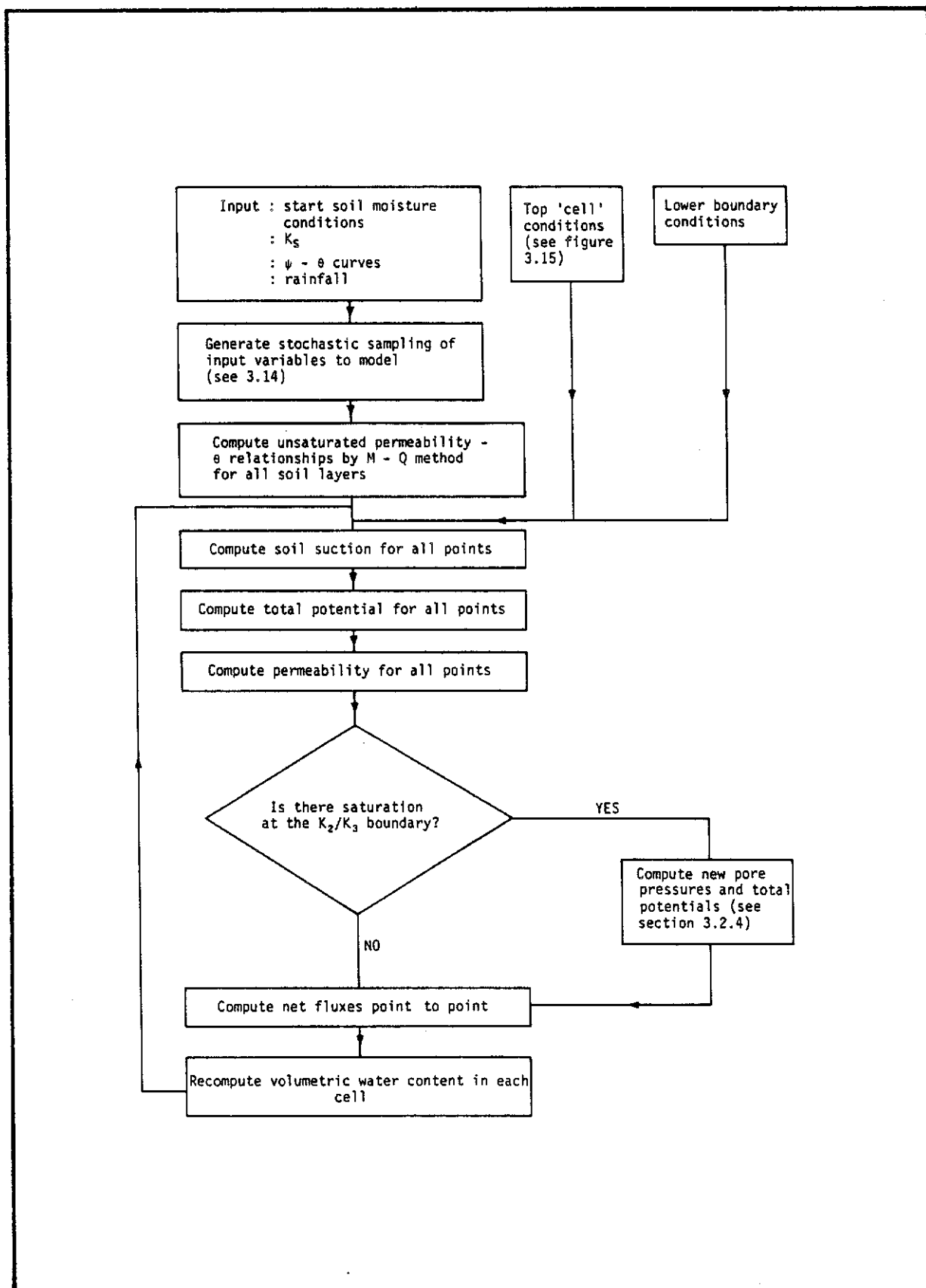


Figure 3.16 - Flow diagram illustrating overall model approach
(also see Figure 3.15)

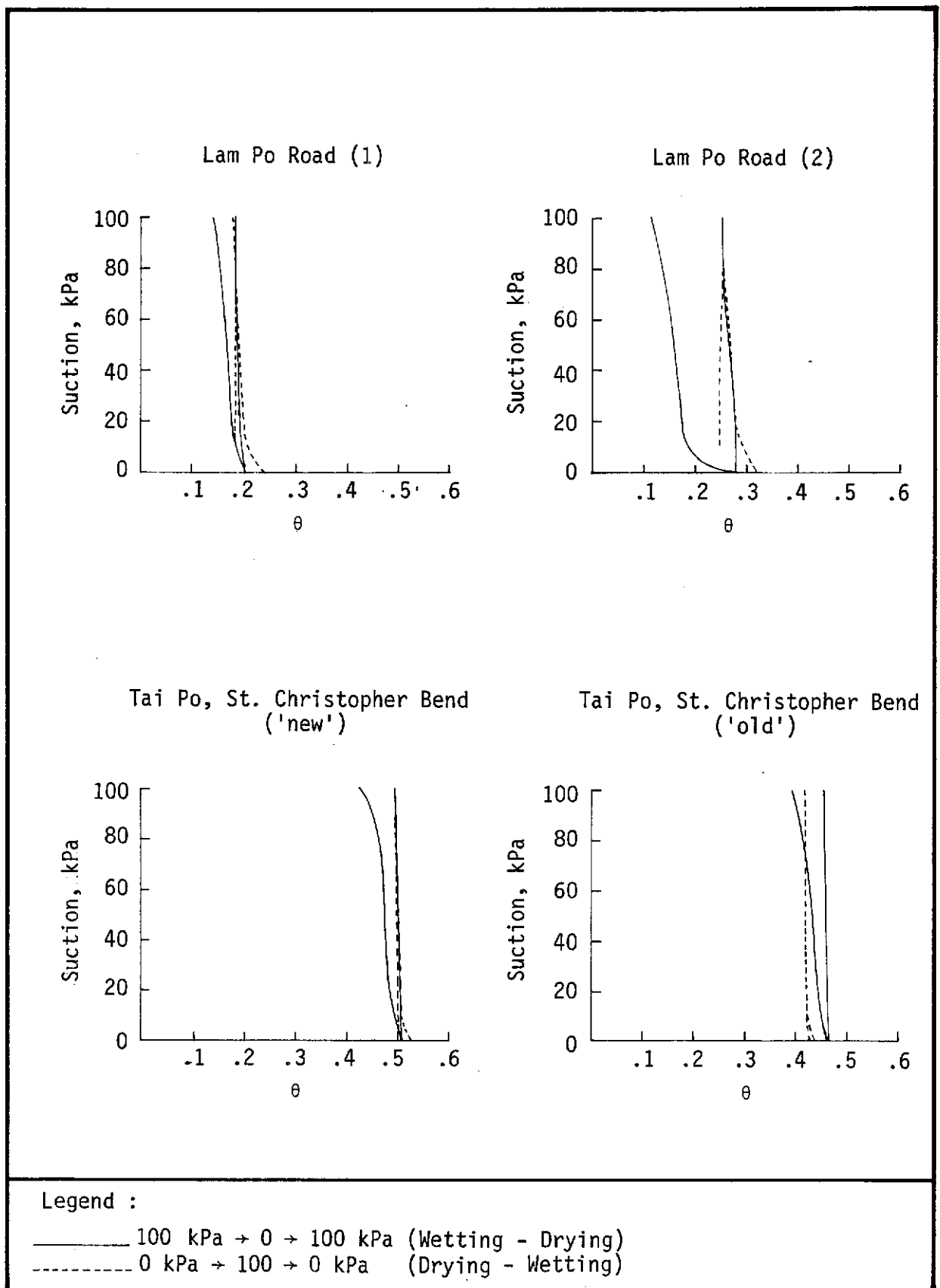


Figure 4.1 - Suction moisture curves for volcanic chunam

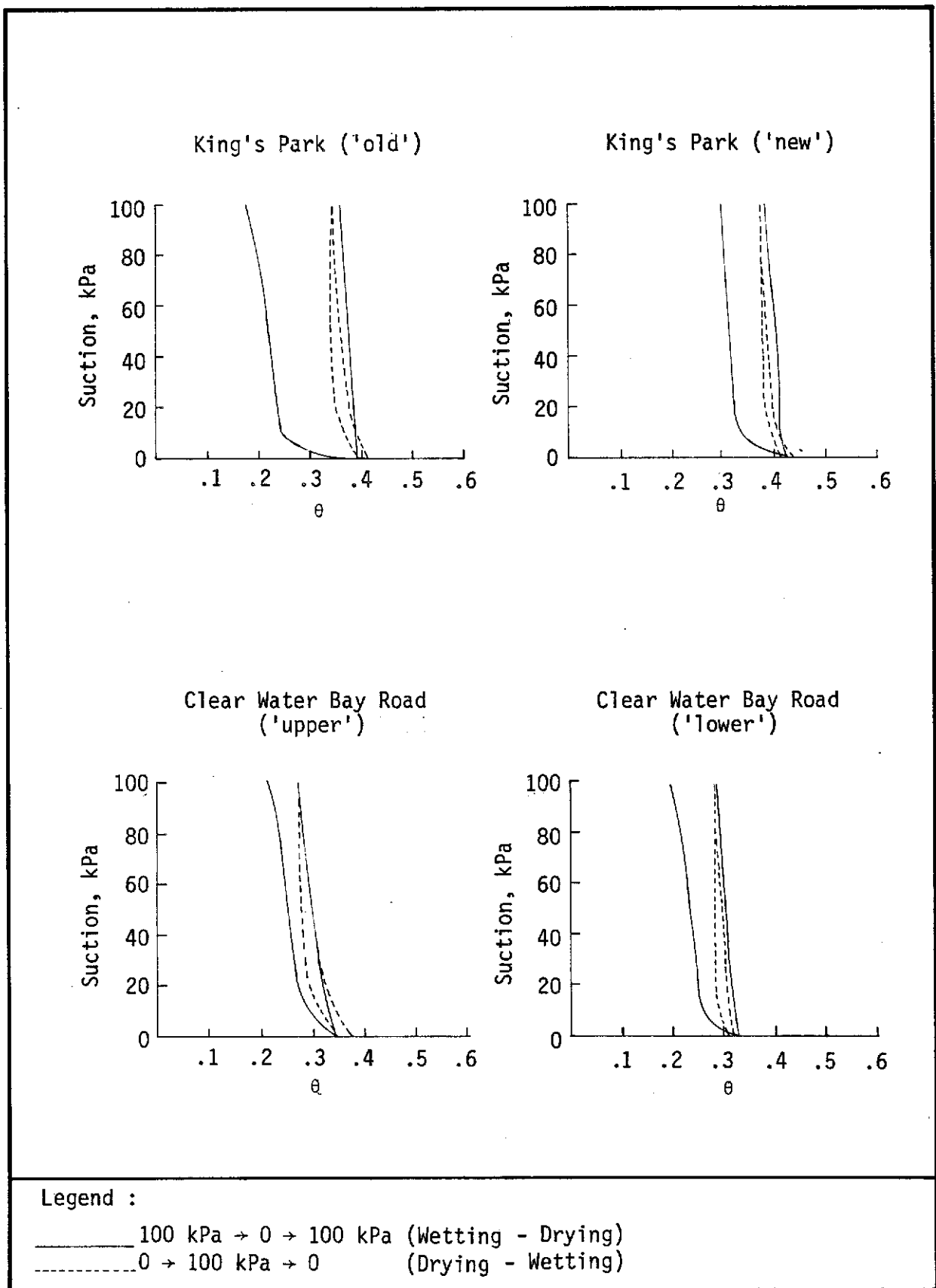


Figure 4.2 - Suction moisture curves for granitic chunam

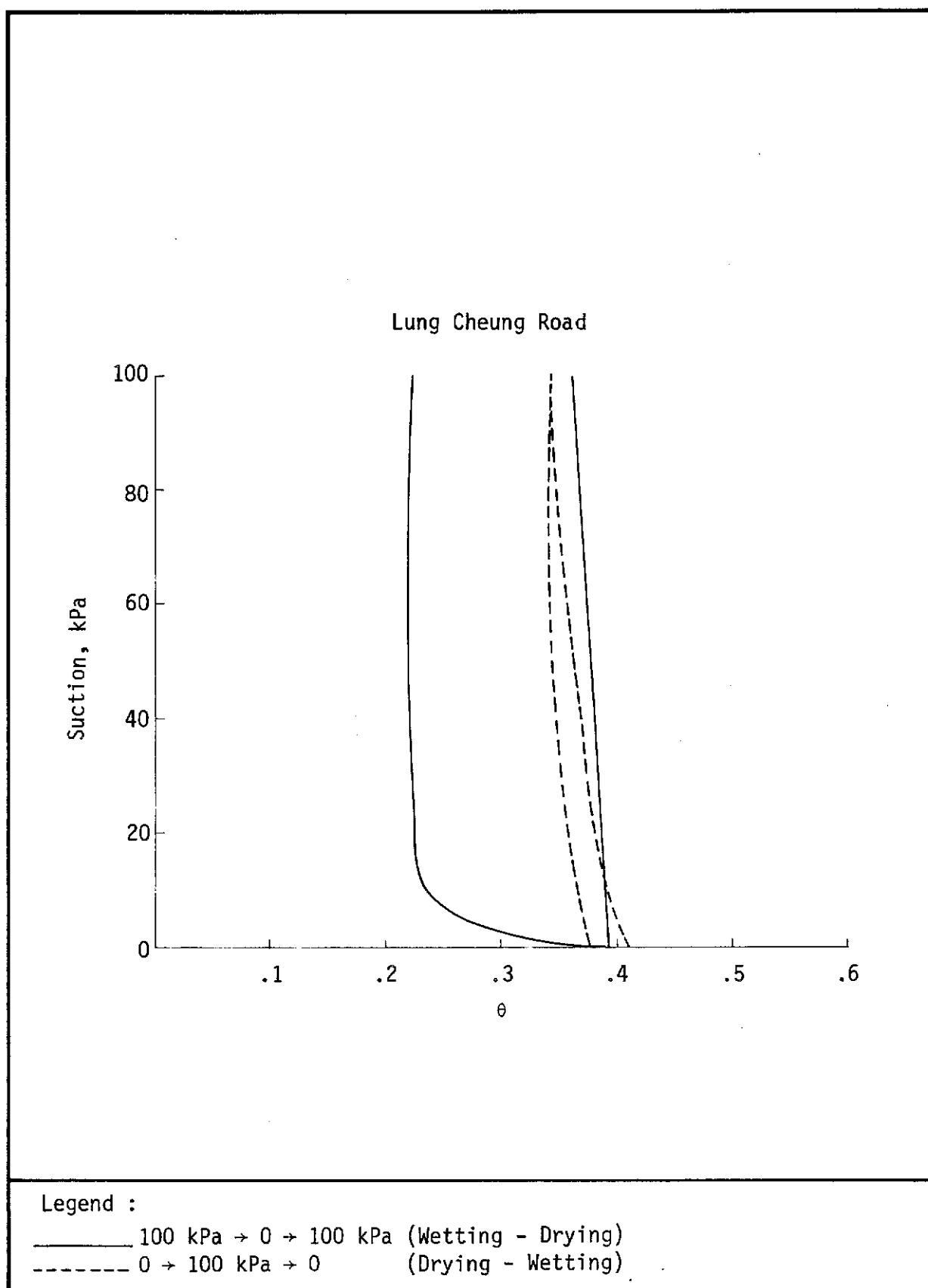
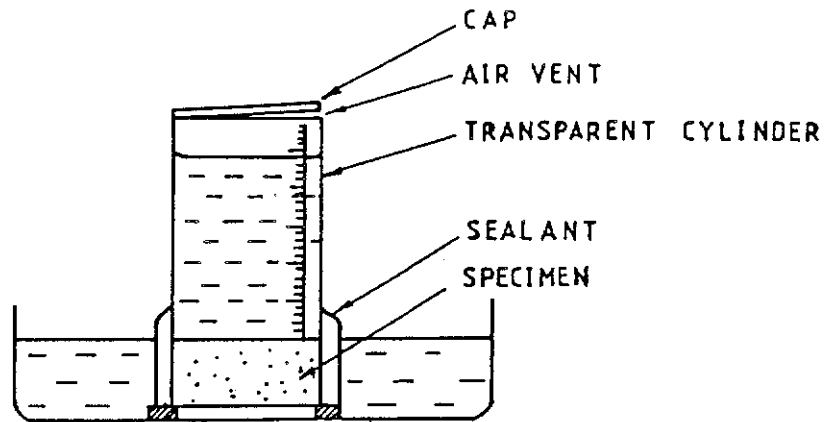
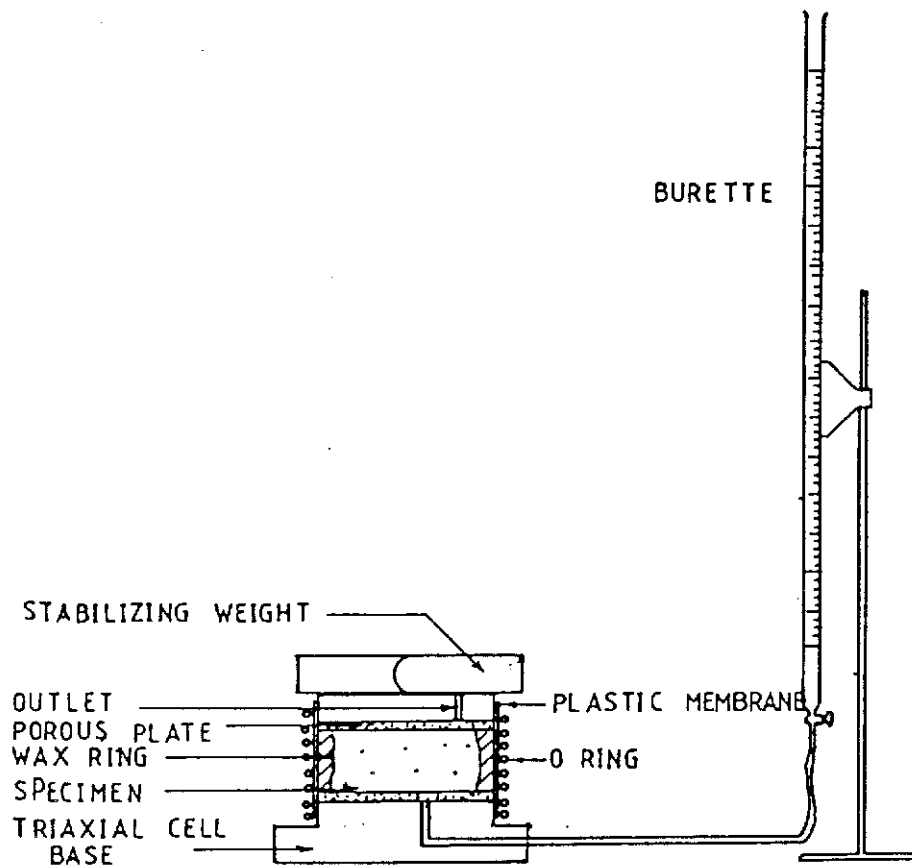


Figure 4.3 - Suction moisture curve for granitic chunam

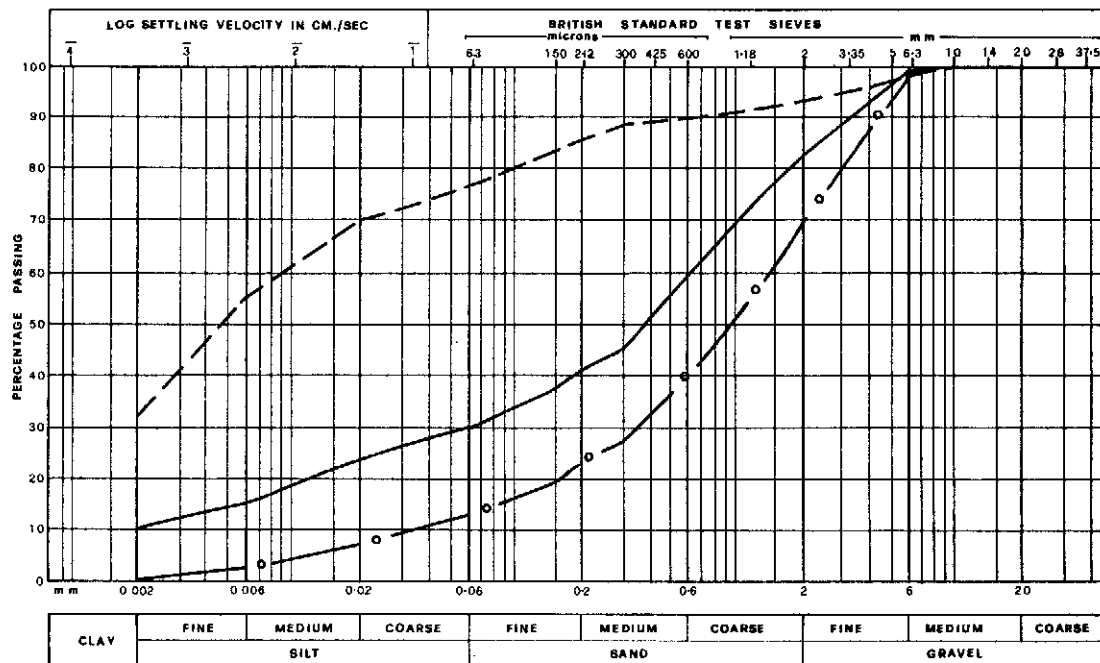


(a) Ponding Test



(b) Burette Test

Figure 4.4 - Ponding and burette methods used to determine the permeability of chunam



Legend :

- Tai Po Decomposed Volcanics : sandy, clayey SILT
- King's Park Decomposed Granite : silty SAND
- o — Clear Water Bay Road Decomposed Granite : clayey, silty, gravelly SAND

Figure 4.5 a - Particle size distributions for soils used in chunam mixes

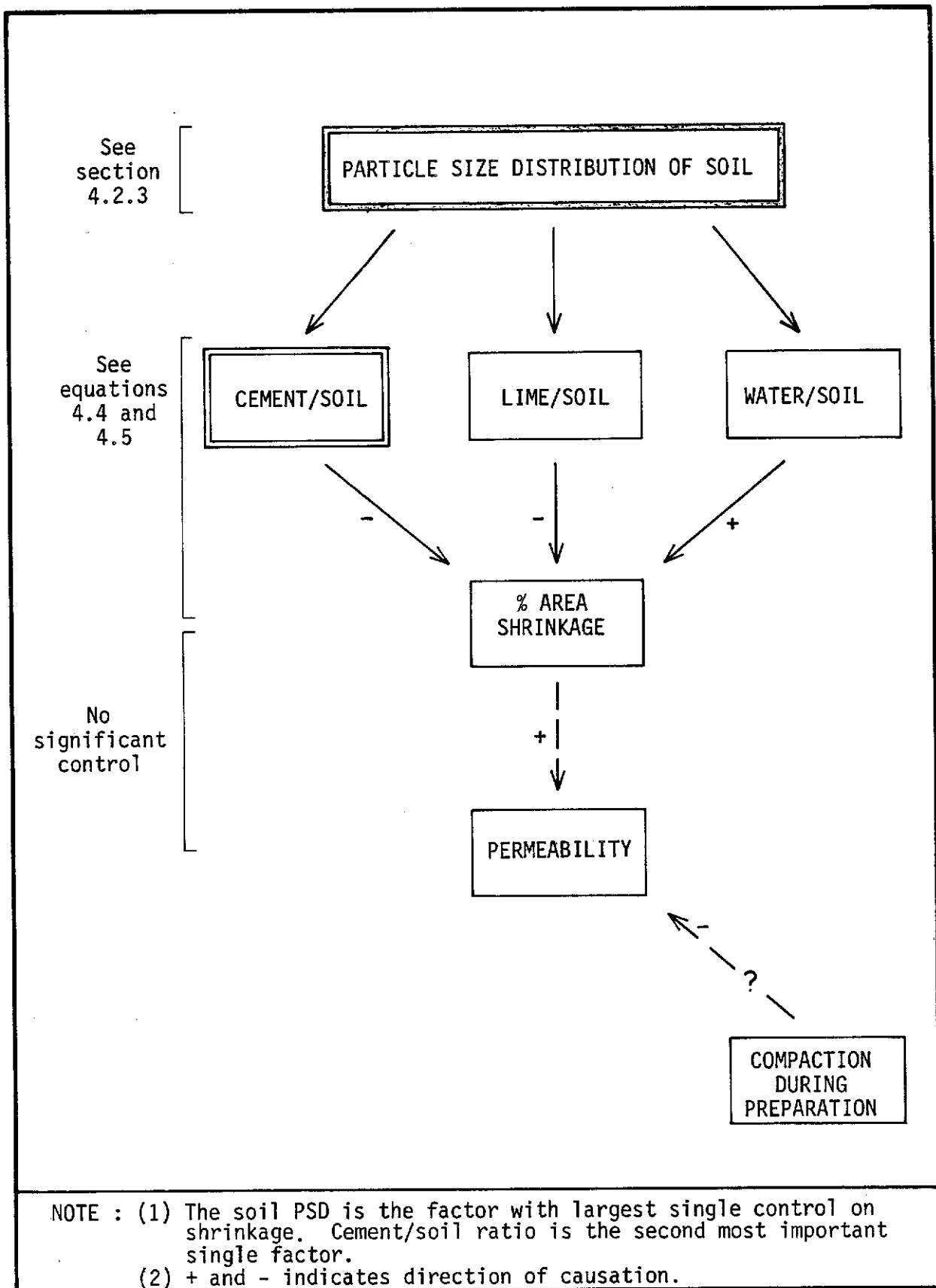


Figure 4.5b - Controls on the shrinkage and permeability of chunam

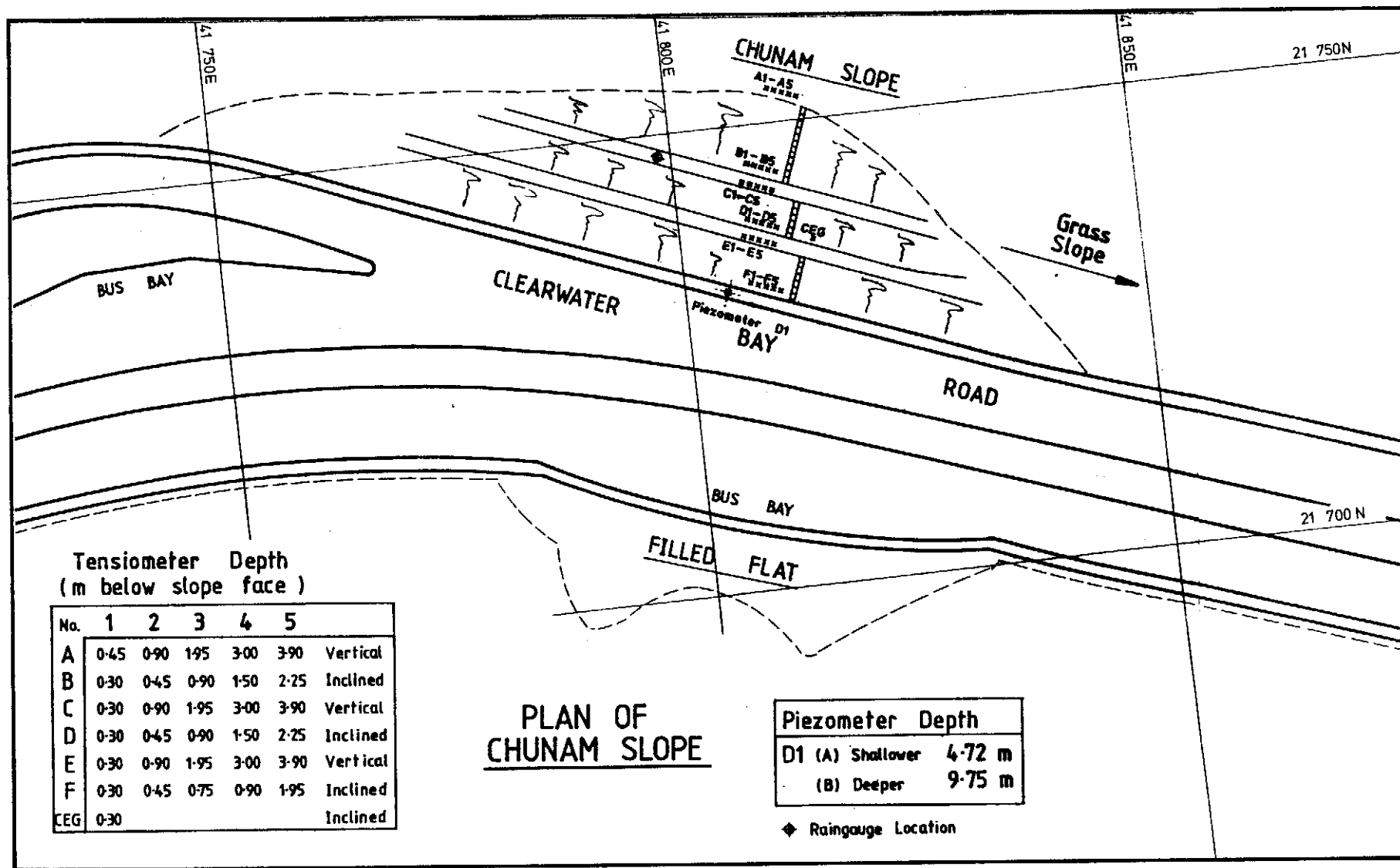


Figure 4.6 - Site plan of the chunam slope, Clear Water Bay Road (see figure 1.7)

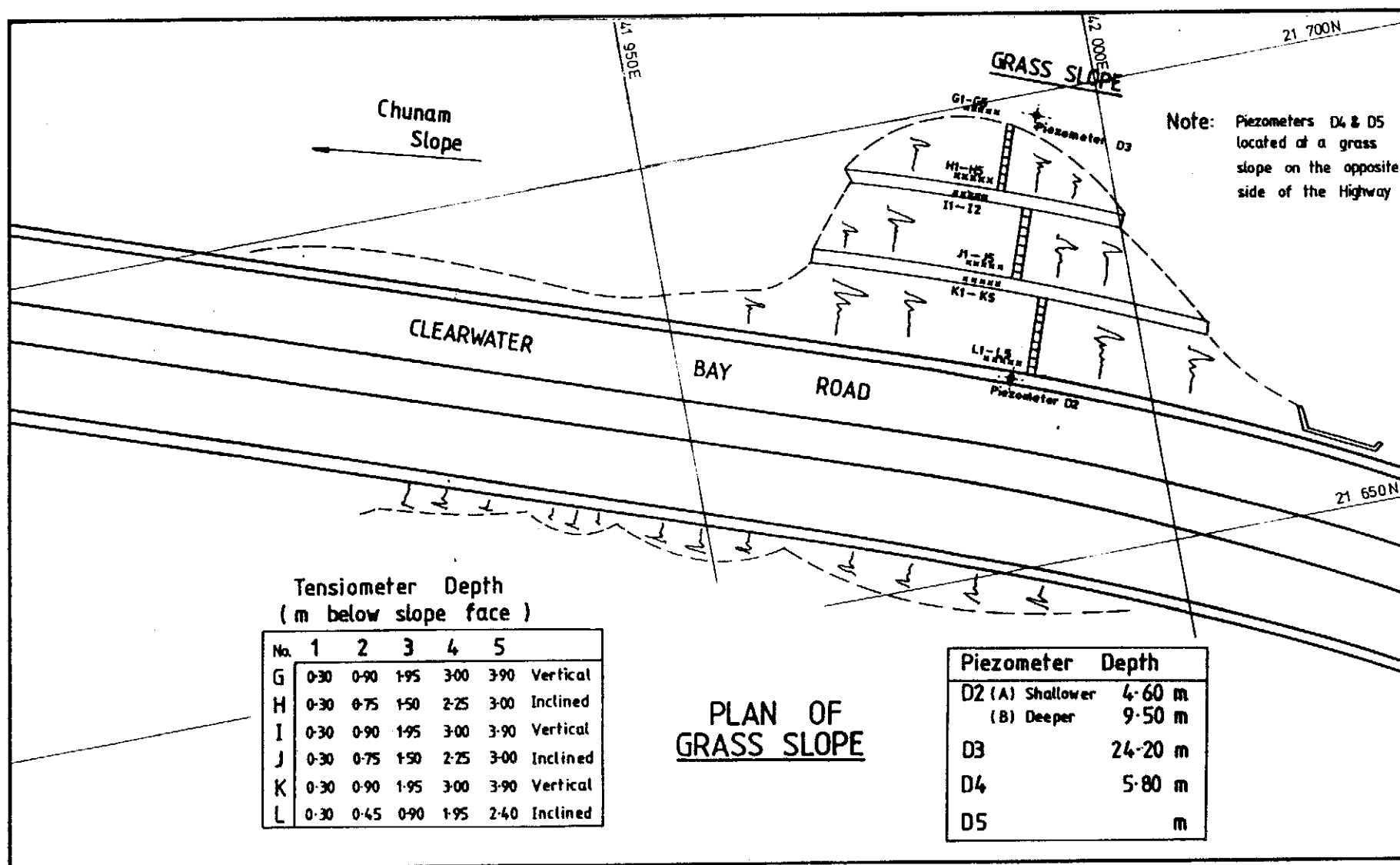


Figure 4.7 - Site plan of the grass slope, Clear Water Bay Road (see figure 1.7)

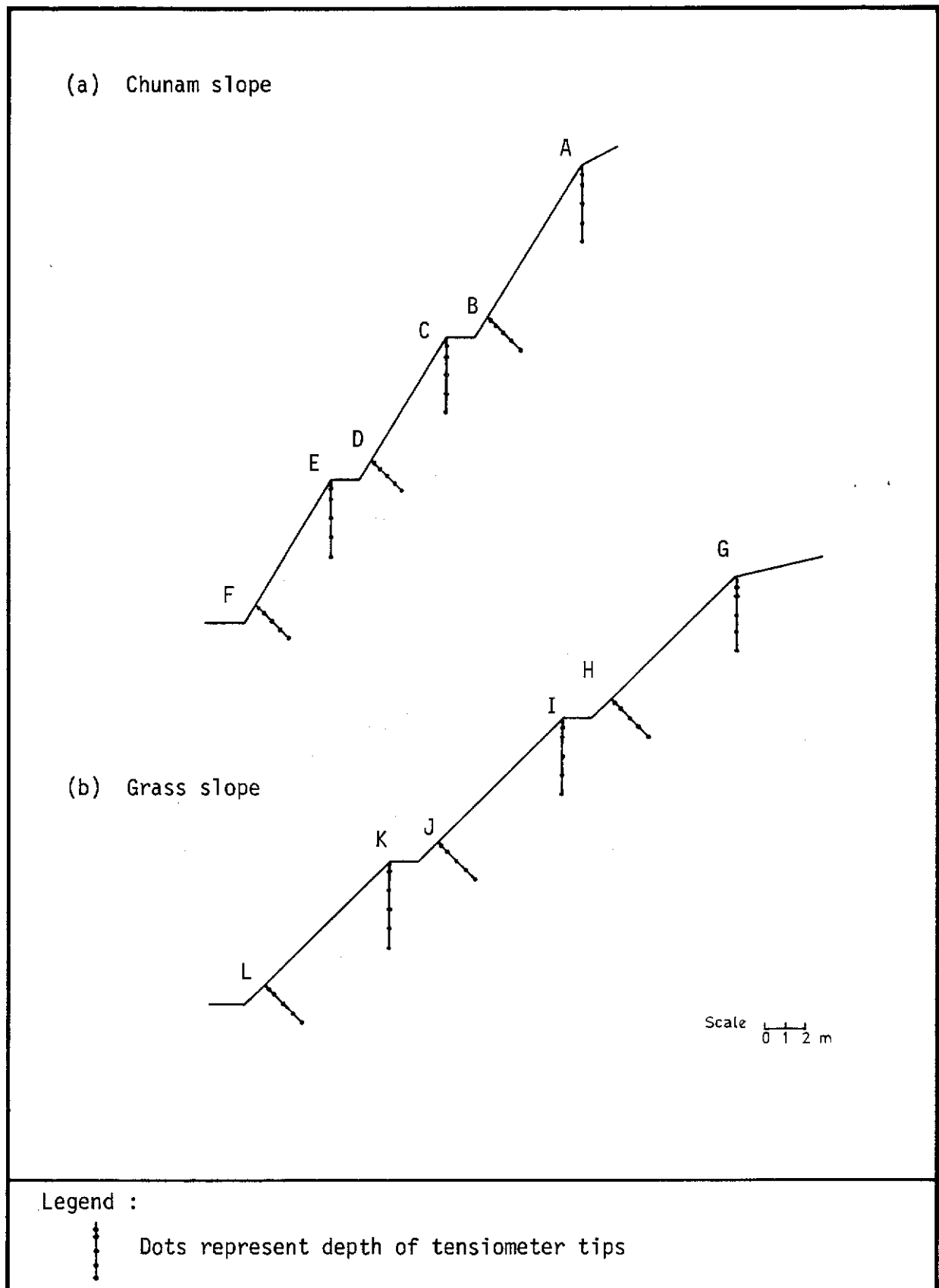


Figure 4.8 - Tensiometer locations at the Clear Water Bay Road site
(see figures 4.6 and 4.7)

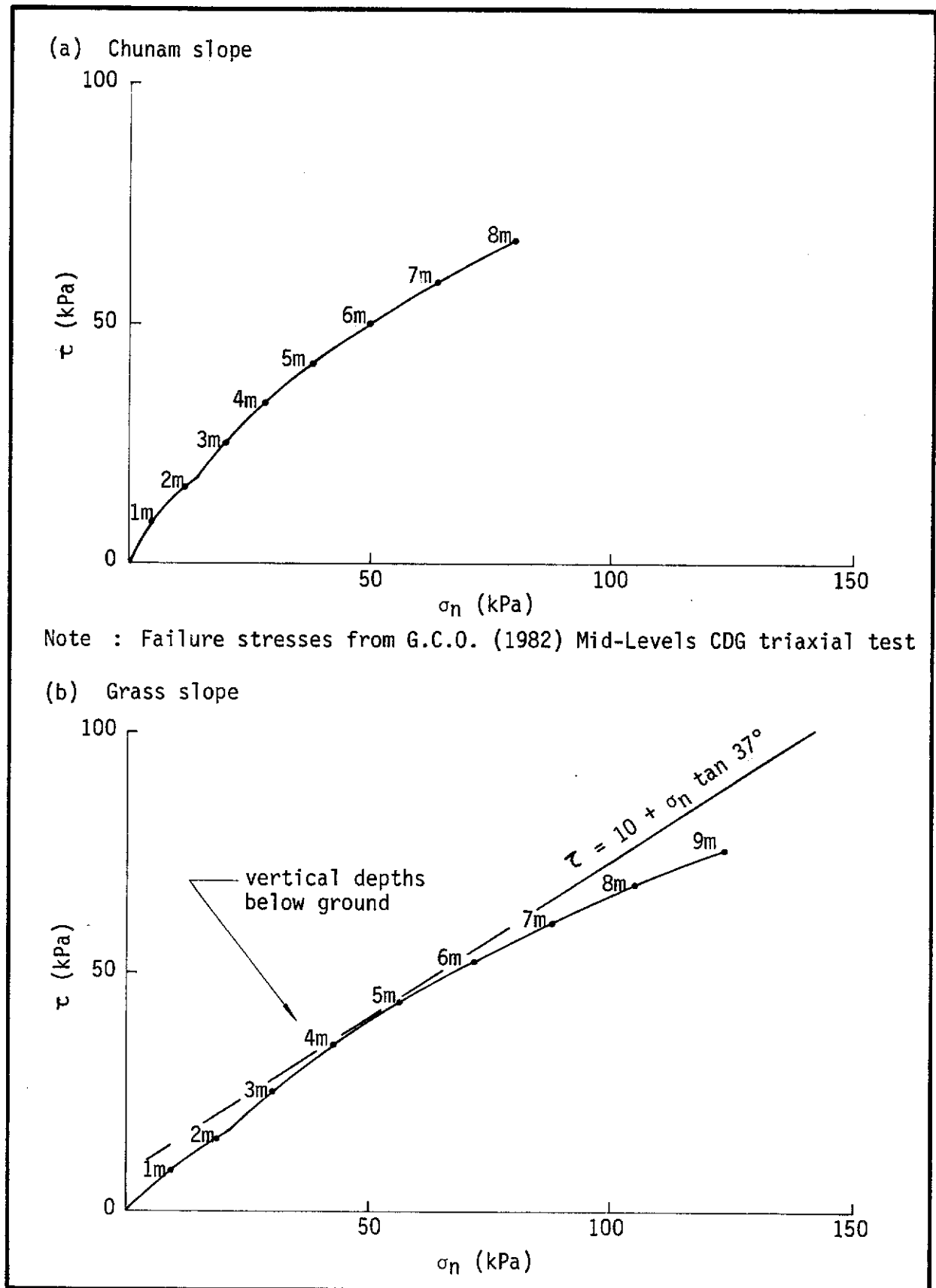


Figure 4.9 - Resistance envelopes for the grass and chunam slopes at Clear Water Bay Road

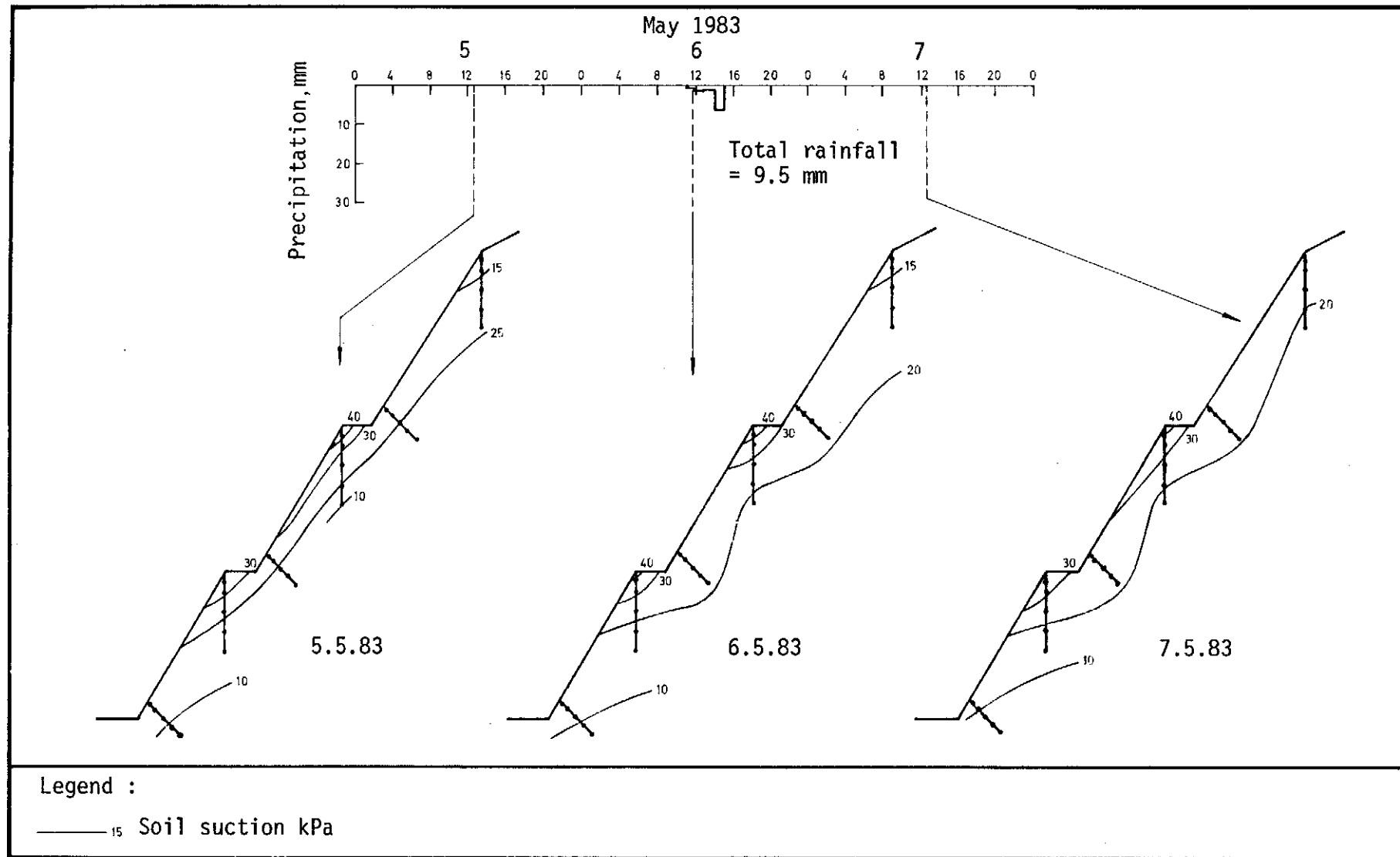


Figure 4.10 - Soil suctions on chunam slope relating to the storm of 6 May 1983

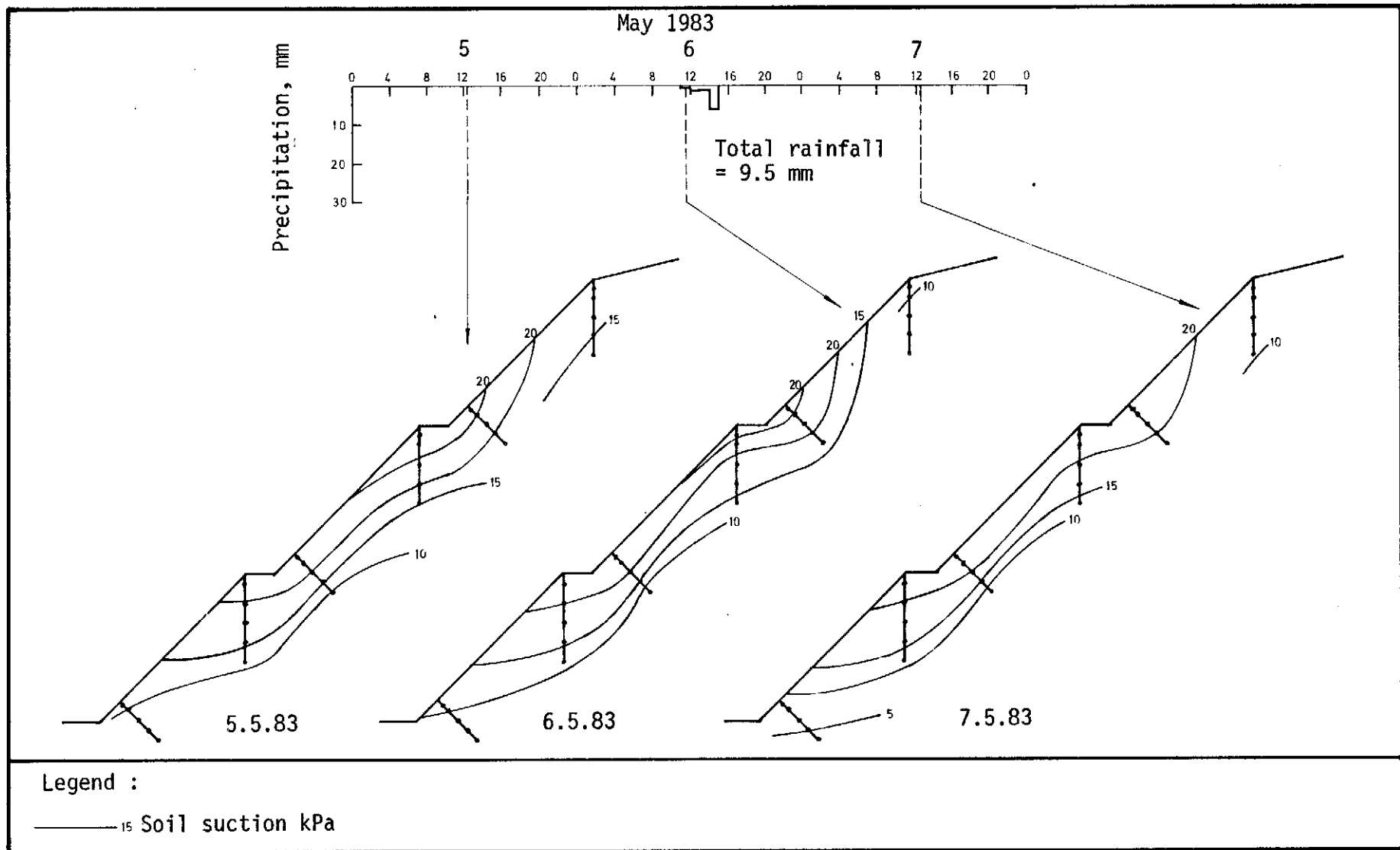


Figure 4.11 - Soil suctions on grass slope relating to the storm of 6 May 1983

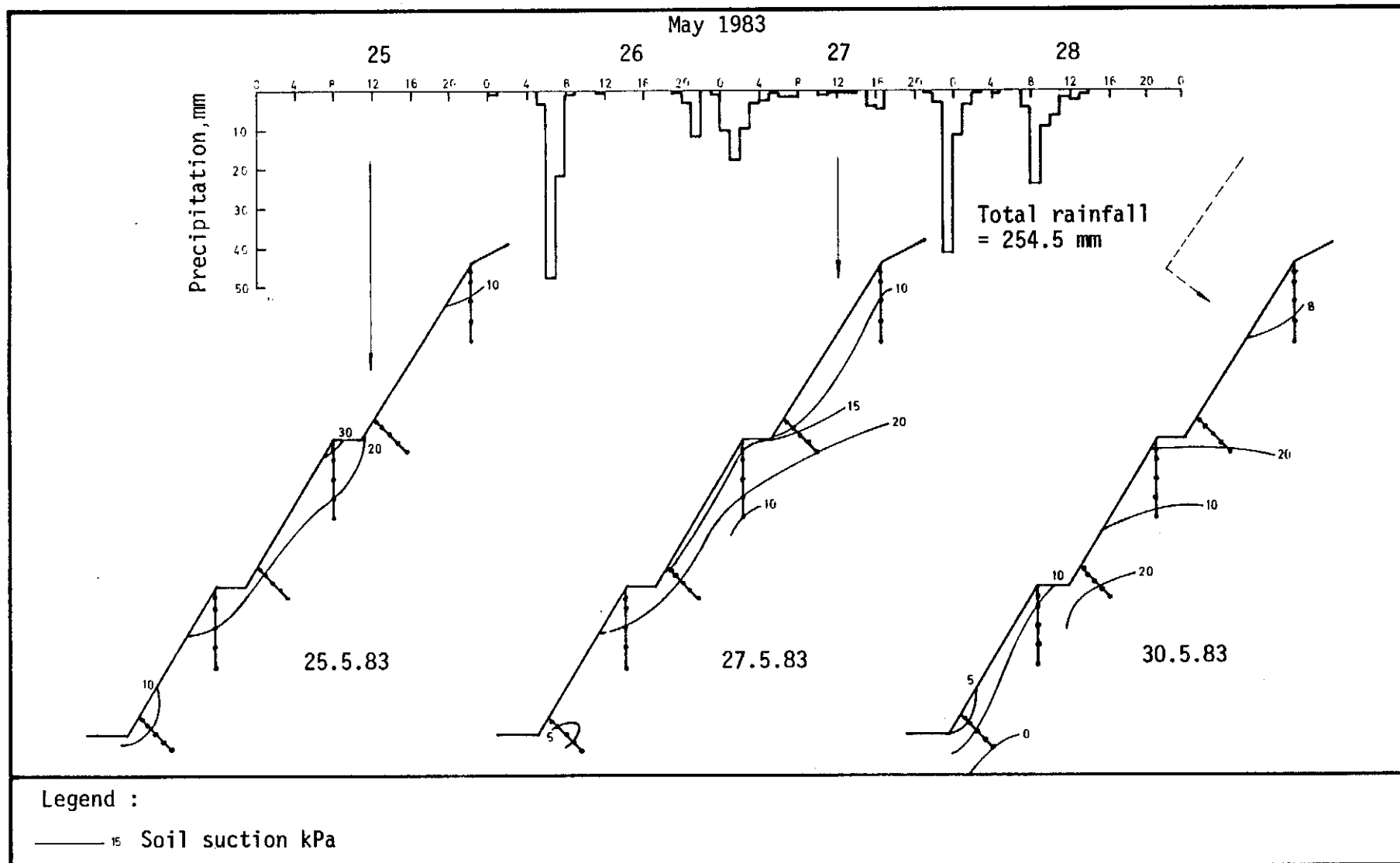


Figure 4.12 - Soil suctions on chunam slope relating to the storm of 16-28 May 1983

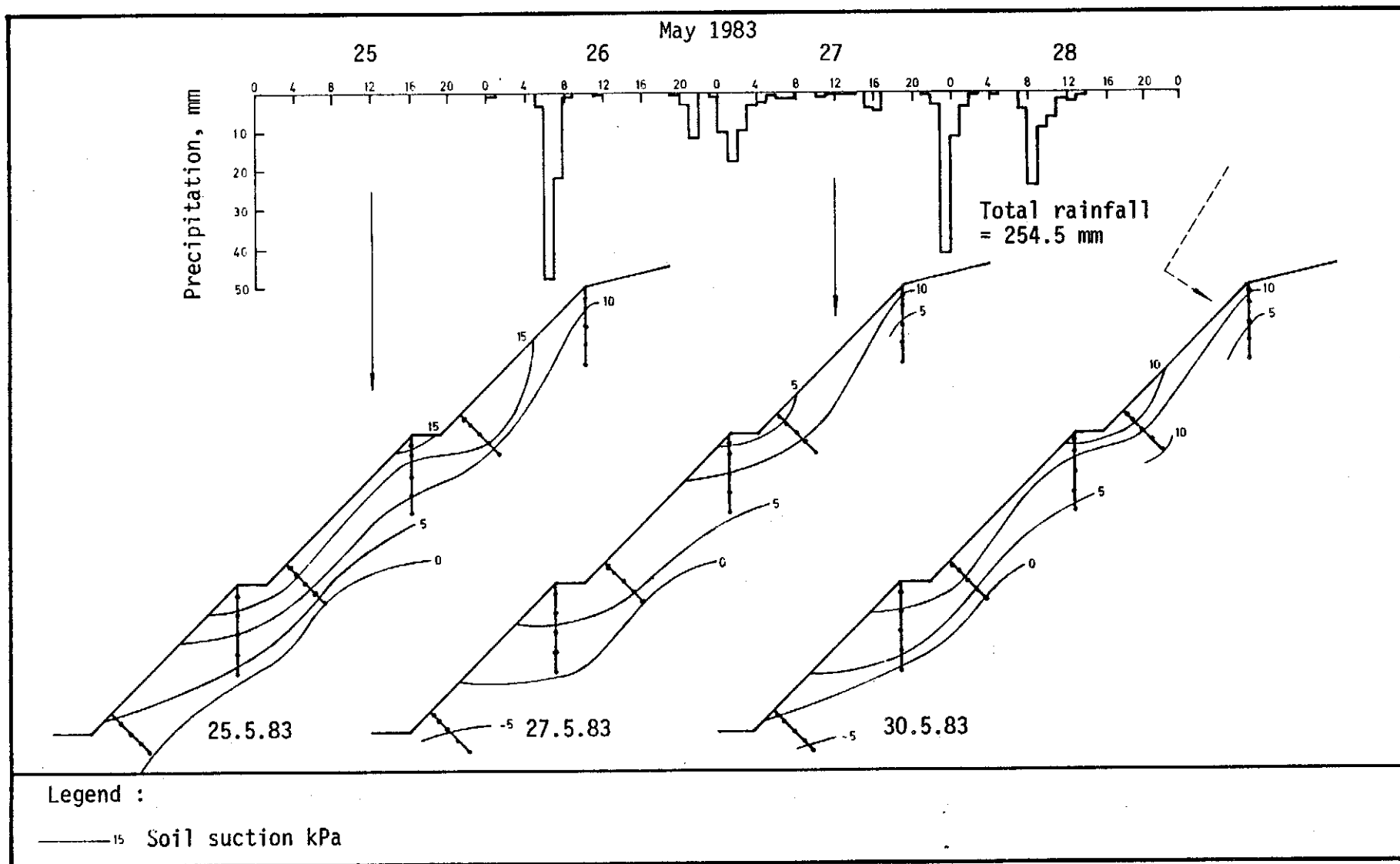


Figure 4.13 - Soil suctions on grass slope relating to the storm of 26-28 May 1983

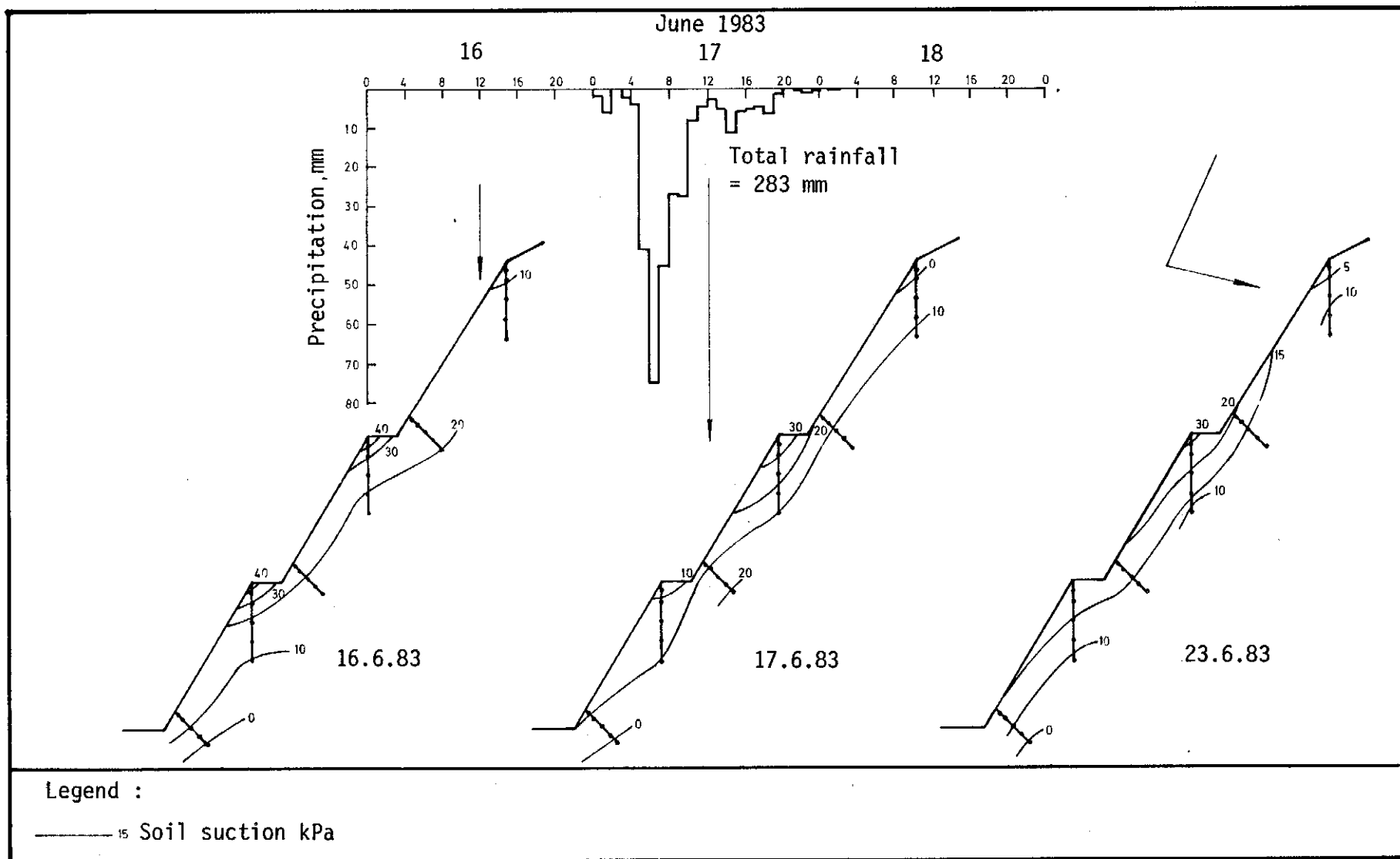


Figure 4.14 - Soil suctions on chunam slope relating to the storm of 17 June 1983

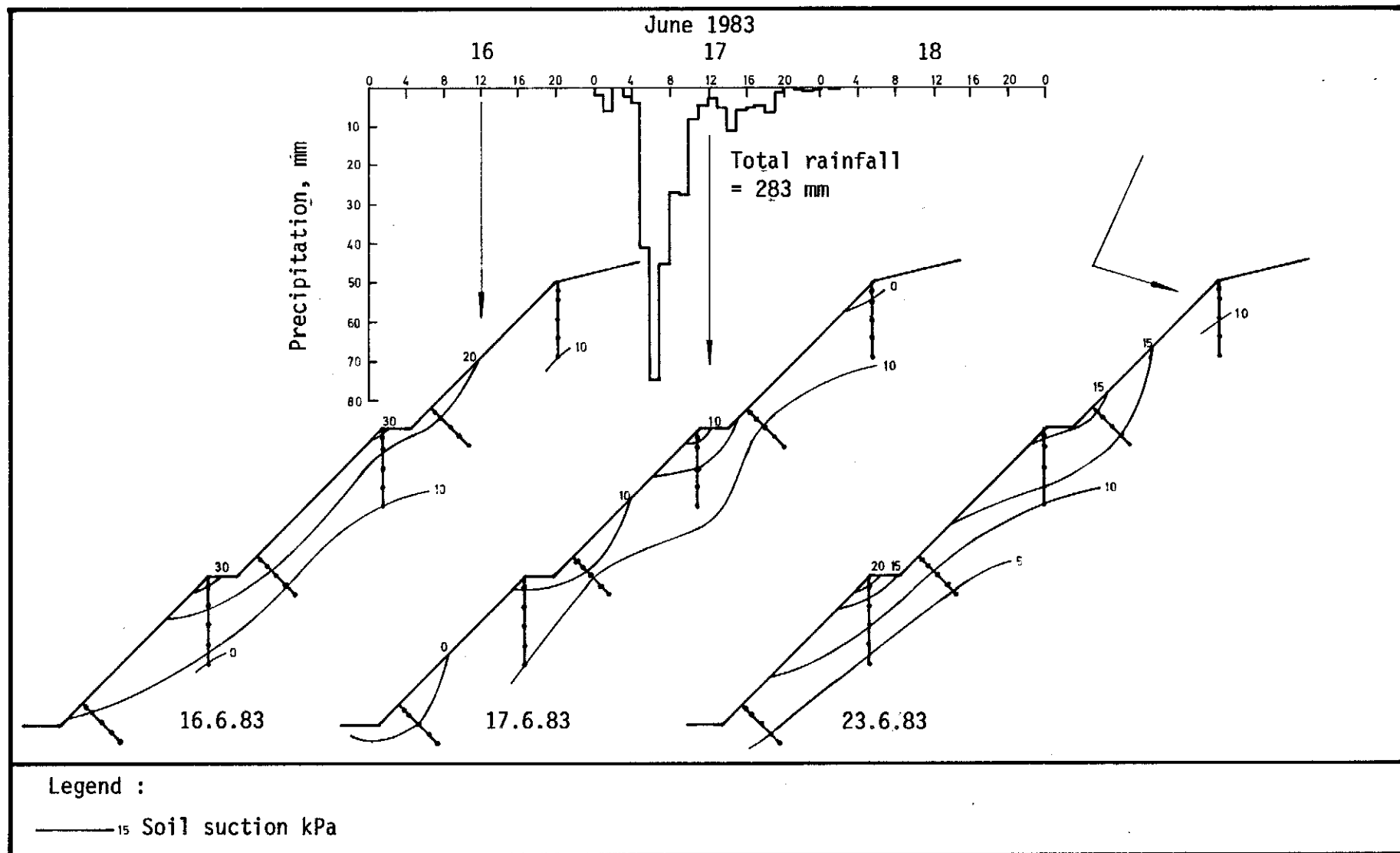


Figure 4.15 - Soil suctions on grass slope relating to the storm of 17 June 1983

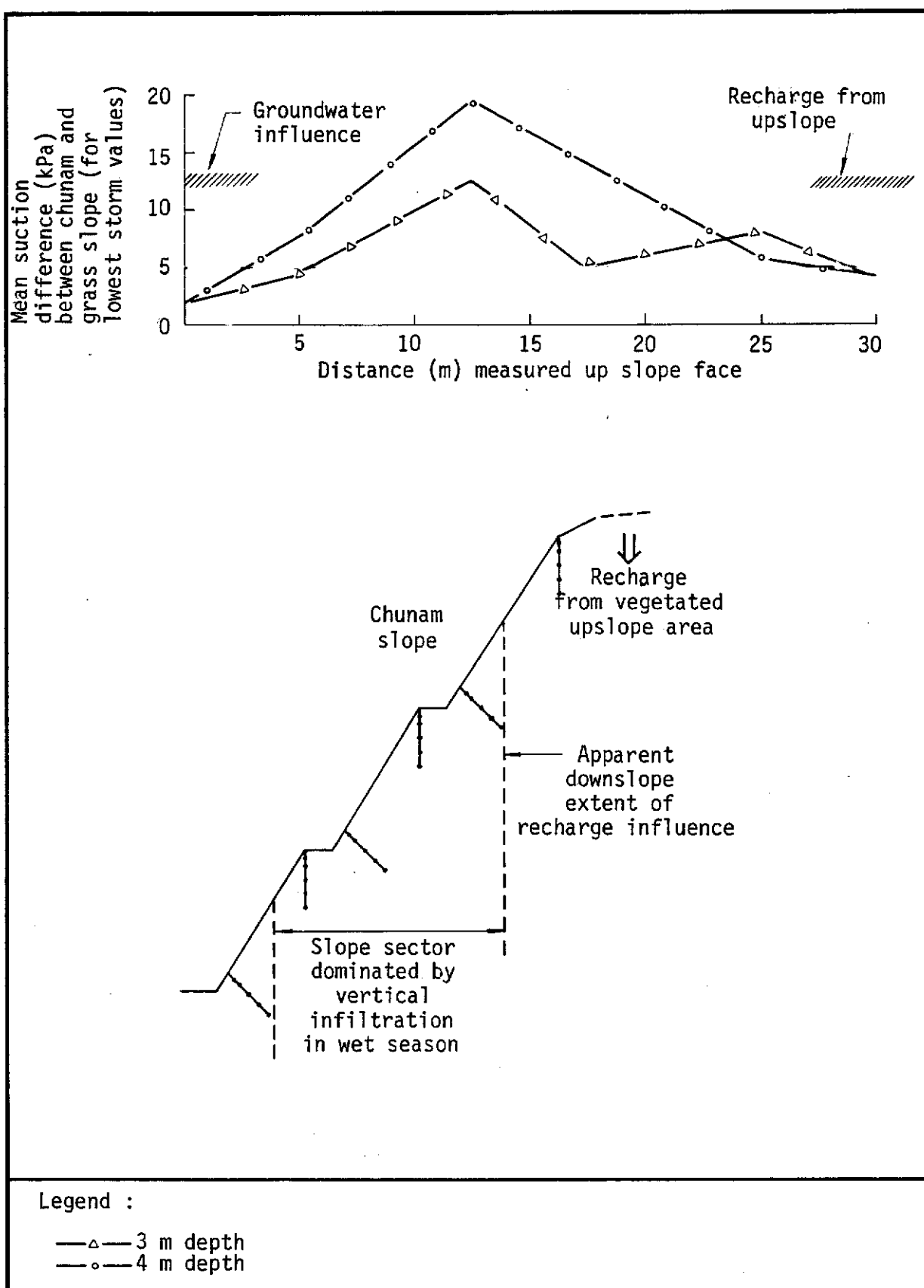
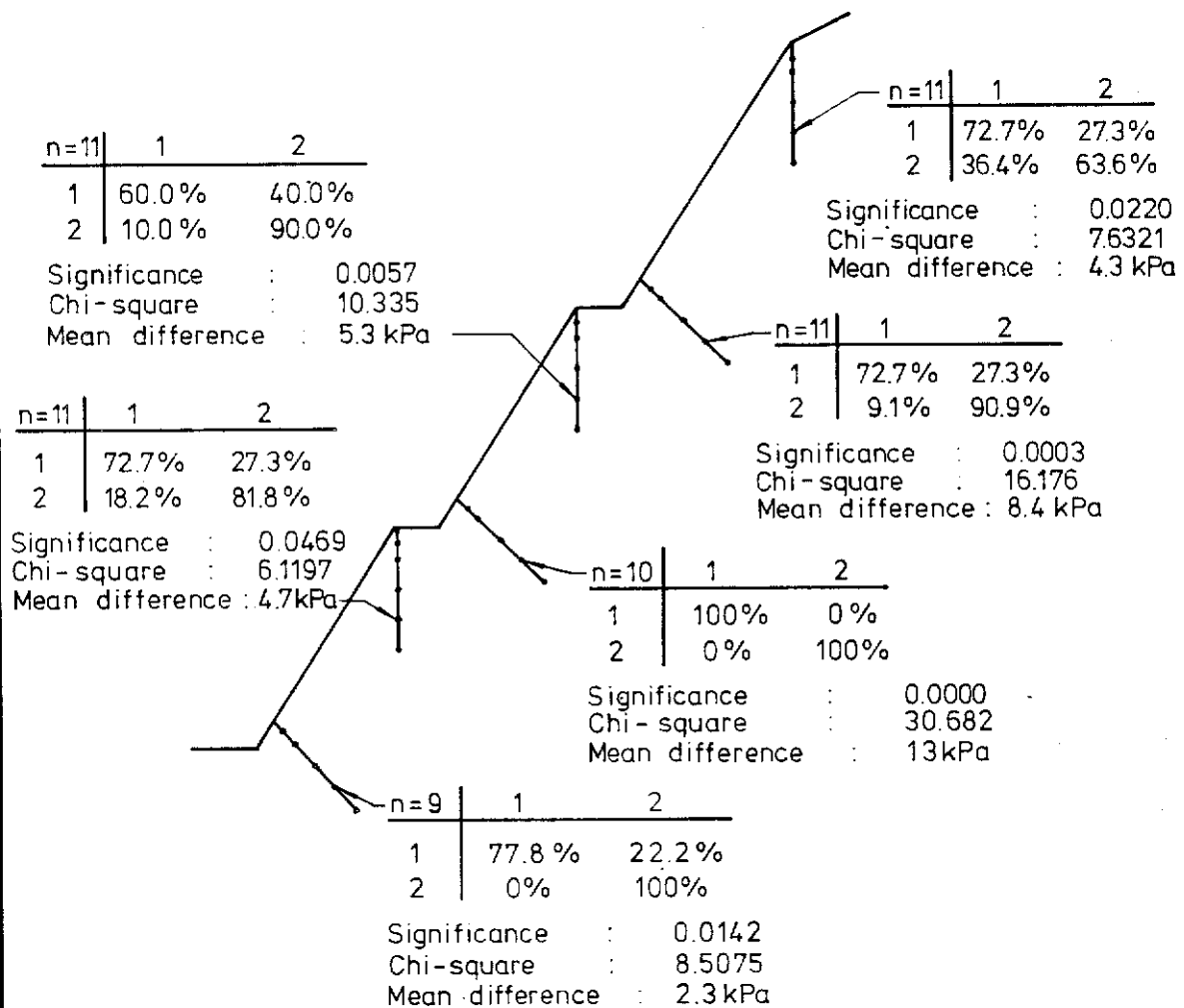


Figure 4.16 - Summary of principal soil water conditions on the chunam and grass slope

3m depth



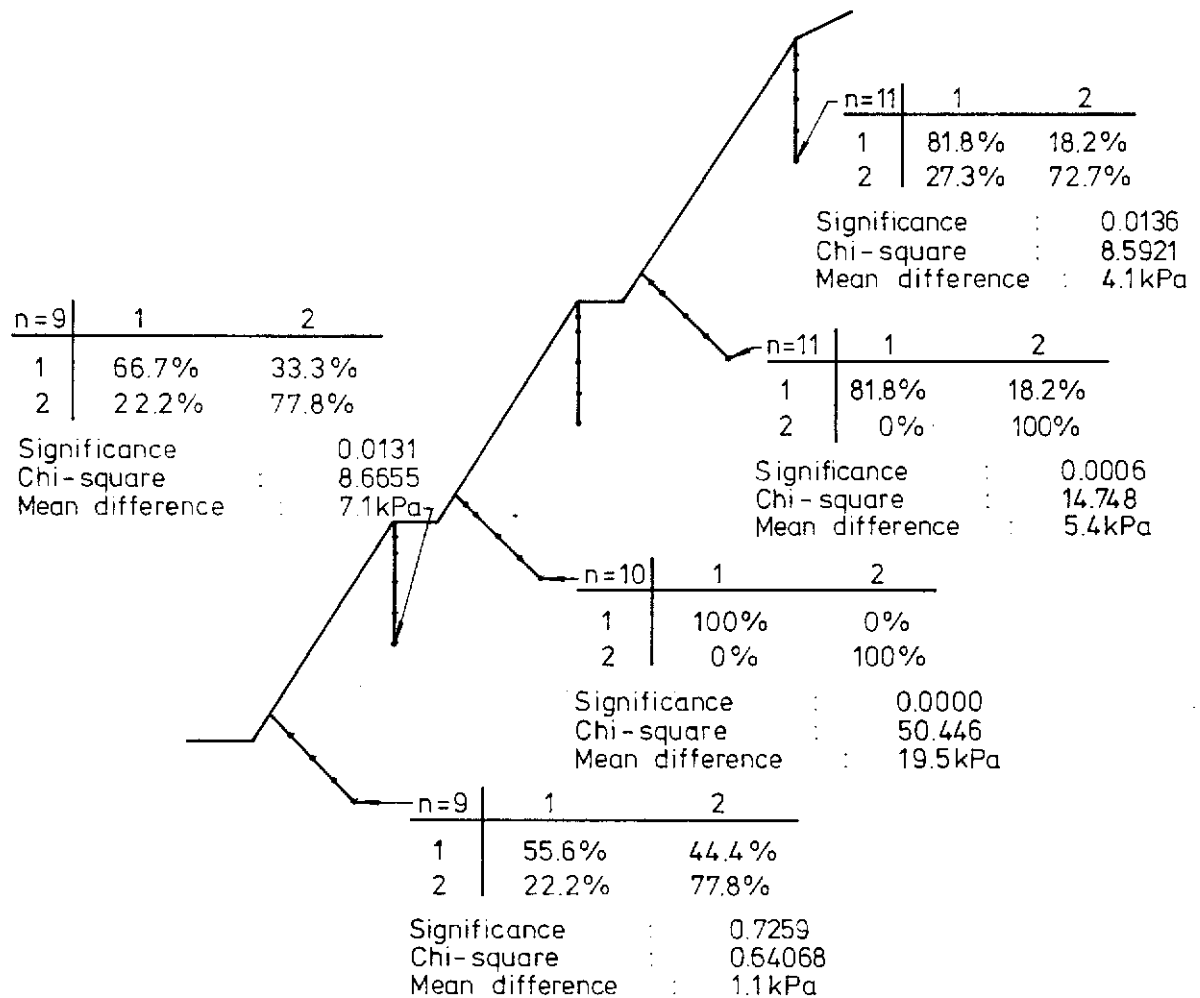
Legend :

Number of storms used
in the analysis

	n=9	1	2	
grass : group No. 1		77.8%	22.2%	← % allocated to group 1 and and assigned to group 2
chunam : group No. 2		0%	100%	
				← % allocated to group 1 and assigned to group 1

Figure 4.17 - Significance of differences between lowest storm suction at 3 m depth on chunam and grass slopes using discriminant analysis

4m depth



Legend :

Number of storms used
in the analysis →

	n=9	1	2	
grass : group No. 1	55.6%	44.4%		← % allocated to group 1 and assigned to group 2
chunam : group No. 2	22.2%	77.8%		
				← % allocated to group 1 and assigned to group 1

Figure 4.18 - Significance of difference between lowest storm suction at 4 m depth on chunam and grass slopes using discriminant analysis

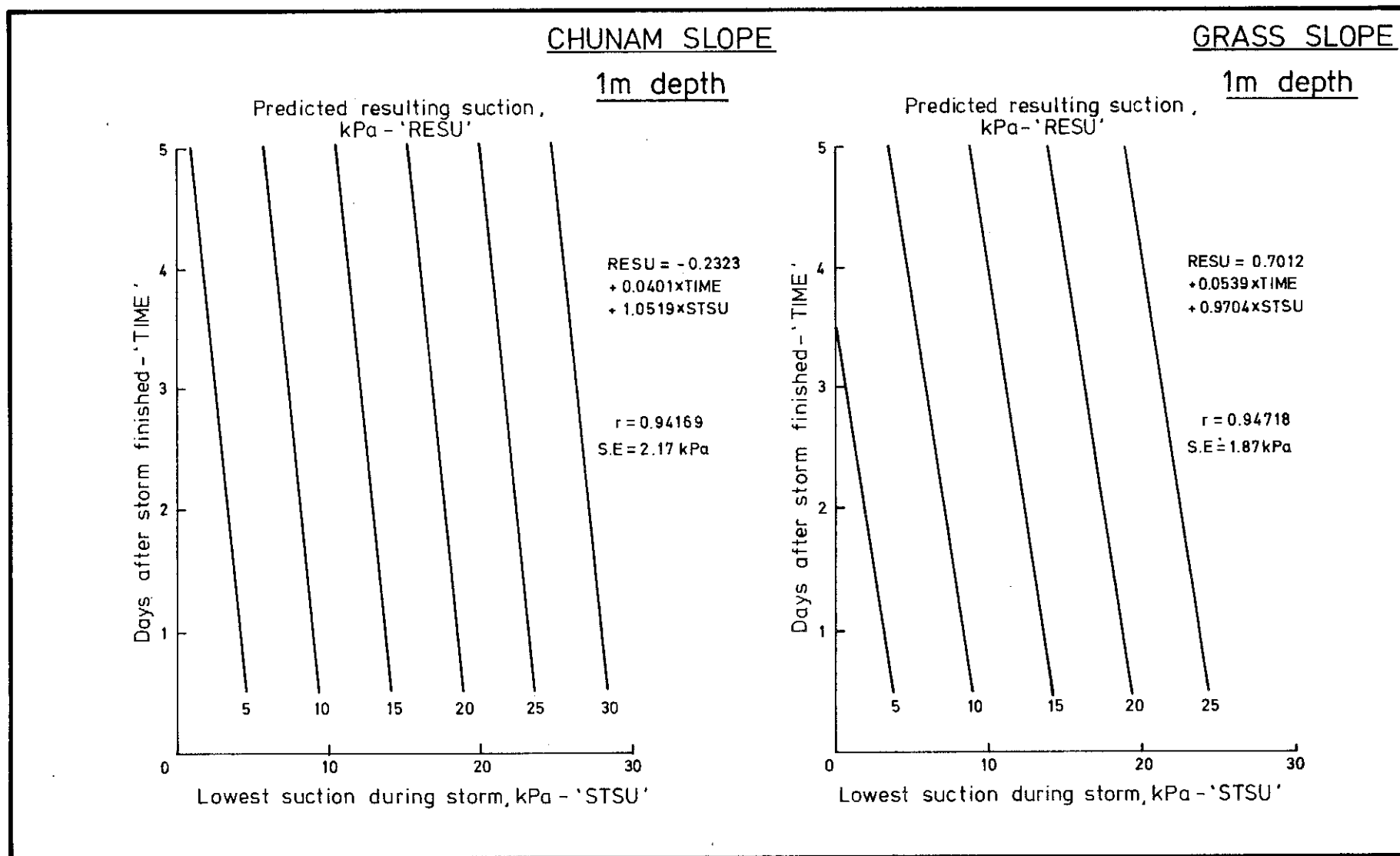


Figure 4.19 - Plot of equations 4.6 and 4.7

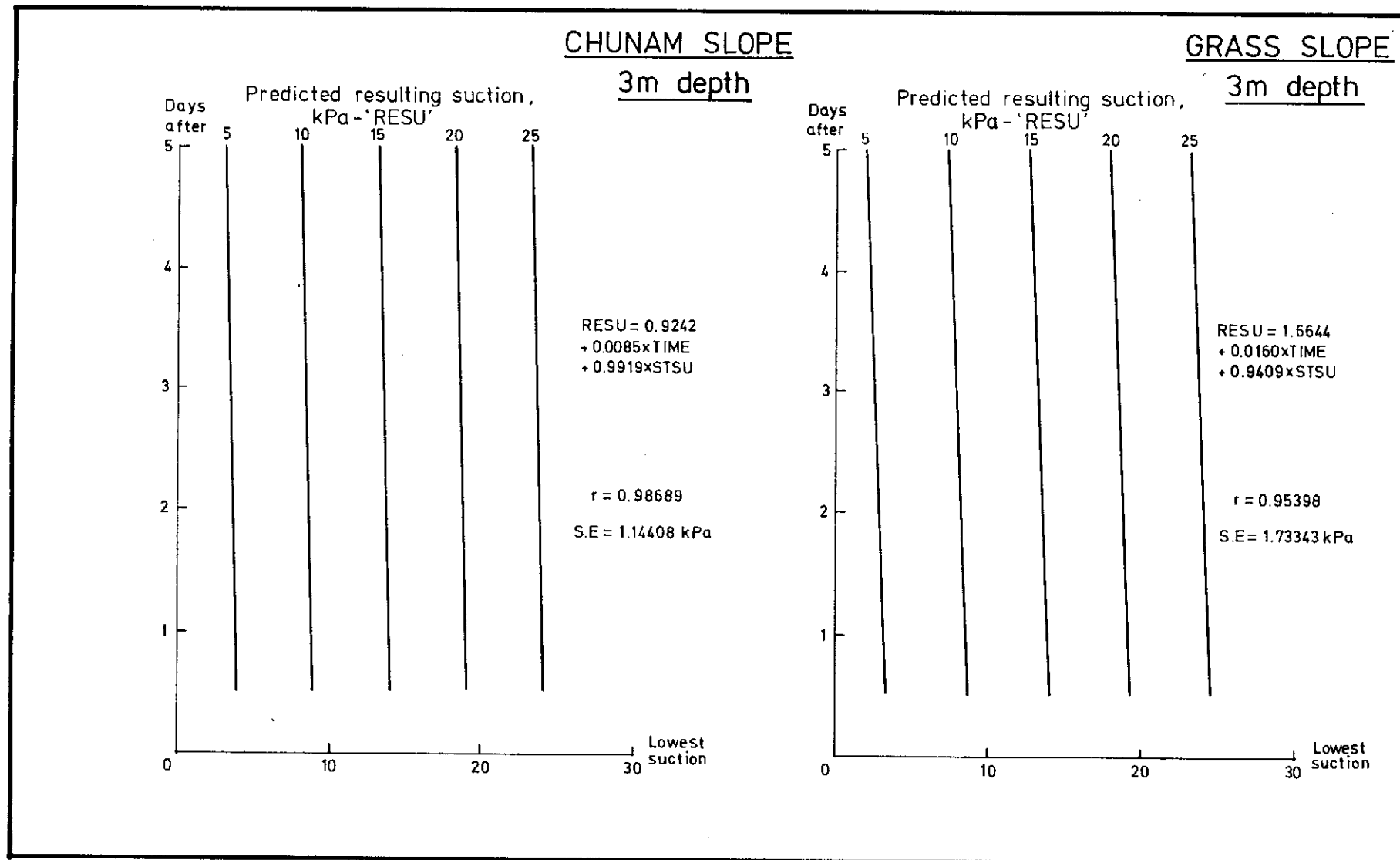


Figure 4.20 - Plot of equations 4.8 and 4.9

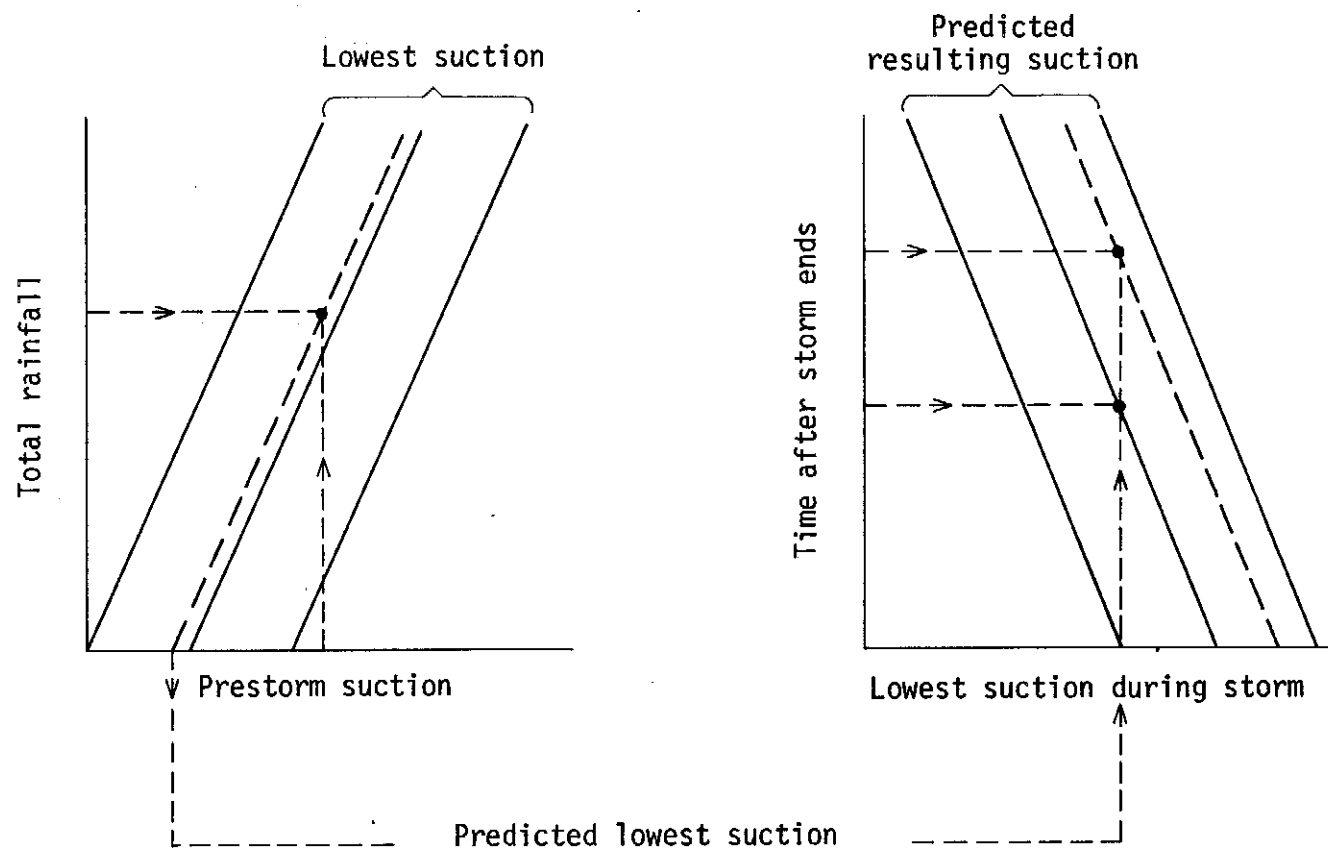


Figure 4.21 - Summary of prediction procedure for estimating both lowest storm suction and subsequent suction recovery

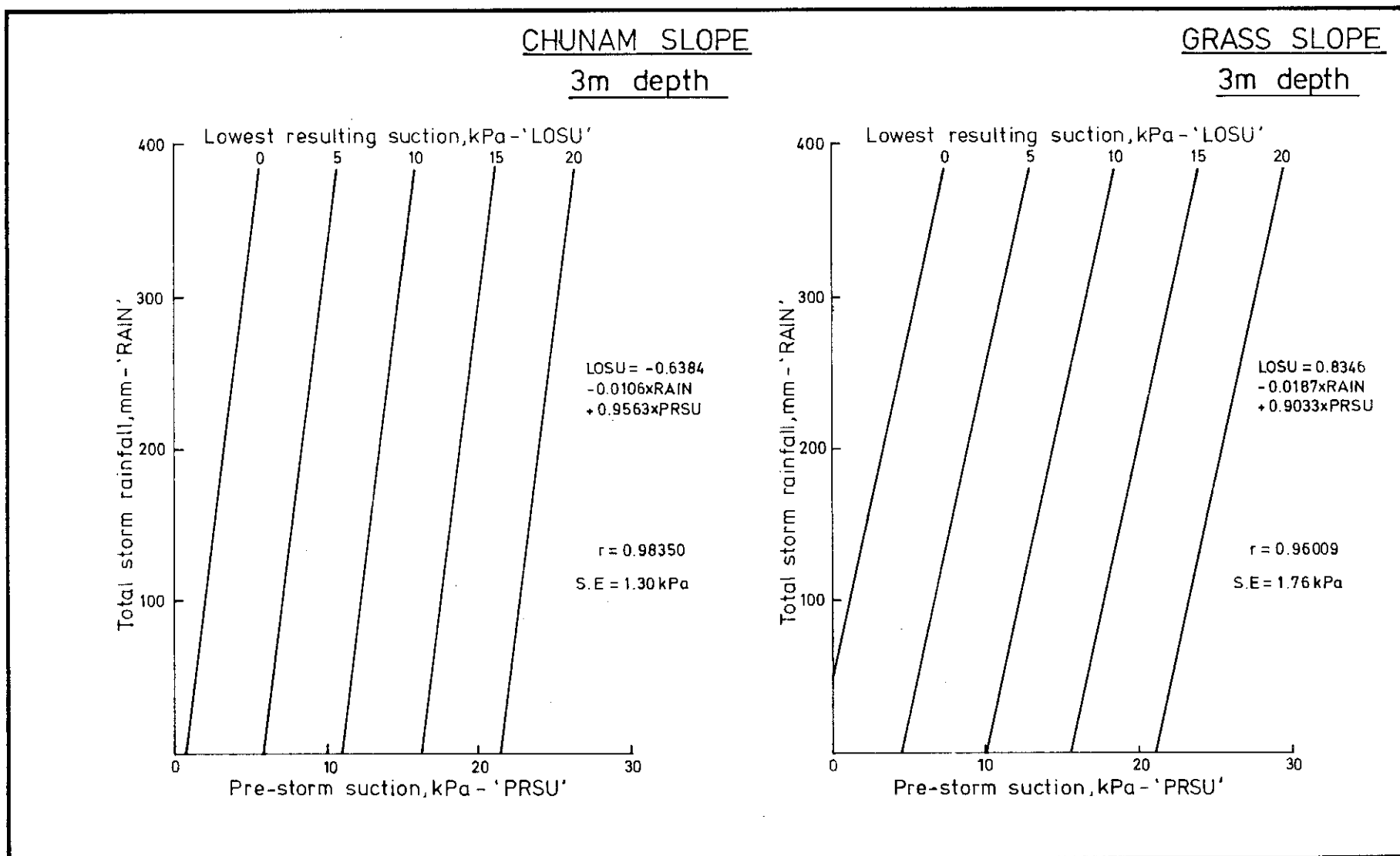


Figure 4.22 - Plot of equations 4.10 and 4.11

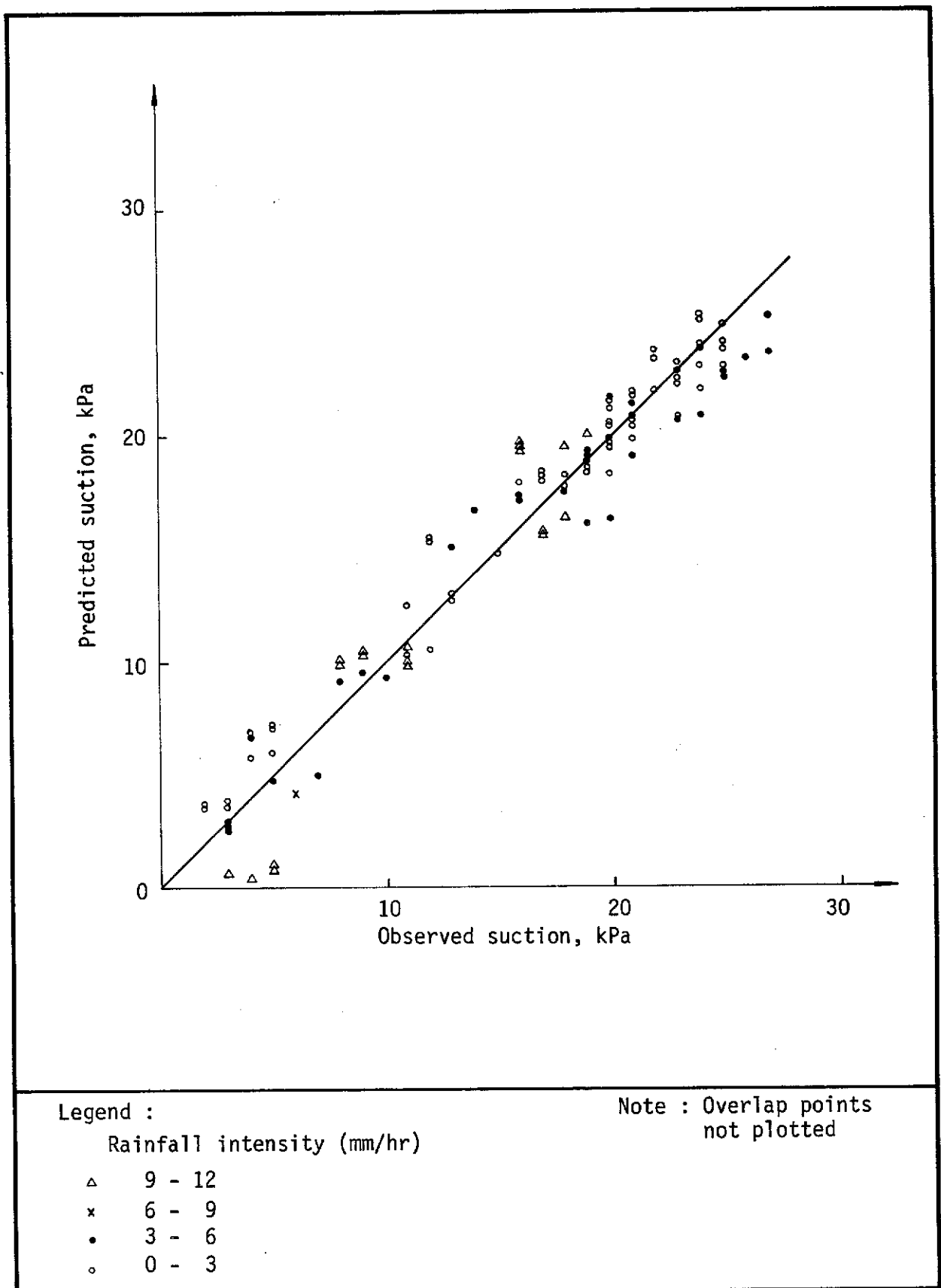


Figure 4.23 - Comparison of observed and predicted suctions during recovery on chunam slope (3 m depth)

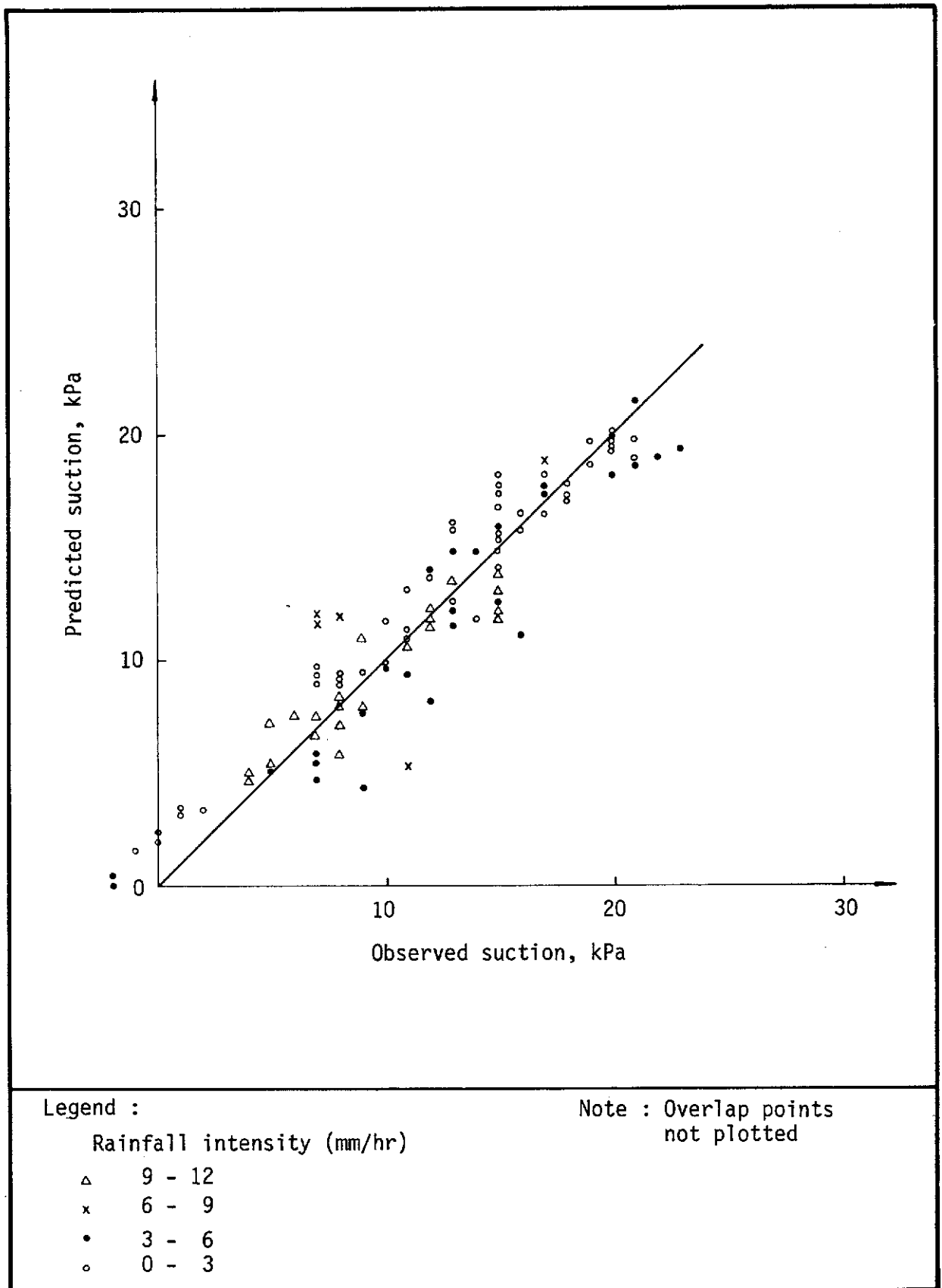
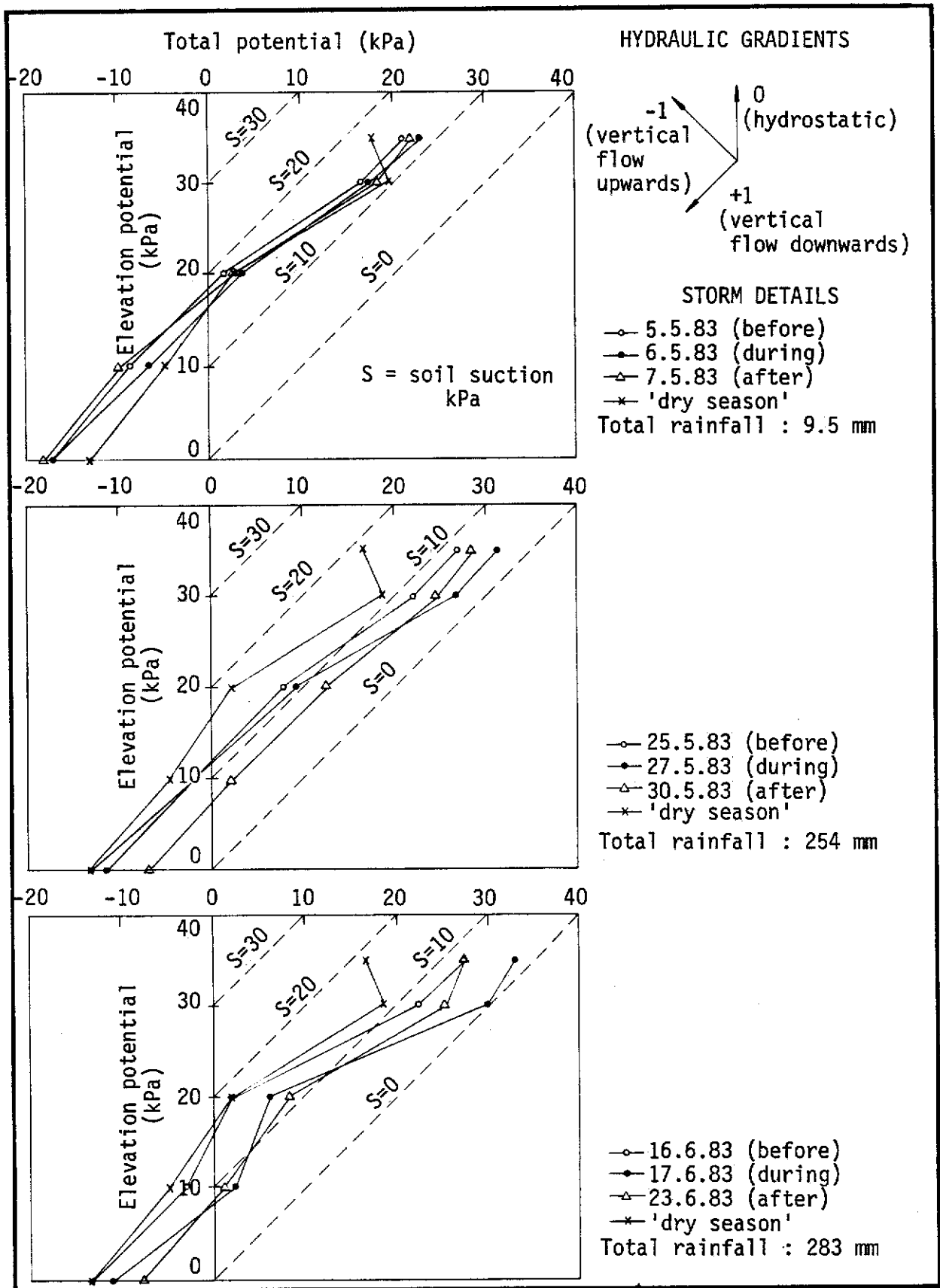


Figure 4.24 - Comparison of observed and predicted suctions during recovery on grass slope (3 m depth)



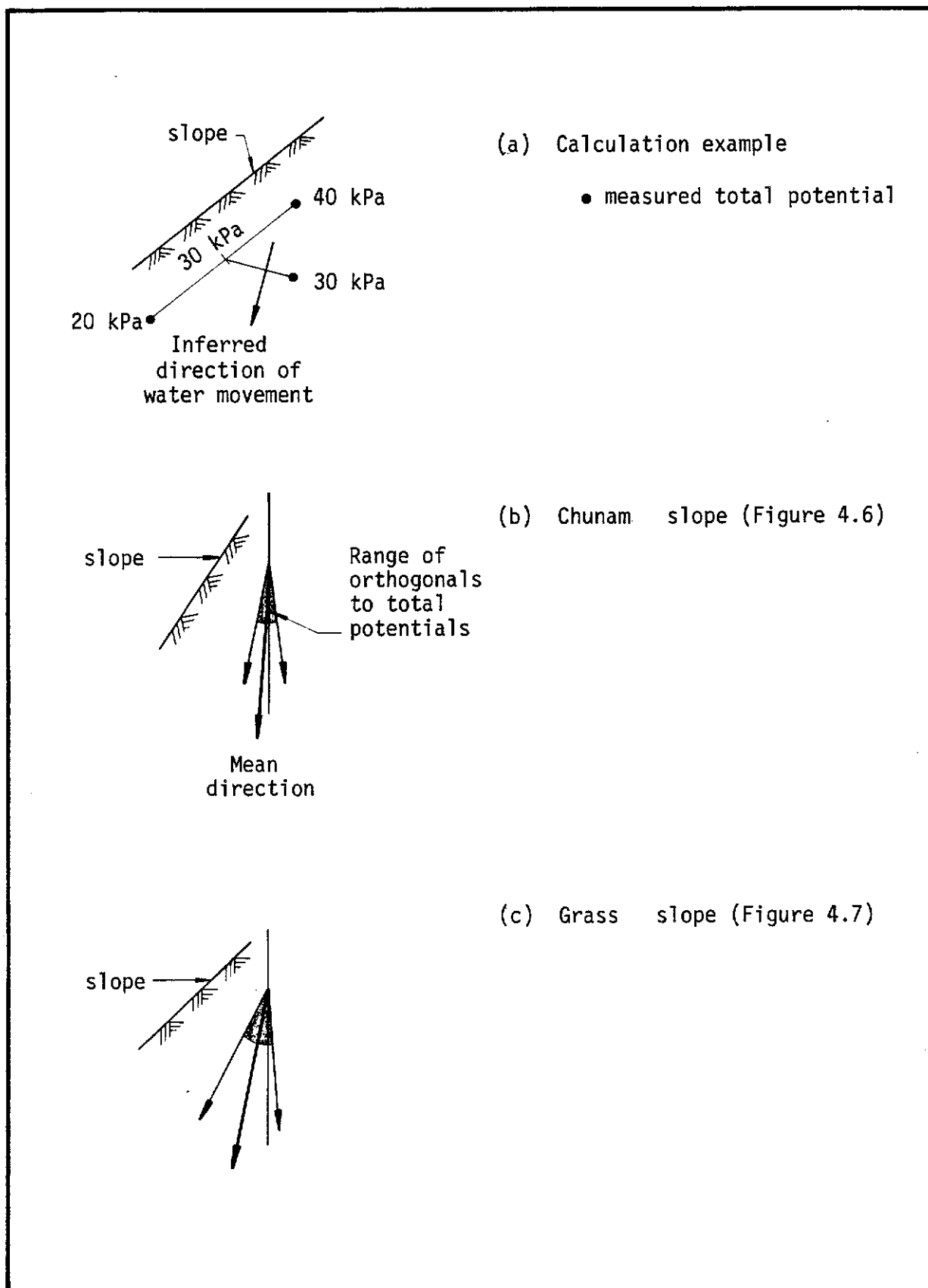


Figure 4.26 - Directions of near surface soil water movement at the Clear Water Bay Road Site (see Figures 4.6 and 4.7)

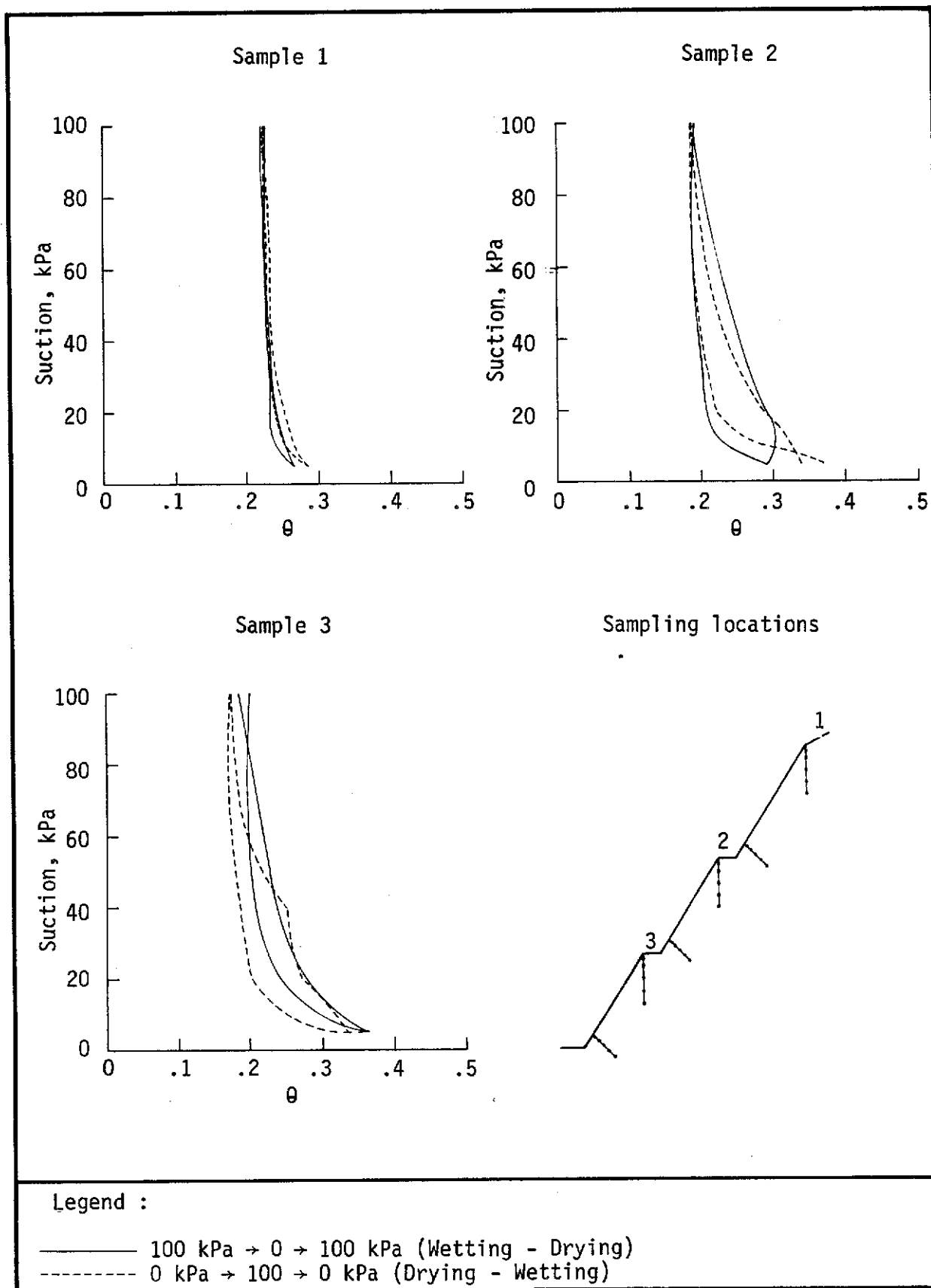


Figure 4.27 - Suction-moisture curves for the CDG on the chunam slope at Clear Water Bay Road (see Figure 4.6)

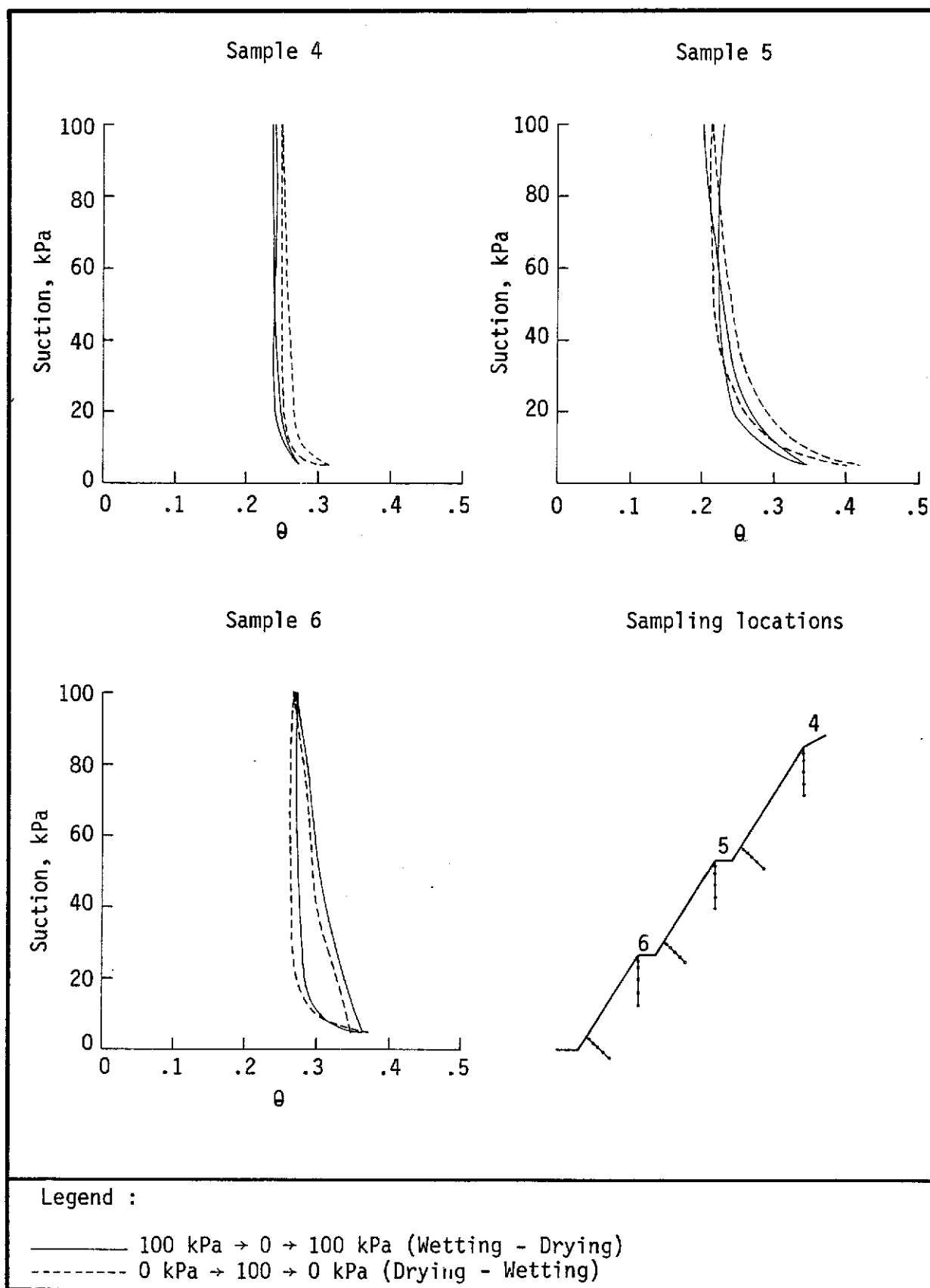


Figure 4.28 - Suction-moisture curves for the CDG on the grass slope at Clear Water Bay Road (see Figure 4.7)

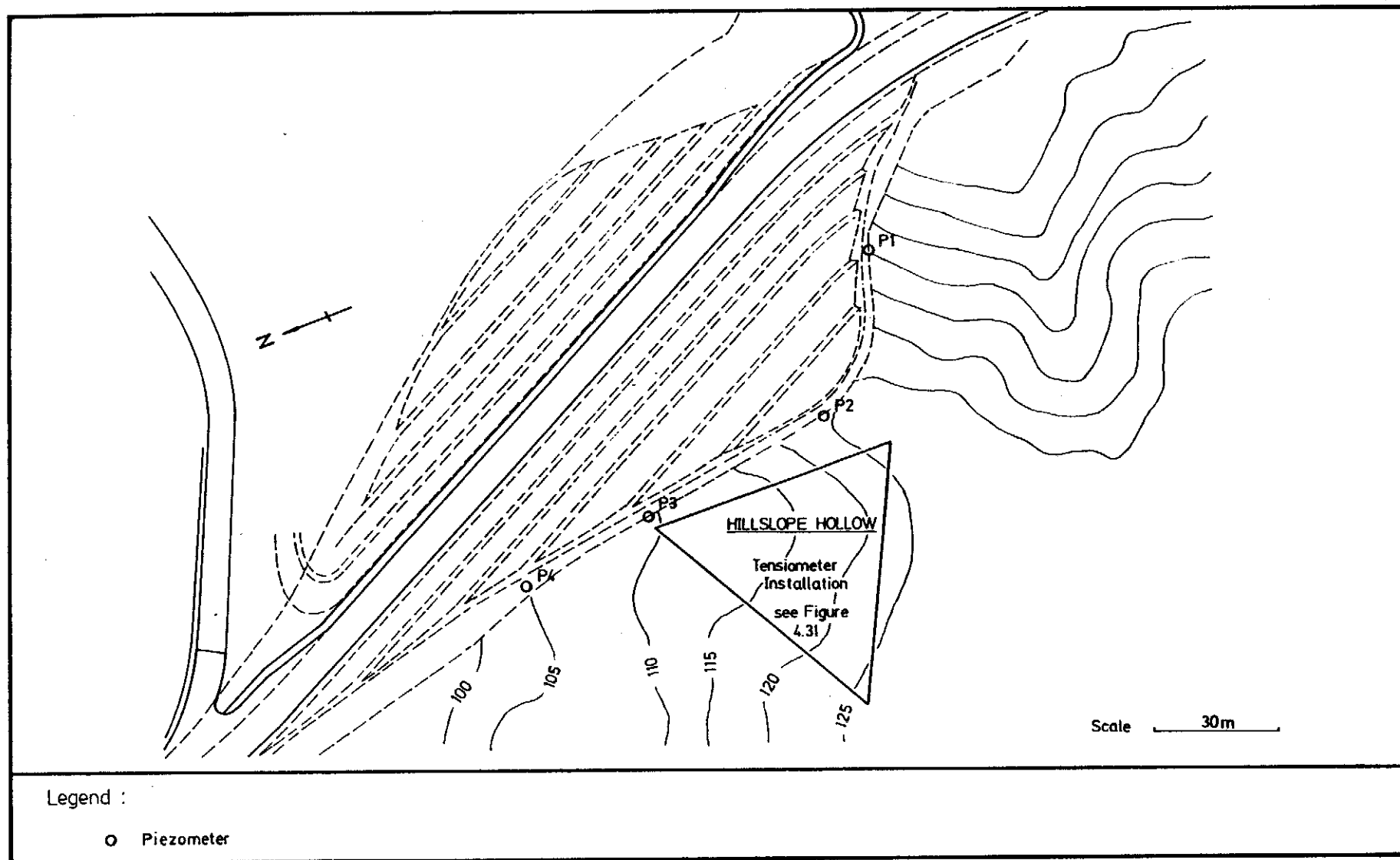


Figure 4.29 - Tai Po, St. Christopher Bend, Study site (see figure 1.7)

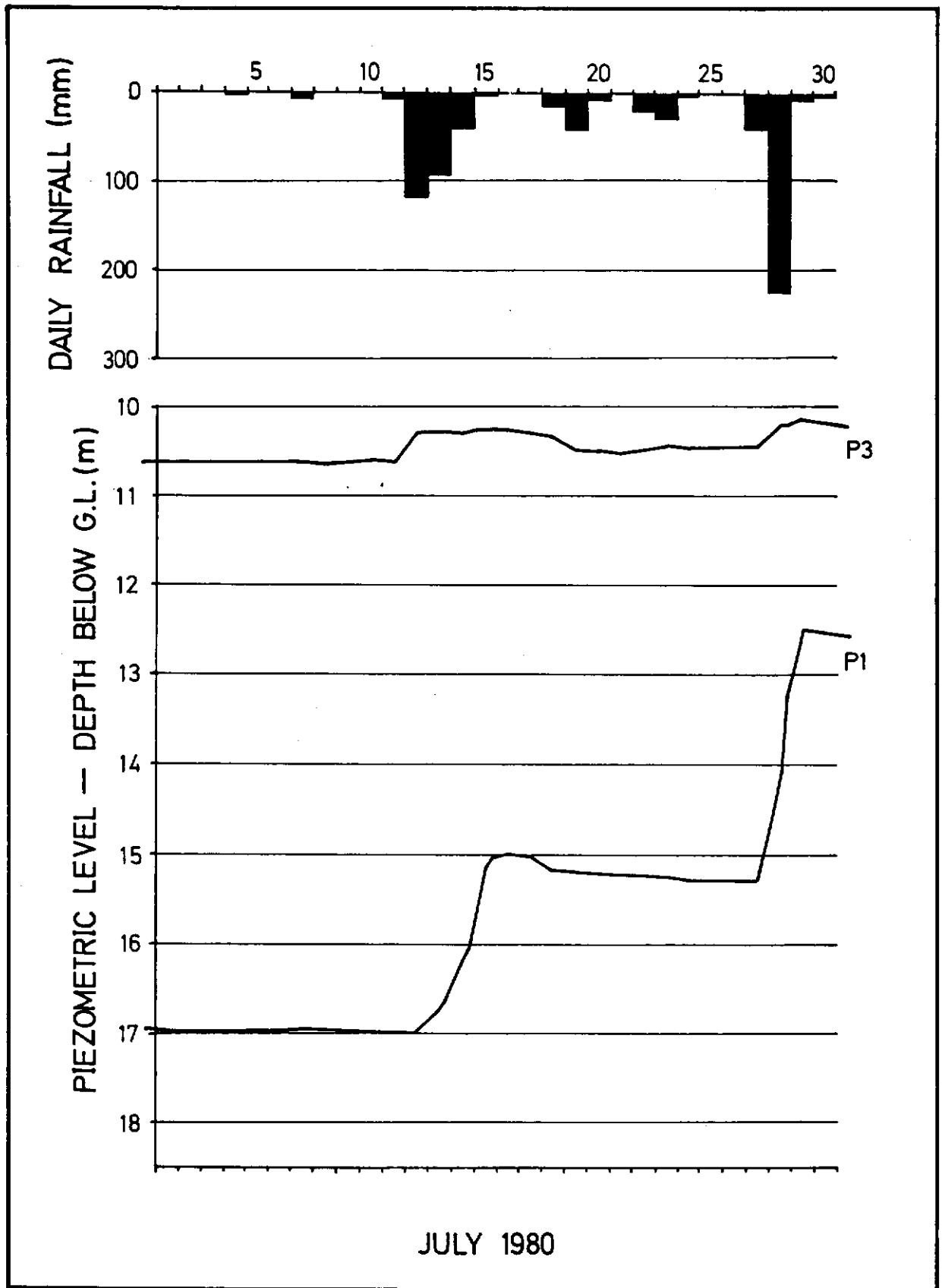


Figure 4.30 - Typical piezometer responses. P1 and P3 are at the same elevation (109.3 mPD)

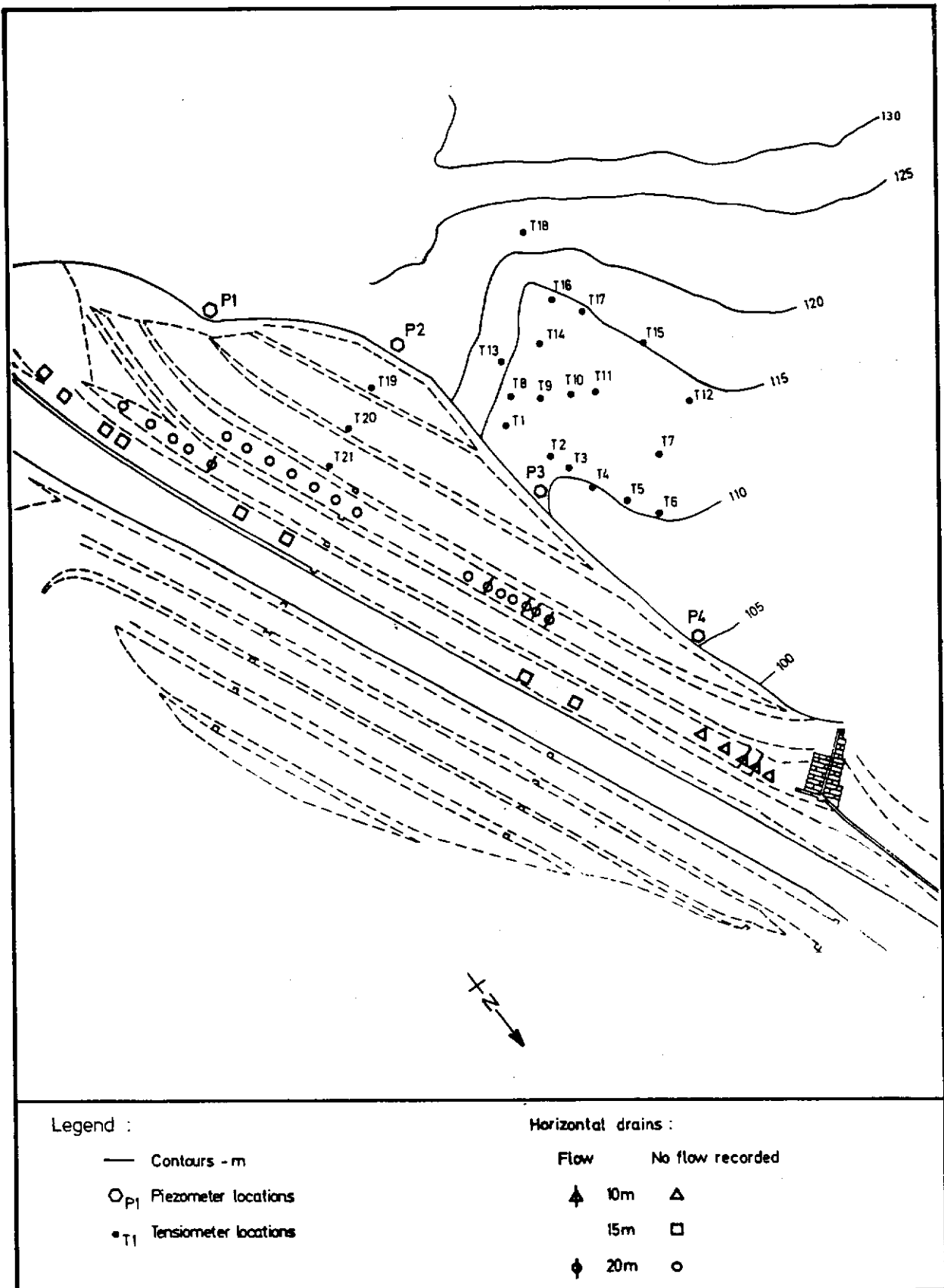


Figure 4.31 - Instrumentation plan, showing tensiometer, piezometer and horizontal drain locations

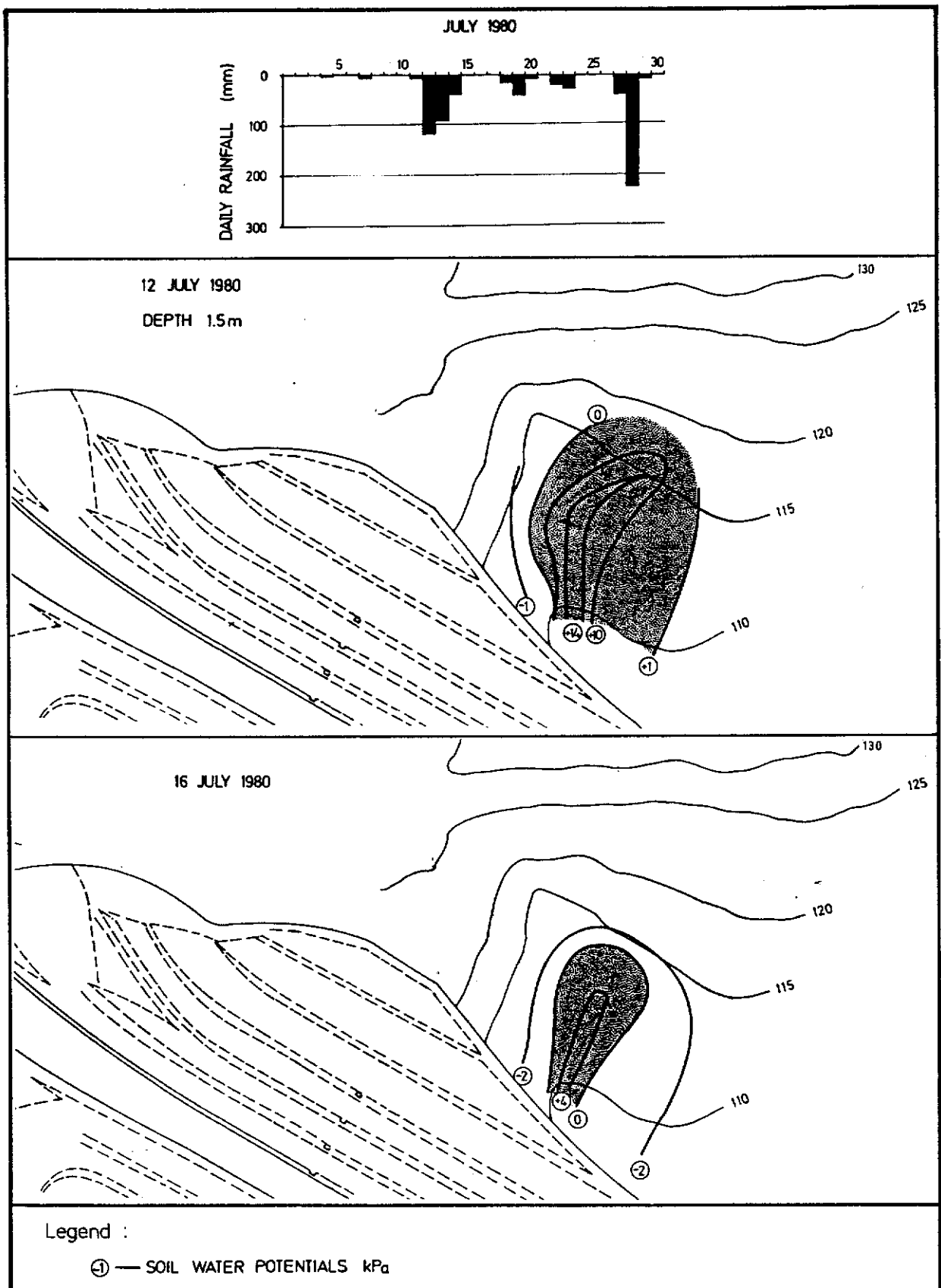


Figure 4.32 - Storm of July 11-14 1980 with the associated soil water conditions on July 12 and July 16 1980 at 1.5 m depth

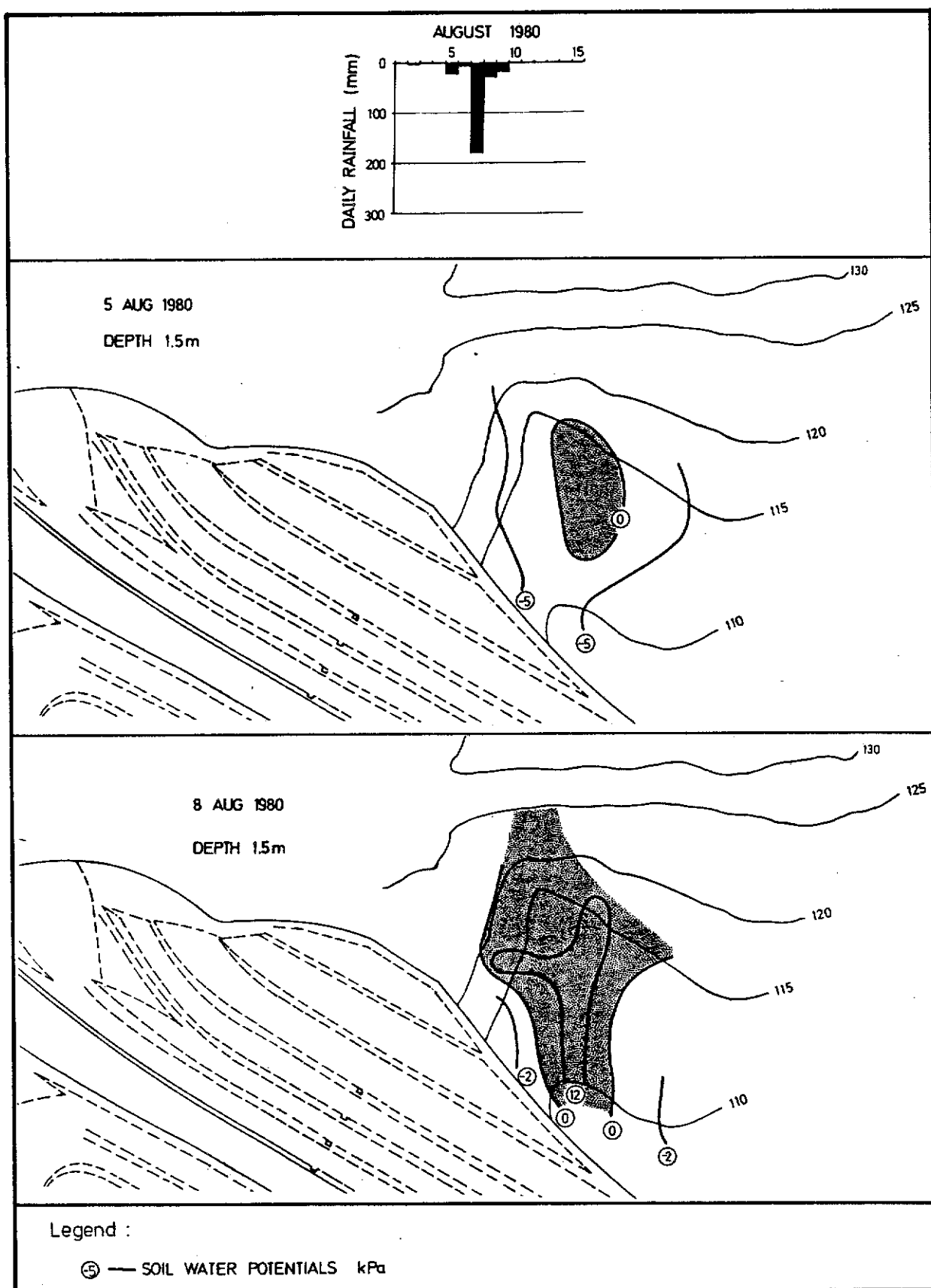


Figure 4.33 - Storm of August 5-9 1980 with the associated soil water condition on August 5 and August 8 1980 at 1.5 m depth

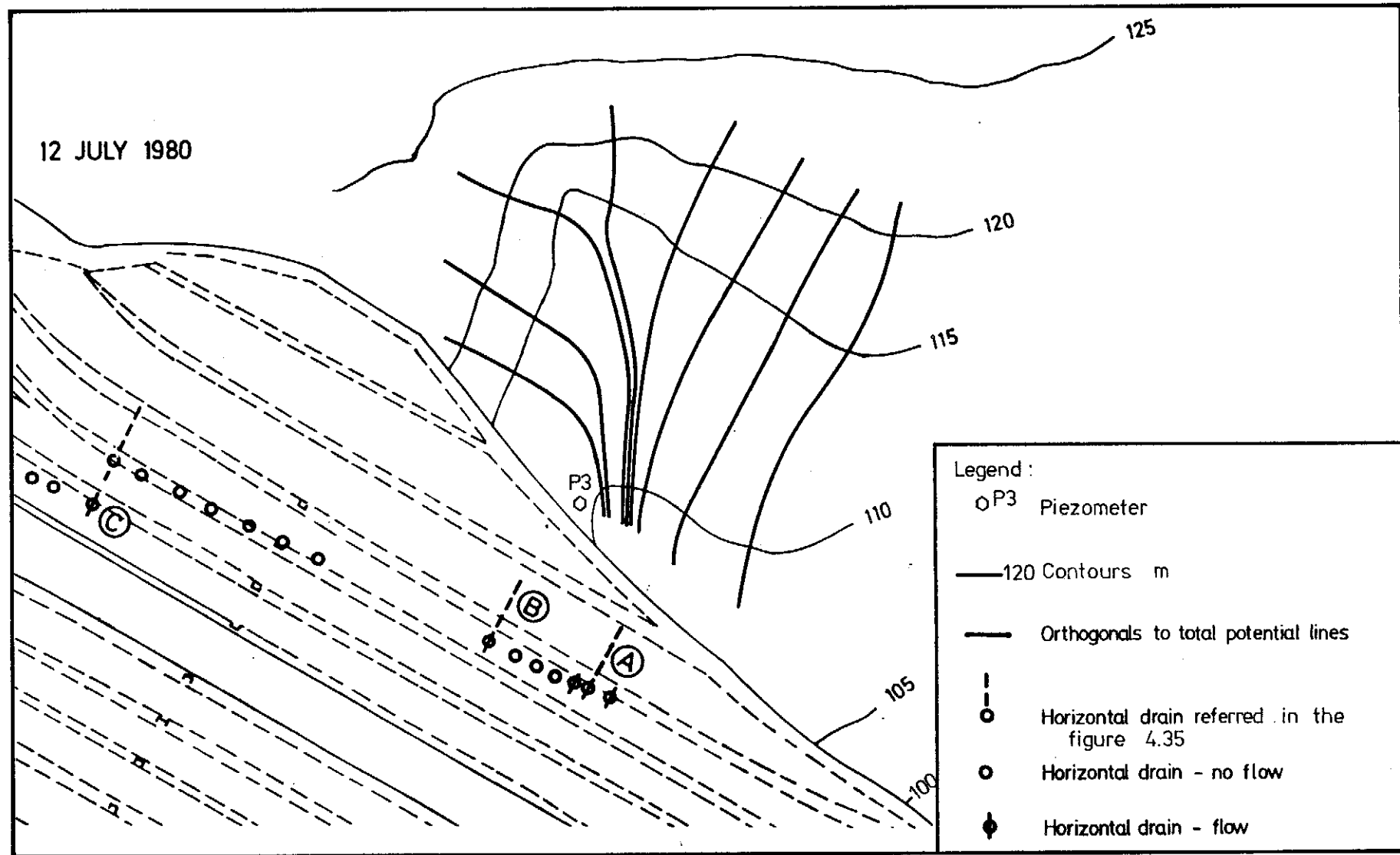


Figure 4.34 - Orthogonals to total potential lines for July 12 1980 illustrating soil water convergence at 1.5 m depth

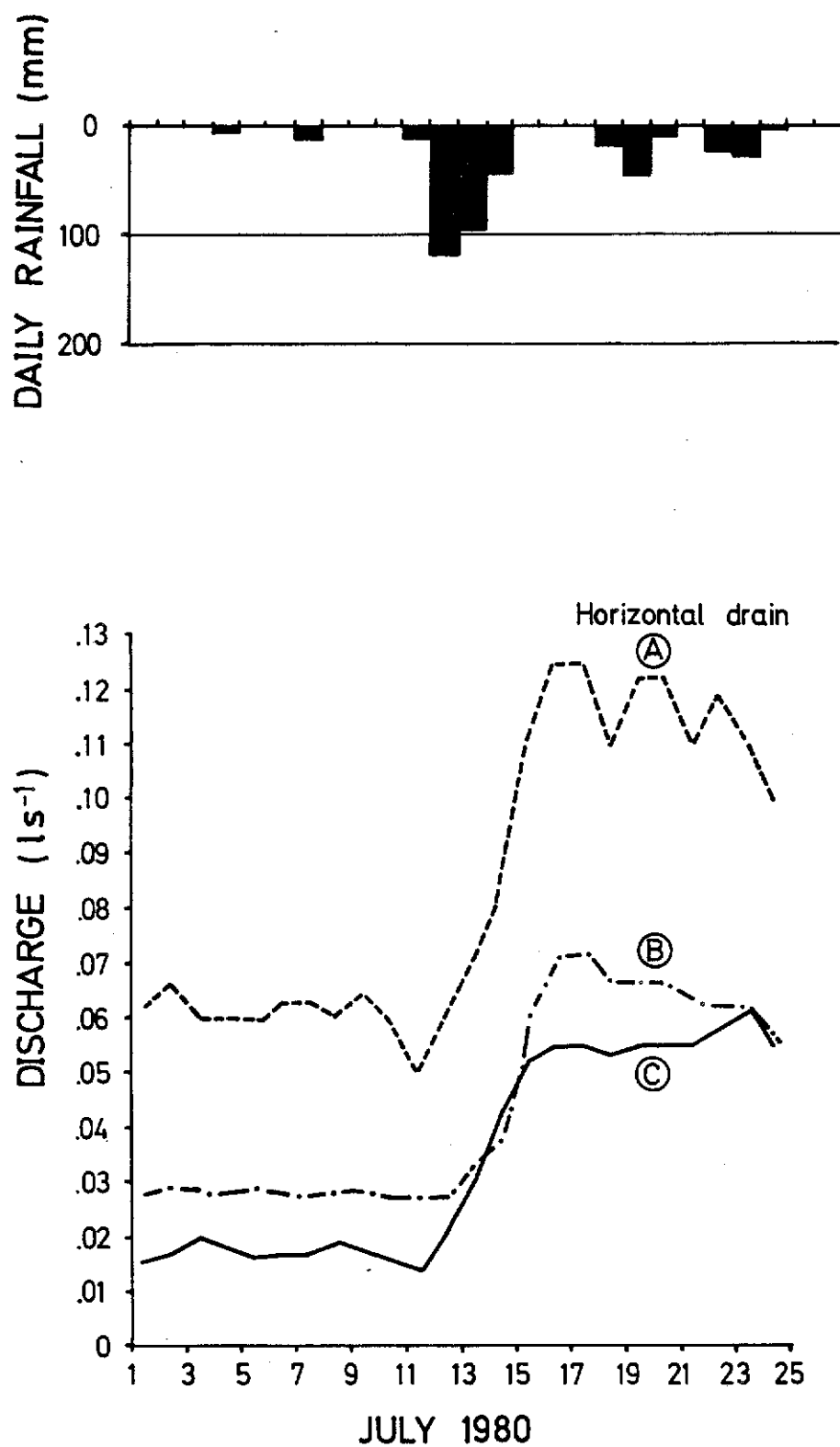


Figure 4.35 - Discharge from three horizontal drains in July 1980 - note the relatively higher discharge from drain A located at the focus of the backslope topography

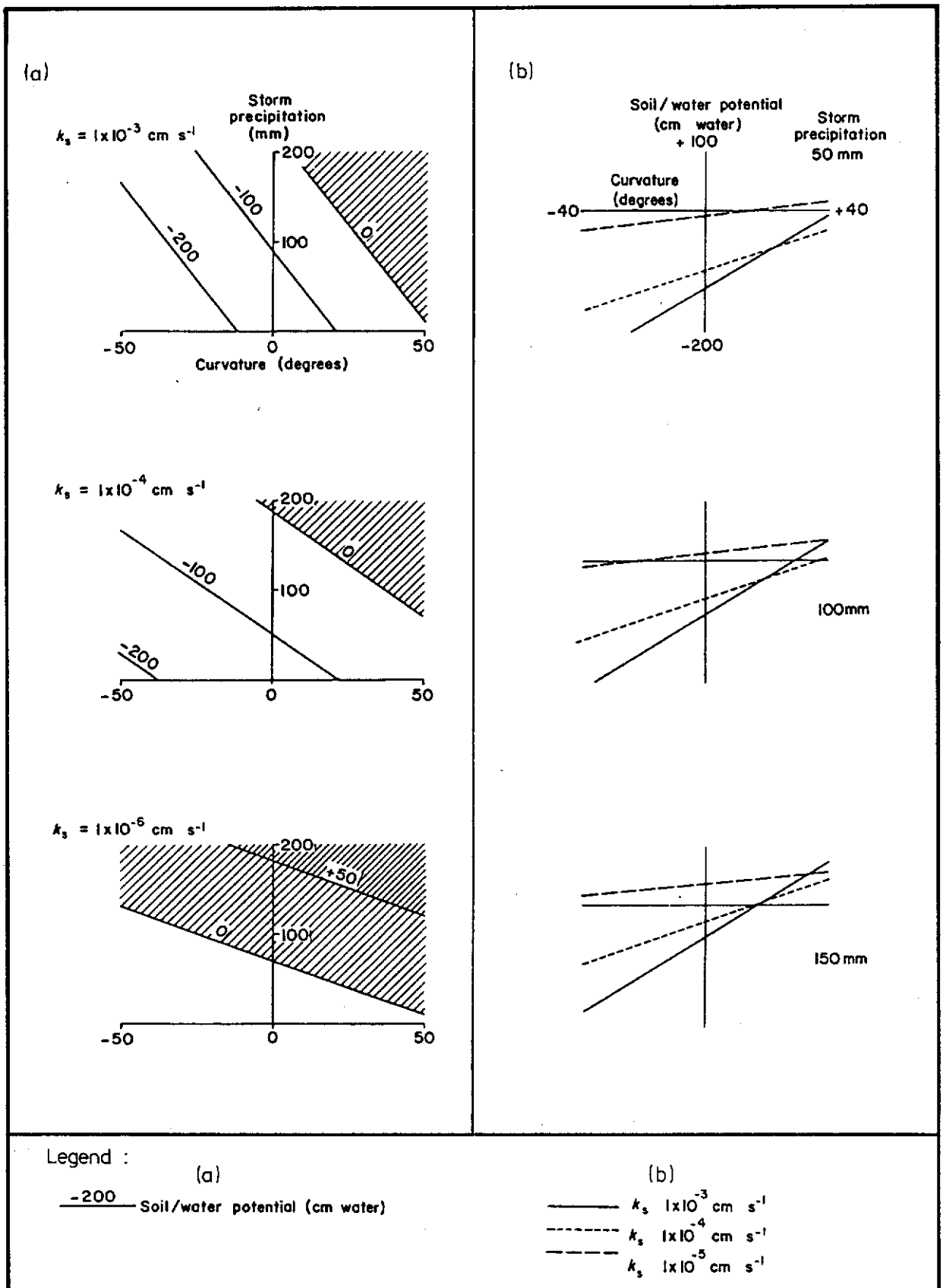


Figure 4.36 - Predicted response of soil suction to slope plan curvature (positive concave) by (a) permeability group and (b) storm size. (after Anderson, 1982)

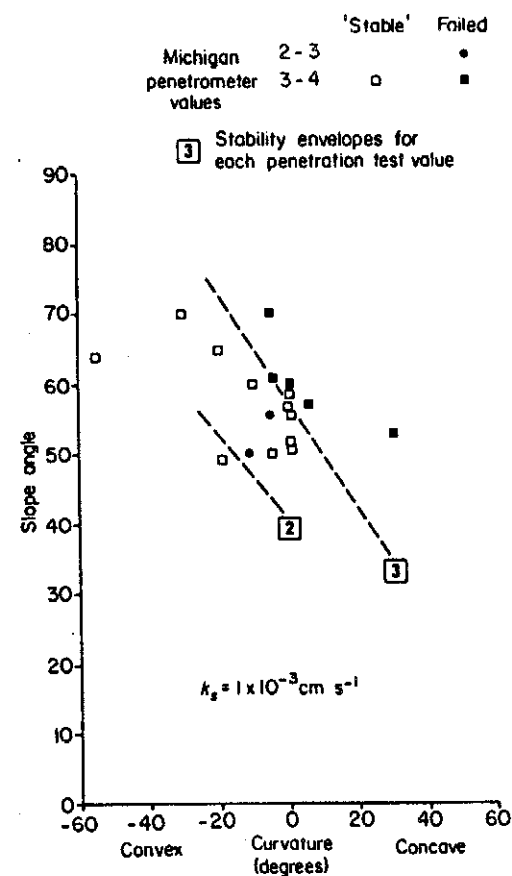
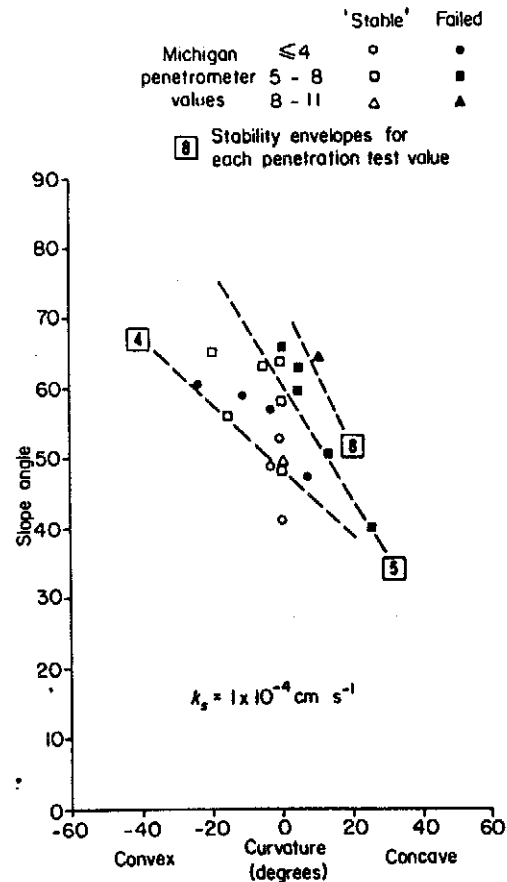
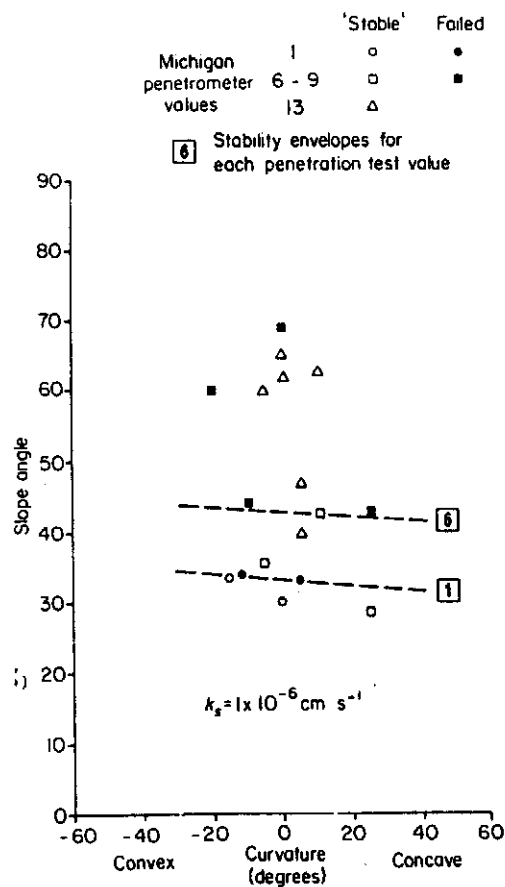


Figure 4.37 - Relationship of failed and 'stable' cut slopes to unconfined strength, slope plan curvature and slope angle for three permeability groups. (after Anderson, 1983)

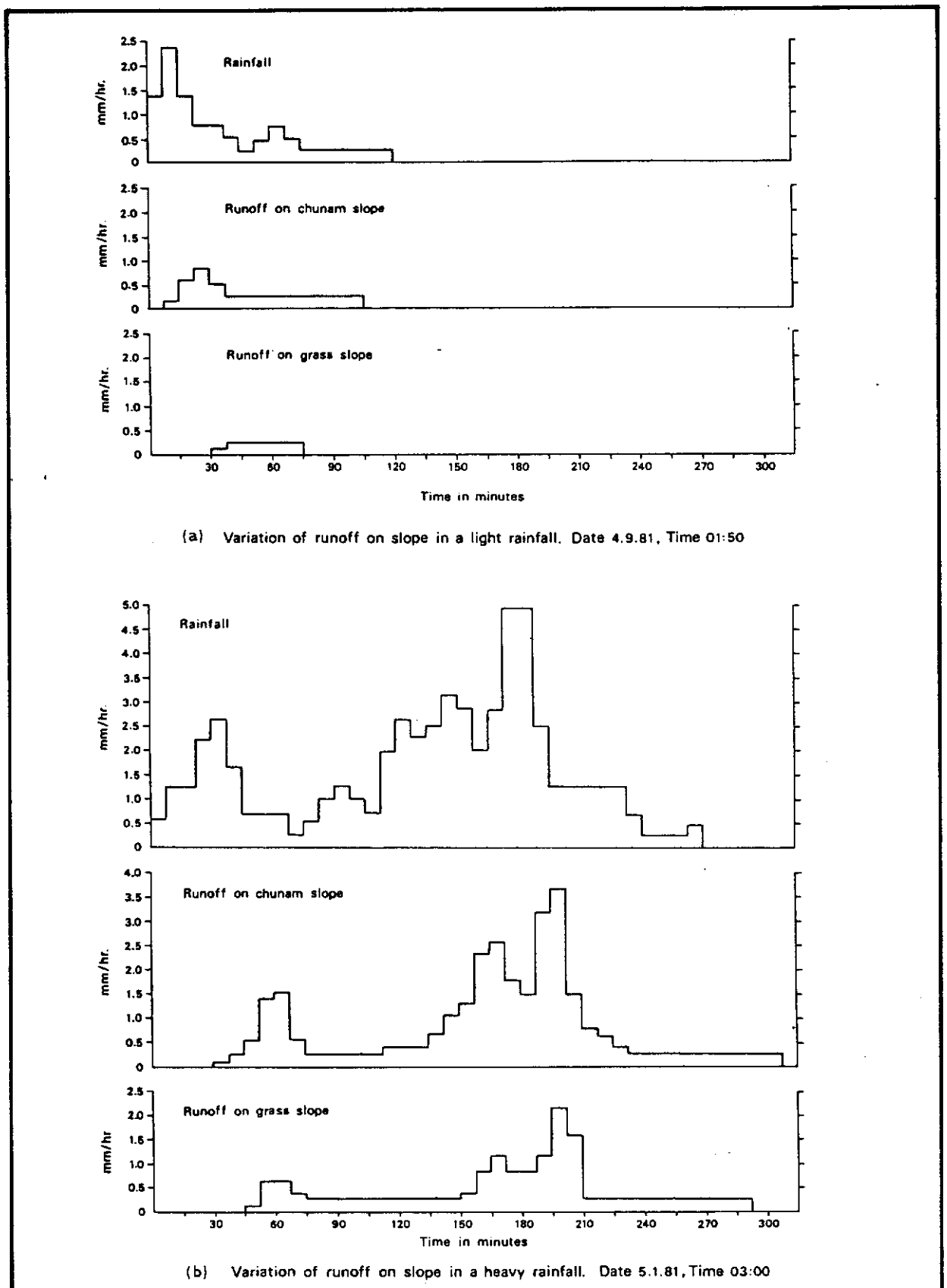


Figure 4.38 - Variation of runoff with rainfall. (after Hsu et al, 1983)

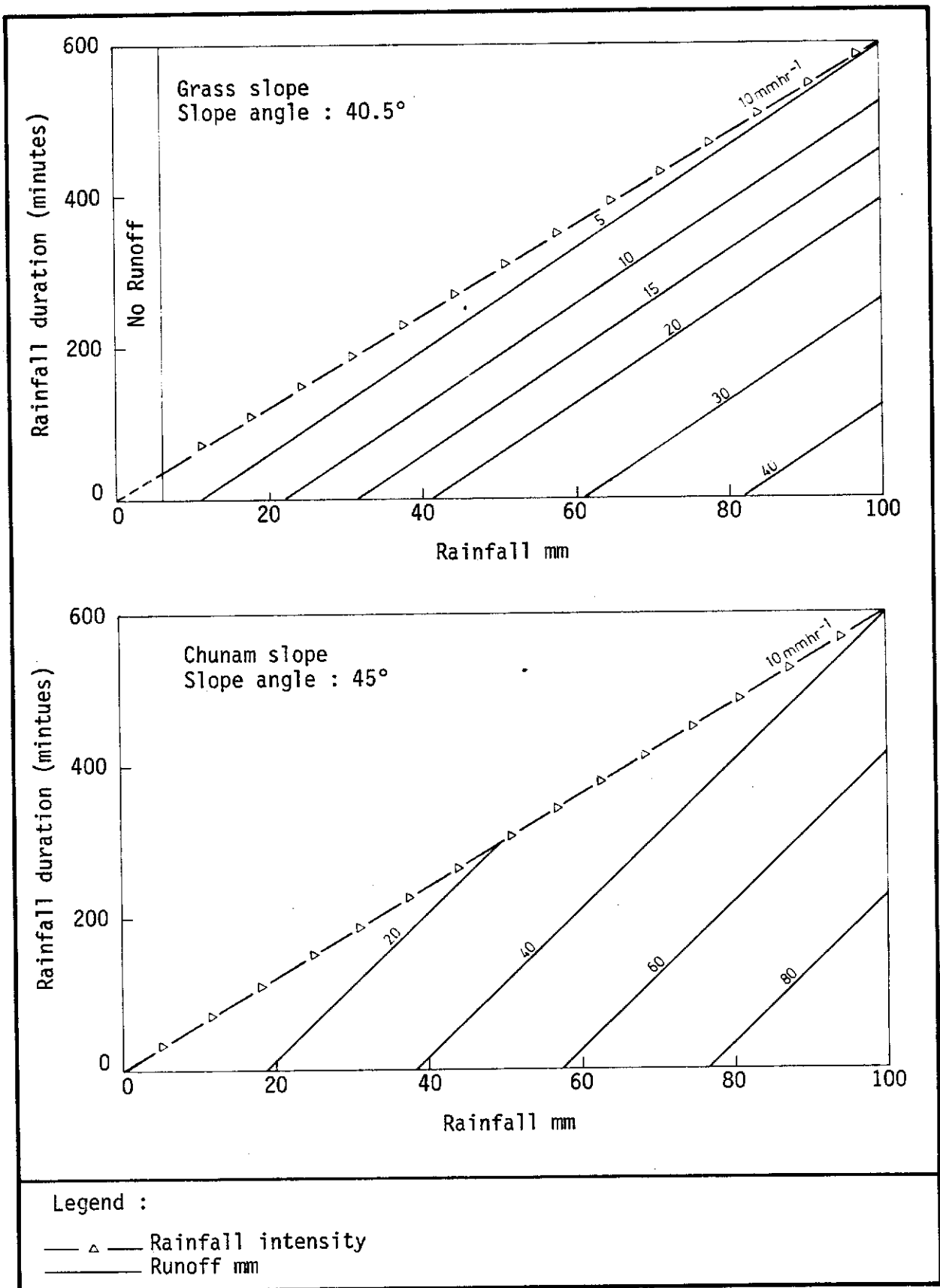


Figure 4.39 - Summary of runoff production on chunam and grass slopes after Hsu et al, (1983)

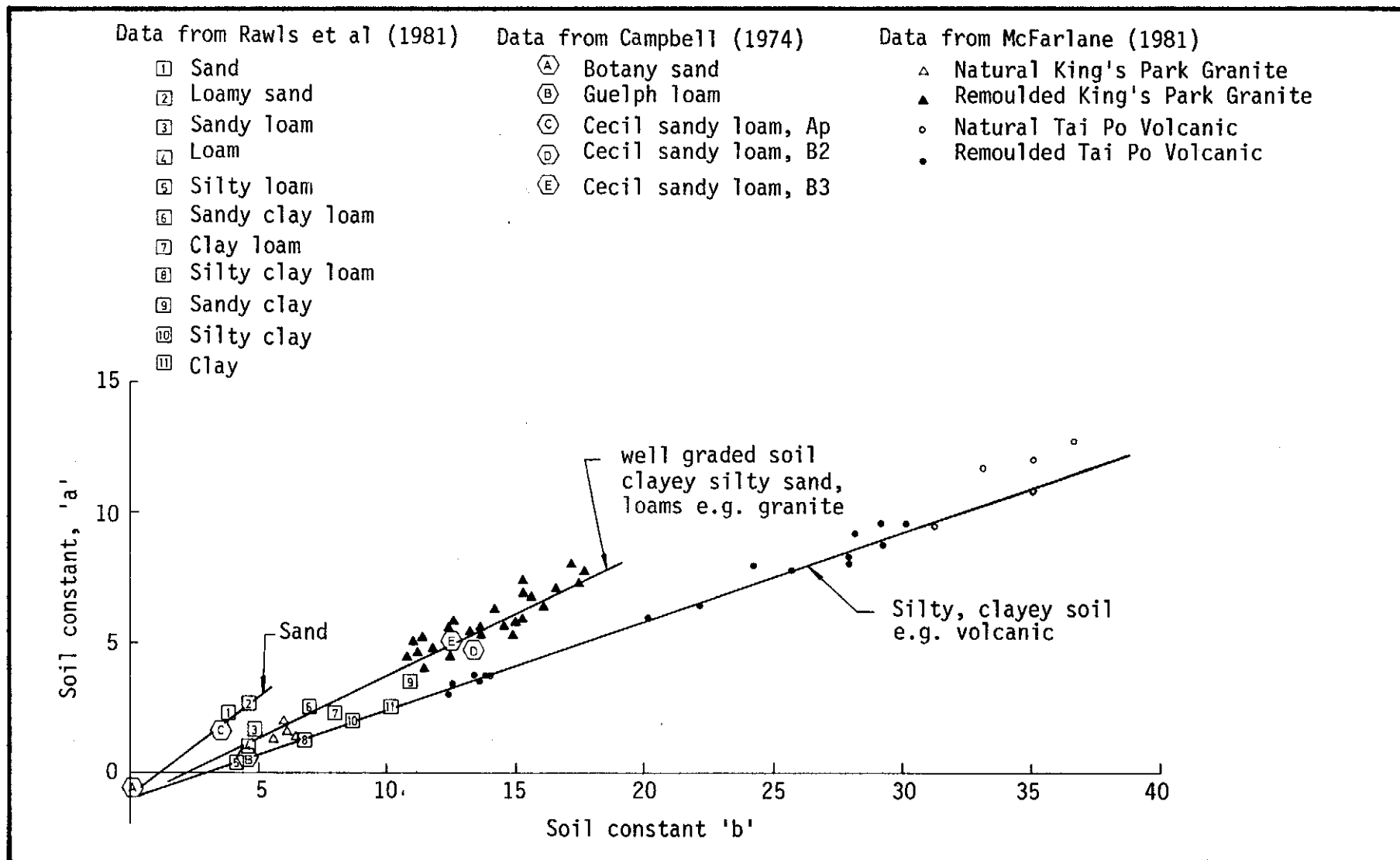


Figure 5.1 - Selected soils plotted on 'a' and 'b' coefficients (see equation 3.22)

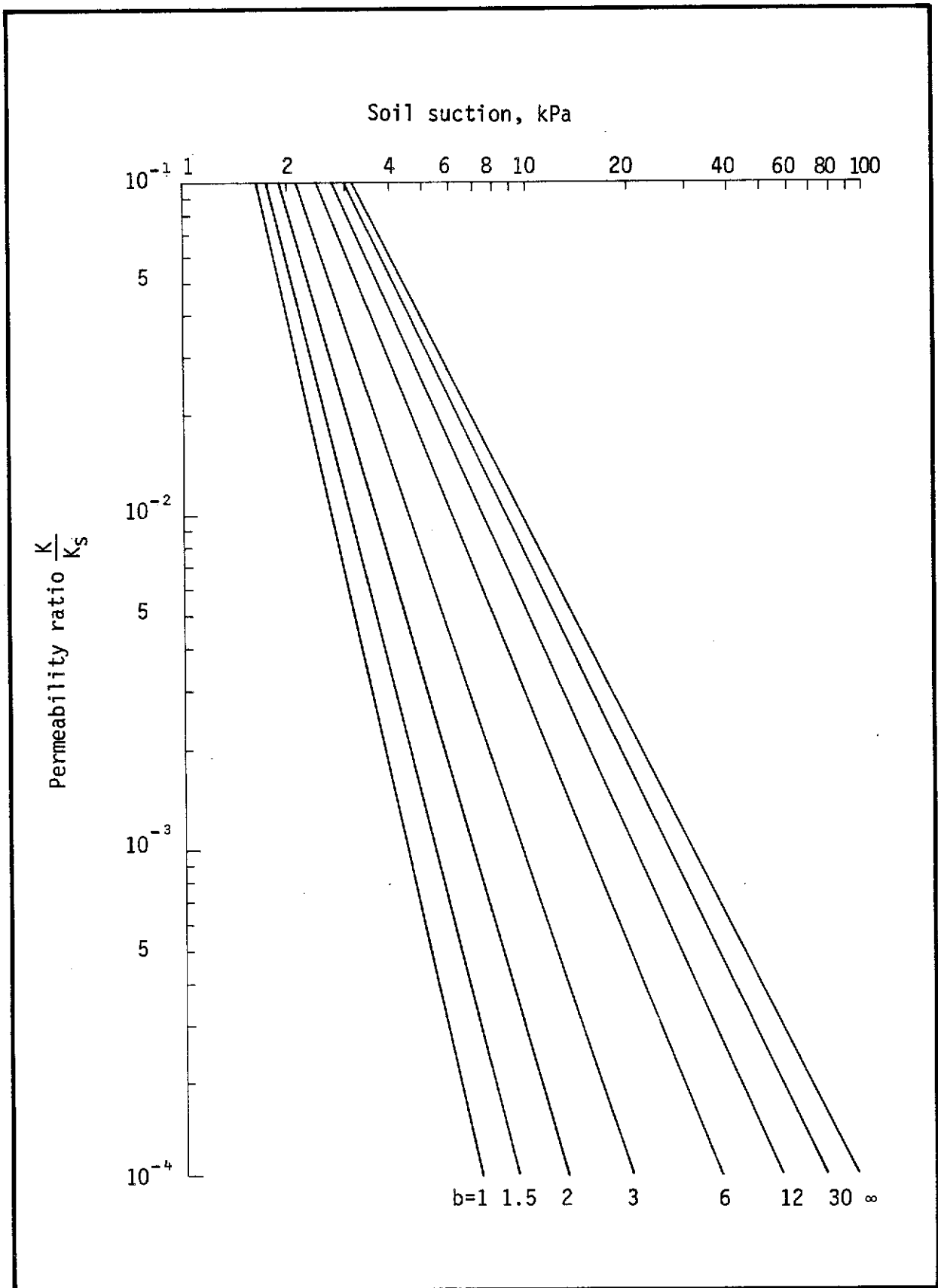


Figure 5.2 - Plot of equation 5.2 used to predict the effect of a protective cover

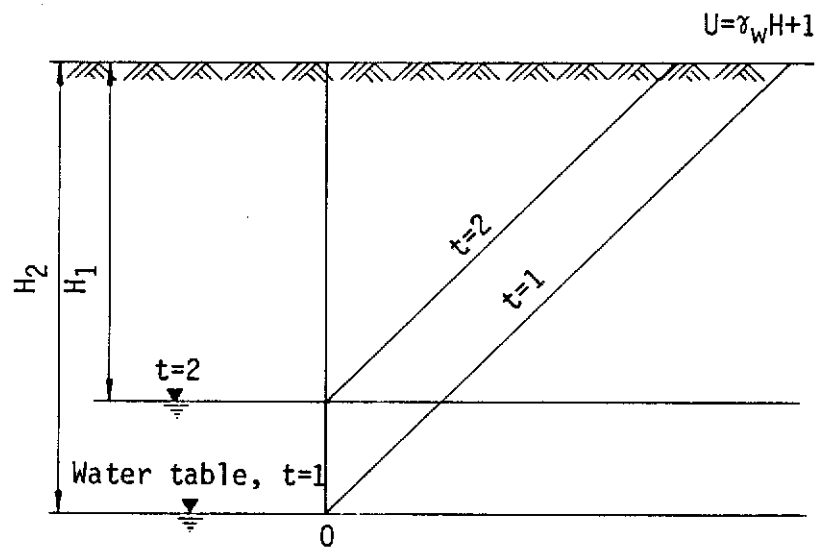
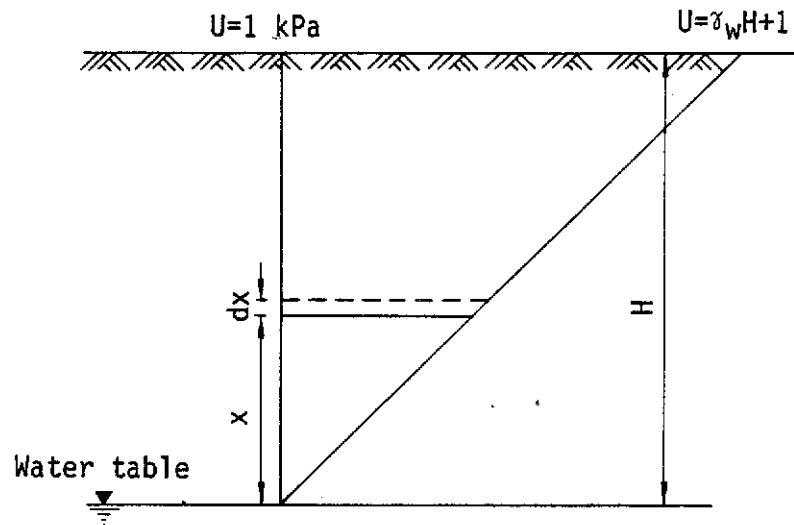


Figure 5.3 - Definition diagrams for equations 5.3 - 5.6

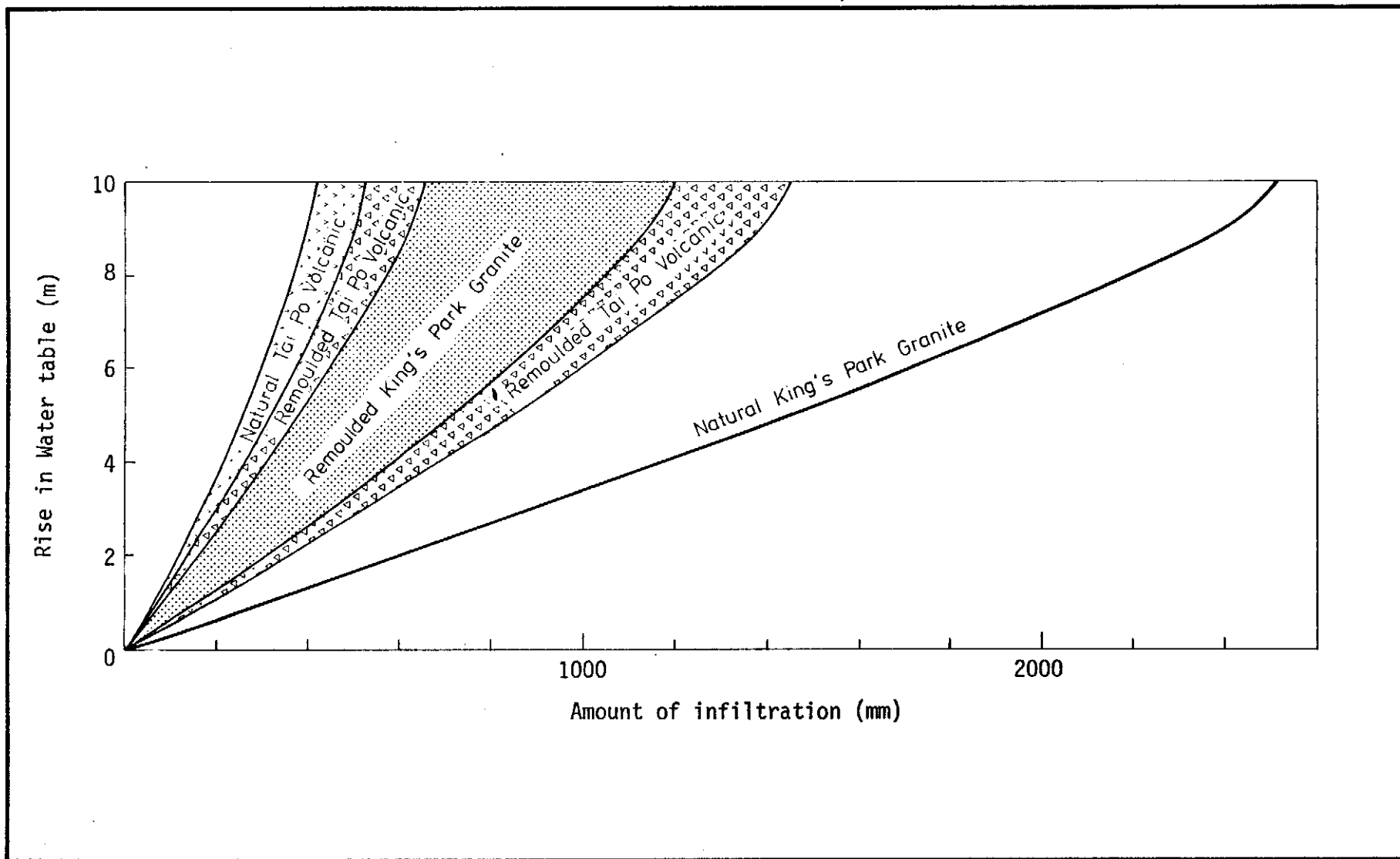


Figure 5.4 - Water table response in selected soils as predicted by equation 5.6 Soil depth 10 m

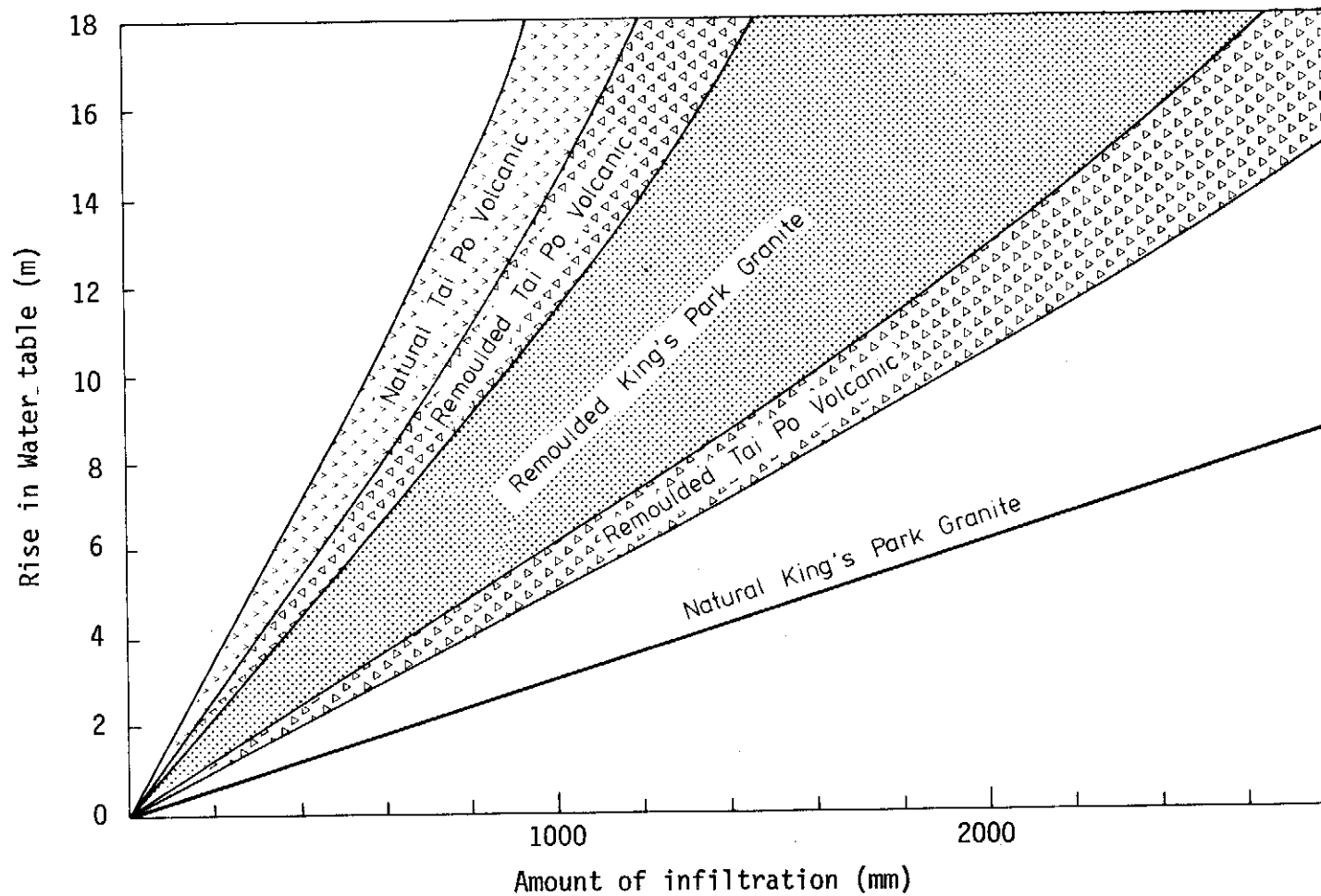
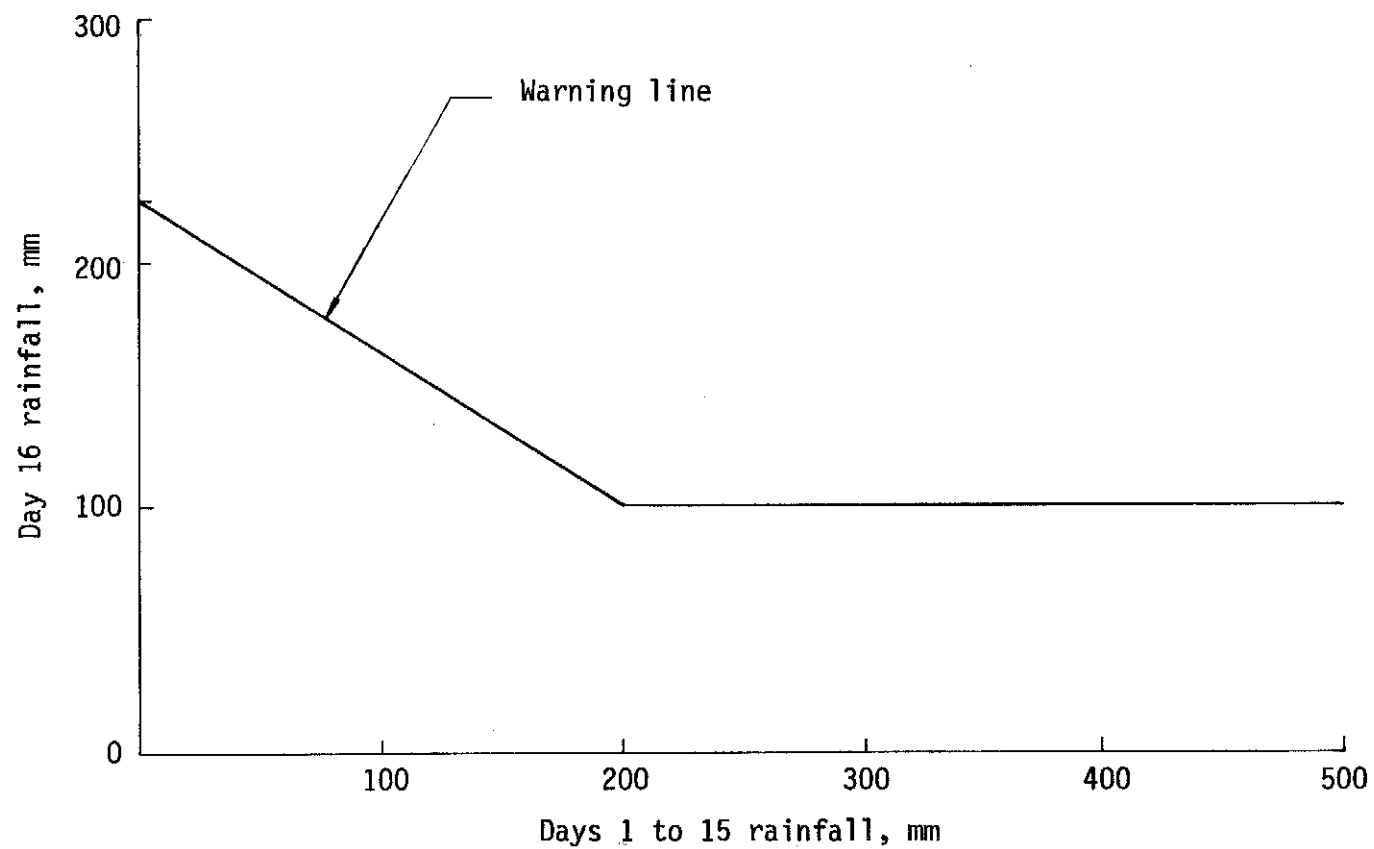


Figure 5.5 - Water table response in selected soils as predicted by equation 5.6. Soil depth 20 m



Legend : (1) Day 1-15 rainfall is that measured at the Royal Observatory.
(2) Day 16 rainfall is that recorded over the past 20 hours plus that forecast for the next 4 hours.

Figure 5.6 - Current procedure (1983) for the issue of a landslip warning

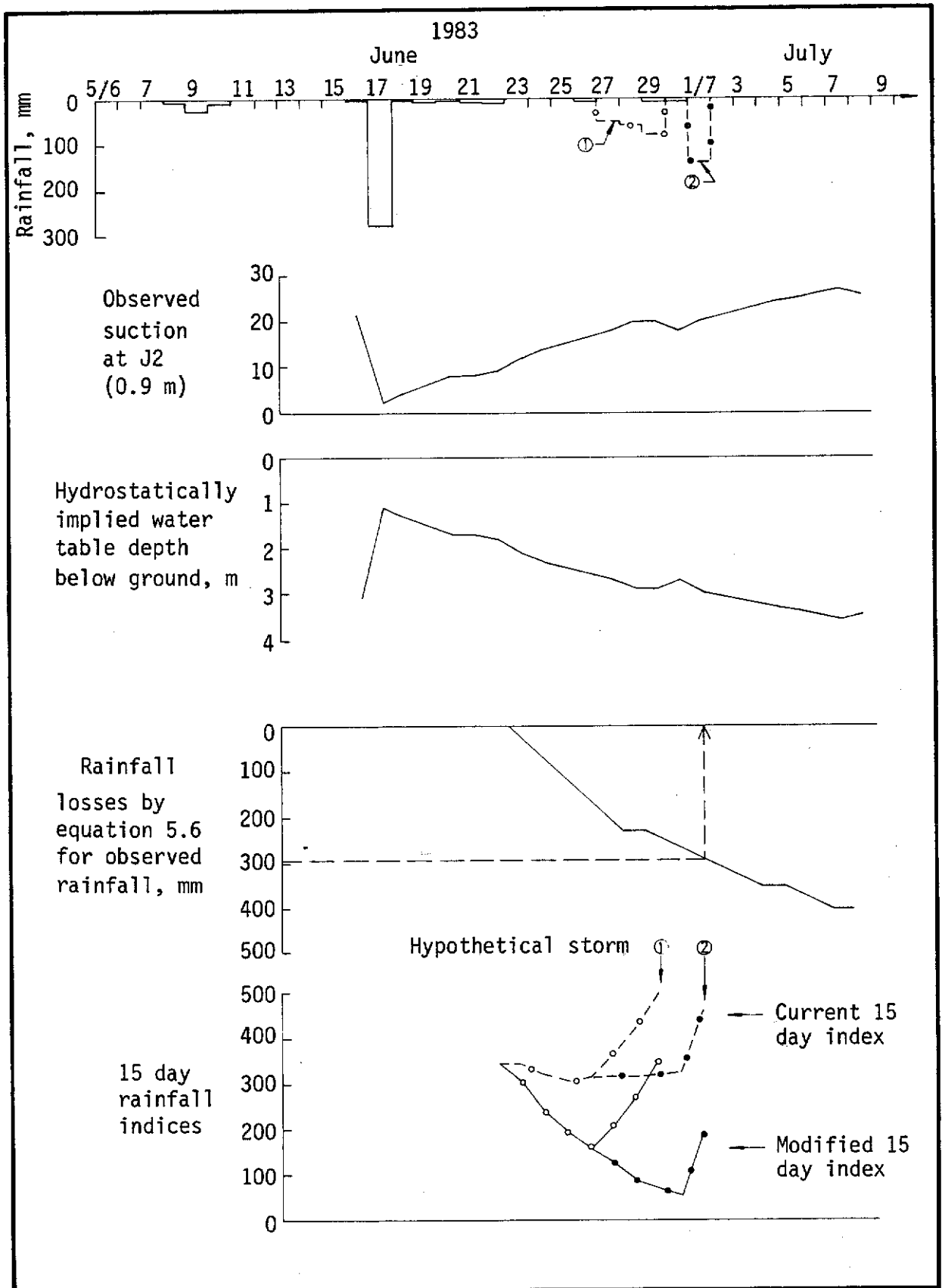


Figure 5.7 - Illustration of a suggested method for improving the current (1983) landslip warning procedure

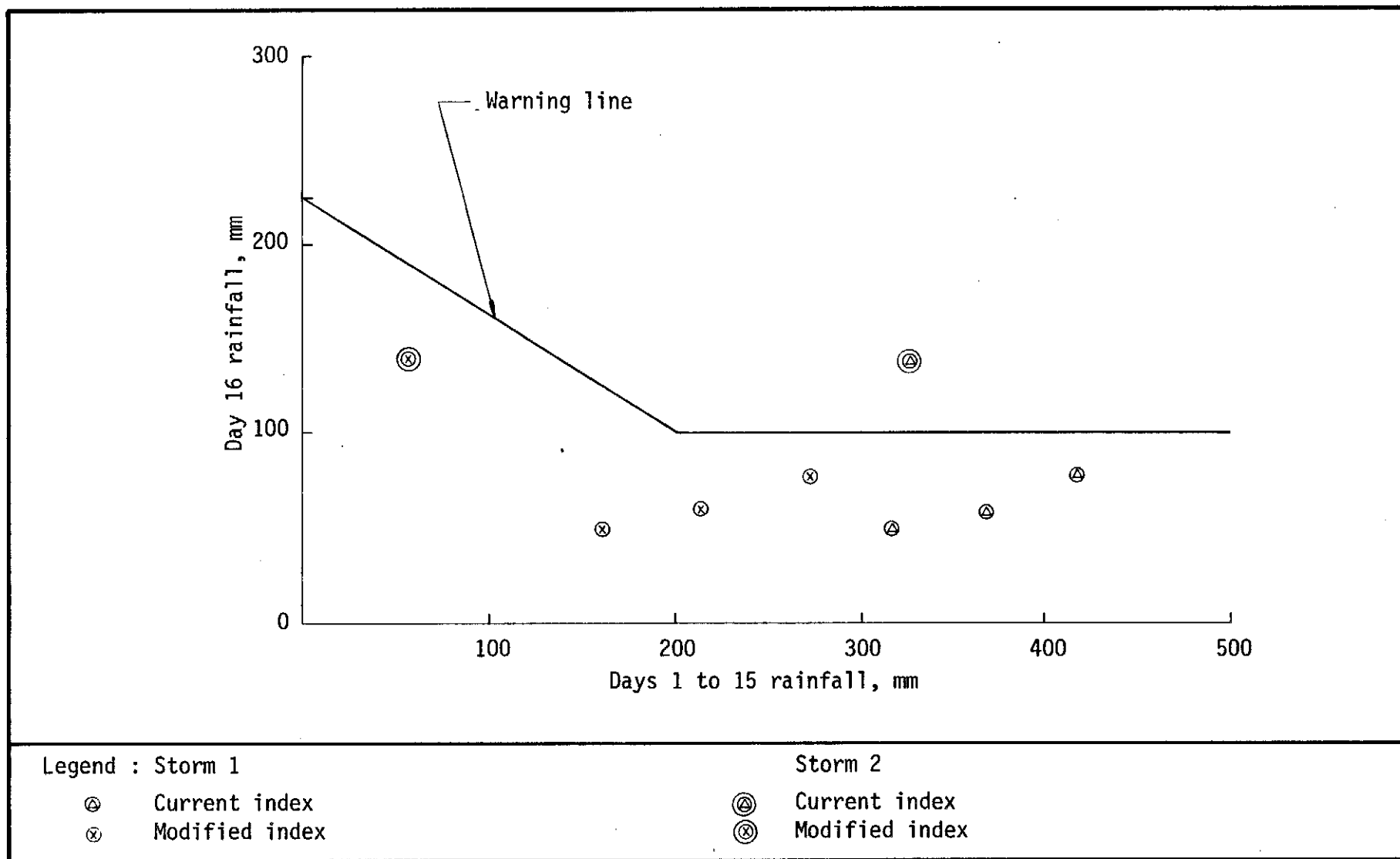


Figure 5.8 - Plots of the two hypothetical storms in figure 5.7 on the current (1983) landslip warning relationship

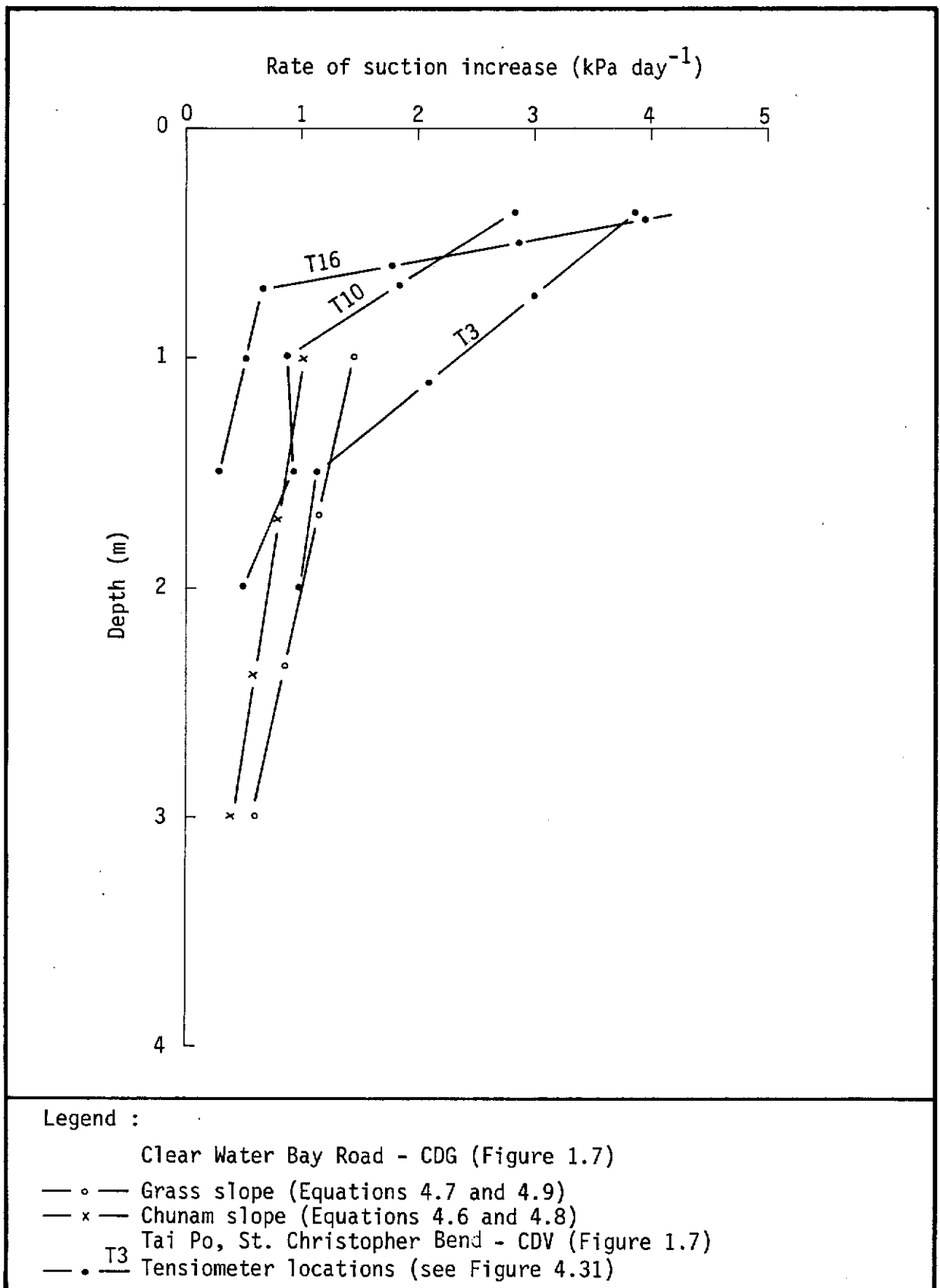


Figure 5.9 - Examples of post storm suction recovery

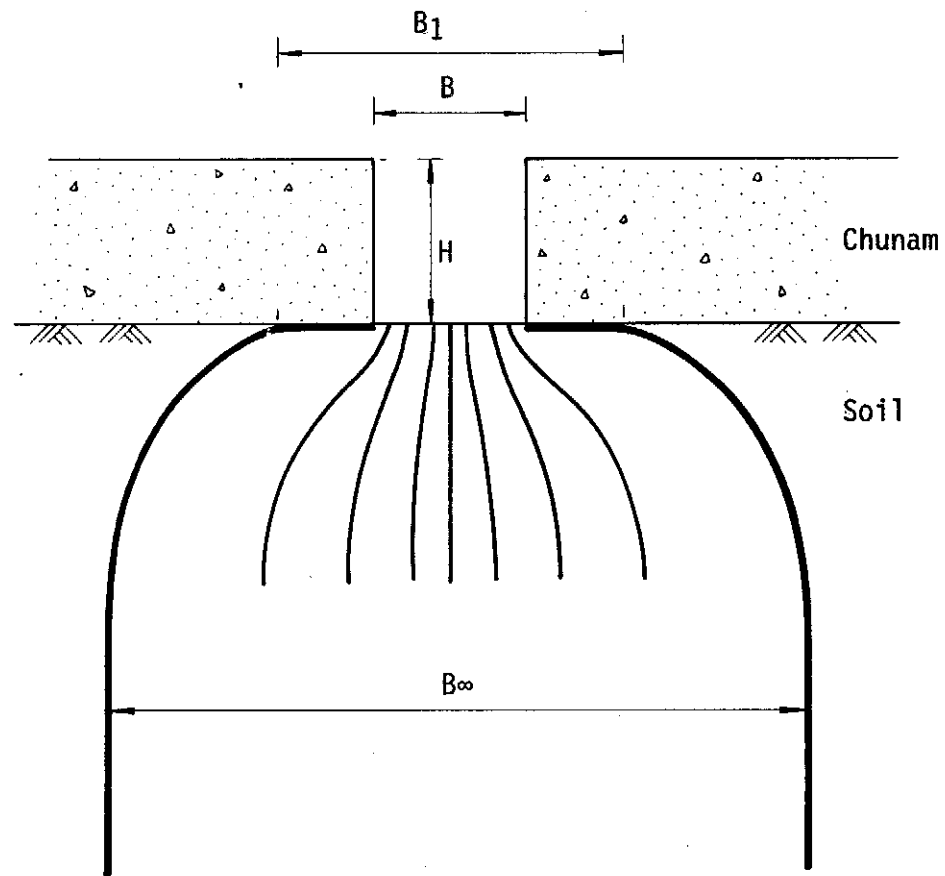
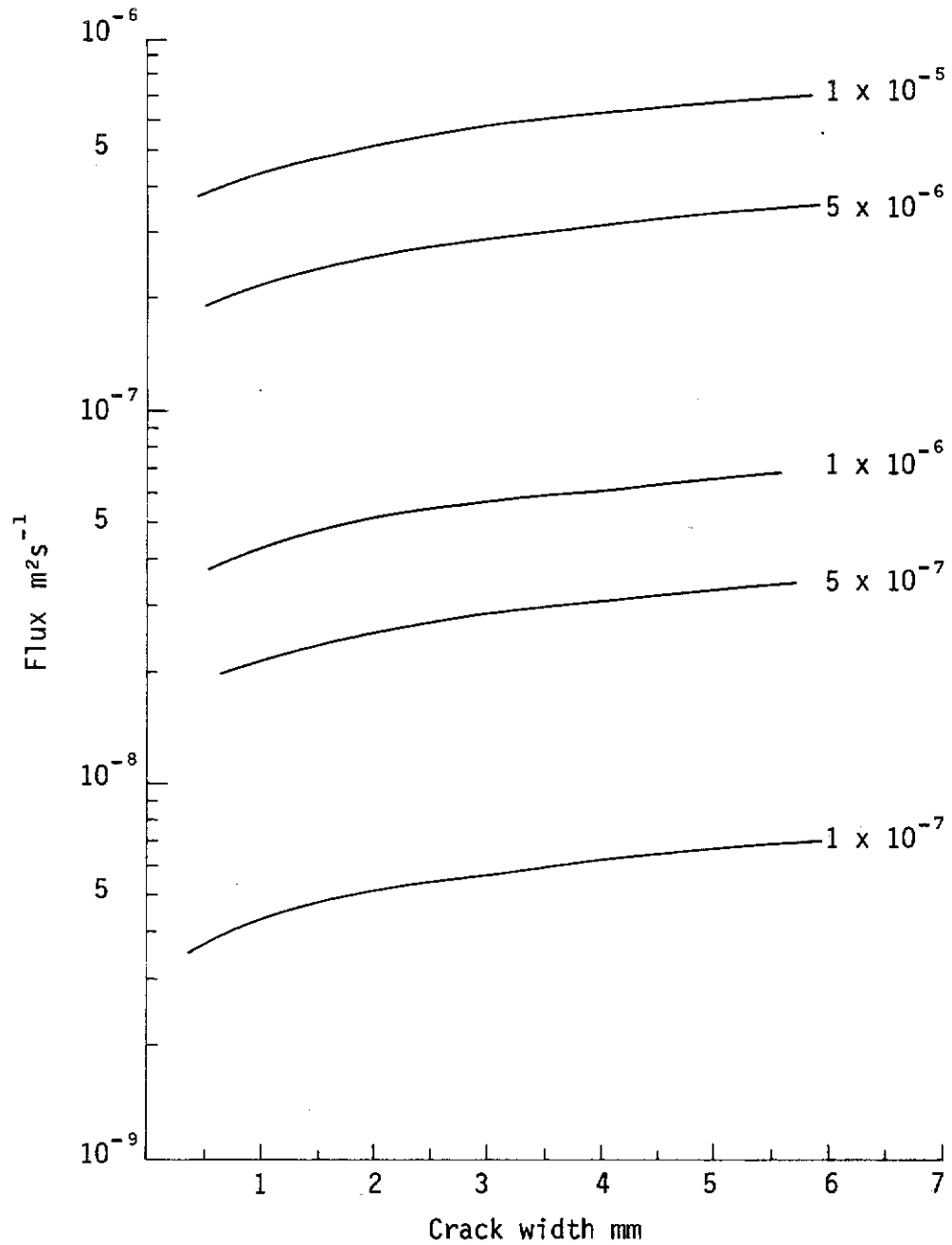
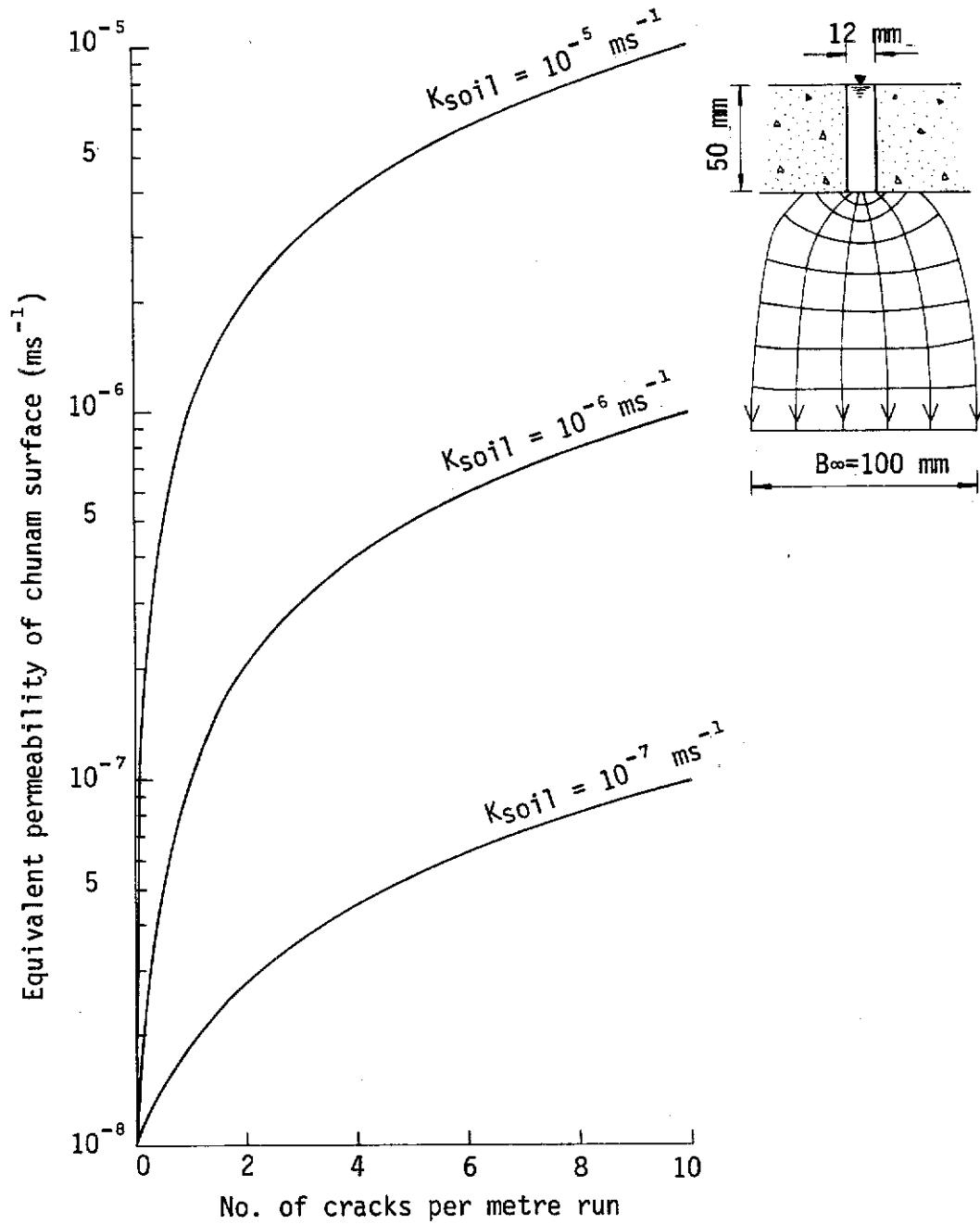


Figure 5.10 - Definition diagram for crack model - see equations 5.7 - 5.9



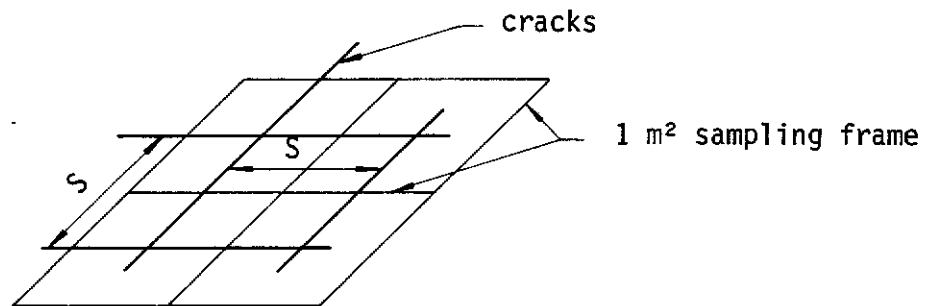
Note : (1) Water head, $H = 50$ mm
(2) 1×10^{-5} : Soil K_s in ms^{-1}

Figure 5.11 - Seepage predicted by the crack model under the conditions specified

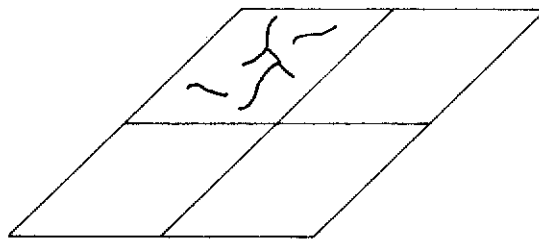


Note : Permeability of intact chunam
 $= 10^{-8} \text{ ms}^{-1}$

Figure 5.12 - Effective permeability of chunam predicted by the crack model



Total crack length per $m^2 = \frac{2}{S}$
 where : S = crack spacing, m
 $K_e = K_i + \sum_{i=1}^j q_i \frac{2}{S_i}$



$$K_e = K_i + \sum_{i=1}^j q_i L_i$$

Where : L_i = field measured crack length per m^2 for crack width, i .

Note : (1) i = crack widths.

Figure 5.13 - Alternative approaches to the estimation of K_e in terms of regular and irregular crack spacing

		CHUNAM CONDITION (1)		
CHUNAM K_i (2)	SOIL K	BAD	POOR	AVERAGE
1×10^{-8}	1×10^{-6}			
	1×10^{-5}			
	1×10^{-4}			

CHUNAM EFFECTIVE PERMEABILITY	PREDICTED EFFECTIVE CHUNAM PROTECTION		$\Delta i-e$ (3)
$< 1 \times 10^{-6}$		Very good	< 0.5
		Good	$> 0.5 \quad < 2.0$
$> 1 \times 10^{-6}$		Poor	$> 2.0 \quad < 2.5$
		Ineffective	> 2.5

Notes : (1) As assessed by 'CHASE' report
 (2) Permeability of intact chunam $K_i \text{ ms}^{-1}$
 (3) Order of magnitude difference between intact and effective chunam permeability

Figure 5.14 - Predicted effective chunam protection

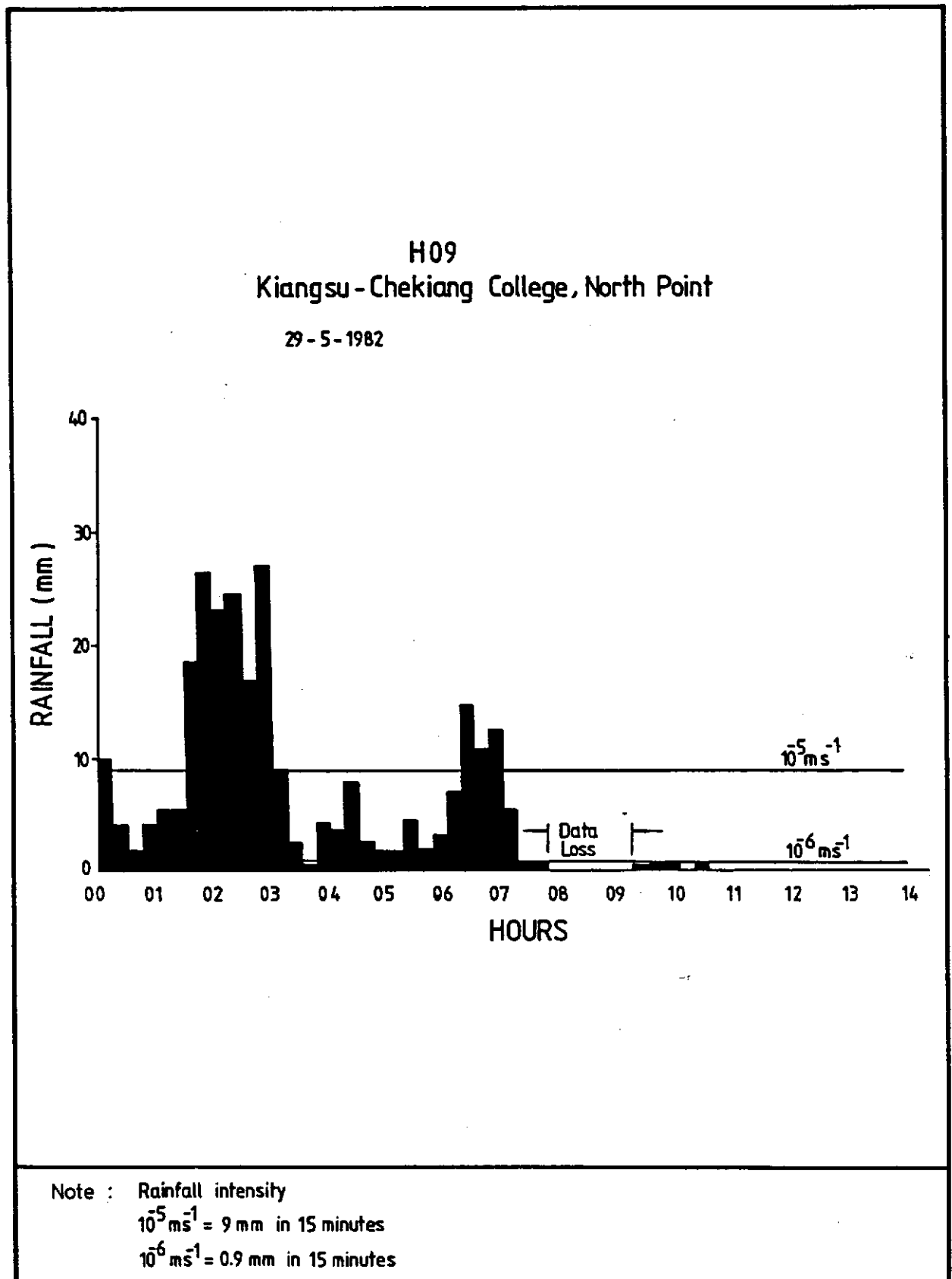
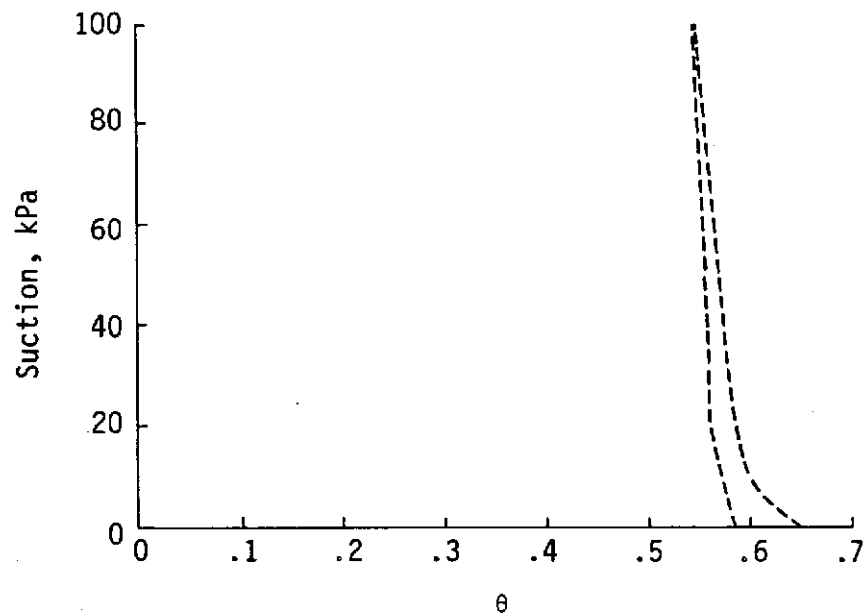
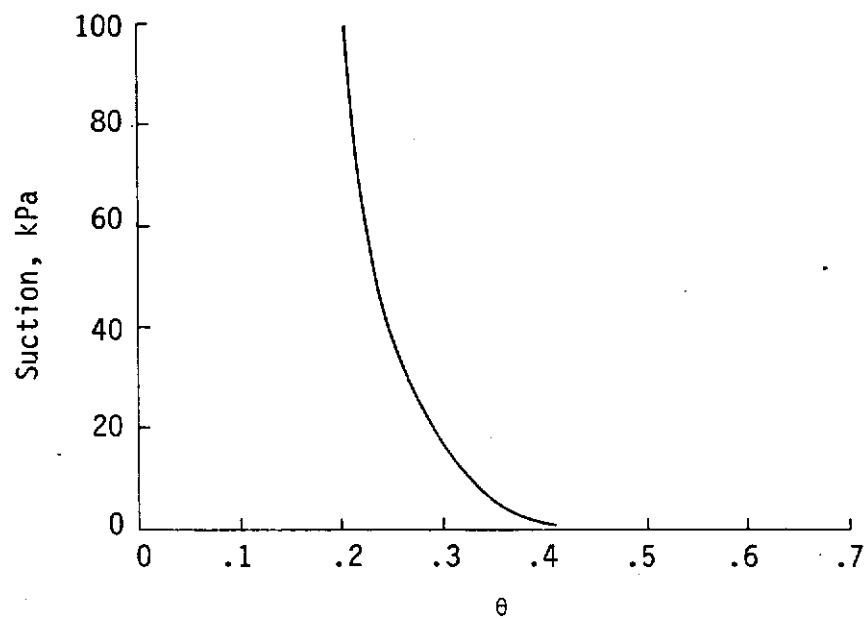


Figure 5.15 - Illustration of rainfall intensities in relation to permeability values

(a) Tai Po Volcanic



(b) Colluvium



Legend :

----- 0 kPa \rightarrow 100 \rightarrow 0 kPa (Drying - Wetting)

Note : Colluvium suction - moisture curve obtained by PSD method

Figure 6.1 - Suction moisture curves used in soil water simulations at locations 1 - 3

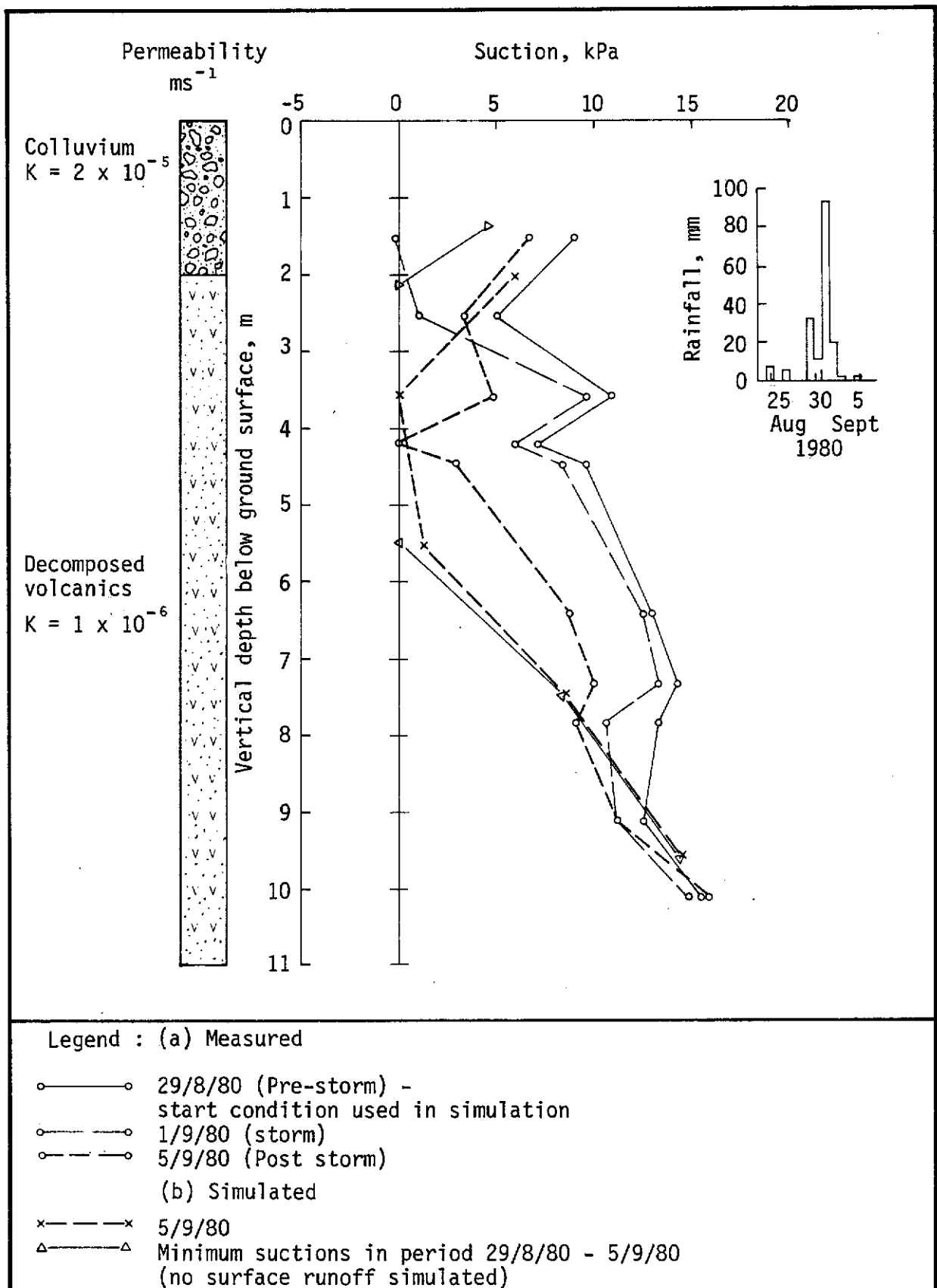
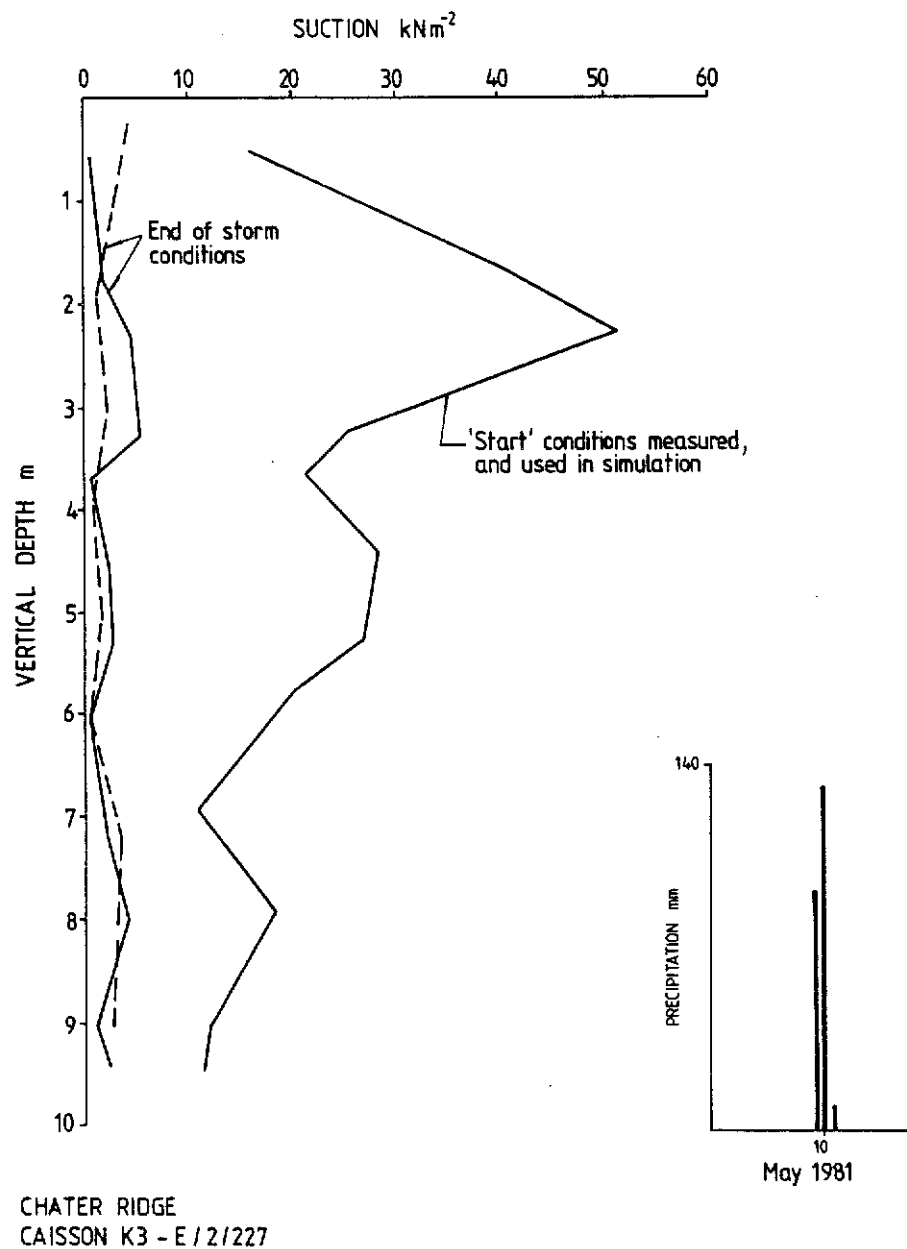


Figure 6.2 - Simulation of soil water conditions at Realty Ridge



Legend :

- Measured
- - - Simulated

Figure 6.3 - Simulation of soil water conditions at Chater Ridge using 1 dimensional soil water model (section 3.0)

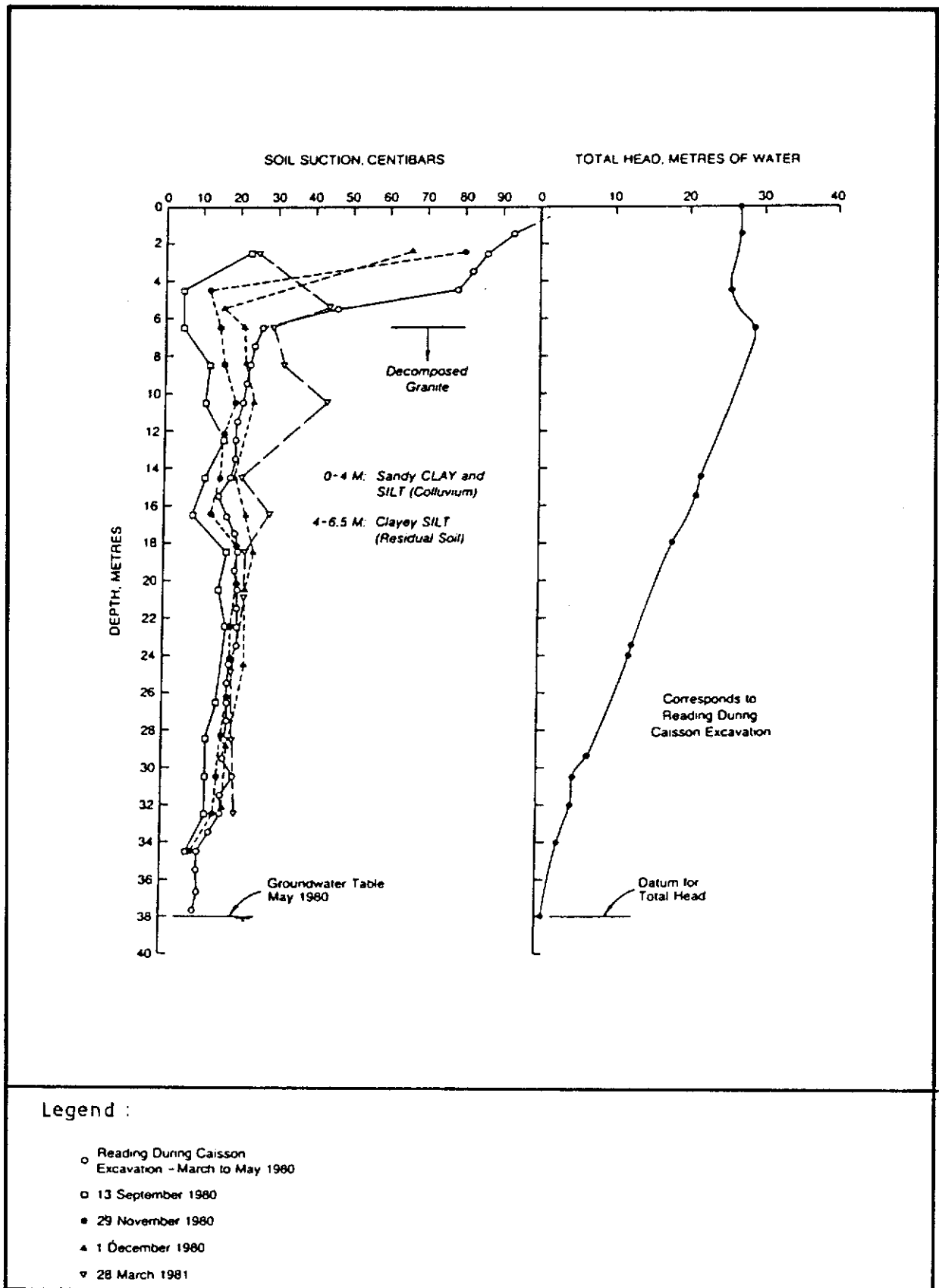


Figure 6.4 - Suctions reported by Sweeney (1982) for a site in Mid-levels

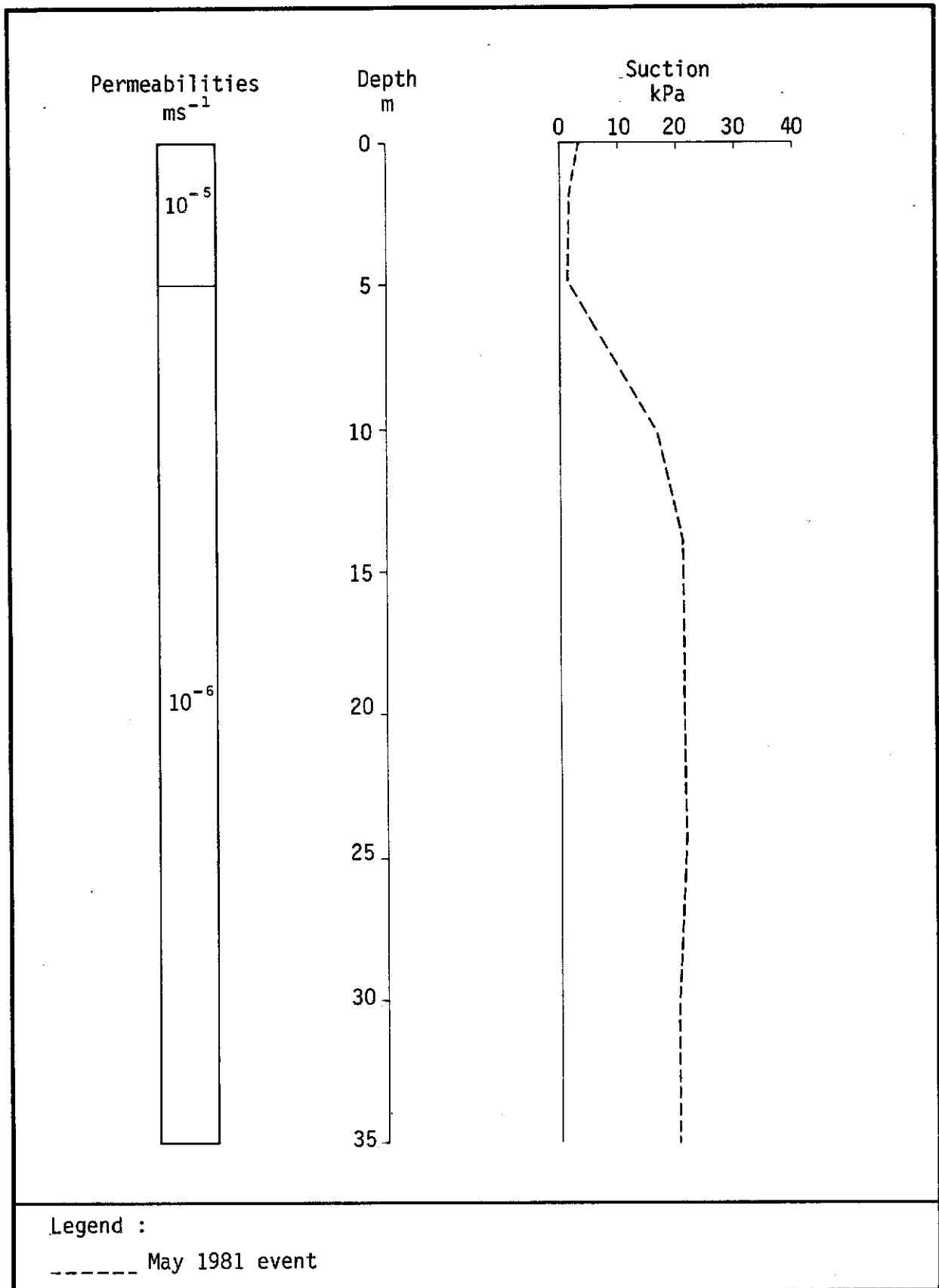


Figure 6.5 - Simulation of soil water conditions based upon the site reported by Sweeney (1980)

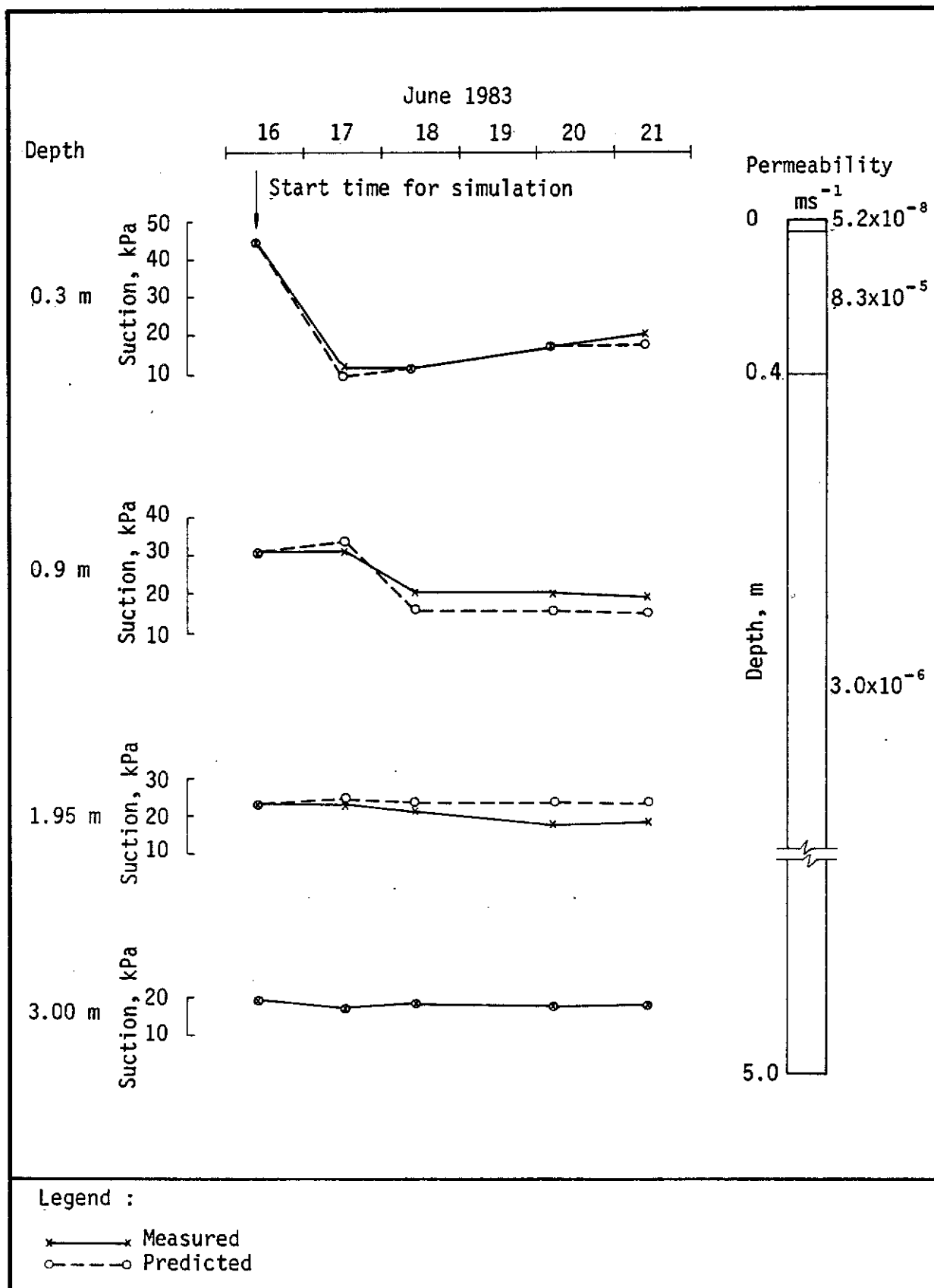


Figure 6.6 - Simulation of soil suctions at Clear Water Bay site, chunam slope, location C (see Figures 4.6 and 4.14)

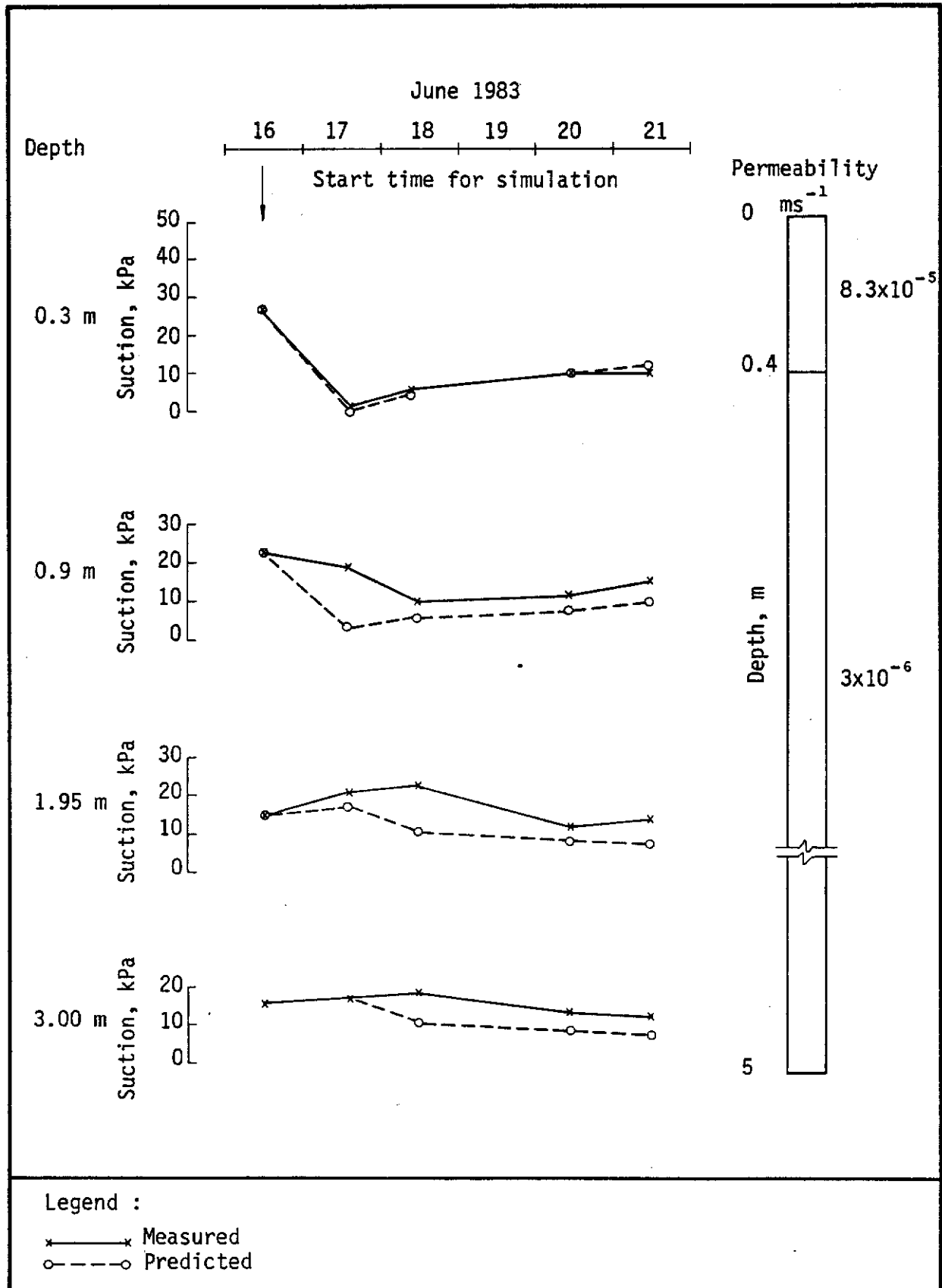


Figure 6.7 - Simulation of soil suctions and Clear Water Bay site, grass slope, location I (see Figure 4.7 and 4.15)

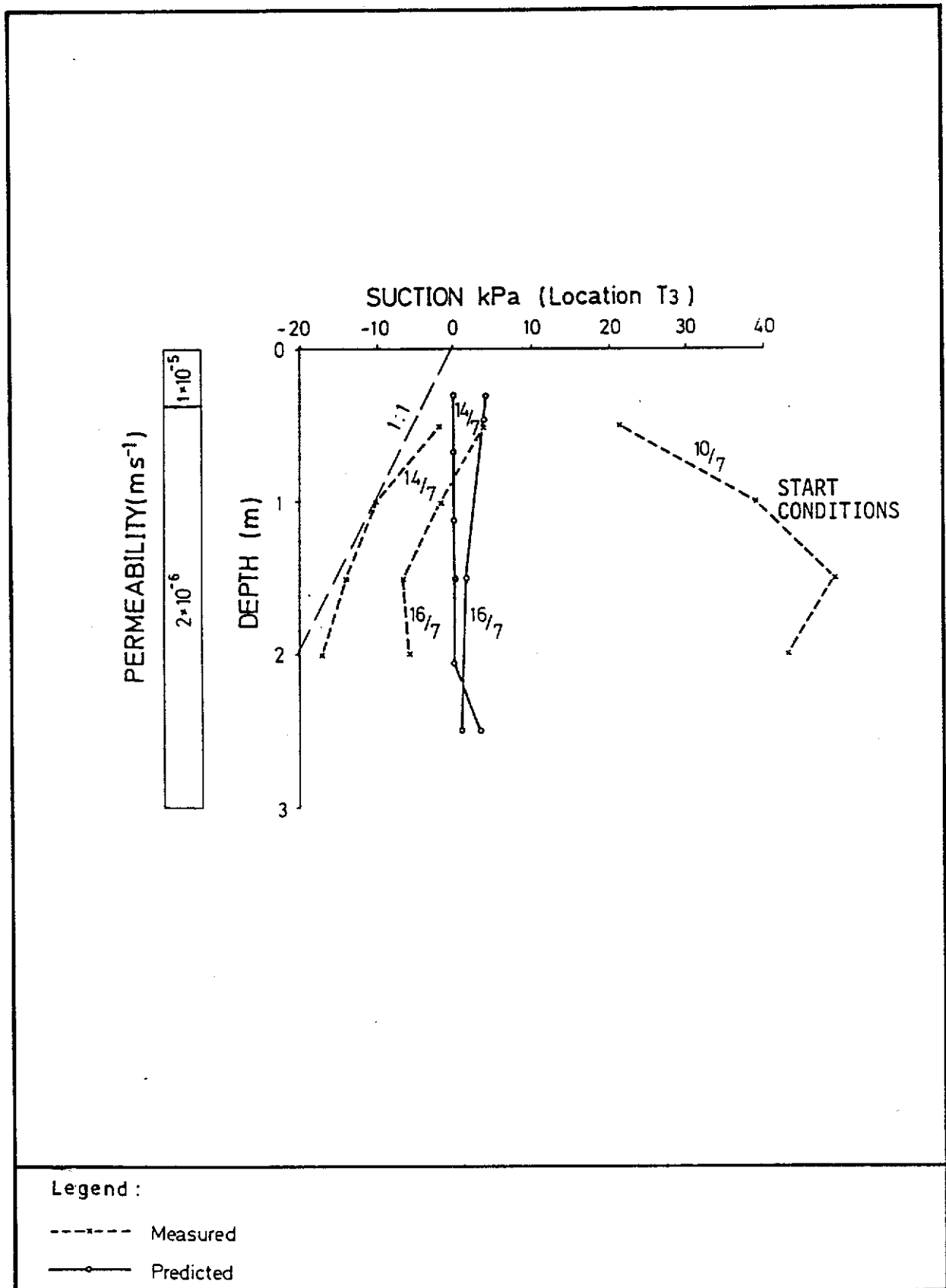


Figure 6.8 - Simulation of soil water conditions at Tai Po, St. Christopher Bend site (see Figure 4.31)

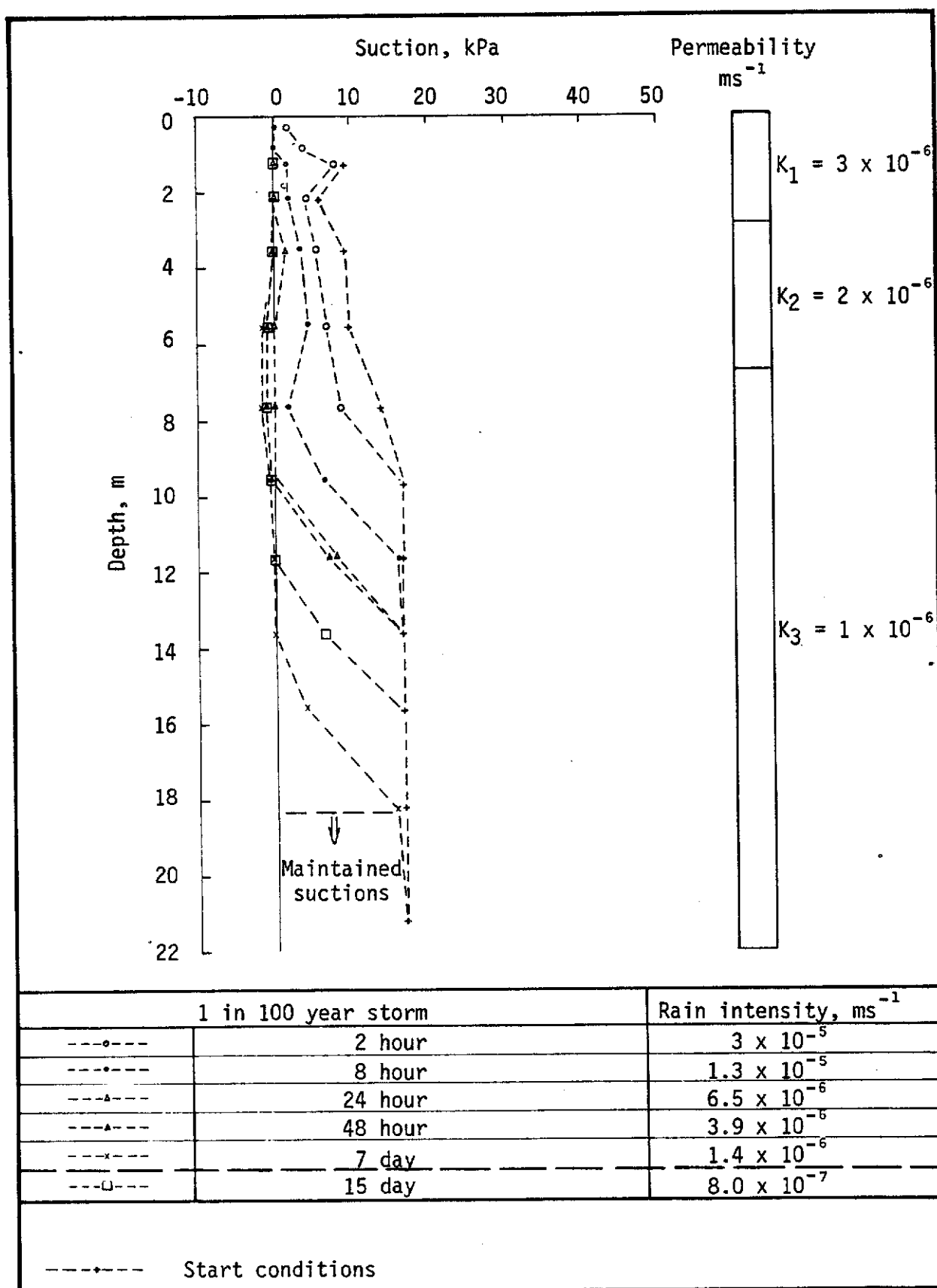


Figure 6.9 - Simulation of soil water conditions resulting from even intensity rainstorms as shown

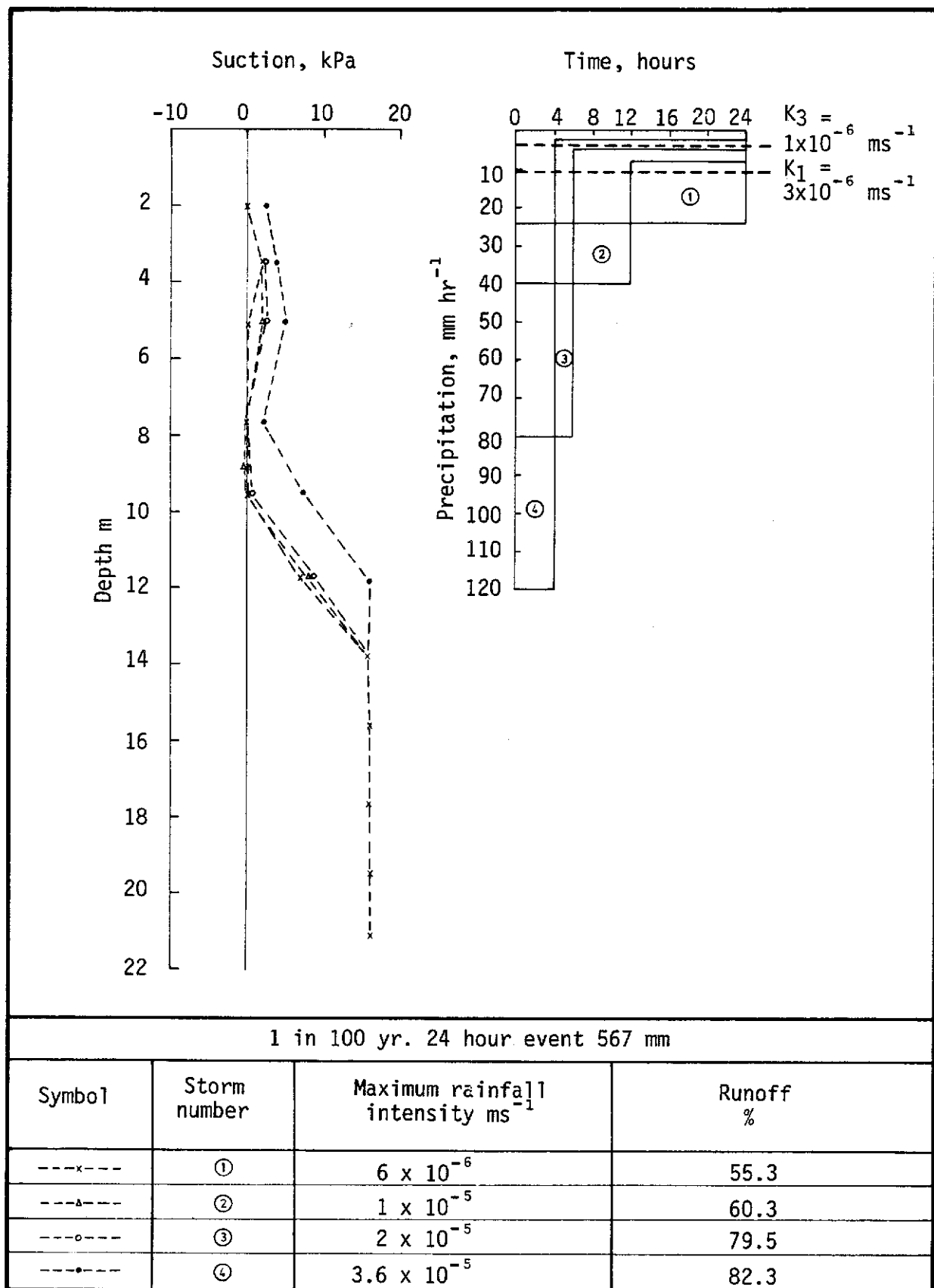


Figure 6.10 - Sensitivity of resulting soil suctions to changes in rainfall distribution within a 24 hour storm (see Figure 6.9)

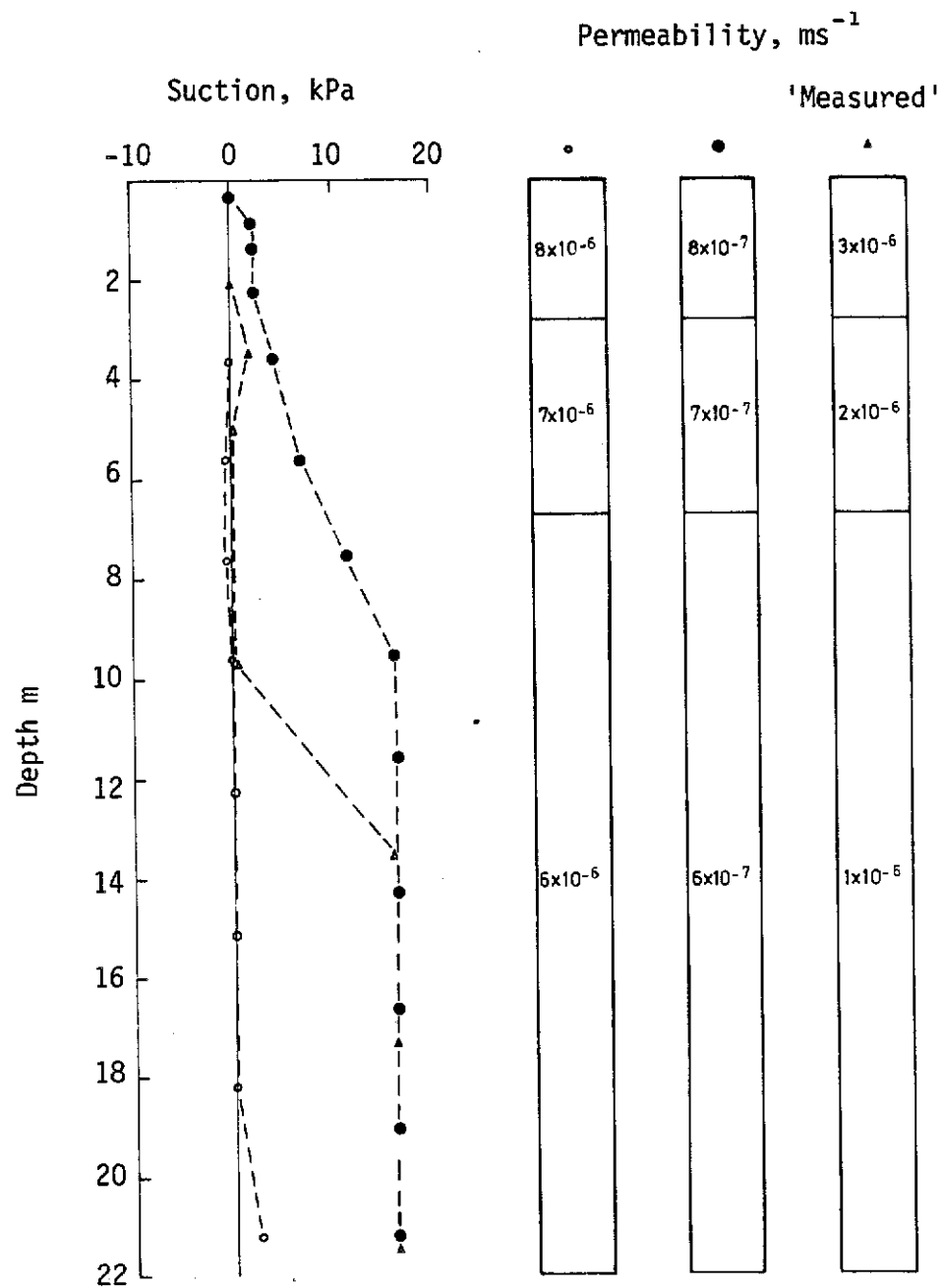


Figure 6.11 - Sensitivity of resulting minimum suctions to permeability changes with regard to the 24 hour storm shown in Figure 6.9

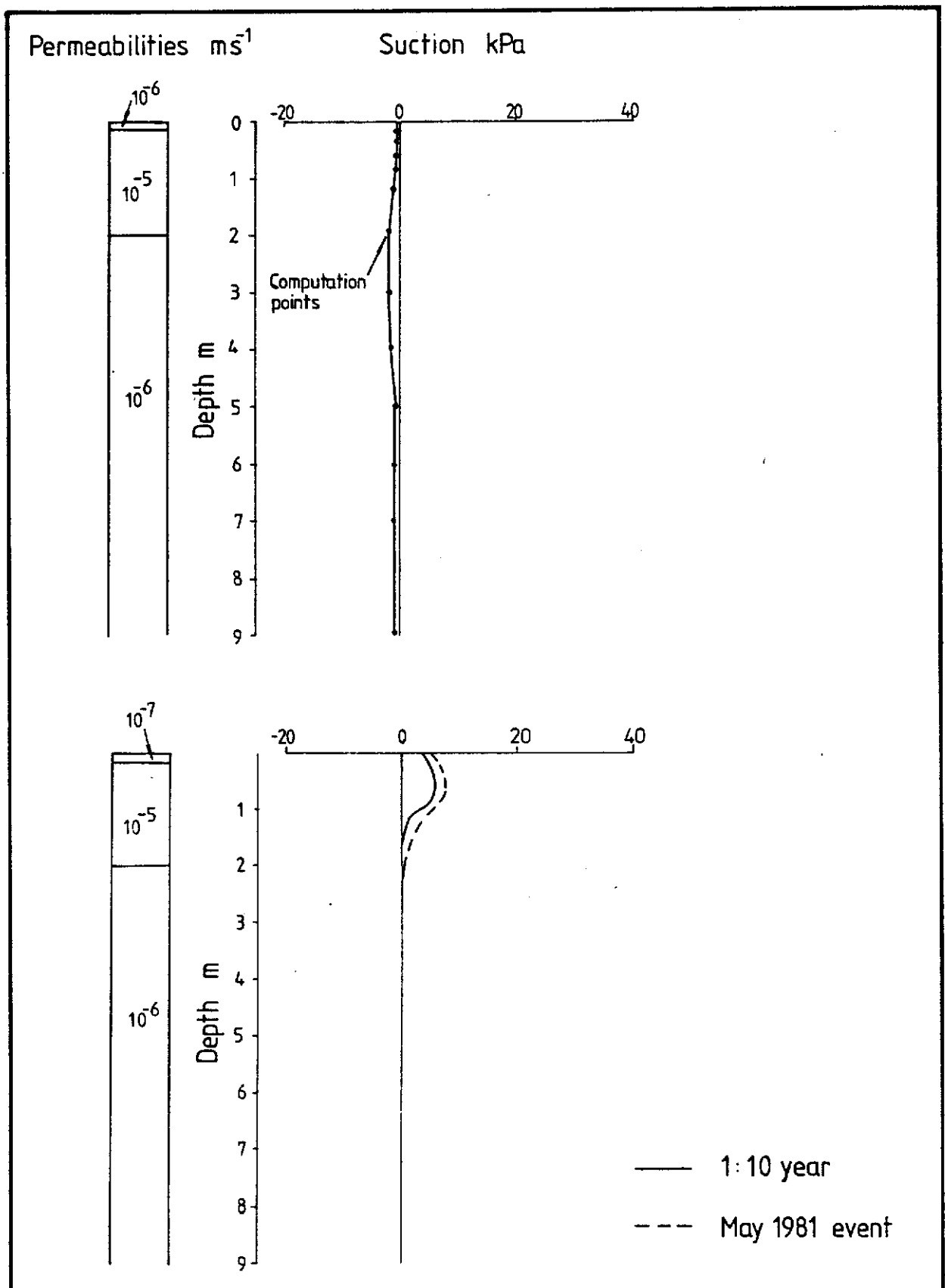


Figure 6.12 - Simulation of soil water conditions with chunam cover. Lowest suctions shown

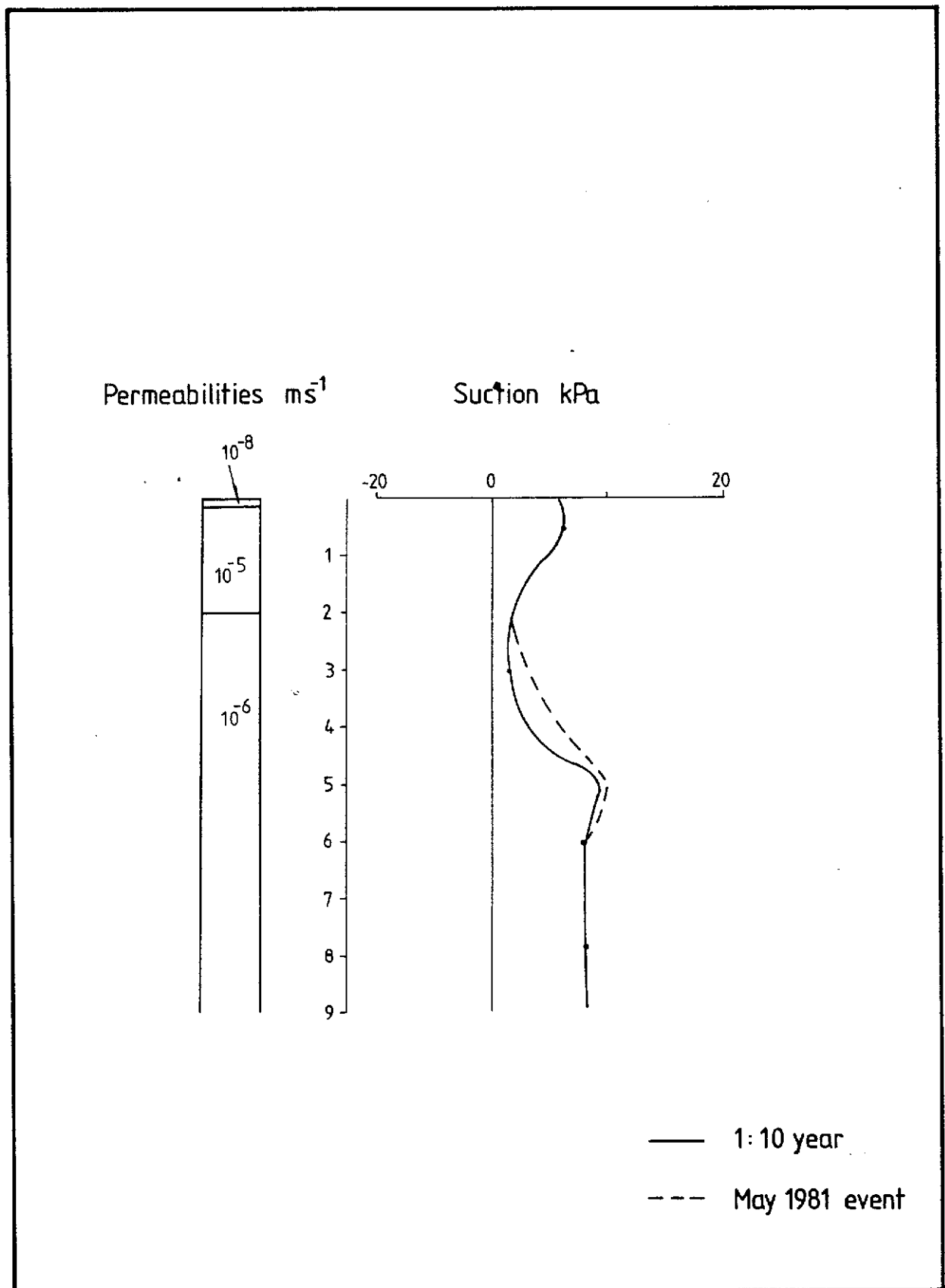
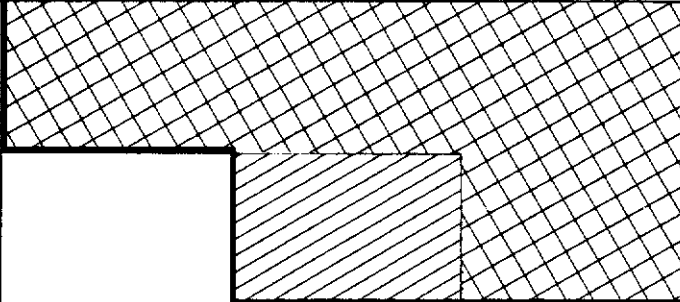


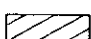


Figure 6.13 - Simulation of soil water conditions with chunam cover.
Lowest suctions shown

		CHUNAM CONDITION		
CHUNAM K_i	SOIL K	BAD	POOR	AVERAGE
1×10^{-8}	1×10^{-6}			
	1×10^{-5}			
	1×10^{-4}			

Legend :

-  Conditions likely to ensure maintenance of some degree of soil suction ($K_e < 10^{-7} \text{ ms}^{-1}$)
-  Good protection ($K_e < 10^{-6} \text{ ms}^{-1}$)

Note : These assessments based on crack model predictions (Equations 5.7-5.9) to determine K_e , and the subsequent utilisation of K_e in soil water finite difference model (e.g. Figures 6.12 and 6.13)

Figure 6.14 - Predicted effectiveness of chunam using crack model coupled to soil water model

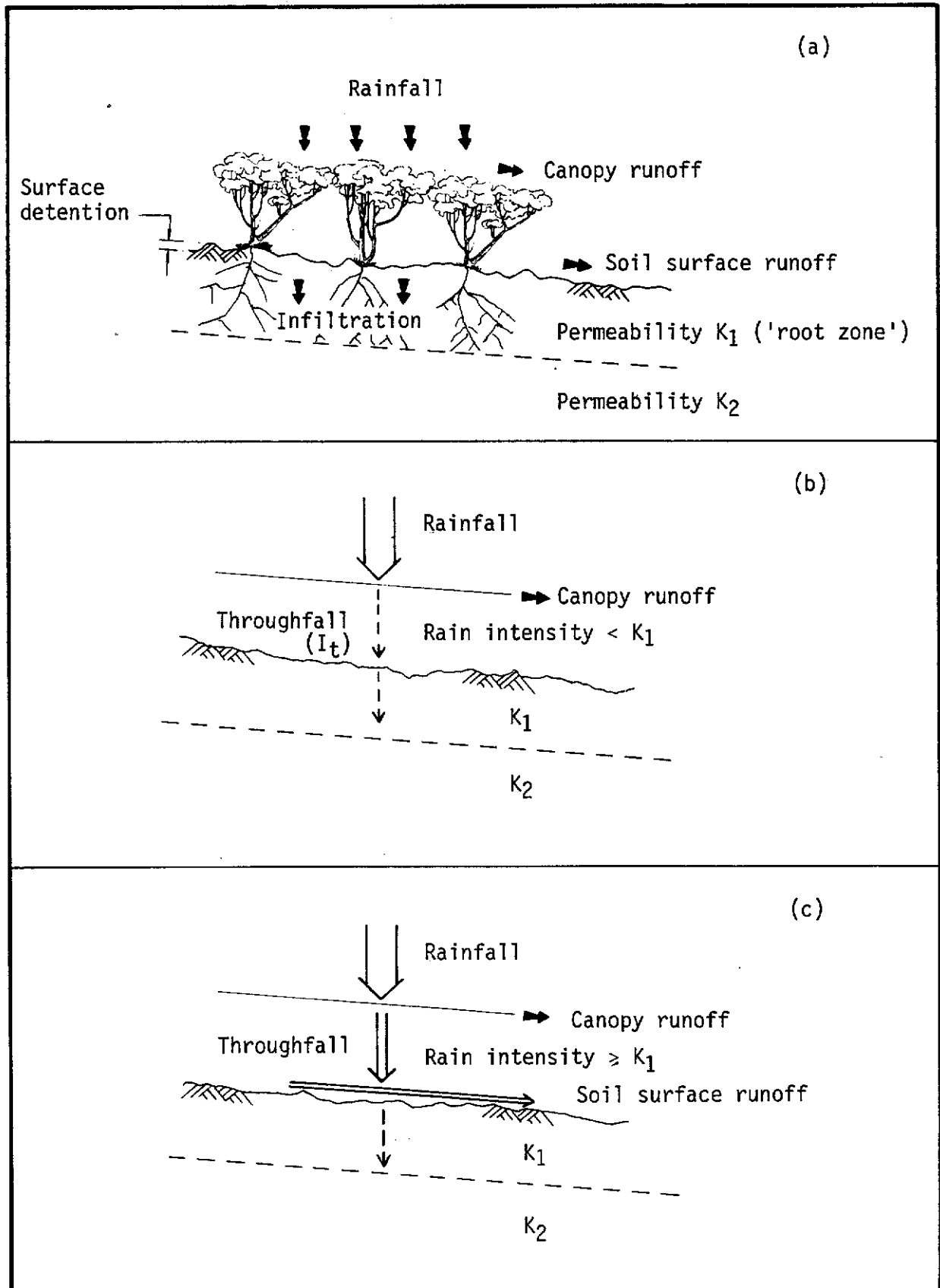
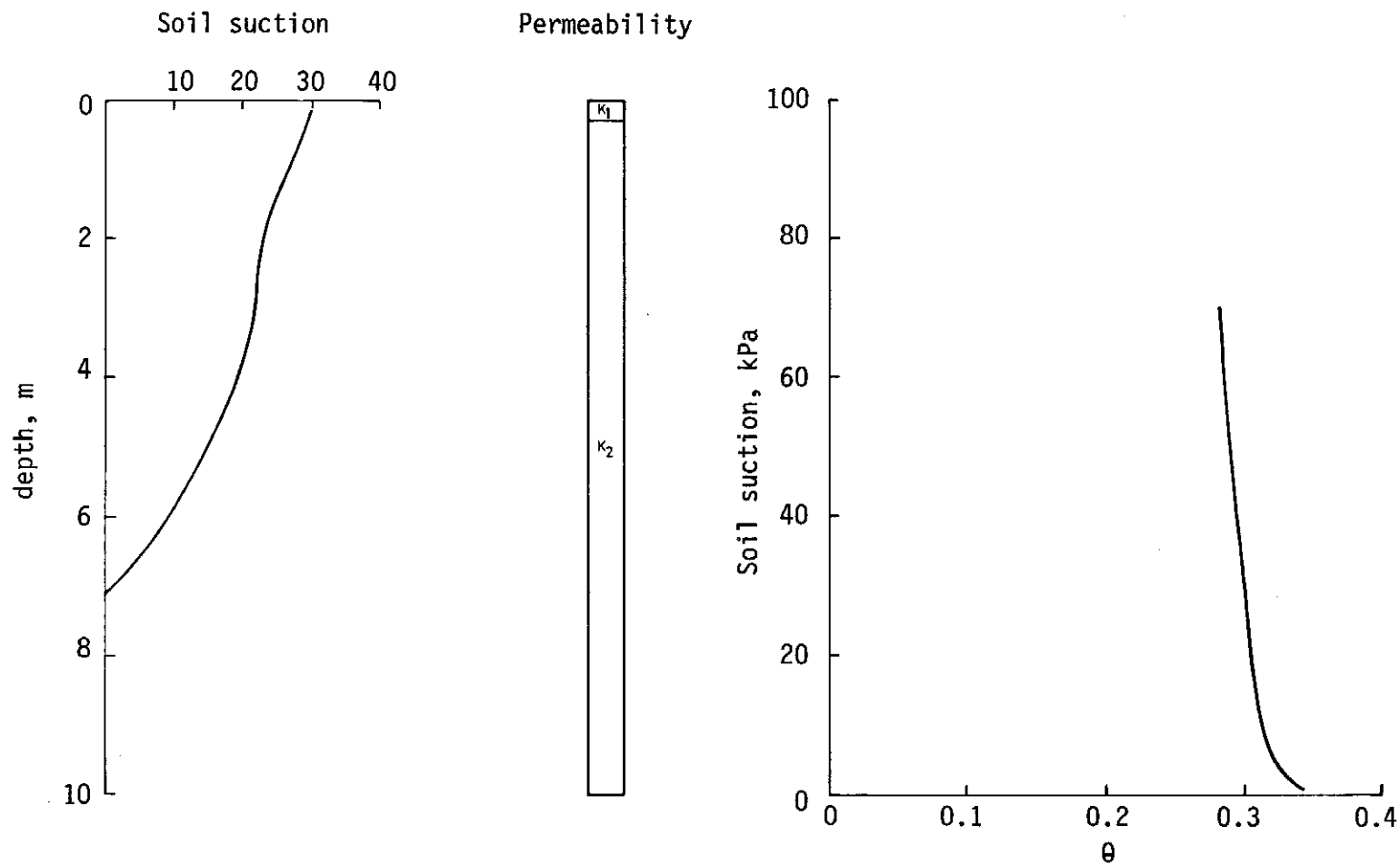


Figure 6.15 - Two simplified conditions of the production of runoff (b and c)



Note : $K_2 = 1 \times 10^{-5} \text{ ms}^{-1}$

Figure 6.16 - Input parameters used in soil water model to illustrate vegetation - runoff relationships (see Figures 6.17 and 6.18)

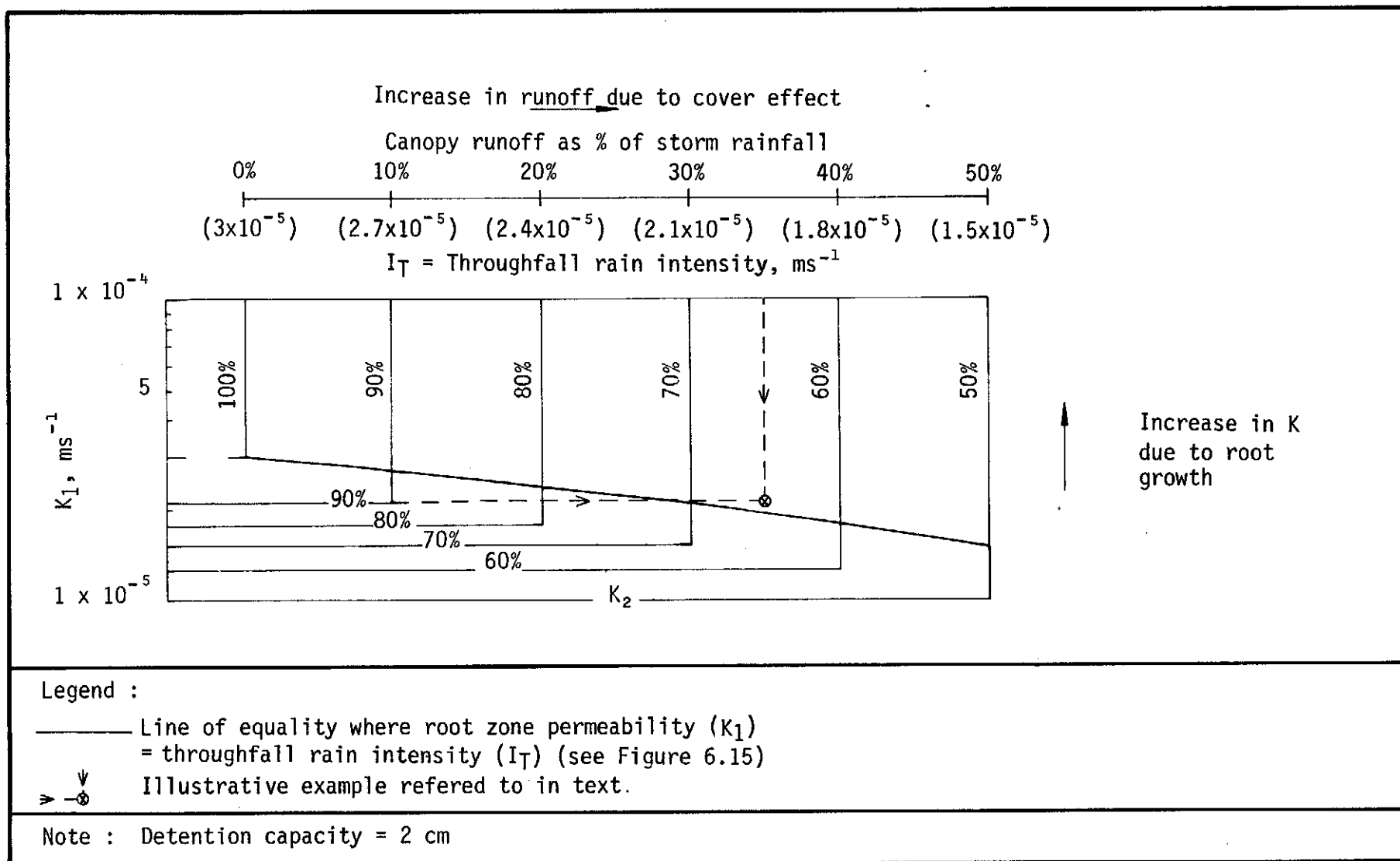


Figure 6.18 - Infiltration, as a percentage of storm rainfall, shown for selected values of K_1

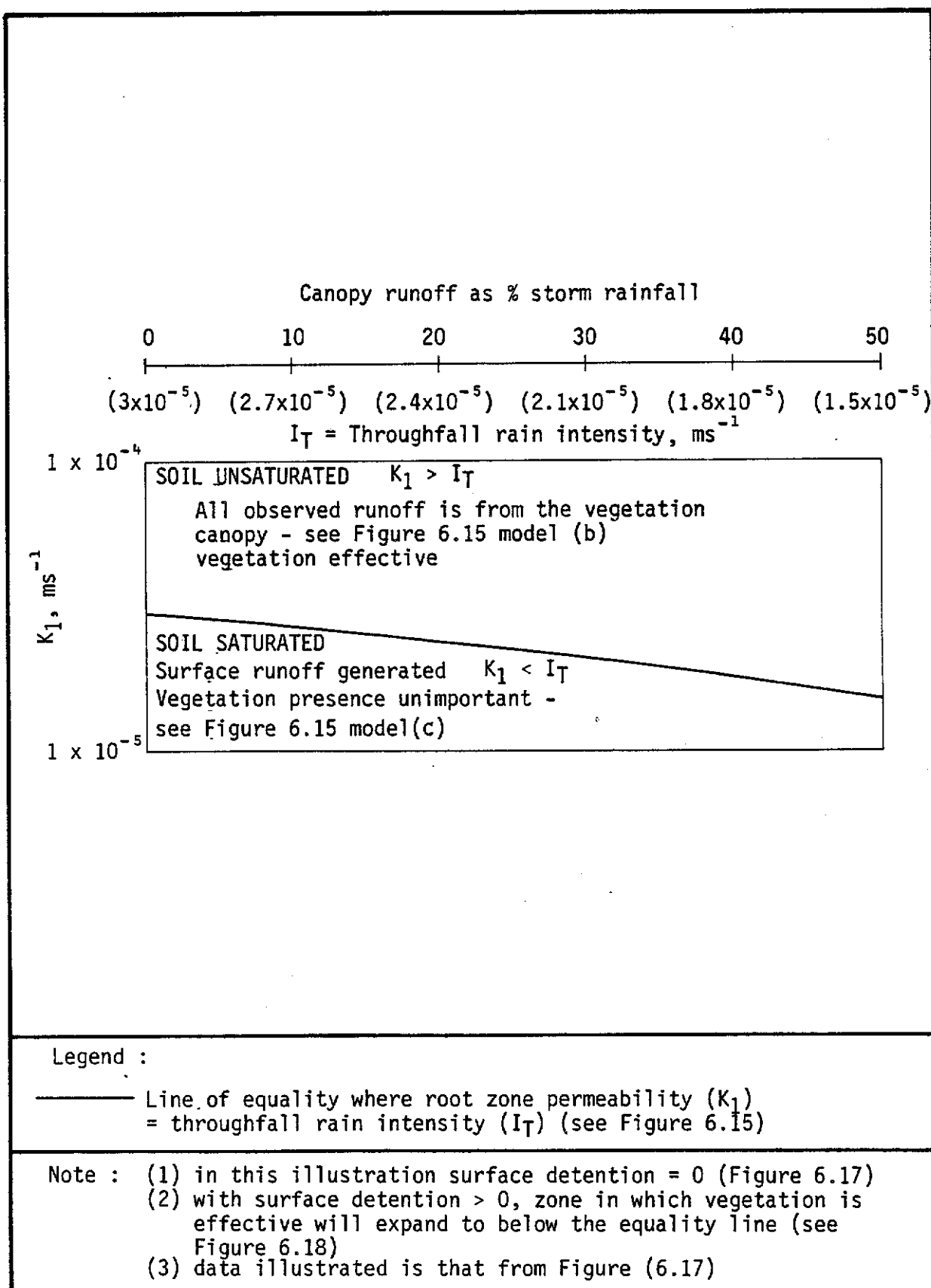


Figure 6.19 - Summary of implications of initial vegetation runoff generation models shown in figure 6.15

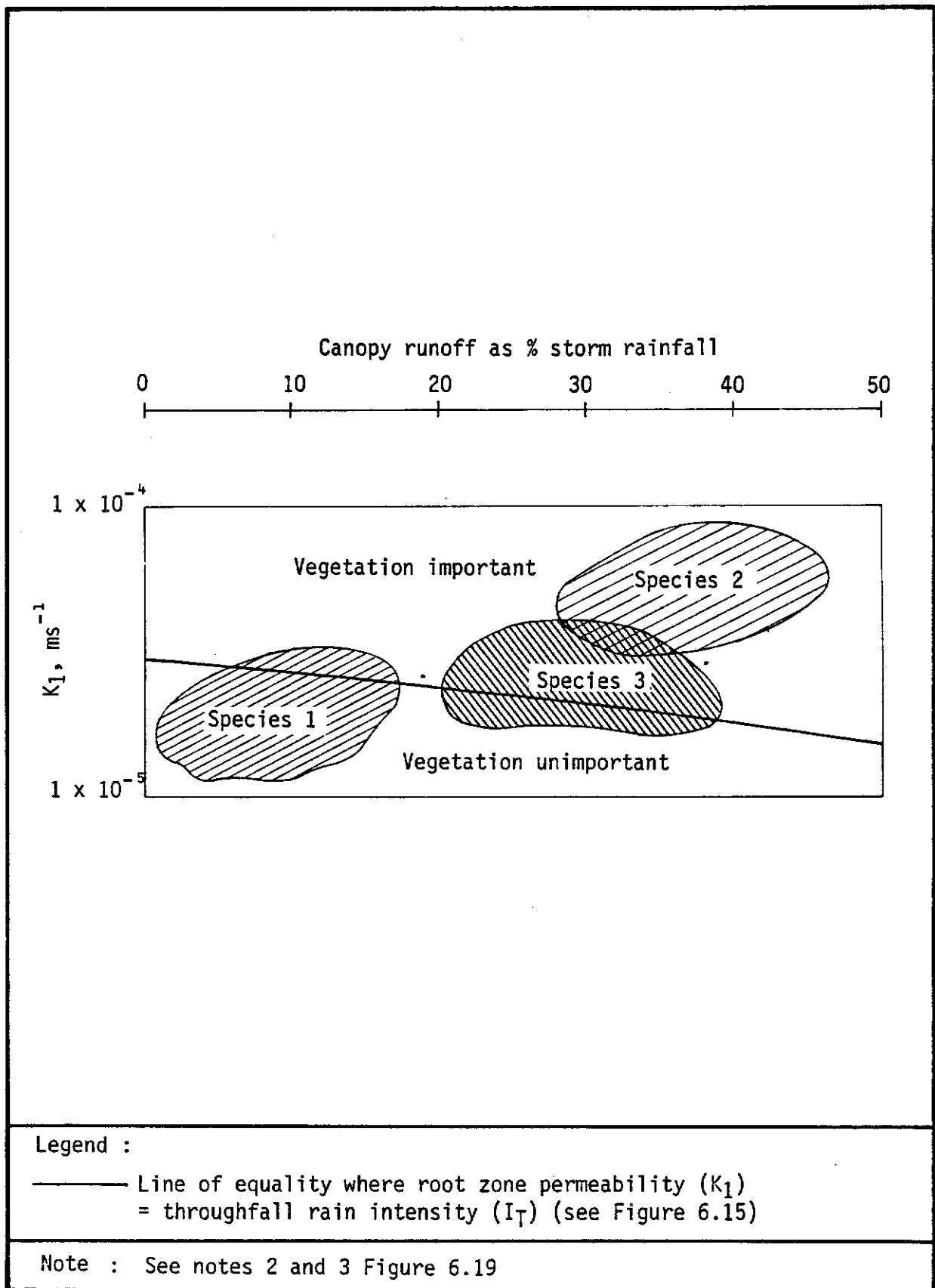


Figure 6.20 - Hypothetical relationships which may emerge from runoff plots and soil water simulations

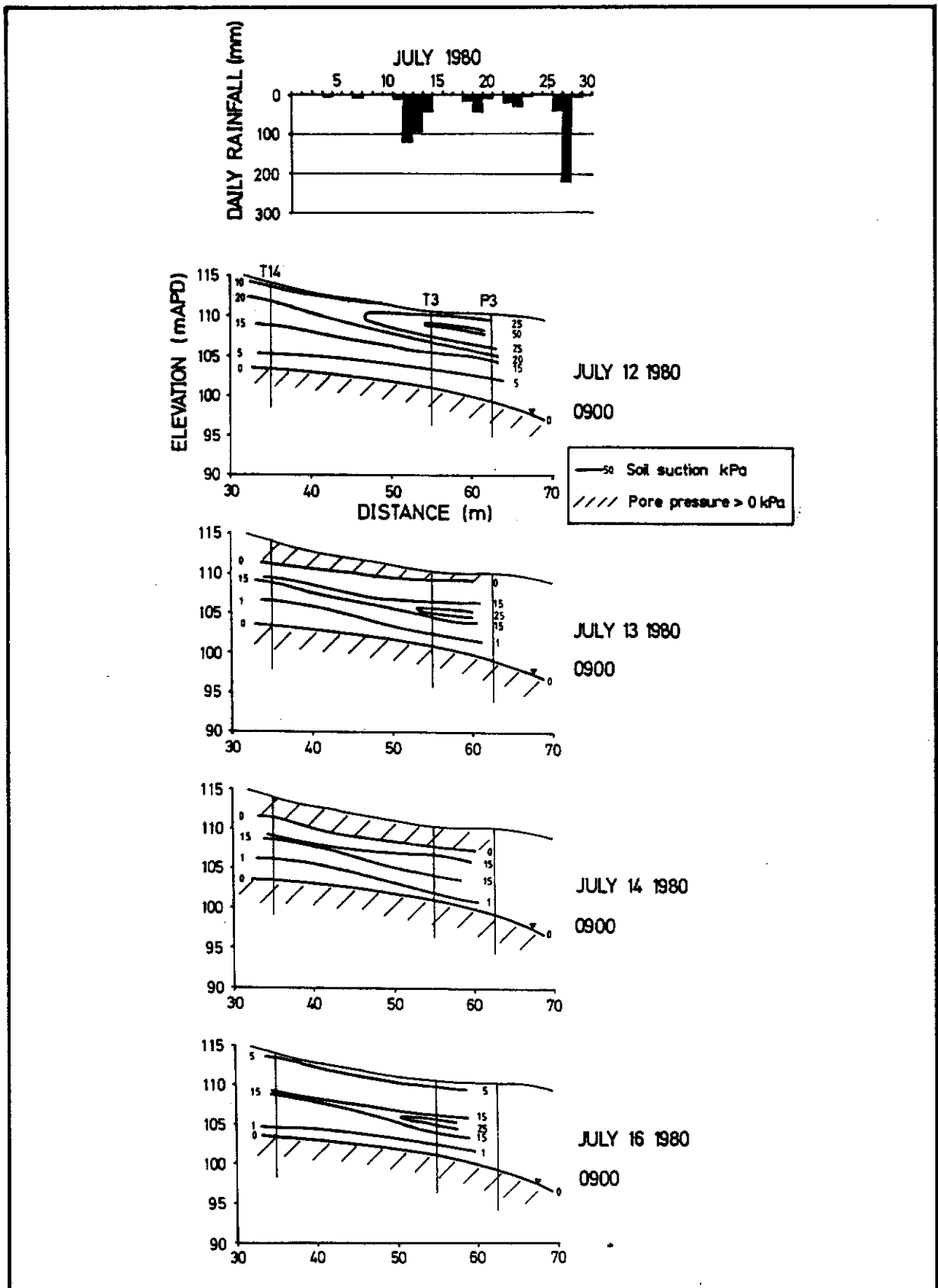


Figure 6.21 - Two dimensional simulation of soil water conditions at Tai Po, St. Christopher Bend site (see Figure 4.31)

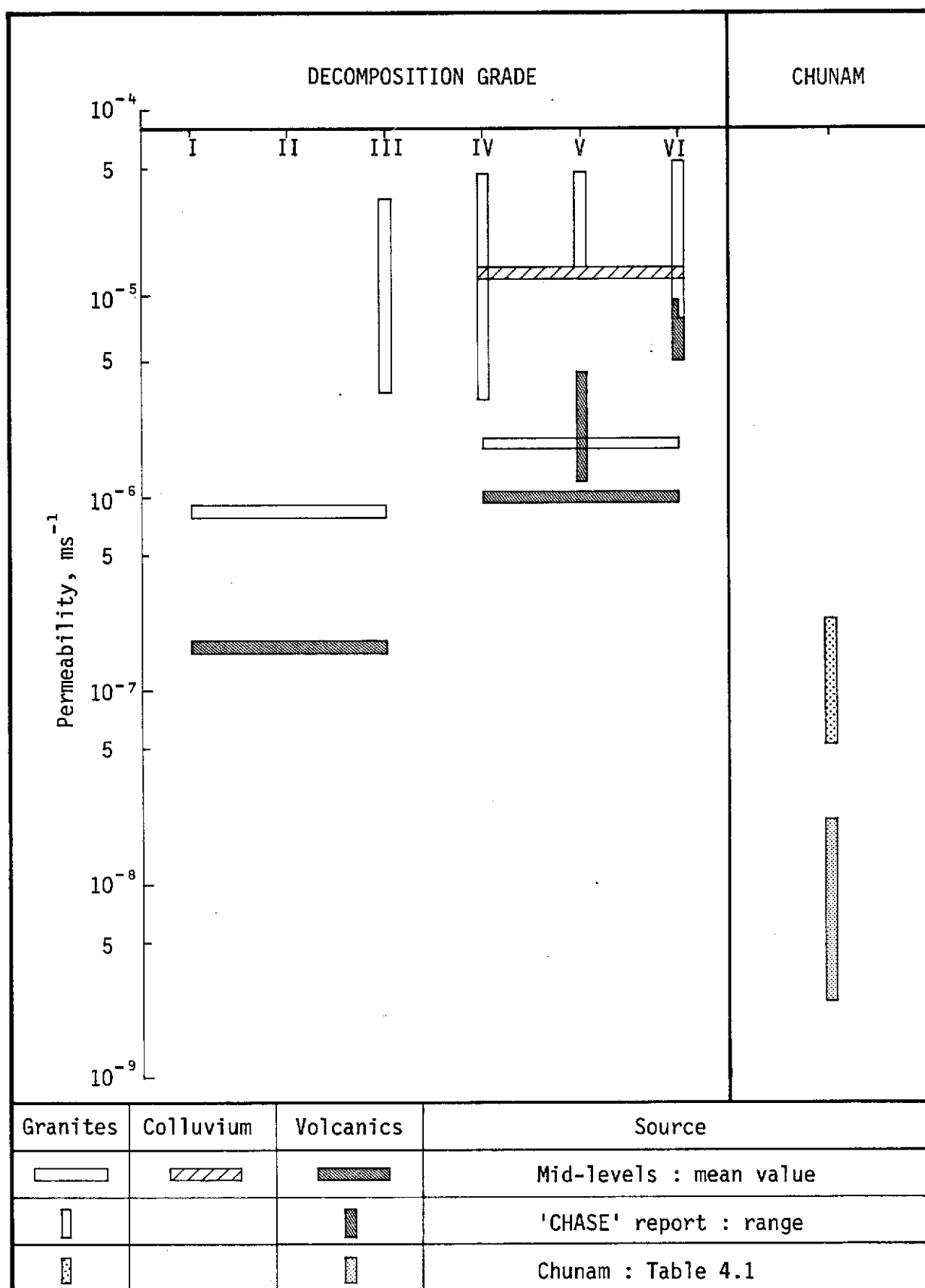


Figure 6.22 - Summary of selected permeability determinations made in Hong Kong

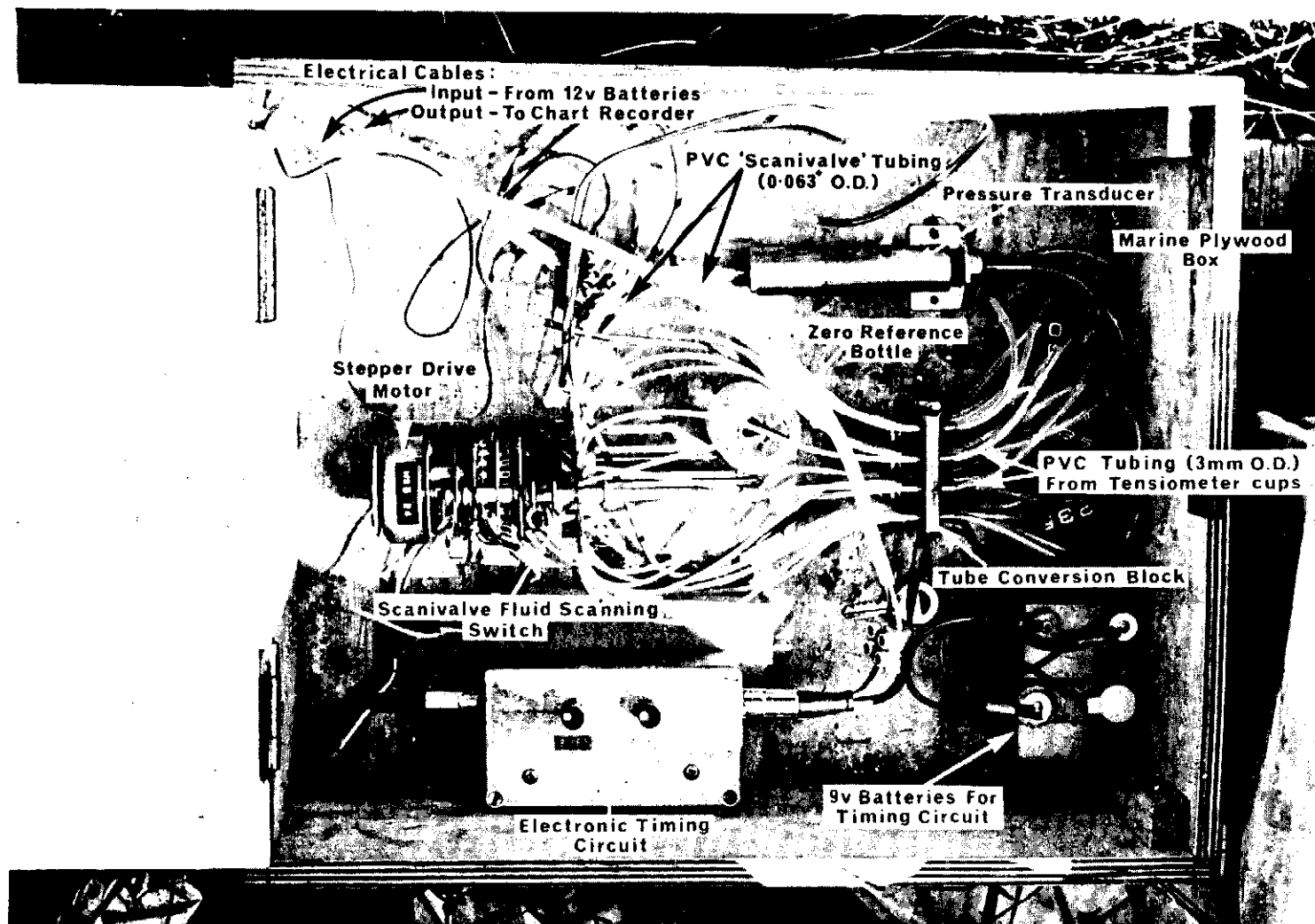


Plate 2.1 - Prototype tensiometer - scanivalve system
 (after Anderson and Burt, 1977)

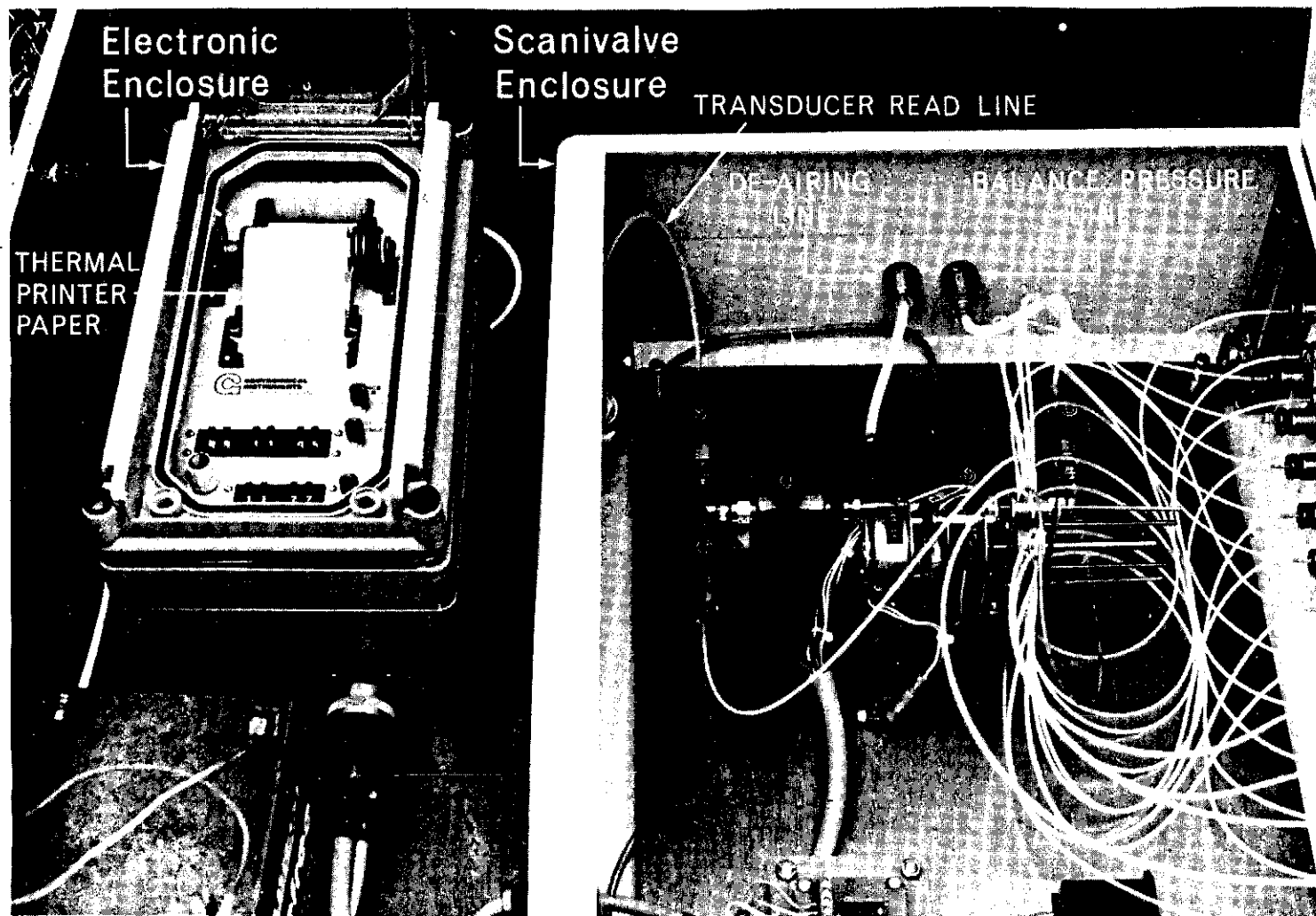


Plate 2.2 - Redesigned tensiometer - scanivalve system employing microprocessor control unit
(after Anderson and Kneale, 1980a)

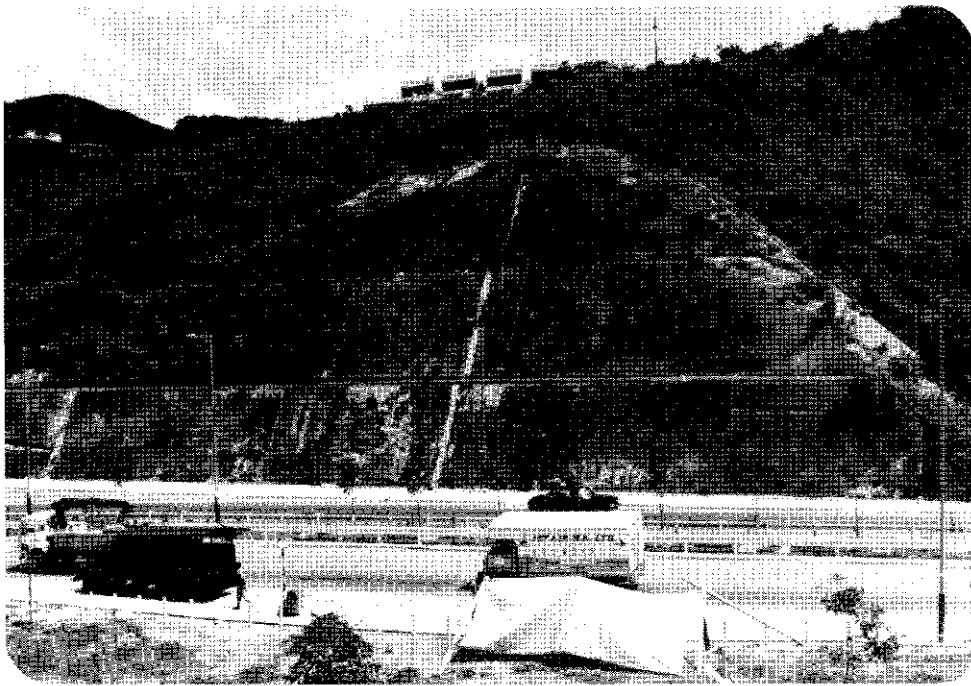


Plate 4.1 - Chunam slope instrumented as shown in figure 4.6

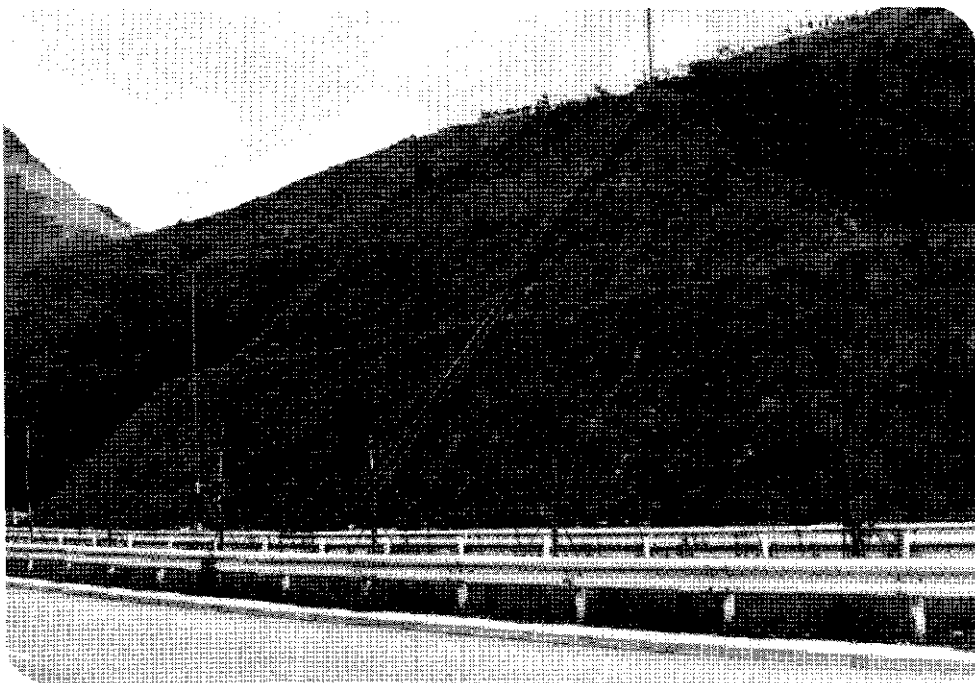


Plate 4.2 - Grass slope instrumented as shown in figure 4.7

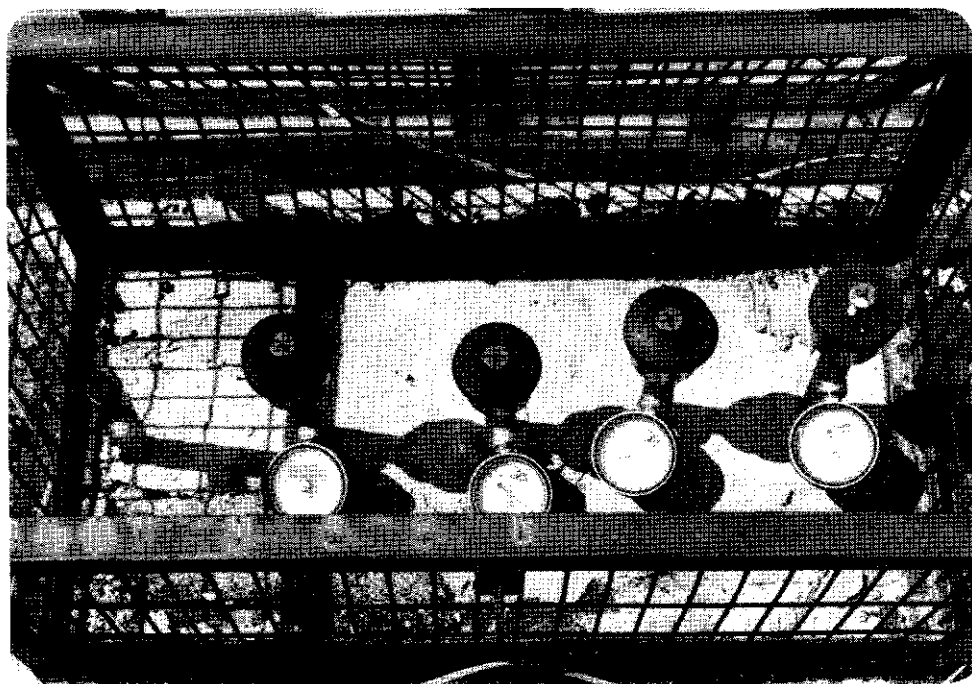


Plate 4.3 - Jetfill tensiometers installed at location C on chunam slope (see figure 4.6).

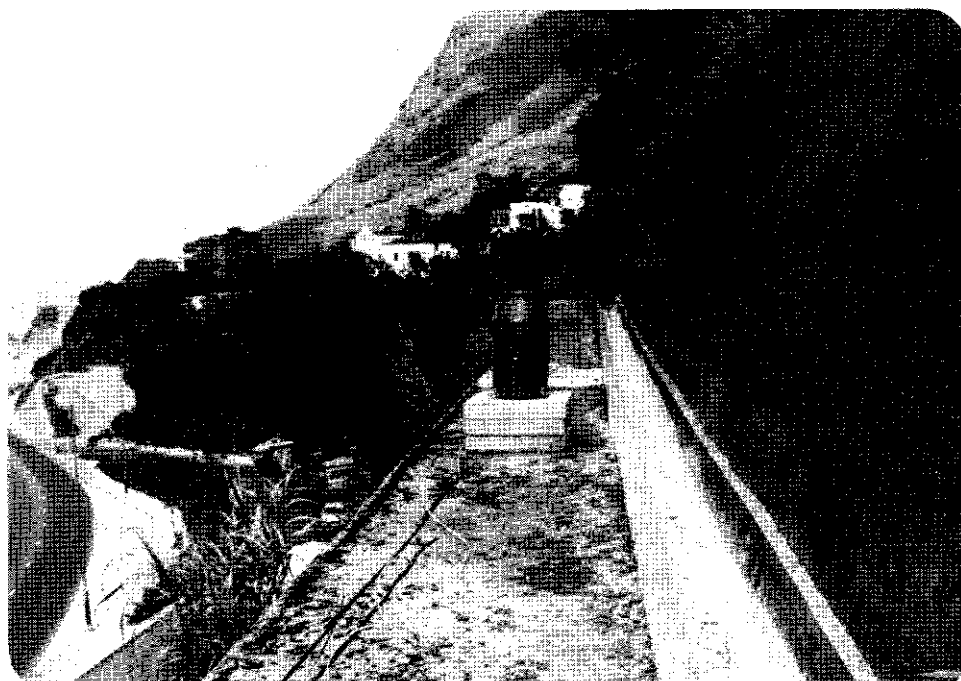


Plate 4.4 - Raingauge location on chunam slope (see figure 4.6)



Plate 4.5 - Tai Po, St. Christopher Bend site

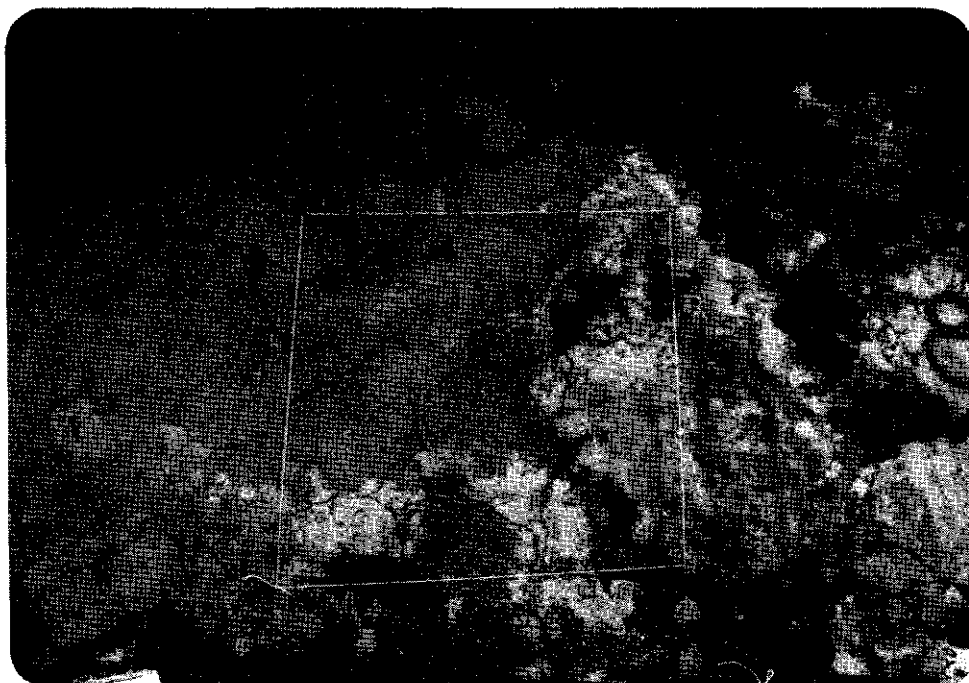


Plate 5.1 - Crack survey - slope 89 - see table 5.3

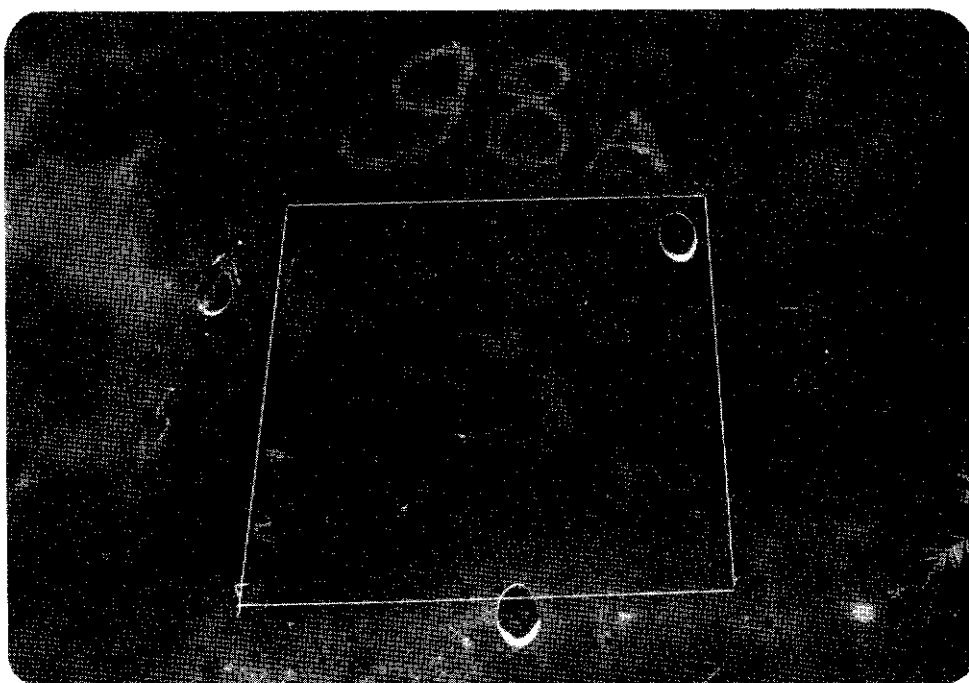


Plate 5.2 - Crack survey - slope 98A - see table 5.3

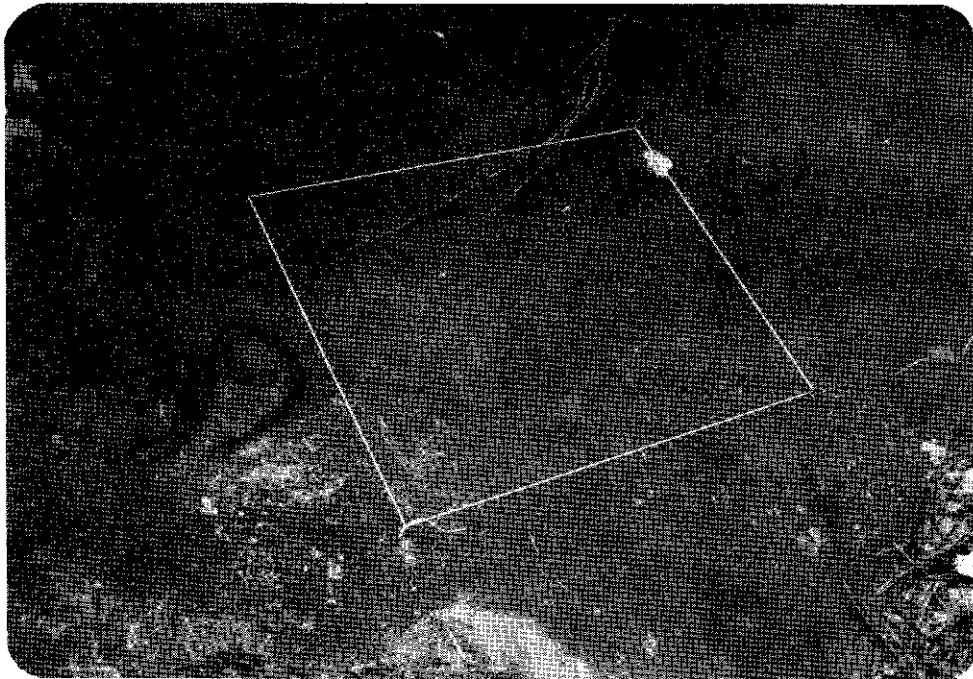


Plate 5.3 - Crack survey - slope 99 - see table 5.3

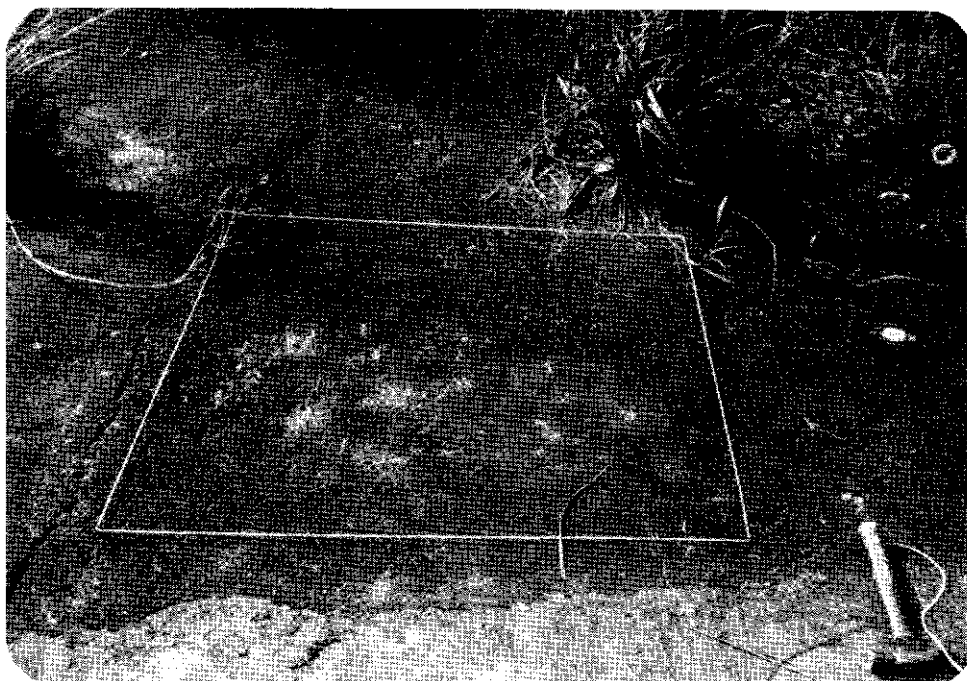


Plate 5.4 - Crack survey - slope 102 - see table 5.3

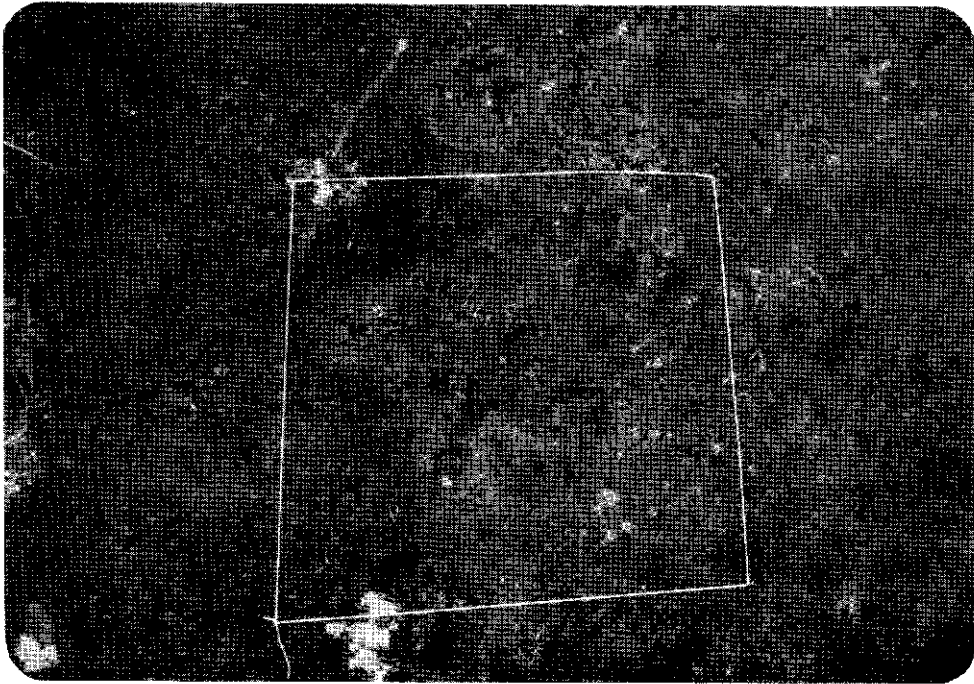


Plate 5.5 - Crack survey - slope 106 - see table 5.3



Plate 5.6 - Crack survey - slope 112 - see table 5.3

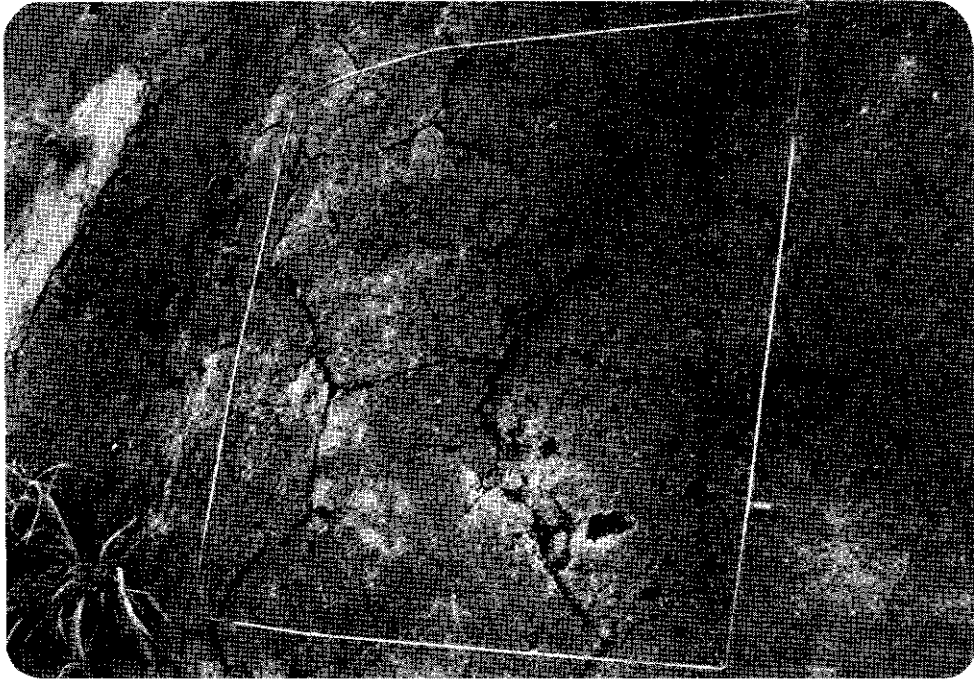


Plate 5.7 - Crack survey - slope 113 - see table 5.3

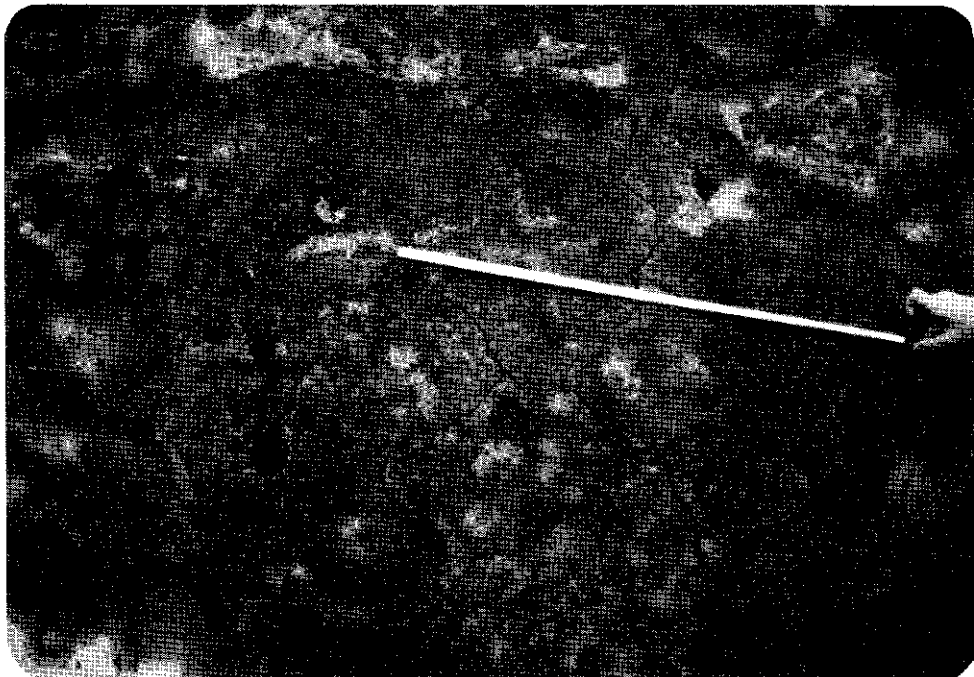


Plate 5.8 - Crack survey - slope 114 - see table 5.3

Appendix A

Laboratory Verification of Crack Model Used in Section 5.2

In view of the programme of work utilising the seepage model outlined by Harr, and discussed in section 5.2, it was seen necessary to obtain some verification of the effective chunam permeability predicted by the model. A laboratory column was set up, being 300 mm diameter and 225 mm high. The lower 50 mm contained a filter above which was placed 125 mm of soil. Chunam was then formed on top of the soil according to PWD specification. A crack forming strip of desired width (within the range 1 mm to 6 mm) was placed on the soil before the chunam was poured.

The complete apparatus could be used to measure (a) the permeability of the soil prior to the chunam pouring, (b) the discharge through the 'cracked' chunam, and (c) the final permeability of the soil (with the chunam removed). Plate A1 shows the laboratory equipment.

In the initial trials undertaken crack widths of approximately 1, 3, 4 and 6 mm were formed and the crack and chunam discharge measured through a soil of $K_s = 6.9 \times 10^{-5} \text{ ms}^{-1}$. A further trial on a soil of $K_s = 1 \times 10^{-6} \text{ ms}^{-1}$ with a 6 mm wide crack was also completed.

Table A1 summarises the measured discharge through the crack widths stipulated. In addition, the flows predicted by equations 5.7-5.9 are also shown.

It can be seen that the measured flow exceeds the predicted flow in the case of the more permeable soil. This difference is of the order of half an order of magnitude.

It is to be noted that for the less permeable soil the disparity between predicted and measured flow is somewhat larger, and in this instance the predicted flow exceeds the measured flow.

By reference to figure 5.10 and the analysis in section 5.2 it is clear that the initial spread below the chunam (B_1) is a critical determinant in the resulting discharge. The nature of the bonding between the soil and chunam is obviously important in this regard. In the context of the laboratory experiment it was observed that in the less permeable soil the chunam, rather than remaining as a distinct layer above the soil, had bonded very strongly with the underlying soil during the curing process. For the case of the less permeable soil, the depth of bonding within the soil was observed to be much less.

Permeability tests confirmed this, as table A1 indicates. The question upon which interpretation of the results hinges, is therefore the nature of the chunam/soil bond under field conditions. If the field application of chunam results in a somewhat superficial degree of bonding (by which it is implied that the chunam layer and soil layer are readily distinct in permeability terms, and without the permeability gradation shown in the less permeable soil - table A1), then the Harr model (equations 5.7-5.9) slightly under-estimates the discharge and effective chunam permeability. The nature of this degree of bonding is judged to be that commonly exposed in field conditions where substantial areas of

cracked chunam are exposed. If this association is accepted, then the predictions based upon the Harr model in chapters 5 and 6 are not over estimating the effective chunam permeability required to prevent infiltration according to the selected criteria.

The indications from this laboratory testing programme are therefore that the results given in table 5.5 and figures 5.14 and 6.14 are broadly supported, with the possibility that the chunam effective permeabilities in table 5.5 may be slightly under predicted, but to a degree that does not alter the conclusions stated in chapter 7.

Table A1 : Results of chunam crack discharge tests

Soil permeability ms^{-1}		Flow $\text{m}^3 \text{s}^{-1} \text{m}^{-1}$	Crack width mm			
before test	after test		1.4	2.9	4.4	6.0
6.9×10^{-5}	5.9×10^{-5}	measured	1.6×10^{-5}	1.9×10^{-5}	2.2×10^{-5}	2.4×10^{-5}
		predicted	4.4×10^{-6}	6.6×10^{-6}	7.2×10^{-6}	7.9×10^{-6}
1.2×10^{-6}	2.1×10^{-7}	measured				5.2×10^{-9}
		predicted				3.1×10^{-8}

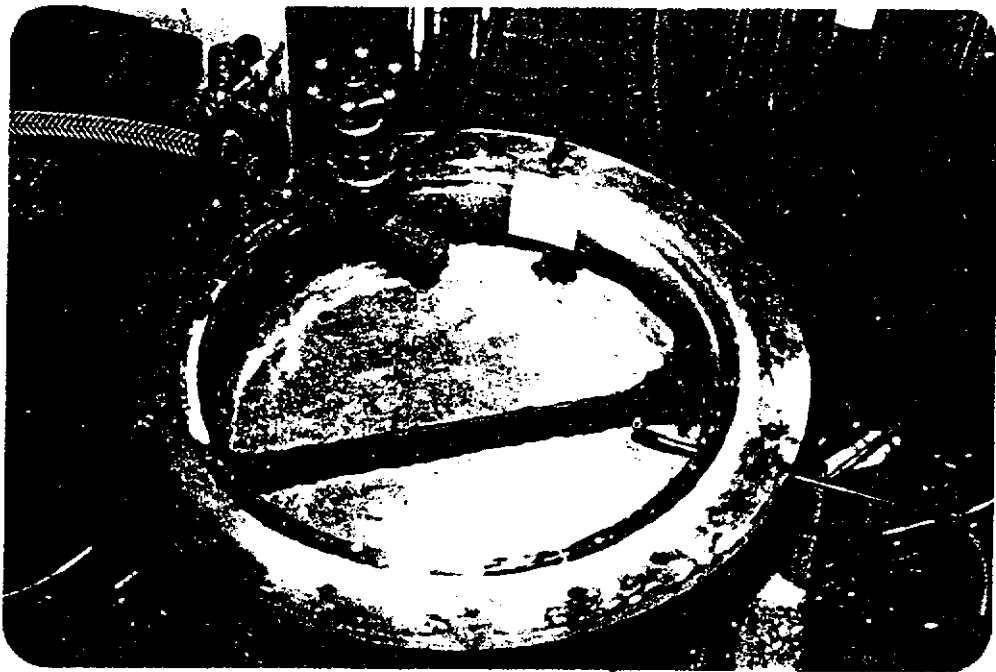


Plate A1 : Laboratory equipment used to test crack model
(equations 5.7-5.9)